DiSTAR Dipartimento di Scienze della Terra,
dell'Ambiente e delle Risorse

UNIVERSITÀ DEGLI STUDI DI NAPOLI FEDERICO II
SCUOLA POLITECNICA E DELLE SCIENZE DI BASE

PhD School in Earth, Environment and Resources Sciences

- XXX Cycle -

PhD Thesis

Tectonic evolution and current deformation of the NW Sicily Channel and the Lampedusa Plateau based on multi-resolution seismic profiles analysis

Melania Meccariello

Advisor

Prof. L. Ferranti

PhD Coordinator
Prof. M. Fedi

Co-advisor
Prof. F. Pepe

2017

ABSTRACT

This thesis deals with the tectonic evolution and the active deformation of the NW part of the Sicily Channel and of the offshore area around the Lampione-Lampedusa islands in the central part of the Channel. While the study sector in the northwest spans across both the offshore prolongation of the Sicilian foreland fold and thrust belt and the Saccense sector of its foreland, the sector in the central part is located in the Pelagian sector of the foreland. As such, they are representative of the two main tectonic processes, namely contraction and extension, that acted together in the Channel during the Pliocene-Quaternary.

In a paleogeographic reconstruction, both study areas belong to the Pelagian Block that represents part of the northern continental margin of Africa. During the Miocene-Pleistocene, Mesozoic-Miocene carbonate platform, seamount and slope rocks found in the NW part of the Channel were deformed and incorporated within the chain as a result of Africa-Europe convergence, whose front migrated from NW towards the SE (ARGNANI et al., 1986; 1990; CATALANO, 1986; CATALANO et al., 1996; ANTONELLI et al., 1988; ROURE et al., 2012; CIVILE et al., 2014).

In light of new advancements in knowledge on the current geodynamics of the central Mediterranean and Pelagian block in the last years (e.g., FACCENNA et al., 2004; 2005; 2007; 2014; BILLI et al., 2007; 2011; ROURE et al., 2012; DEMETS et al., 2015; SOUMAYA et al., 2015), the goal of this research was to improve the understanding of the tectonic setting and evolution of these key areas of the Channel. In addition, specifically for the sector spanning the transition between the present front of the belt and the Saccense foreland, we aimed at providing new constraints on the active deformation pattern.

We based the research on a multi-scale analysis of seismic reflection profiles at different resolution and of deep well logs, and integrated these data

with other geophysical and geological datasets. Specifically, we used multi-channel seismic (MCS) reflection profiles from the ViDEPI and ENI databases and newly acquired high-resolution single-channel sparker (SCS) profiles calibrated with borehole data and outcrops from western Sicily.

In the NW part of the Channel, following and partly refining previous views (CATALANO, 1987; CATALANO et al., 1995 a; b; ANTONELLI et al., 1988; ROURE et al., 2012; CIVILE et al., 2014), we performed an accurate location of the actual front of the chain and proposed a deep-seated deformation style. The latter feature is expressed by fault systems that cut, with a broadly planar geometry and a relatively high dip angle (~ 60° on average), at least down to the investigation depth (~ 7 km) allowed by MCS profiles. A recent analysis of gravity data in the region (LO RE, 2017) also supports this tectonic model of deformation and specific features of our reconstruction.

During Early-Middle Miocene, contractional deformation affected the Egadi area with deep-seated thrusts (ETS, Egadi Thrust System), limited to the east by a major thrust ramp (ETF, Egadi Thrust Front) that separate the Pre-Panormide domain from the Trapanese-Saccense domain. These two domains were differentiated on the base of the seismic facies and of well log analysis. Deformation in the thrust belt was associated to the growth of a foredeep basin in the area of the Adventure Bank.

Through well calibration and seismic facies analysis, we were able to distinguish three seismo-stratigraphic facies pertaining to the Miocene foredeep basin. The lower and middle facies are correlative of the Serravallian-Lower Tortonian pelites (Castellana formation) and conglomerates (Terravecchia fm.), respectively. A high amplitude reflector separates the lower and middle seismic units from the upper unit, which is correlative of the sandy-pelitic sediments pertaining to the younger (Upper Tortonian-Messinian) member of the Terravecchia fm. (BASILONE, 2012).

During the Late Miocene, a new thrust front (ATF, Adventure Thrust Front) acted along the eastern side of the Adventure Bank and the previous foredeep basin was involved in the thrust belt (ATS, Adventure Thrust System). Based on well log analysis, we suggest that the ATS reactivated an inherited crustal boundary that, during the Mesozoic, separated the proximal shelf facies (Trapanese domain) from the distal ramp facies (Saccense domain). The boundary acted also in the Miocene when it separated proximal from distal foredeep facies in the Terravecchia formation. Activity along the ATS with involvement of the older foredeep basin sediments largely ended by ~ 8 Ma ago, as evidenced by the high-amplitude reflector associated to the sandy member of Terravecchia formation that apparently seals deformation of the older foredeep sediments.

Contraction during the latest Miocene and the Plio-Quaternary shifted offshore Capo Granitola, where the Trapanese-Saccense domains were affected by a reverse reactivation of Lower Miocene extensional faults, probably formed to accommodate bending of foreland ahead of the advancing Miocene chain, which generated a pop-up structure.

The offshore area between Capo Granitola and Sciacca is ahead of the contractional belt, and experienced Pliocene-Pleistocene transcurrent deformation along two tectonic belts. The array to the west is the SELFB (Selinunte Fault Belt), which experienced a positive inversion of inherited normal faults. To the east, offshore Sciacca, the SFB (Sciacca Fault Belt) is characterized by a transpressional deformation expressed by positive flower structures. Contemporarily, in the Egadi area we assist to a transpressional re-activation of inherited faults and a new generation of distributed back-thrust faults which are traced up to the sea-floor.

During the Pliocene-Pleistocene, rifting of the Pantelleria basin took place along the central part of the Channel, and the associated extensional faults extended toward Sicily shore. We define an asymmetric basin, which narrows from ~ 20 km in the south to ~ 7 km in the northwest of Pantelleria

Island. The basin is characterized by NW trending extensional structures with a domino style, where half-grabens are separated by sub-vertical normal faults arrays with offsets of a few hundred meters. Seismic images also highlight some reverse faults in the rift basins which can be connected to a local reactivation of normal faults, as already proposed by ARGNANI (1990). Based on age constraints, Plio-Pleistocene reactivation is coeval to the last compressive events of the chain in the offshore of Sciacca and Agrigento along the SFB and Gela Nappe (GN) and also to transpressional reactivation in the Egadi offshore.

The analysis of high-resolution SCS profiles calibrated with well-log data and outcrops on the coastal belt allowed to reconstruct the Pleistocene-Holocene structural framework and evolution of the offshore area between Capo Granitola and Sciacca. The area was divided in two zones based on different tectonic style. The sector to the west, between Capo Granitola and Capo San Marco is characterized by deformation expressed by NE-trending folds of relatively low amplitude and wavelength and low-medium aspect ratio between amplitude and length. These folds, which are associated to slumping and fluid seepages, can be traced for a minimum of 9 km from the coast. They affect Lower Pleistocene sediments and are cored by uplifted Pliocene substratum. Growth of these folds is responsible of marked changes in dip angle and dip direction, relatively to the regional sea-ward directed trend, of the Lower Pleistocene reflectors. Differently, the area between Capo San Marco and Eraclea Minoa to the east is controlled by NNE-trending folds with high amplitude and wavelength, and high aspect ratio between amplitude and length. These folds, which can be traced for a minimum of 20 km from the coast, are associated to fluid infiltration along high angle faults and fractures. These folds are considered to ensue from slip on underlying blind faults whose upper tip is localized at the transition from the brittle-behaving Mesozoic rocks to the ductile-behaving Paleogene-Miocene rocks. Based on the different geometrical parameters outlined above, the western folds are interpreted as

fault-related features, whereas the folds to the east are considered of transpressional origin and being localized on a blind transcurrent zone.

The space-temporal distribution of seismic units highlights a major tectonic control on the thickness distribution of the Middle Pleistocene-Holocene unit, compared to that of the Lower-Middle Pleistocene unit, as it better follows the structure trends. So, it can be inferred that tectonic activity pulsed in the Middle Pleistocene-Holocene.

An estimate of fold vertical growth rate was made for the two areas. The results evidence for the Selinunte anticline uplift rates of ~ 0.1 mm/yr and of 0.03 mm/yr for the short- (1.5 Ma) and long- term (5.3 Ma) interval, respectively. Instead, the estimates for the Sciacca fold are ~ 0.08 mm/yr (short-term) and ~ 0.13 mm/yr (long-term). Note that this estimate for the Sciacca Fold reflects less directly the slip rates on the underlying fault, which, as suggested by the different fold parameters relative to the Selinunte folds, we believe is a high-angle strike-slip fault. On the contrary, the estimate for the Selinunte fold reflects the slip accommodated on the underlying blind thrust ramp.

The joint analysis of MCS and SCS profiles and the definition of fold and fault geometrical parameters extend in the offshore the deformation belt traced in south-western Sicily. This area is spatially adjacent to the macro-seismic zone of the destructive 1968 Belice earthquake sequence in which the active compression at the front of the Sicilian chain is accommodate by south-eastward displacing deep-seated thrusts with poor surface expression. Gentle folds interpreted as the forelimb of a fault-related fold affect the Quaternary deposits between Campobello di Mazara and Punta Granitola (BARRECA et al., 2014; GUZZETTA, 2014). According to our analyses, the transition from the on-land to the offshore domain is marked by an en echelon arrangement and is transferred to the Selinunte anticline which is part of the SELFB.

Summing up, active deformation related to plates convergence is diffuse in the Channel and is evidenced in the Egadi offshore, expressed by back-

thrusts and transpressional/transtensional structures, and in the Mazara and Sciacca offshore by folding and faulting of Pleistocene sediments associated to the most recent thrust front and to the transcurrent belt, respectively.

For what concerns the foreland domain in the central part of the Channel, we analysed the northern part of the Lampedusa Plateau (central sector of the Pelagian Block). The analysis was based on joint analysis of multichannel seismic reflection profiles calibrated with well-logs, and of structural data collected on Lampedusa island. The investigation evidenced that this part of the plateau forms an anticlinorium (Lampedusa Plateau Anticlinorium, LPA).

The LPA developed during Paleogene to Early Miocene intraplate contraction followed by Miocene to current strike-slip deformation. It is formed by WNW-ESE striking highs and lows, which have an ~ 20 km average wavelength and culminate at the Lampione-Lampedusa High. These broad folds are underlain or locally bounded by high-angle faults with a reverse component of displacement, which cut Eocene to Lower Pliocene strata offshore, and Late Miocene strata on Lampedusa. Extensional faults, that have a bathymetric expression and are responsible for marked stratal tilting due to their listric geometry, are only found to the NE of the island and are associated to the rifting that, as seen further NW at Pantelleria, affected the central part of the Sicily Channel in the Pliocene-Quaternary. Seismic reflection profiles show that normal fault activity peaked during the middle part of the Pliocene and strongly diminished afterward.

Appraisal of recent plate motion reconstructions and of published and new structural data offshore and on-land suggests that the main growth phase of the LPA occurred during (Late Cretaceous?) Paleocene-Early Miocene ~N-S convergence between Nubia and Eurasia and associated intraplate shortening. Starting from Early Miocene, likely in response to a CCW rotation of the plate convergence direction, strike-slip deformation occurred with a ~NW-SE shortening axis and ~NE-SW extension axis. During this time span the previous contractional structures were locally reactivated in transpression.

A geodetic velocity field for the Channel was purportedly realized as a collaborative project during this thesis research, and combined velocities of sites on the islands and on the northern shore of the Channel. This analysis evidenced that the two different strain regimes, extensional and transpressional that established since Miocene still persist today as documented by GNSS geodetic velocities. Specifically, Lampedusa and the region north-northeast of it until the Sicily shore at Agrigento is reached, and probably swinging to NW toward Campobello, has similar greatest contractional and extensional vector magnitudes, which reflect a strike-slip deformation regime. Moving northeast of Lampedusa toward Malta and the southeast Sicily shore, the magnitude of the extensional vector gradually prevails, starting from the area where we mapped Plio-Quaternary extensional basins. Between Lampedusa, Pantelleria and the north-western part of the Sicily shore of the channel, a NW-SE trending contractional axis dominates, reflecting an increasing transpression degree. Hence, the deformation gradually changes from compressive in the northwest to transpressive south-eastward but is also influenced by extensional processes.

INTRODUCTION

The Sicily Channel is the relatively shallow sea portion, with an average depth of ~ 350 m, located in the central western Mediterranean between Sicily and Tunisia (Fig. 1). It shows a NW–SE elongated shape and is geographically bounded by the Sicilian coasts to the north and north-east, the Malta Escarpment to the south-east, the 35th parallel to the south, the Tunisian coast to the west and the Skerki Bank to the north-west (Fig. 1, COLANTONI, 1975). It is characterized by a series of topographic highs and lows: the continental shelves Adventure, Malta and Pelagian, banks of sedimentary (e.g. Bannock, Madrepore) or volcanic (e.g. Graham, Terrible, Nameless) origin, the rift basins of Malta, Pantelleria and Linosa that run along the central part of the Channel.
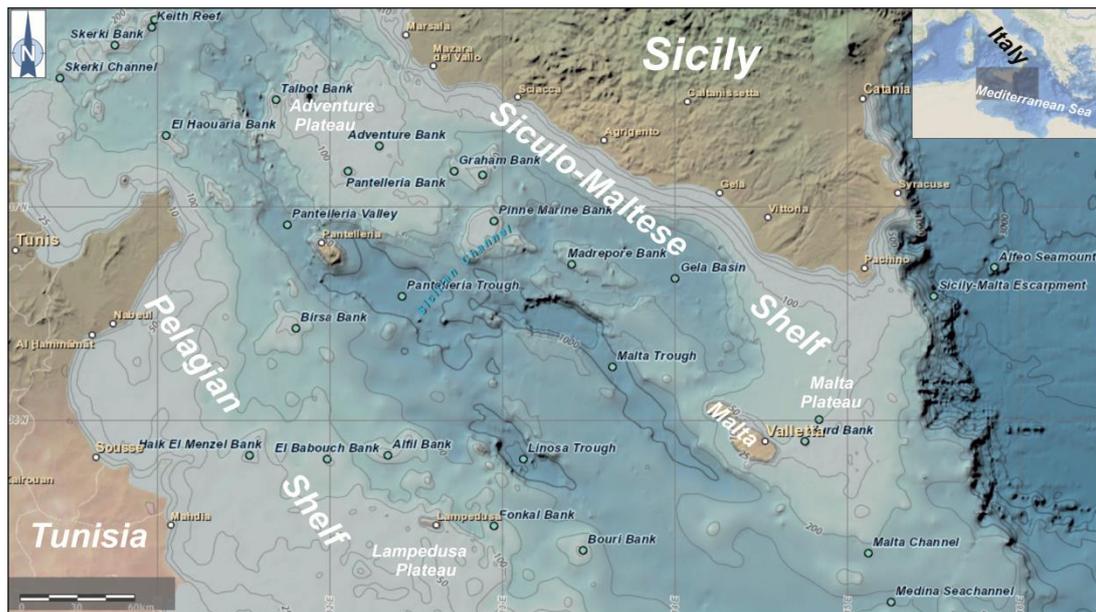
Fig. 1 – Shaded–relief bathymetric map of the Sicily Channel. Data from GEBCO (General Bathymetric Chart of the Oceans) Digital Atlas. (From MONACO et al., 2015).

The Channel represents a key area within the geodynamic framework of the central Mediterranean embodying the submerged prolongation of the Apennines-Maghrebides belt, which outcrops in northern Tunisia and Sicily, and part of the foreland domain represented by Hyblean Plateau in Sicily and

by southern Tunisia. The area floored by the Channel belongs to the northern margin of the African continental plate, which is named Pelagian Block. Part of the continental margin was accreted within the Apennines-Maghrebides orogenic belt, which ensues from collision between Africa and Europe. The fold and thrust belt is now submerged in the north-western part of the Channel, with the remaining part of the Channel being floored by intact or mildly deformed Pelagian foreland.

Most studies regarding the area focused on the origin and evolution of the rift system along the central axis of the Channel, and attributed an Early Pliocene age to the main rift basin development. Different explanations were proposed describing the Channel as: (a) a dextral shear zone located in front of the collisional belt, where tectonic depressions of the rift represent large pull-apart basins involving deep crustal levels (FINETTI, 1984; JONGSMA et al., 1985; REUTHER & EISBACHER, 1985; BEN-AVRAHAM et al., 1987; BOCCALETTI et al., 1987; CELLO, 1987; FINETTI & DEL BEN, 2005); (b) the product of intraplate rifting, related to NE–SW-oriented displacement between Sicily and Africa (ILLIES, 1981); c) the product of mantle convection developed during the rollback of the African lithosphere slab beneath the Tyrrhenian Basin (ARGNANI, 1990); d) the effect of the NW–SE directed impingement of the Pelagian Block against the Maghrebian collisional belt causing the lateral extrusion of the NE portion of the Pelagian Block towards weak segments of the continental margin represented by residual basin areas (CATALANO et al.; 2009); e) a result of slab rupture (FACCENNA et al., 2004).

The offshore continuation of the Sicilian chain was comparatively less investigated. The first models regarded the NW part of the Channel as a locus of shortening active since the Tortonian age (ARGNANI et al., 1986; ARGNANI, 1987; ANTONELLI et al., 1988). The submerged chain was described as characterized by a diachronous system of two foredeep basins with different structural trends and evolution related to a Miocene western and a Plio-Pleistocene eastern front. The two fronts were separated by a transcurrent belt

13

also responsible of Pantelleria and Malta-Linosa grabens separation in the central Channel.

More recently, CORTI et al. (2006) highlighted the coexistence of both contractional and extensional structures related to the occurrence of two independent tectonic processes, shortening in the Sicilian–Maghrebian orogenic belt and extension in the rift system, that acted simultaneously since the Pliocene overlapping each other. Following, CATALANO et al. (1994; 1995a, b; 1996; 2000) and CIVILE et al. (2014) focused on the Adventure Plateau distinguishing three main deformational zones, from NW to SE compressive, transcurrent and extensional.

In light of the present-day knowledge about the Sicily Channel, the present thesis work was carried with the purpose of improving the understanding the tectonic setting of the area through integration of available ministerial data, represented by multi-channel seismic reflection profiles and boreholes, with more high resolution seismic reflection profiles from ENI industrial database. This dense dataset was useful to investigate the area with a more critical perspective by detailing the areas of major interest and clarifying structurally complex zones. The need of an updated analysis arises because previous works only relied on low-resolution ministerial seismic profiles; because significant advancements in knowledge on the current geodynamics of the central Mediterranean and Pelagian block have been achieved in the last years (e.g., FACCENNA et al., 2004; 2005; 2007; 2014; BILLI et al., 2007; 2011; ROURE et al., 2012; DEMETS et al., 2015; SOUMAYA et al., 2015), an update of current tectonic models using better resolution data appears mandatory to date.

The research focused on two key areas of the Channel, the first represented by the marine zone between Egadi Island and Sciacca offshore and the second by Lampedusa-Lampione offshore. The choice of these two areas was dictated by the fact that they are located in the sector of chain and in the rifted foreland domain, respectively. The goal was to determine the relationship between the two areas, specifically how contraction in the NW

and extension in the central part of the Channel interact. With a deeper insight into the tectonic evolution of these two areas, highlights on the geodynamic implications within the Mediterranean geological contest could be gathered. The work presented here on the Lampedusa Plateau integrates different methodologies, as specified in Chapter V, and has been published on the official journal of the Italian Geological Society, named Italian Journal of Geosciences, with the title "*New insights on the tectonics of the Lampedusa Plateau from the integration of offshore, on-land and space geodetic data*" (MECCARIELLO et al., 2017).

An important hint to the current interaction between contraction and extension in the Channel is provided by GPS geodetic analysis (PALANO et al., 2012), which document transtension at ~ 1-2 mm/yr across the Sicily Channel between Malta and Lampedusa, and a shortening of ~ 3 mm/yr along the rift between Pantelleria and Lampedusa. The amount of shortening accommodated on-land is poorly established; it is estimated at 0.5-1 mm/yr along the Sicily front (FERRANTI et al., 2008; DEVOTI et al., 2011), and appears to increase to the east to up to 4.4 mm/yr along a narrow east-west-trending contractional belt located along the northern rim of the Hyblean Plateau in southern Sicily. A remaining part of the current and geological (last 5–6 Myr) convergence between Africa-Eurasia at a rate of 1–2 cm/yr, which is estimated at ~ 1–1.5 mm/yr (PALANO et al., 2012) is accommodated along a narrow east-west-elongated belt of contraction extending offshore northern Sicily from Ustica to Stromboli across the Aeolian Islands. Given the uneven coverage of geodetic sites and the low deformation rates, the locus of the remaining shortening related to plate convergence is unknown, as it is poorly understood how in reality frontal to rear belt contraction and foreland extension interact.

In this perspective, this work aims at contributing to know where the geological deformation associated to Africa-Eurasia convergence is accommodated elsewhere in the Channel.

Furthermore, the possibility of collecting, processing and interpreting new high resolution Sparker profiles for a restricted region of the Channel offshore western Sicily allowed to bring new implications regarding the active tectonics of the area. As a matter of fact, the tectonic deformation in western Sicily is still active as dramatically testified by the 5.9 magnitude destructive earthquake occurring in the Belice valley in 1968. Previous works suggest a NNW-dipping crustal blind thrust ramp (MONACO et al., 1996) belonging to a regional-scale seismogenic structure (LAVECCHIA et al., 2007) as the possible source for the 1968 Belice earthquake sequence. Archaeo-seismological studies also indicate that the ancient Greek colony of Selinunte located in between Mazara del Vallo and Sciacca, was destroyed between 370 and 300 BCE and between 300 and 600 A.D. (GUIDOBONI et al., 2002; BOTTARI et al., 2009), thus providing evidence that the 1968 earthquake was not an isolated event for the area. Recent studies confirm that oblique thrusting and folding in response to NW–SE oriented contraction of the Sicilian chain is still active in an area spatially coincident with the macro-seismic zone of the Belice earthquake sequence and along a SW–NE oriented blind thrust system that extends from Campobello di Mazara to Castelvetrano, and possibly offshore Punta Granitola (BARRECA et al., 2014).

Thus, the effective prolongation in the Sicily Channel of the on-land thrust system seems to be of great importance for the definition of active deformation, a key ingredient in the evaluation of the seismic hazard of a densely populated area such as the western Sicily.

CHAPTER I

1. BACKGROUND GEOLOGICAL SETTING

1.1 The Sicily Channel in the regional geological contest

The Sicily Channel, located between Tunisia and Sicily, is part of the central Mediterranean Sea, which marks the African-European plate boundary and links the African Maghrebides with the Sicilian chain (Fig. 1.1).

The Sicily chain and its submerged western and northern extensions are bounded by the Sardinia block and the southern Tyrrhenian Sea in the hinterland, and by the Pelagian-Hyblean sector in the foreland.
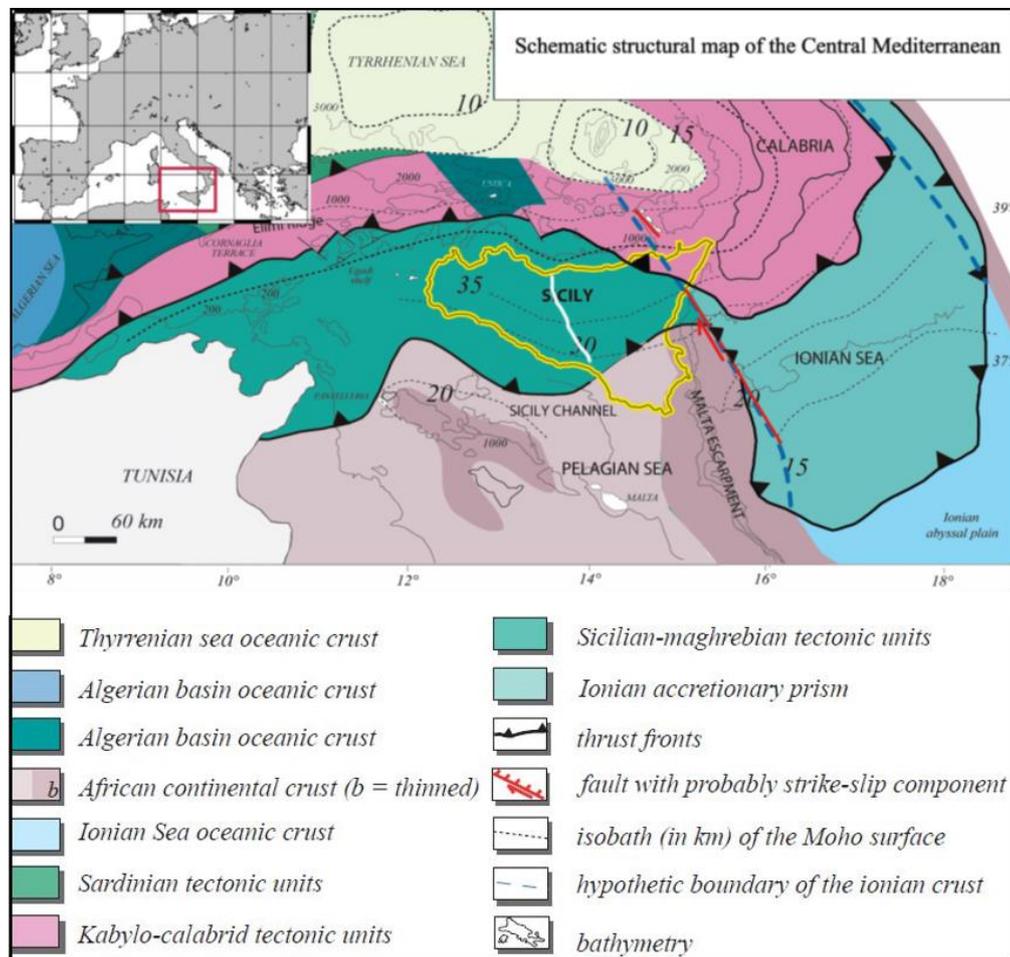
Fig. 1.1 – Schematic structural map of the central Mediterranean area (from CATALANO et al., 2011).

According to CATALANO et al. (1996), the Late Triassic paleogeographic reconstruction of the portion of the North African continental margin now

incorporated in the Sicilian fold and thrust belt consisted of a carbonate platform, setting including the Panormide, Trapanese-Saccense and Hyblean domains.

The carbonate platform passed north and east to a basinal area, where the Sicilide, Imerese and Sicanian deep water domains developed (Fig. 1.2 on the right, *Paleogeographic reconstruction of the southern Tethyan margin during the Late Triassic showing the spatial distribution of the Sicilian-Appennines domains, from CATALANO et al., 1996*).
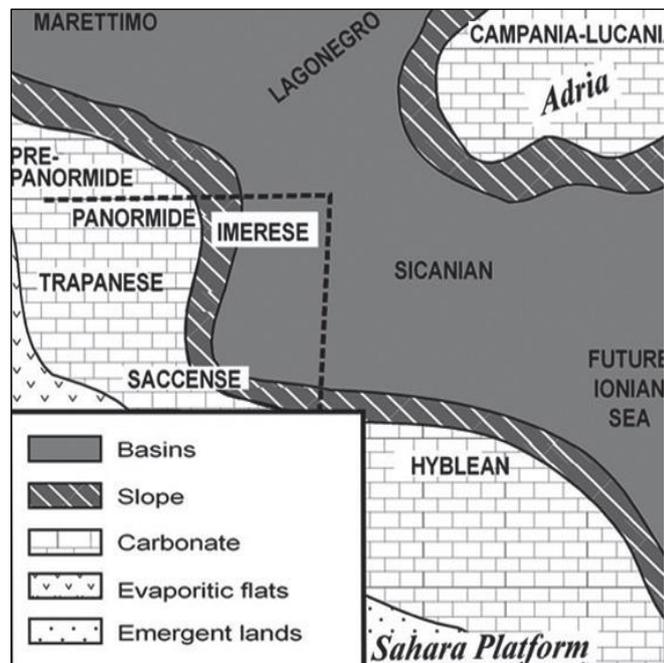
The evolution of the margin was influenced by syn-sedimentary extensional tectonics related to continental rifting and then to oblique oceanic spreading in the Tethyan ocean. During the Jurassic, N-directed extension linked to the sinistral transcurrent motions between Africa and Europe (DEWEY et al., 1989) dissected the Triassic-Liassic carbonate platform with the formation of margins and pull-apart troughs, and drowning of substantial portion of the Trapanese and Hyblean domains (CATALANO & D'ARGENIO, 1982). The Mesozoic platform consisted of steep-faulted margins and was characterized by low rate of sedimentation on the remaining highs, pelagic deposition accompanied by basaltic volcanism (pillow lavas) in the basins, seamount and atolls.

Plate tectonic reconstructions indicate that, from Late Cretaceous to Miocene, Africa and Europe converged along a direction varying from NE-SW to N-S moving from east to west across the Mediterranean Sea (DEWEY et al., 1989). Since the Miocene and through the Pliocene-Quaternary, the plate

convergence direction turned to NW-SE (see Fig. 1.10; Dewey et al., 1989; Rosenbaum et al., 2002; Demets et al., 2015). Present-day geodetic motion indicates a ~ 20° CW rotation of the convergence direction relative to the geologic reconstructions in the Sicily Channel (Demets et al., 2015 and references therein).
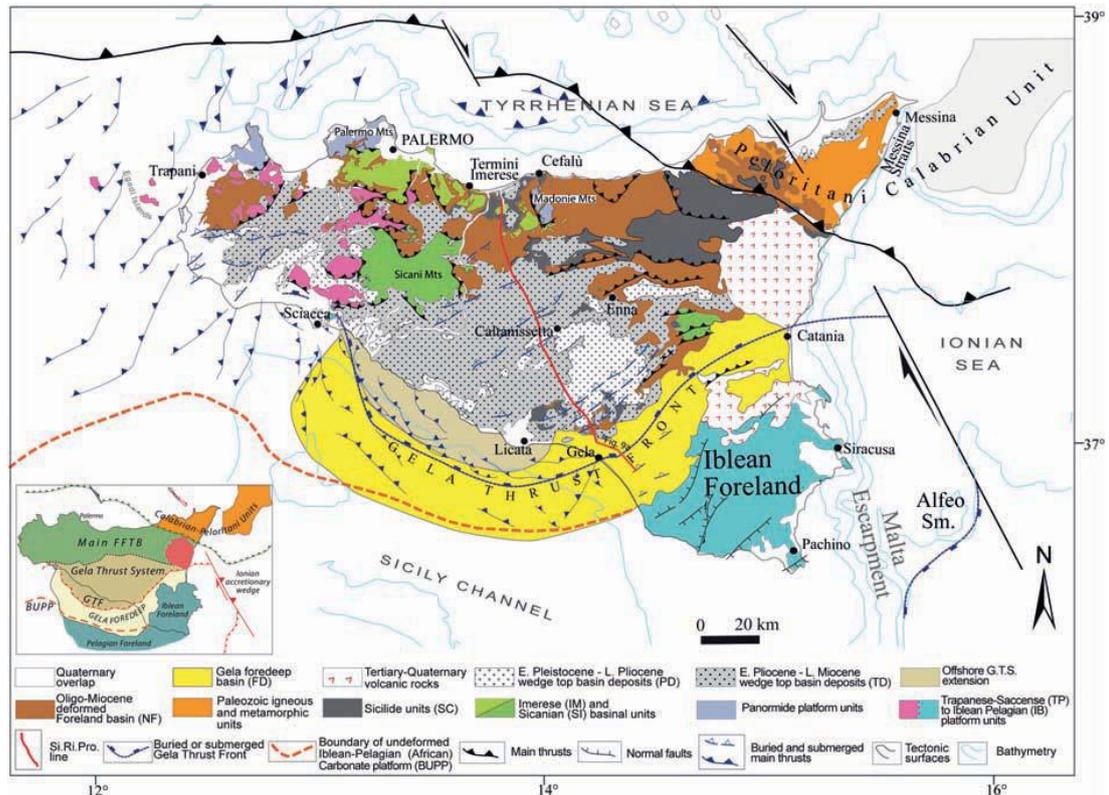
Fig. 1.3 – Structural map of Sicily (from Catalano et al. 2013). Inset map shows the main elements characterizing the collisional complex of Sicily.

The main compressional deformation in the central Mediterranean Sea began with the latest Oligocene-Early Miocene counter clockwise rotation of Corsica-Sardinia and its collision with the African continental margin. Orogenesis occurred in connection with the westward subduction of the Adriatic, northern African and Ionian lithosphere beneath the Corsica-Sardinia block. Subduction and thrusting were contemporaneous with back arc-type extensions in the Tyrrhenian Sea. Today, a ~ 450 km northwest-dipping Benioff zone beneath the southern Tyrrhenian Sea and the related calc-alkaline

volcanism in the Aeolian Islands indicate the remnant of this subduction (FINETTI & DEL BEN, 1986; MALINVERNO & RYAN, 1986; FACCENNA et al., 1996; ROSENBAUM & LISTER, 2004; FINETTI et al., 2005; CHIARABBA et al., 2008; NERI et al., 2009).

The Sicily fold and thrust belt (SFTB) is composed of tectonic units derived from the deformation of the above described paleogeographic domains, which were progressively accreted from west to east (CATALANO et al., 2013 and references therein). Three elements characterize the collisional complex of Sicily and adjacent offshore areas (Fig. 1.3):

- an E and SE-vergent fold and thrust belt, which outcrops in Sicily and is submerged in the adjacent western, northern and eastern seas; this more than 15 km thick complex consists, from the internal to the external sectors, of a "European" element (Peloritani Units), a "Tethyan" element (Sicilide Units) and an African element (Maghrebian-Apenninic Units);

- a WNW-ESE trending foredeep which extends from the Ionian margin of Sicily to the southern Sicily offshore (Gela basin), and is a narrow, more or less deformed depression, partially buried by the frontal arcuate termination of the Sicilian chain;

- a foreland which outcrops in the Hyblean plateau and is submerged in the Pelagian sea and in the adjacent Ionian Sea. The autochthonous sedimentary wedge (about 9 km thick) overlies an "African" continental crust and consists of thick Triassic-Liassic platform and slope to basin carbonates, overlain by Jurassic-Eocene pelagic carbonates and Tertiary open shelf clastic deposits (PATACCA et al., 1979; CATALANO & D'ARGENIO, 1982; ANTONELLI et al., 1988).

1.2 Structural setting and active deformation of SW Sicily

A focus on structural framework of western Sicily is made.

The interest portion of Sicily mainland is part of the SFTB that cross the island with a west-east trend and consists of an African verging thrust wedge.

It is characterized by a duplex geometry composed of two superposed thrust systems and separated by a regional décollement (CATALANO et al., 1998; 2000; FINETTI et al., 2005). The shallower system consists of a 1-3 km thick middle-late Miocene stack of thrust sheets, the deeper is a ca. 10 km thrust system structured since the Late Miocene-Early Pliocene (BELLO et al., 2000; CATALANO et al., 2000; AVELLONE et al., 2010).

Starting from Late Miocene, the south-eastward deep thrust migration was accompanied by large antiformal folding (e.g. Fiume Freddo anticline, Vita and Belice syncline, MONACO et al., 1996; Fig. 1.4) of the tectonic units previously structured at the upper level and passively transported, including satellite sedimentary basins (e.g. the upper Miocene Castelvetrano Basin). The frontal thrust faults show flat-ramp geometries and are involved in lateral extrusion processes produced by the indentation of the orogenic wedge against the rigid part of the Pelagian foreland block (MONACO et al., 2000).

The pre-orogenic sequences involved in the thrust deformation consist of Permian-Cenozoic carbonates and marls pertaining to carbonate and pelagic platform domains and deep-water basins representing the sedimentary cover of paleogeographic domains pertaining to African continental margin prior to the onset of deformation (CATALANO et al., 2002). Whereas, the Miocene-Pleistocene rocks were deposits during the deformation of the continental margin.

The pre-Panormide succession is made up of Triassic-Lower Liassic carbonate platform dolomites and limestones; Lower Cretaceous to Eocene cherty limestone and marls; Middle Oligocene-Lower Miocene biocalcarenites, sandy pelites and Numidian quarzarenites. Lower-Middle Miocene shallow-water limestone and glauconitic arenites with marls follow upward (CATALANO et al., 2002).

The Panormide type successions crop out in the north-western part of Sicily at Capo San Vito. Upper Triassic–Middle Liassic carbonate platform deposits are followed by Jurassic pelagic platform rocks that are onlapped by

Upper Jurassic–lowermost Oligocene reefoidal and slope facies limestone. Lower Miocene open shelf to reef limestones unconformably cover the eroded Meso-Cenozoic carbonate body (ABATE et al., 1993).
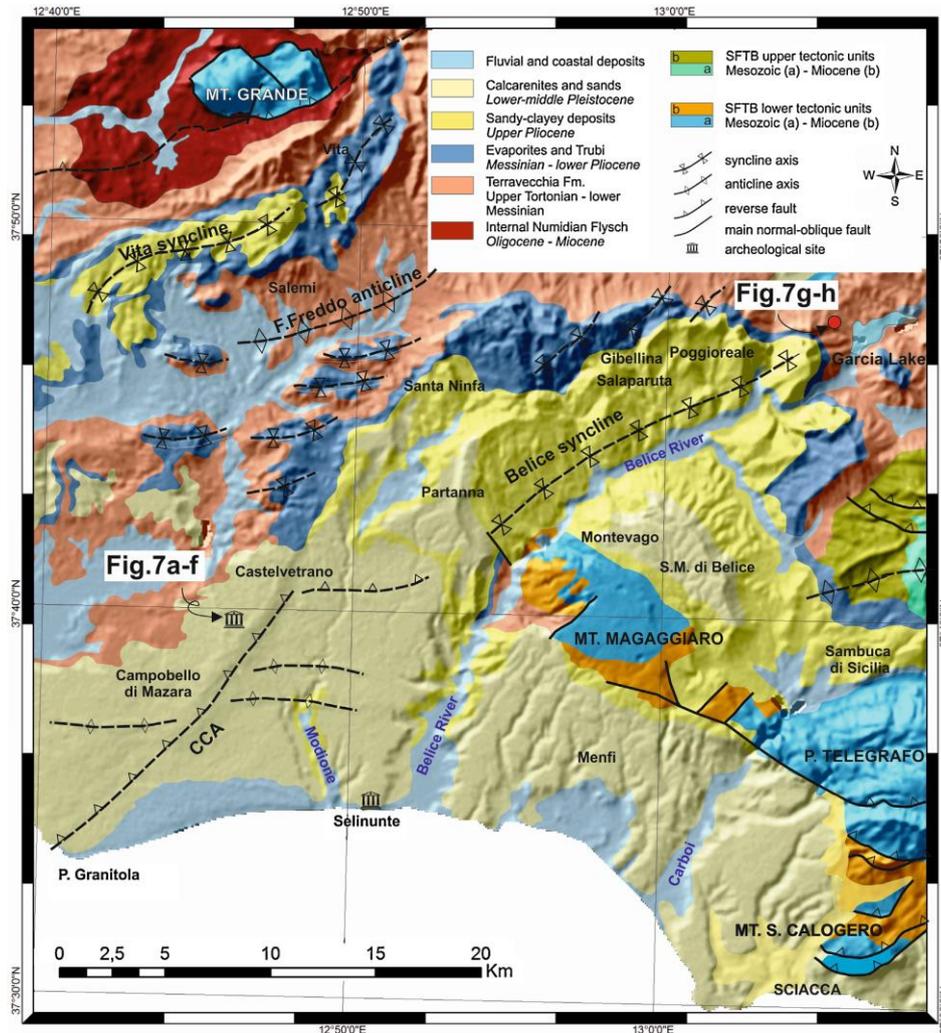
Fig. 1.4 – Geological map of south-western Sicily showing thrust faults and axial traces of major folds including the CCA (Campobello di Mazara–Castelvetrano) alignment (from BARRECA et al., 2014).

The Trapanese type succession outcrops at the Inici–Montagna Grande ridge, M. Bonifato, Trapani, Castellammare, Monti di Alcamo, Dorsale di Rocca Busambra, Monte Kumeta, and was penetrated by several exploration wells. Upper Triassic–Middle Liassic carbonate platform dolomites and limestones (Sciacca and Inici facies) are followed by Jurassic–Lower

23

Oligocene pelagic platform deposits that include Buccheri, Lattimusa, Hybla and Scaglia formations (locally known as Amerillo fm.). Upper Oligocene–lowermost Miocene re-sedimented biocalcarenites and breccias follow unconformably (Corleone calcarenites and San Cipirello marls). Burdigalian to Langhian, open shelf to coastal, glauconitic calcarenites and sandstones unconformably cover the Meso-Cenozoic carbonates.

The carbonate platform rocks which crop out to the south in the Magaggiaro ramp anticline and are buried in the Castelvetrano–Mazara area have been described as pertaining to the Saccense domain (CATALANO & D'ARGENIO, 1978). The Saccense type succession is similar to the Trapanese one, except that the Oligocene–Lower Miocene deposits display open shelf to reef environmental characteristics.

Serravallian to Tortonian terrigenous deposits crop out all over western Sicily, either paraconformably overlying the Lower Miocene glauconitic limestone and sandstone of the Trapanese succession, or unconformably overlapping the already deformed Panormide (ABATE et al., 1993) or pre-Panormide rock units (CATALANO et al., 1989; ABATE et al., 1993; INCANDELA, 1995). This unit is capped unconformably by conglomerates, clayey sandstone and marls of Terravecchia Fm. (Late Tortonian–Early Messinian). Messinian evaporites lap over an erosional surface cutting the underlying strata. The Messinian evaporitic succession is predominantly eroded north of Montagna Grande, becoming widespread to the south, in outcrops (Biddusa–Vita and Gibellina– Castelvetrano synforms), or in the subsurface of southernmost western Sicily.

The evaporitic strata are overlain disconformably by the marl–carbonate Trubi fm. A thick sedimentary wedge of mostly carbonate-clastic rocks (turbiditic sandstone and resedimented biocalcarenites, hemipelagic shales with interbedded siltstones and calcarenite mudstones), locally known as "Marnoso Arenacea del Belice" (Belice marly-arenaceous) fm., overlies the Trubi limestone. Its age is bracketed between 3.8 and 2.5 Ma (VITALE, 1996).

It occurs particularly in southwestern Sicily along the NE–SW synforms of Biddusa–Vita, Gibellina– Castelvetrano and the Menfi area.
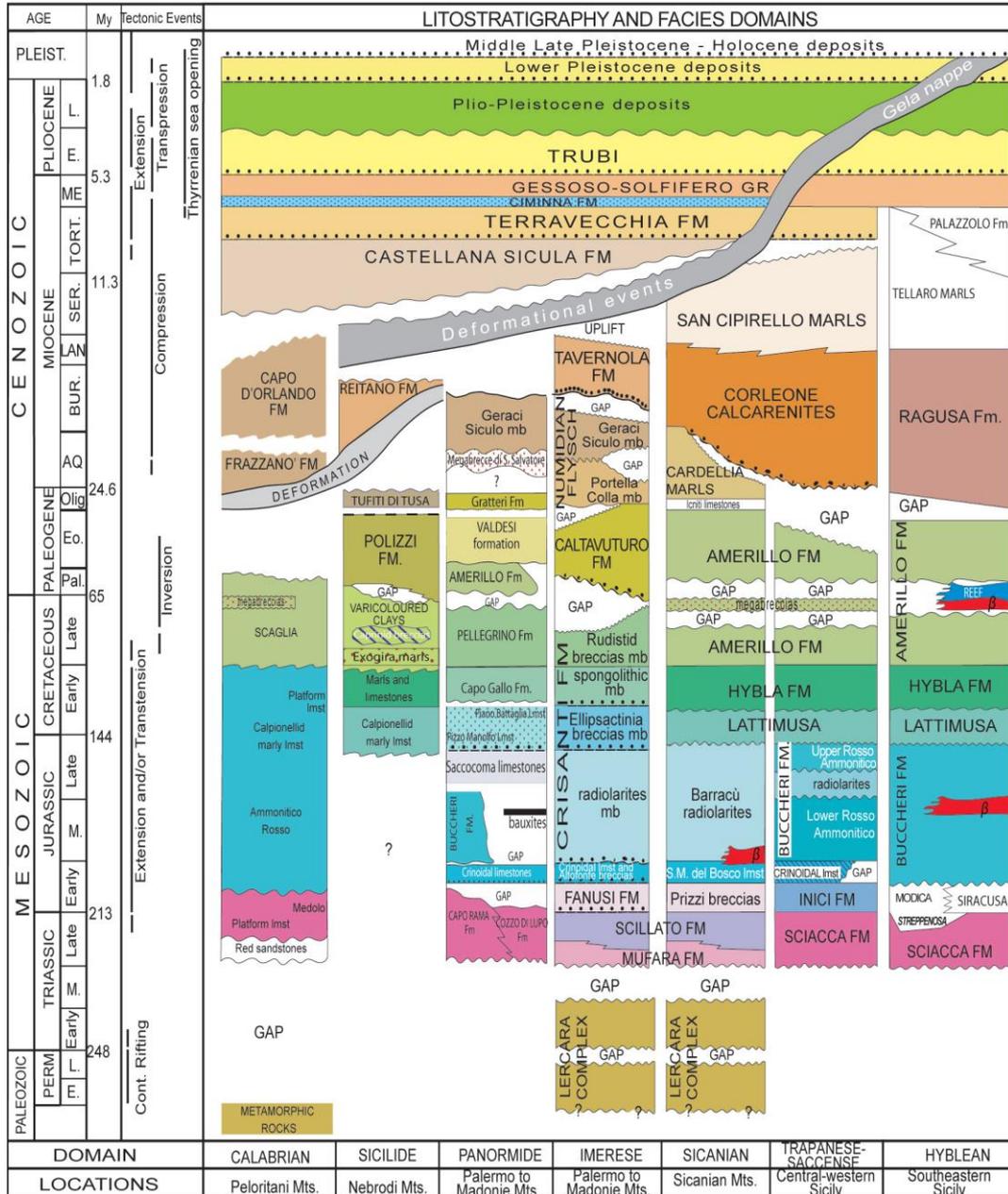
Fig. 1.5 – Chronostratigraphic scheme of the Permo-Cenozoic Sicilian lithostratigraphic units divided in facies and paleogeographic domains (from CATALANO et al., 2011).

Uppermost Pliocene–Lower Pleistocene sandy shales, calcarenites and shallow-water carbonates cover the westernmost and southern areas of western Sicily.

The studied offshore area of the NW part of the Channel is bounded by the coastal belt extending from Mazara del Vallo to Sciacca. This coastal area has a rather flat morphology with slope angles ranging between 0° and 5° and is crossed by Belice and Modione river.

Recent tectonic activity is testified by folded Late Quaternary terraces and lacustrine deposits, outcropping at the frontal and shallower sector of the thrust and fold system south of Pizzo Telegrafo (MONACO et al., 1996), and by the 1968 Belice Valley destructive earthquake sequence (MONACO et al., 1996; MORELLI & PONDRELLI, 1998; DISS Working Group, 2010).

According to previous authors (MONACO et al., 1996; CATALANO et al., 1998) the deep-seated ramp thrusts of the SFTB are part of a unique regional system which deforms the northernmost margin of the Pelagian block. This regional system has been incorporated by LAVECCHIA et al. (2007) in a geodynamic model that attributes to the active thrust belt (the Sicilian Basal Thrust, SBT), which deepens northward from the front and reaches sub-crustal depths, the role of single seismogenic source of western Sicily.

The 1968 Belice earthquake sequence, characterized by several shocks with M ~ 5, and considered the strongest seismic event recorded in western Sicily in historical times, did not produce surface rupture breaks. The seismic event was the result of multiple ruptures of a still active crustal thrust ramp under the Belice Valley area that remains blind and flattens into a flat detachment within the sedimentary cover splaying into a series of minor contractional structures (MONACO et al., 1996).

Before the 1968 Belice seismic sequence, the westernmost segment of the SFTB was considered a seismically almost quiescent region.

Geoarchaeological evidences indicate the occurrence of two ancient earthquakes documented by the collapse of Greek temples in Selinunte,

located 4 km west of the Belice River mouth (Fig. 1.4), occurred between 370 and 300 B.C. and between 300 and 600 A.D. (GUIDOBONI et al., 2002; BOTTARI et al., 2009).
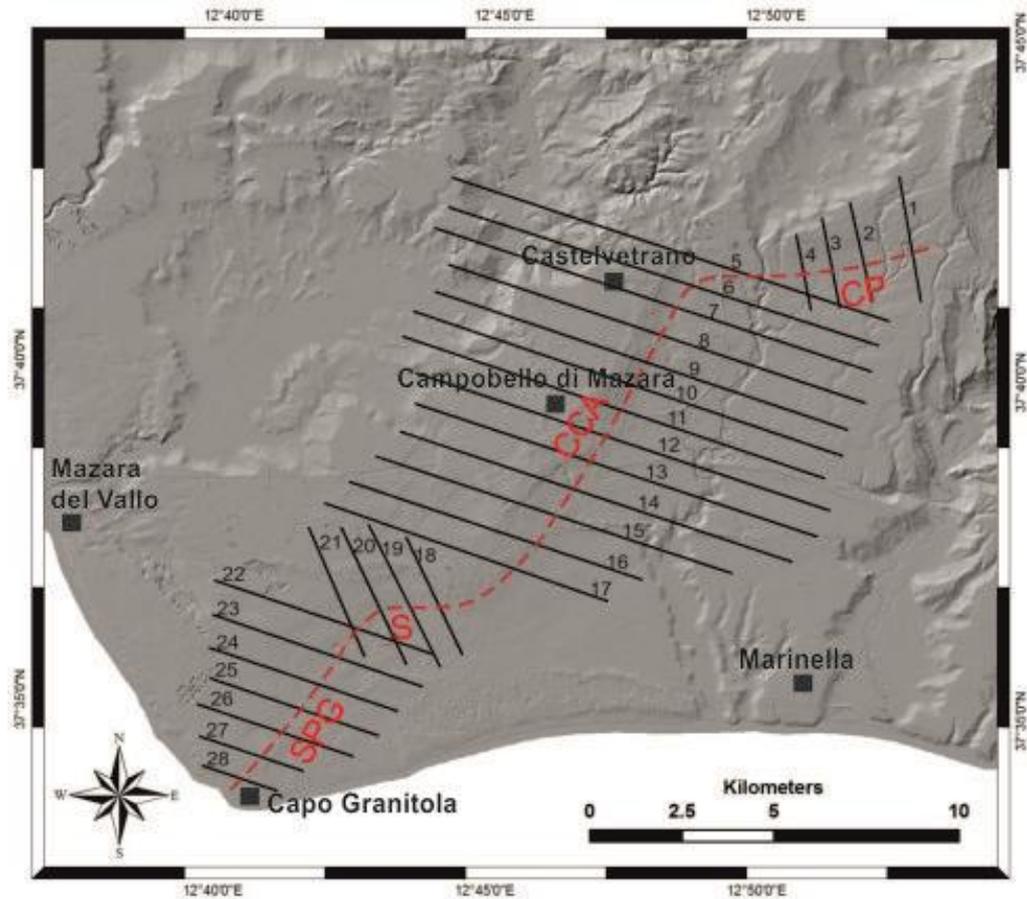
Fig. 1.6 – Hillshade of the SW Sicily with the topographic profiles (from 1 to 28) normal to the morphologic lineament divided into 4 segments: CP, CCA, S, SPG (from GUZZETTA, 2014).

GUZZETTA (2014) studied the western part of the frontal thrust system and distinguished four morphological segments expressed by escarpments which deform Quaternary deposits in the area of Castelvetrano and Capo Granitola: CP (Castelvetrano-Partanna), CCA (Castelvetrano-Campobello di Mazara), S (Straglio) and SPG (Straglio-Punta Granitola). They show variable lengths (between 2 and 12 km) and trends (NNE-SSW, for the CCA and SPG, and ~ E-W, for the S). The CP segment is characterized by a slope with height

varying from 300-200 m dipping towards the coast. The CCA segment with NE-SW trend is represented by a ~ 5 km wide, marked asymmetric ridge with a prominent escarpment on the SE side. The escarpment appears steep, rapidly growing toward southwest and reaching the highest altitude south of Castelvetrano (58 m on a length of 1.1 km). Towards Straglio area, the scarp is unrecognizable and appears to be segmented in several smaller slopes ~ 10 m in height.

On the third segment S (Straglio), articulated and seaward degrading topography varies from 80 to 20 m. Slightly steep slopes dipping toward SSE are characterized by gentle gradients.

Along the southern segment SPG, a wide undulation is recognized with no evident slopes. As it moves towards the coast, the feature decreases in height and extension, also showing an asymmetrical profile with a maximum altitude of 9 m on an average length of 275 m. The ridge tends to flatten toward the coast.

Except for the more regular S segment, interpreted as a relay zone, the variation in height of the scarp along the other segments has been related to the growth of distinct folds bounding fault segments.

The CCA displays an asymmetric morphologic scarp with NNE-SSW trend and amplitude of ~ 1 km, which is part of a gentle ~ 5 km wide ridge. The sharp topographic break within the Lower-Middle Pleistocene calcarenites along the CCA (Fig. 1.6) is attributed to blind, thrust-related antiformal folding nucleated in response to south-eastward slip on a deep-seated thrust which cores a blind culmination of the SFTB internal units (GUZZETTA, 2014; BARRECA et al., 2014).

Recent activity of the CCA is testified by the discovery of dislocated archaeological remains about 25 km south-west from the epicentral zone between Castelvetrano and Campobello di Mazara (BARRECA et al., 2014), and not associated to the 1968 Belice sequence but to past earthquakes that destroyed the old Greek colony of Selinunte (GUIDOBONI et al., 2002;

BOTTARI et al., 2009). And along the CCA that extends offshore in the Sicily Channel as shown by the preliminary analysis of high resolution seismic reflection profiles (GUZZETTA, 2014; BARRECA et al., 2014).

1.3 Regional distribution of lithostratigraphic units

The analyzed offshore areas surrounding SW Sicily coasts pertain to Trapanese-Saccense and Hyblean domains.

ANTONELLI et al. (1988) presented a lithostratigraphic scheme (Fig. 1.7) based on well and seismic reflection data obtained from surveys conducted in the northern portion of the Sicily Channel. They evidenced the facies pertaining to the Trapanese-Saccense and Hyblean paleogeographic domains of continental Sicily for the northernmost part of the Channel and to Tunisian and Malta domains of the Pelagian block for the southernmost portion.

The Trapanese-Saccense facies extends between the Adventure Bank and offshore Agrigento. The sequences consist of Triassic-Eocene carbonates and marls underlying Oligocene-Quaternary clastic deposits. The carbonate sections include platform carbonates of Triassic-Liassic age (Sciacca and Inici fm.) that pass to limestone and deep-sea marls (Buccheri, Chiaramonte, Hybla and Amerillo fm.). Instead, the clastic sections exhibit sedimentary rocks of the coastal and outer platform (Fortuna, Ain Grab, Corleone, Terravecchia and Ribera formations) interbedded with open platform and shallow water marls and limestone (San Cipirello, Mahmoud and Nilde fm.) and evaporite deposits.

The Hyblean sequence extends into the northeastern Agrigento offshore and the Ragusa-Malta Plateau. During the Jurassic, the eastern region (Ragusa-Aretusa) differed from the western (Perla-Vega): while shallow platform deposits prevailed in the east, a thick basinal succession sedimented in the west.

29
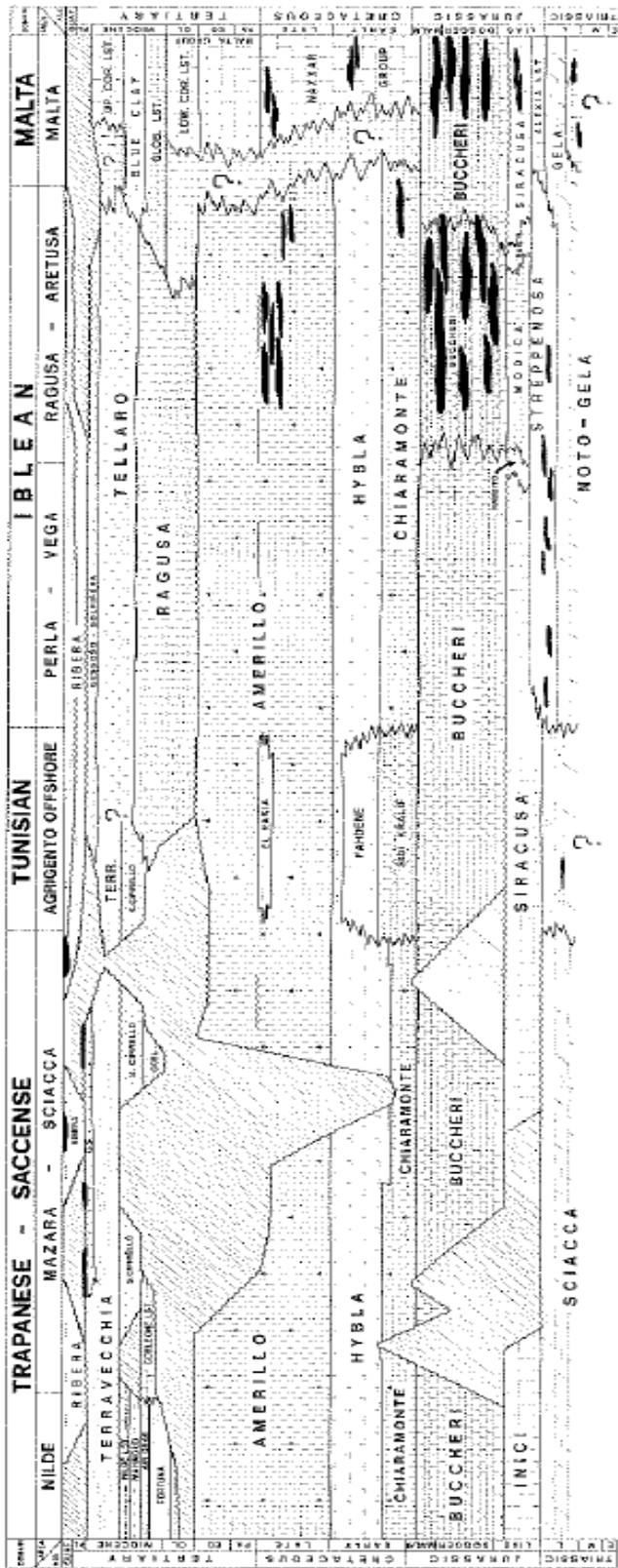
Fig. 1.7 – Lithostratigraphic correlation chart along the central and eastern part of NW Sicily Channel (from ANTONELLI et al., 1988).

The sequence exhibits deep sea and platform carbonate and sedimentary rocks of Triassic-Liassic age (Gela, Noto, Streppenosa, Siracusa and Modica

fm.) followed by pelagic and deep-sea rocks (Buccheri, Chiaramonte, Hybla and Amerillo fm.). This section is overlain by outer platform carbonates, marls and evaporates of Oligocene-Miocene age and Plio-Quaternary clastic deposits (Ribera fm.).

The Tunisian facies covers the southern side of the Adventure Bank and southern Agrigento offshore. It presents Jurassic shallow platform and pelagic carbonates comparable with the Trapanese and Hyblean domains (Siracusa and Buccheri fm.) underlying a Tithonian-Eocene section of deep marine carbonate and clastic rocks (Sidi Kralif, Fadhene, Aleg, Abiod, El Haria, Souar). At the top, Oligocene-Quaternary deposits equivalent to those of Trapanese domain are found.

The Malta facies, developed on the Ragusa-Malta Plateau, was characterized by shallow marine carbonate deposits during the most part of Meso-Cenozoic.

1.4 Structural frame of the Sicily Channel

The Sicily Channel is characterized by a broad shelf that reaches maximum extension towards Malta and towards southwestern Sicily on the Adventure Bank, connected to the central and deeper part by an irregular slope with basins and banks, some of which of volcanic origin (ARGNANI et al., 1986).

Seismic reflection, gravimetric, magnetic and well data collected by oil companies and research institutions have allowed to reconstruct the paleogeographic evolution and the structural setting of the northern (Italian) sector of the Sicily Channel (Fig. 1.8; ANTONELLI et al., 1988; ARGNANI, 1987; ARGNANI et al., 1986; 1987; 1999; TORELLI et al., 1991; 1992; CATALANO et al., 1994; 1995b; 1996; 2000; CIVILE et al., 2010; 2014; 2015; COLTELLI et al., 2016).
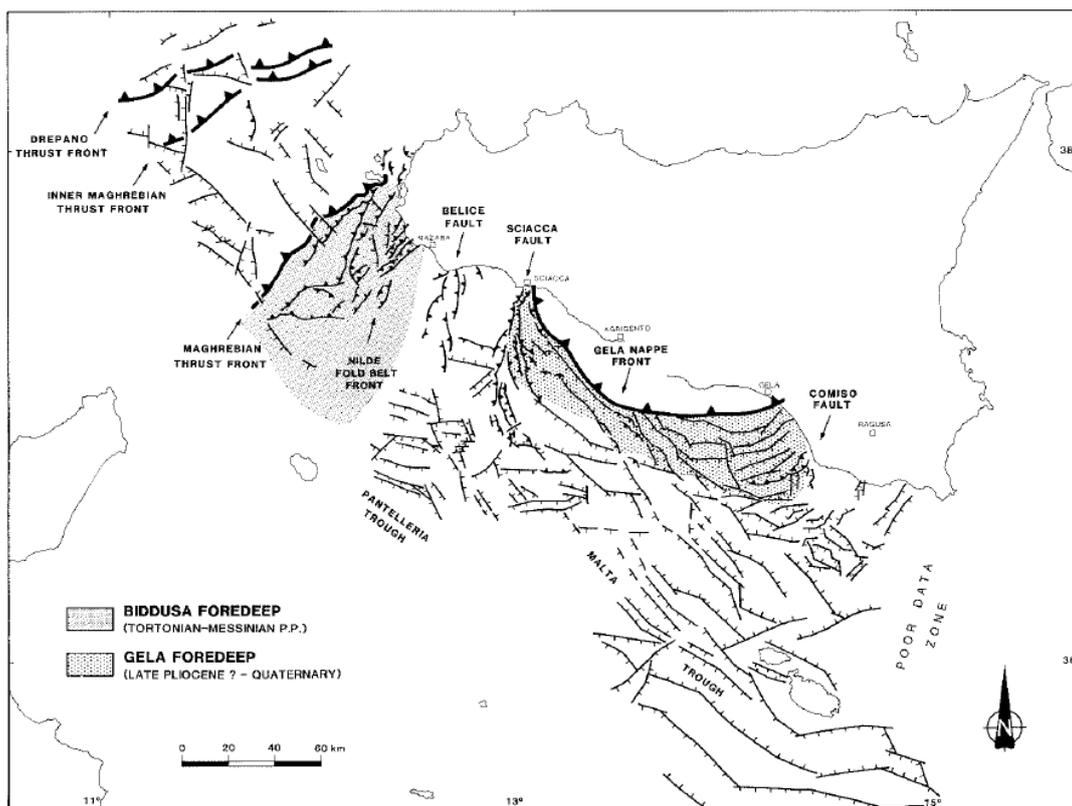
Fig. 1.8 – Tectonic map of Sicily Channel Neogene-Quaternary evolution (from ANTONELLI et al., 1988).

Several domains are recognized moving from W to E:

- a western segment of the chain, SE verging, whose outer front (Nilde Fold Belt Front, NFBF) is located offshore Mazara involving structural features belonging to the Belice fault zone and recognized further to the east by ARGNANI et al. (1986);

- a transcurrent belt along the eastern part of Adventure Plateau and corresponding to the onshore Mazara-Sciacca regional high;

- an eastern segment of the chain with SW vergence represented by the Gela Nappe Front (GNF) that extends offshore only on its external front between Sciacca and Gela;

- a foreland area, from Gela offshore to Malta, which is part of the Pelagian foreland block from which it is separated by extensional faults related to the Sicily Channel rift.

The SE verging western segment of the chain was emplaced during the Miocene and represents the most deformed inner sector of the chain (ANTONELLI et al., 1988) derived from the deformation of the Sicilide, Imerese and Sicanian domains. It is made up of a thick pile of rootless nappes which underlies the Adventure Bank (CIVILE et al., 2014). The thrust front is visible on the north-western sector of the bank, named Egadi thrust front (ETF; CATALANO et al., 1995b) or Maghrebian thrust front (MTF; ANTONELLI et al., 1988), whose associated structures seem to be reactivated in recent time locally affecting the sea floor (CIVILE et al., 2014; TORELLI et al. 1993).

From the Messinian, the Adventure Bank was involved in the deformation and emplacement of the NFBF.

The NE-SW trending Adventure foredeep (ARGNANI, 1993a, b) or Biddusa foredeep (Fig. 1.8; ANTONELLI et al., 1988) of Miocene age is located on the western side of the homonymous Bank limited to the west by the MTF and truncated on the south by the Pantelleria trough. It is filled by silico-clastic sediments pertaining to the Terravecchia formation (Tortonian-Messinian age) with maximum thickness of 2-3000 m. The foredeep is correlated with the onshore Castelvetrano basin.

Based on the age of the associated foredeep, a Late Miocene and Pliocene-Pleistocene age was attributed to the emplacement of the western and eastern segments of the chain, respectively.

The NNE-SSW trending transcurrent belt, named Separation Belt (SB) by ARGNANI (1990), constitutes the link between the two segments of the chain and the faulting is thought to involve the basement (ARGNANI et al., 1986; ANTONELLI et al., 1988; ARGNANI, 1993a, b; GRASSO, 2001). The SB is also highlighted by the distribution of the magnetic anomalies, which extend from Linosa Island to the eastern margin of the Nameless Bank (Fig. 1.9; LODOLO et al., 2012).

During the Early Tortonian, the SB experienced an intense transtensional phase, contemporaneous to the emplacement of the NFBF (ANTONELLI et al.,

1988; CIVILE et al., 2014). The SB was reactivated in transpression during the Plio-Pleistocene along two major lineaments (Belice and Sciacca faults; Fig. 1.8) producing inversion structures in the Miocene sedimentary units with a right-lateral displacement and connected with the individuation eastward of the Gela foredeep (ANTONELLI et al., 1988; CIVILE et al., 2014).

The SB is considered a lithospheric transfer zone, interpreted as a left-lateral strike-slip, due to the differential amount of opening between the Pantelleria Graben, to the east, and the Malta and Linosa Graben, to the west (REUTHER et al. 1993; GHISETTI et al. 2009).

The eastern segment of the chain in the offshore is the Gela Nappe (GN; Figs. 1.3, 1.7), which represents the youngest and outermost thrust sheet of the SFTB. The blind basal thrust of the GN delineates a large SSW-facing arc, laterally constrained against salients of the Pelagian-African platform (Sciacca high to the west and Hyblean Plateau to the east), and frontally advanced above the Plio-Pleistocene flexural foredeep (ARGNANI, 1987; LICKORISH et al., 1999; GHISETTI et al., 2009). The WNW-ESE trending Gela foredeep (Fig. 1.8) is partially buried by the Gela Nappe, and is limited to the east by the Hyblean foreland. Plio-Pleistocene silico-clastic, turbiditic and pelagic sediments fill the trough that passes to the Caltanissetta basin landward.

The GN is a Mio-Pliocene allochtonous body initially interpreted as an olistostrome and a gravity driven emplacement was considered dominant (OGNIBEN, 1969; COLANTONI, 1975; WINNOCK, 1981). The second hypothesis, actually largely accepted by literature, on the nature of GN invokes a tectonic origin explained in terms of a wedge-shaped prism of weak material resting above more rigid block and pushed from behind by a buttress stronger than the material in the wedge (LENTINI, 1982; ARGNANI, 1987; ANTONELLI et al., 1988). Therefore, the GN is considered the product of compressional movements related to the SFTB that caused offscraping and accretion from a wedge of weak sediments.
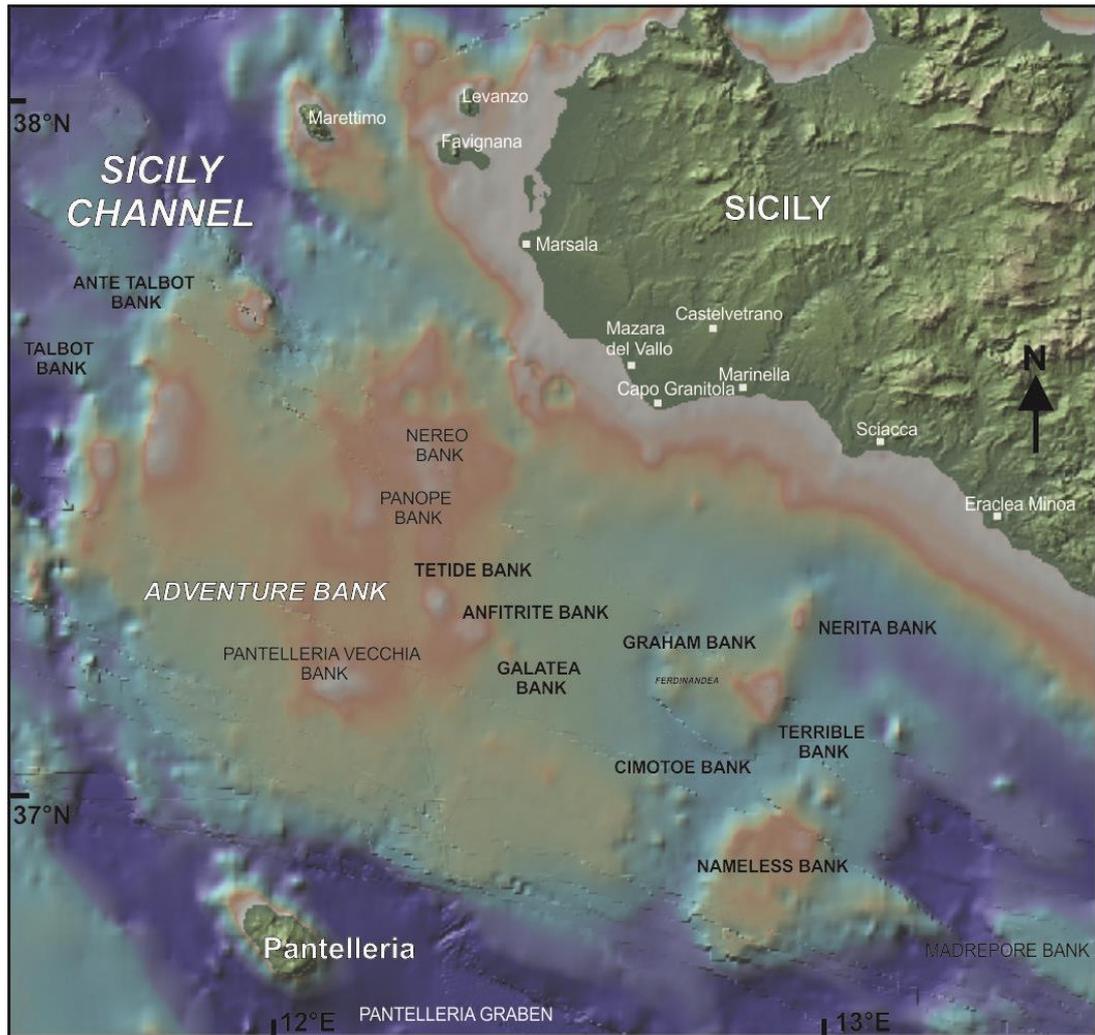
Fig. 1.9 – Bathymetric map of NW Sicily Channel with location of sedimentary and volcanic banks.

The GN displays a sequence of interfering deformations represented by a first generation of E-W folds that deform the Messinian evaporitic sequence and the overlying Lower Pliocene Trubi Formation, refolded by a set of N-S to NNE-SSW folds, that involve the Pliocene and the Lower Pleistocene sequences. GHISETTI et al. (2009) argue that late stage E-W shortening of the GN was imposed by the compressional reactivation of inherited, Mesozoic N-S and NNE-SSW normal faults in the carbonate substratum, during the progressive incorporation of the Pelagian Foreland in the thrust belt. These faults are oblique to subparallel to the regional trajectories of maximum horizontal shortening in the GN and their reactivation (probably with

transpressive components) appears to accommodate the differential buoyancy and the flexure of the rigid carbonate substratum beneath the thrust belt. In light of this, the authors retain that the thrust belt-foreland interaction results in a mixed style of thin- and thick-skinned tectonics, and in components of finite shortening at 0° to 90° from the regional transport direction.

The offshore Gela Nappe emplacement occurred during three different main stages, Zanclean Piacenzian and top of Calabrian, since its internal thrusts involved the Messinian, the base Gelasian and the 0.8 Ma unconformities (CAVALLARO et al., 2017).

The foreland is part of the Pelagian Block (BUROLLET et al., 1978; BEN-AVRAHAM & GRASSO, 1991), a 25–30 km thick crustal portion of the African continental margin which extends from the Sahel region of Tunisia to eastern Sicily (Fig. 1.10). Here, it is interrupted by the Malta Escarpment, a regional tectonic boundary that separates the Pelagian Block from the Ionian Basin.

Following Mesozoic syn- and post-rift sedimentation, a broad positive tectonic inversion affected the Pelagian shelf starting from the Late Cretaceous (BEN-AVRAHAM et al., 1990; GRASSO et al., 1999; TAVARNELLI et al., 2004).

During the Neogene and up to the present, the block acted as a foreland of the Sicilian-Maghrebian collisional orogen (Fig. 1.1; BEN AVRAHAM et al., 1990; LENTINI et al., 2006).

The north-central sector of the Sicily Channel between Sciacca and Licata was affected by a complex poly-phasic deformation belt coeval with the Neogene–Quaternary migration of the Gela Nappe (CAVALLARO et al., 2017). The belt is characterized by set of high-angle WNW–ESE to NW–SE early Miocene extensional faults deriving from the flexure of the foreland plate beneath the advancing SFTB (COGAN et al. 1989). Some of these show evidences of a Zanclean-Piacenzian right-lateral strike-slip reactivation producing releasing and restraining bends geometries and by local positive tectonic inversion in Piacenzian time (CAVALLARO et al., 2017). A transpressional reactivation is documented by the occurrence of roughly

symmetrical, up to 10-km-large push-up structures affecting all the Jurassic–Miocene sequence.

Since Late Miocene and mostly during the Pliocene, extension occurred in the central part of the Pelagian Block and led to the formation of the Sicily Channel rift zone (Fig. 1a; ARGNANI, 1990; FINETTI & DEL BEN, 2005, and references therein). Extension was concentrated north of the plateau where deep basins developed (e.g. Malta, Linosa and Pantelleria grabens, Fig. 1.11). Thick sequences of clastic sediments accumulated within the basin depocenters (COLANTONI, 1975; ARGNANI, 1990; ARGNANI & TORELLI, 2001).

Different hypothesis on the development of Sicily Channel Rift Zone have been proposed. Some authors consider the tectonic depressions as large and discrete pull-apart basins involving deep crustal levels, developed along a major dextral wrench zone (JONGSMA et al., 1985; REUTHER & EISBACHER, 1985; BEN-AVRAHAM et al., 1987; BOCCALETTI et al., 1987; CELLO, 1987; FINETTI,1984; CATALANO et al., 2009). ARGNANI (1990) interprets the rifting as due to mantle convections developed during the roll-back of the African lithosphere slab beneath the Tyrrhenian basin. A mechanism of formation of transform faults (REUTHER et al., 1993) and intraplate rift, related to NE directed displacement of Sicily away from the African continent, has been also proposed (ILLIES, 1981; WINNOCK, 1981; FINETTI, 1984). Tomographically detected high-velocity anomalies lead to support that the Sicily Channel rift is a surface manifestation of a rupture in the western Mediterranean subduction zone (FACCENNA et al.,2004). Analogue modeling has shown that independent tectonic processes, i.e., the Maghrebian–southern Apennine accretionary prism and the NE-SW trending Sicily Channel rift, may coexist and overlap each other, suggesting that plate boundaries are passive features rather than the driving mechanisms of plate tectonics (CORTI et al., 2006).

Recent studies on the Pantelleria rift evolution support the content of a 'passive' rifting model controlled by slab-pull forces of the northward-

subducting African slab and characterized by the chronological sequence of events (rifting-doming-volcanism), through two tectonic events: lithospheric-scale continental rifting (Early Pliocene), which caused the graben formation, and a successive phase (Late Pliocene–Pleistocene) characterized by a magma-assisted extensional mechanism (CIVILE et al., 2010).
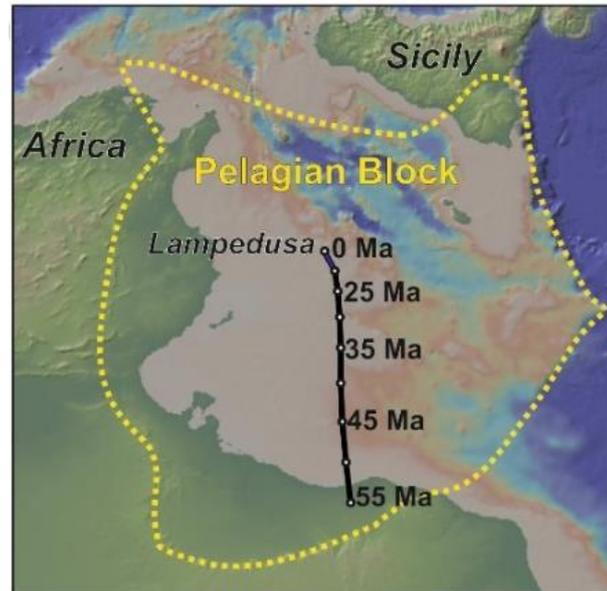
Fig. 1.10 – Limit of the Pelagian Block and path of a point located at 35.5°N, 12.6°E (LAMP GNSS station), reconstructed back in time relative to Eurasia, using finite rotations from DEMETZ et al. (2015) for the present to 19.7 Ma (blue path) and from ROSENBAUM et al. (2002) for 25 to 55 Ma (black path).

Other submarine magmatic manifestations have been identified in the Adventure Plateau, Graham and Nameless banks. In particular, the main volcanic centres, Tetide, Anfitrite, Galatea and Cimotoe (Fig. 1.9), have been recognized in the Adventure Plateau and considered to be of Plio–Pleistocene age (CIVILE et al., 2014). Tetide, Anfitrite and Galatea volcanic centres very close each other and aligned N-120 seem to be associated with a NW trending fault belonging to same fault system limiting the Pantelleria Graben, but in an external position with respect to the shoulders of the rift (CIVILE et al., 2014).

The tectonic configuration of the Pelagian Block south of the Channel rift system consists of a series of mostly WNW-ESE trending structural highs

and basins bordered by variously oriented faults of Neogene-Quaternary age (SEBEI et al., 2007). The Lampedusa Plateau forms a large wavelength high in the central sector of the Pelagian Block. The plateau is underlain by Meso-Cenozoic carbonate platform and open shelf rocks characterized, since the Late Paleozoic, by a long-lasting history of extension and subsidence (GRASSO et al., 1999). During Lower–Middle Cretaceous, shallow-water carbonates, marls and fine siliciclastic sediments were deposited within NW–SE trending half-grabens along the flanks of the plateau. Post-rift sediments consist of Middle–Upper Cretaceous marls and open-shelf carbonates.

According to most investigators (GRASSO & PEDLEY, 1985; GRASSO et al., 1993; CATALANO et al., 1995a; TORELLI et al., 1995; GRASSO et al., 1999; ARGNANI & TORELLI, 2001), the present structural pattern of the Lampedusa Plateau is dominated by structures linked to Late Tertiary extensional faulting in the rift zone, although significant Tortonian strike-slip syn-sedimentary tectonics is documented at Lampedusa (GRASSO & PEDLEY, 1985).

During Paleocene-Eocene, regional uplift and shortening are documented south and west of Lampedusa Island and adjacent Lampione, a small rocky islet west of Lampedusa (Figs. 1.10, 1.11). This process caused emersion and erosion as testified by *hiatuses* in the stratigraphic record (GRASSO et al., 1999; SEBEI et al., 2007). Shortening was accommodated by folds, wrench faults and thrusts, which partly reactivate Early Cretaceous extensional structures (GRASSO et al., 1999; TAVARNELLI et al., 2004; SEBEI et al., 2007).

During Late Miocene, strike-slip tectonics occurred and is well documented at Lampedusa Island (GRASSO & PEDLEY, 1985). During Messinian, sea-level fall in response to closure of the Mediterranean basin (RYAN & CITA, 1978) caused erosion of a large part of the plateau. During this stage, evaporites only deposited in the deeper parts of the Mediterranean basins.

1.5 Seismo-tectonic frame of the Sicily Channel

The present-day seismo-tectonic frame of the Sicily Channel is characterized by a low seismicity level with predominance of 10-20 km deep, and occasionally deeper strike-slip earthquakes (Fig. 1.11) attributed to reactivation of inherited faults (SOUMAYA et al., 2015).
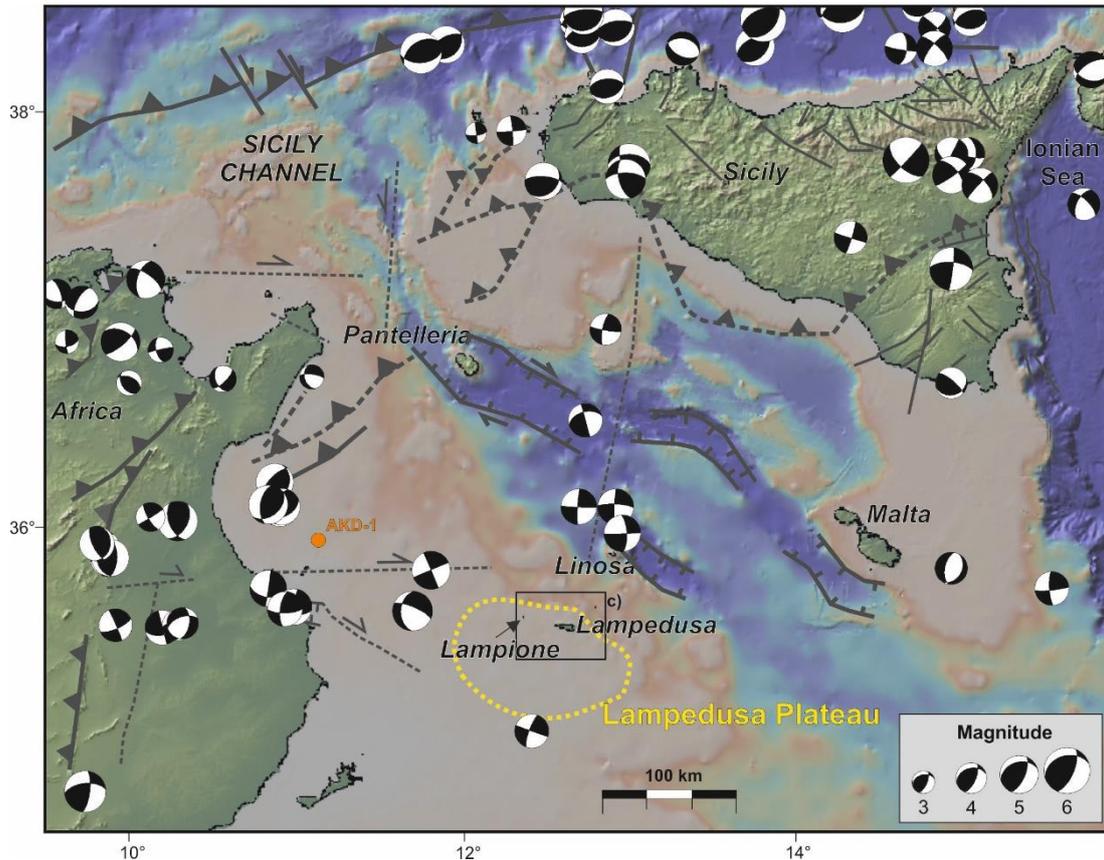
Fig. 1.11 – Map of the central Mediterranean region, showing the major tectonic structures. Focal mechanisms of 3≤M≤4 earthquakes occurred between 1957 and 2014 in the Sicily Channel were redrawn from SOUMAYA et al. (2015).

West and north of the channel, on mainland Tunisia and Sicily, and offshore northern Sicily, focal mechanisms are mostly contractional and are related to the Siculo-Maghrebian collisional belt.

The strike-slip earthquakes around the Lampedusa Plateau have dextral and sinistral nodal planes with ~ E-W and ~ N-S direction, respectively. Supplementary information on the active tectonics of the Pelagian Block

derive from geodetic data published by PALANO et al. (2012) which indicate that the Channel is currently subject to ~ 1.4 mm/yr NE-SW extension, coupled to ~ 2.9 mm/yr NW-SE contraction.

1.6 Volcanism in the Sicily Channel

A widespread volcanic activity related to the rift occurred during the Plio-Pleistocene, especially on Pantelleria and Linosa Islands. Minor activity was registered in the Adventure, Nameless, Graham and Terrible banks (Fig. 1.9; COLANTONI et al., 1975; BECCALUVA et al., 1981; CALANCHI et al., 1989; ROTOLO et al., 2006). Nevertheless, the oldest volcanic rocks have been found in the Nameless Bank with an age of ~ 10 Ma (BECCALUVA et al., 1981).

In 1831 on the Graham bank an ephemeral volcanic island named Foerstner (Ferdinandea, Fig. 1.9) arose up to 65 m above sea level. In 1863 a second eruption took place.

The youngest volcanism is associated to Pantelleria island where an underwater eruption occurred in the 1891, and to the Pinne Marine Bank at the south-eastern wedge of Graham Bank (Fig. 1.9), where emissions of gases were observed in 1941 (CORTI et al., 2006).

Pantelleria represents the largest extent of emerged volcanic rocks of the Sicily Channel with alkaline to peralkaline erupted products which consist mainly of alkali basalts, hawaiites, trachytes, and peralkaline trachytes to peralkaline rhyolites (pantellerites). Whereas, the much smaller island Linosa shows mildly alkaline, scarcely evolved rocks dominated by alkali basalts and trachybasalts (CORTI et al., 2006).

Overall, the volcanic products erupted in the Channel constitute a bimodal sodic, moderately alkaline association. This kind of volcanism points to an anorogenic magmatism akin to that found in continental rift areas (CORTI et al., 2003). The trace element distribution is comparable with that observed in intraplate basalts or ocean island basalts (CORTI et al., 2006).

CHAPTER II

2. FUNDAMENTALS OF SEISMIC REFLECTION ACQUISITION AND INTERPRETATION

2.1 The seismic reflection analysis

One of the most used methods in the study of marine areas is the seismic reflection that allows to gather information on the stratigraphic and tectonic setting. Seismic data provide the basic means for the preliminary understanding of the basin fill in the subsurface, and allow to identify potential hydrocarbon traps (structural, stratigraphic, or combined); evaluate potential reservoirs, seals, source rocks; estimate petroleum charge in the basin, the amount and the nature of fluids in individual reservoirs; develop a strategy for borehole planning and significantly improve the risk management in petroleum-related activities (CATUNEANU, 2006).

A seismic image reflects the interaction between the substrate geology and the seismic waves traveling through the rocks, modulated by the physical properties of the rocks. The seismic waves emitted by a source at the surface are characterized by specific physical attributes, including shape, polarity, frequency, and amplitude. These attributes change as the waves travel through the geological substrate, except for frequency, which is a constant parameter that depends upon the source of the seismic signal.

The physical property of acoustic impedance (velocity multiplied by the rock's density) is very important, because its changes with depth can signify changes in lithology and/or in fluid content, or even diagenetic contrasts.

When a seismic wave travelling through the substrate encounters an interface between two materials with different acoustic impedances, some of the wave energy will reflect off the interface and some will refract through the interface (Fig. 2.1). The seismic reflection technique consists of generating seismic waves and measuring the time taken for the waves to travel from the source, reflect off an interface and be detected by an array of receivers (or geophones) at the surface.

If the travel times from the source to various receivers and the velocity of the seismic waves are known, the pathways of the waves can be reconstructed in order to build up an image of the subsurface.
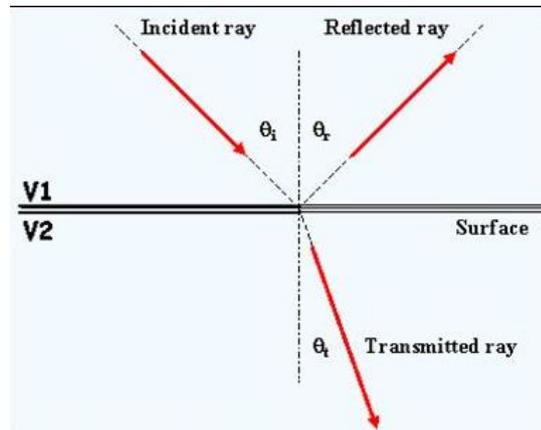
Fig. 2.1 – Relationship between the angles of the incident radius (θ$_i$), the reflected radius (θ$_r$) and the refracted radius (θ$_t$) measured along the normal of discontinuity of two media with different velocities (V1 and V2).

It should also be noted that in addition to the useful signal, there are disturbance signals such as direct and refracted surface waves, multiple reflections, diffractions, etc. The raw seismic data require further processing (e.g., demultiplexing, gain recovery, static corrections, deconvolution, migration, etc.) before they can be used for geological interpretations. The goal is to obtain a better signal-to-noise ratio.

The processed seismic lines, where the horizontal scale is proportional to the distance along the line and the vertical scale to the time of arrival of reflections, provide continuous subsurface information over distances of tens of kilometres and depths of few kilometres. The continuous character of seismic data represents a major advantage of this method with respect to the stratigraphic analysis of well-logs, core or outcrops, which only provide information from discrete locations.

The vertical resolution of seismic data is primarily a function of the frequency of the emitted seismic signal. A high-frequency signal increases the

resolution at the expense of the effective depth of investigation. A low frequency signal can travel greater distances, thus increasing the depth of investigation, but at the expense of the seismic resolution. In practice, vertical resolution is generally calculated as a quarter of the wavelength of the seismic wave. Acquiring the optimum resolution for any specific case study requires therefore a careful balance between the frequency of the emitted signal and the desired depth of investigation.

The nature of the seismic reflector (single contact *vs.* amalgamated strata packages) adds another degree of uncertainty. Where the vertical distance between stratigraphic horizons is greater than the vertical resolution (i.e., seismic reflectors may correspond to single geological interfaces), the polarity of the reflections is more reliable in terms of geological interpretations. However, where seismic reflectors amalgamate closely spaced stratigraphic horizons, polarity interpretations become less reliable, as what can be seen on seismic lines is a composite signal.

2.2 Techniques of acquisition of the analysed seismic reflection profiles

The analysed multichannel seismic reflection profiles downloaded from ViDEPI database (see chapter III) were acquired by AGIP using the technique of water gun acquisition.

A water gun (Fig. 2.2) is a source of energy for marine seismic data acquisition that shoots water from a chamber in the tool into a larger body of water, creating cavitation. The cavity is a vacuum and implodes without creating secondary bubbles. This provides a short time signature and higher resolution than an air-gun source that is a source of seismic energy releasing highly compressed air into water. Air guns are also used in water-filled pits on land as an energy source during acquisition of vertical seismic profiles.

The basic element used to detect the reflected seismic energy is the hydrophone, a piezoelectric device that creates an electrical signal in response

to pressure changes. Multiple hydrophones are mounted in a streamer cable, which is a jacketed tube filled with a liquid less dense than water. Weights and liquid are combined so that the streamer cable is near neutral buoyancy. Then, with the help of depth-controlling devices called birds, the cable can be positioned at a specified depth below the surface of the water. Achieving neutral buoyancy is defined balancing the cable.

Diagram of a marine towed streamer seismic survey with the raypaths that result from a single shot by an airgun into a streamer containing 5 hydrophones.
--- = raypaths to first reflector; --- = raypaths to second reflector;
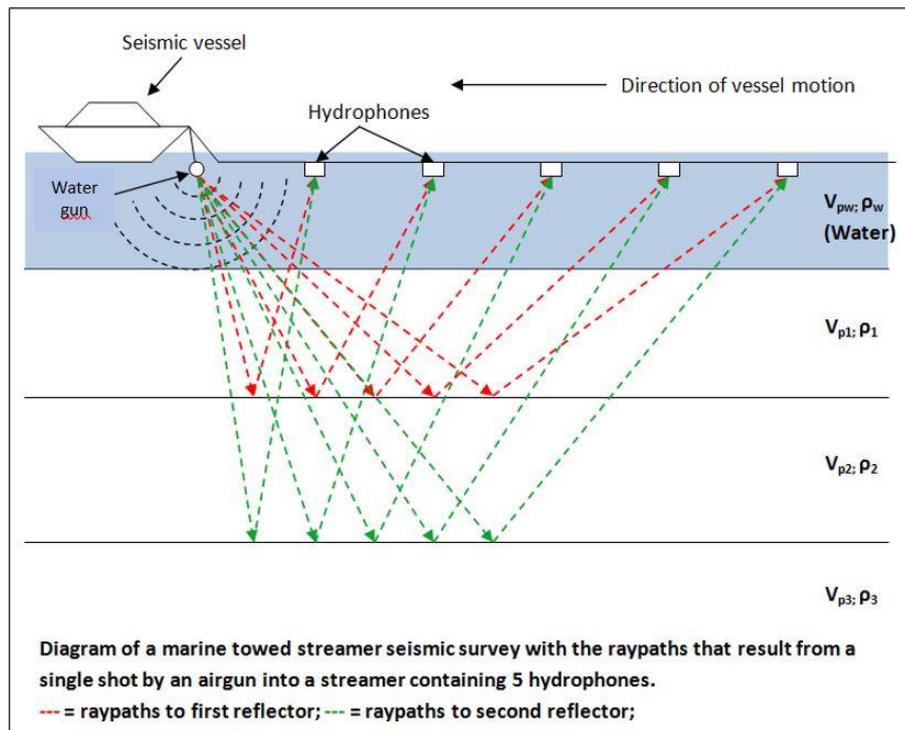
Fig. 2.2 – Diagram shows the layout of a marine seismic survey using towed streamers.

Each seismic profile is then subjected to a processing sequence consisting of:

1. editing, which consists of reading data and correcting geometric spreading, with the purpose of amplifying the signal;

2. deconvolution is an operation aimed to remove the effect of the instrumental response to obtain the ground response signal;

3. normal move out is a technique used to apply a time correction to each trace taking to account for the different lengths of the rays' paths;

4. stacking is used to sum up the traces of the same grouping in order to reduce the number of outgoing tracks and improve the signal-to-noise ratio by eliminating inconsistent noise;

5. filtering has the purpose of eliminating noise and phenomena that do not fall into the frequency band of interest.

The single-channel seismic reflection profiles described in chapter IV were acquired with the Sparker instrumentation.

Sparker, literally a "spark maker", exploits the principle of a high voltage and low power electric discharge between a series of electrodes, immersed in water, which produce a wave blast followed by bubble pulses generated from the expansion and subsequent contraction which they produce. The electrodes produce the spark perfectly in phase. The metal armour generates a potential difference, so that the water crossed by the electric discharge causes one bubble rising rapidly by volume, generating a wave of pressure. This instrumentation, towed by the ship, has an energizing source of 1 kJ and a spectrum of frequency between 100 and 1000 Hz and allows to reach penetration up to 400 ms (about 340 m), with a resolution of one meter or lower depending on the lithology of the crossed rocks, the weather-marine conditions during the survey, and noise in the water column.

As the acoustic waves reach a discontinuity surface, the generated reflections are recorded by an array (8 – up to 24) of hydrophones (streamer), assembled into a tube filled with a protective and insulating coating (generally polyurethane) and towed by the vessel at a safety distance from propellers. To avoid surface ghosts between the primary impulses and their reflection at the sea surface, the electrodes must be constantly dipped within a few decimetres in the water. Finally, the acquired information is returned in files, usually in seg-y format by software imaging seismic profiles.

The processing of sparker profiles made up in this work will be described in the chapter IV.

2.3 Seismo-stratigraphic analysis

Following data recording and processing, the next pass is to understand what they represent. This is the phase of the geological interpretation of seismic data that aims to pass from the information obtained from the propagation of the elastic waves to the structure of the geological bodies.

The seismo-stratigraphic approach is based on the simple principle that seismic reflections (seismic horizons) can be compared to stratigraphic layers. And, the geometry of the reflections corresponds to depositional geometry. Therefore, the geological concepts of classic stratigraphy can be applied to seismic reflections. For these reasons, the seismo-stratigraphy is considered as a geophysical-geological approach applied to stratigraphic interpretation.

Seismic reflections arise from contrasts of acoustic impedance along surfaces that correspond to layer surfaces or other discontinuities, which have a chronostratigraphic significance. Layer surfaces represent ancient depositional surfaces and are geologically synchronous in the areas of deposition. The discontinuities are erosional or non-deposition surfaces corresponding to significant stratigraphic gaps and, even if they represent time-variant events, should be considered as chronostratigraphic surfaces. In light of this, primary reflections reveal the stratigraphic framework and chronostratigraphic relationships rather than the nature of the lithostratigraphic units. Thereby, the lithology of buried rocks cannot be established directly with seismic reflection method, but predictions can be made by studying seismic facies and using calibrating wells.

The seismo-stratigraphic interpretation consists in two phases: the analysis of seismic sequences and the analysis of seismic facies.

A seismic sequence is a depositional sequence recognized on a seismic section. It is represented by a succession of seismic reflectors that correspond to sedimentary layers and is bounded by discontinuity or concordance surfaces.

On-land outcrops allow to identify stratigraphic sequences based on a number of criteria, including the nature of the contact (conformable or unconformable), the nature of facies which are in contact across the surface, depositional trends recorded by the strata below and above the contact, ichnological characteristics of the surface and stratal terminations. In the case of seismic lines, contacts that separate strata packages can be mapped solely on the basis of how strata terminate against the contact. Nevertheless, the surfaces can be traced from local to regional scales based on the stratal terminations (CATUNEANU, 2006), which are defined by the geometric relationship between strata and the stratigraphic surfaces against which they terminate. They are onlap, downlap, toplap, offlap (MITCHUM & VAIL, 1977; MITCHUM et al., 1977) and erosive truncation (Figs. 2.3, 2.4).
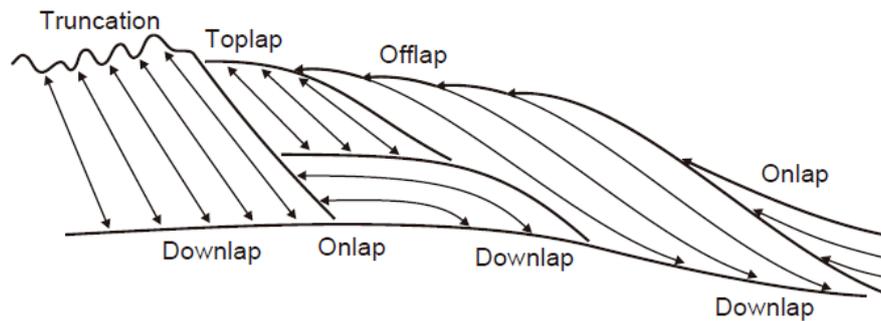
Fig. 2.3 – Types of stratal termination, from CATUNEANU (2006).

A seismic sequence is also a genetic unit, since it deposited during a given geological event.

In seismic images, a discontinuity is expressed by the discordance between the erosive truncation and onlap or downlap overlapping reflections.

The age of a depositional sequence corresponds to the time interval between the age of its boundaries, lower and upper.

The seismic facies analysis consists of geological description and interpretation of the seismic attributes of reflections. A seismic facies unit is a

set of reflectors with similar seismic characteristics, which reflect the same depositional environment and geological asset.

Truncation: termination of strata against an overlying erosional surface. *Toplap* may develop into truncation, but truncation is more extreme than toplap and implies either the development of erosional relief or the development of an angular unconformity.

Toplap: termination of inclined strata (clinoforms) against an overlying lower angle surface, mainly as a result of nondeposition (sediment bypass), ± minor erosion. Strata lap out in a landward direction at the top of the unit, but the successive terminations lie progressively seaward. The toplap surface represents the proximal depositional limit of the sedimentary unit. In seismic stratigraphy, the *topset* of a deltaic system (delta plain deposits) may be too thin to be "seen" on the seismic profiles as a separate unit (thickness below the seismic resolution). In this case, the topset may be confused with toplap (i.e., *apparent toplap*).

Onlap: termination of low-angle strata against a steeper stratigraphic surface. Onlap may also be referred to as *lapout*, and marks the lateral termination of a sedimentary unit at its depositional limit. Onlap type of stratal terminations may develop in marine, coastal, and nonmarine settings:

  - marine onlap: develops on continental slopes during transgressions (*slope aprons*, Galloway, 1989; *healing-phase deposits*, Posamentier and Allen, 1993), when deep-water transgressive strata onlap onto the maximum regressive surface.

  - coastal onlap: refers to transgressive coastal to shallow-water strata onlapping onto the transgressive (tidal, wave) ravinement surfaces.

  - fluvial onlap: refers to the landward shift of the upstream end of the aggradation area within a fluvial system during base-level rise (normal regressions and transgression), when fluvial strata onlap onto the subaerial unconformity.

Downlap: termination of inclined strata against a lower-angle surface. Downlap may also be referred to as *baselap*, and marks the base of a sedimentary unit at its depositional limit. Downlap is commonly seen at the base of prograding clinoforms, either in shallow-marine or deep-marine environments. It is uncommon to generate downlap in nonmarine settings, excepting for lacustrine environments. Downlap therefore represents a change from marine (or lacustrine) slope deposition to marine (or lacustrine) condensation or nondeposition.

Offlap: the progressive offshore shift of the updip terminations of the sedimentary units within a conformable sequence of rocks in which each successively younger unit leaves exposed a portion of the older unit on which it lies. Offlap is the product of base-level fall, so it is diagnostic for forced regressions.

Fig. 2.4 – Description of stratal terminations from CATUNEANU (2006) and references therein.

The seismic facies is described with the acoustic parameters of geometry, lateral continuity, amplitude, frequency and velocity. The parameter of continuity suggests a uniform and continuous stratification, while the amplitude gives information about the spacing of the stratification and variation in velocity and density. The thickness changes of the layers are revealed by the frequency which also depends on the nature of the seismic source impulse. The velocity is associated to the lithology, porosity and fluid content of the investigated deposits.

50

2.4 Eustatism and tectonics controlling continental margin evolution

The integration of seismic and sequence stratigraphy is a powerful method in revealing the main factors that govern the outbuilding of continental margins (VAIL et al., 1977; VAIL, 1987; VAN WAGONER et al., 1988). The interplay of changes in the rate of sediment supply and base level (tectonic subsidence, isostasy, sediment compaction and eustasy) rules stratal stacking patterns defined as transgressive, normal regressive and forced regressive (Fig. 2.5; HUNT & TUCKER, 1992).
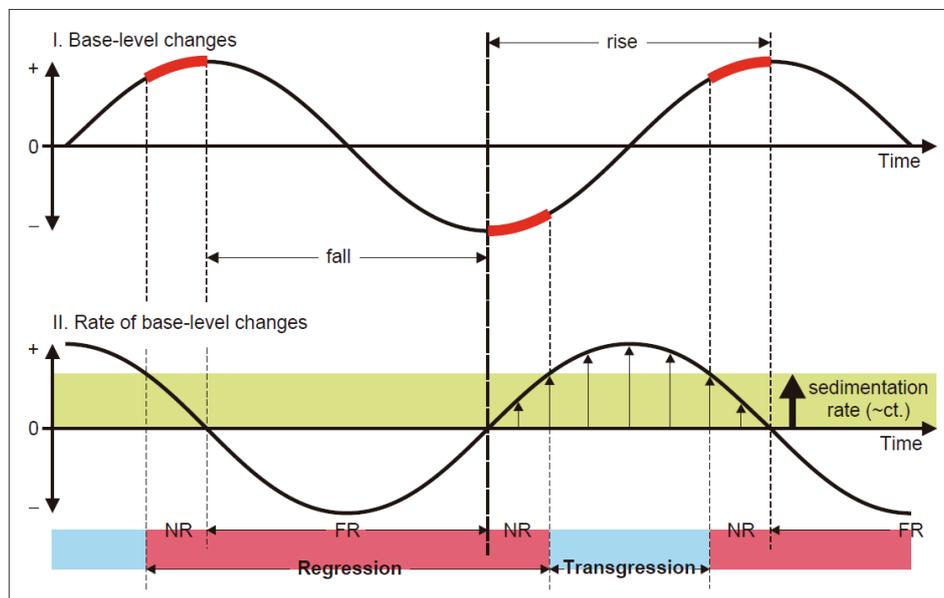

Fig. 2.5 – The top sine curve shows the magnitude of base-level changes through time, the sine curve below shows the rates of base-level changes (from CATUNEANU, 2006). The red portions on the top curve indicate early and late stages of base-level rise, when the rates of base-level rise (increasing from zero and decreasing to zero, respectively) are outpaced by sedimentation rates. Note that the rates of base-level change are zero at the end of base-level rise and base-level fall stages. Transgressions occur when the rates of base-level rise outpace the sedimentation rates.

The base level defines a dynamic surface of balance between erosion and deposition and is strictly related to accommodation, i.e. the amount of space available for sediment accumulation (NEAL & ABREU, 2009): a rise in base level creates accommodation, whereas a fall in base level destroys accommodation. Base level is commonly approximated to relative sea level so

that base-level change becomes equivalent to sea-level change (POSAMENTIER et al., 1988). Base-level changes are idealized by two symmetrical sine curves (Fig. 2.5), one describing the sea level changes at the shoreline and one associated to shoreline shift, also named transgressive-regressive curve (CATUNEANU, 2006).

The cyclic behaviour of the sea-level change curve is underlined by the presence of negative and positive spikes, which indicate low positions (low-stand) and high-stands of the sea level, respectively. Within the climatic record, the former correspond to glacial periods, while the latter are related to interglacial periods.

The associated shoreline shift curve describes changes in depositional trends during base-level shift.

Eustatic oscillations have occurred in association with climatic fluctuations throughout the Quaternary and in turn affected changes in sediment supply to the basin, variations in oceanographic regime and basin interconnectivity (HERNÁNDEZ-MOLINA et al., 2014). After the early to middle Pleistocene transition, high-amplitude (100 m) sea level fluctuations, among other factors, played a crucial role in continental margins outbuilding (VAIL et al., 1977; CATTANEO & TRINCARDI, 1999 for the Adriatic epicontinental sea; AMOROSI & COLALONGO, 2005 for the Po River Plain; RABINEAU et al., 2005 for the Gulf of Lyon). These fluctuations forced the basin-ward and landward migration of the shoreline during periods of sea level lowstand and highstand, respectively.

Transgressions occur when accommodation is created more rapidly than it is consumed by sedimentation, i.e., when the rates of base-level rise outpace the sedimentation rates at the shoreline. This results in a retrogradation (landward shift) of facies. Forced regressions occur during stages of base-level fall, when the shoreline is forced to regress by the falling base level irrespective of sediment supply. Normal regressions occur during early and

late stages of base-level rise, when sedimentation rates outpace the low rates of base-level rise at the shoreline.

CHAPTER III

3. MULTI-CHANNEL SEISMIC REFLECTION PROFILES AND WELL-LOG ANALYSIS

3.1 Materials

The NW part of the Sicily Channel was investigated through analysis of multi-channel seismic (MCS) reflection profiles and well-log data available from a) ViDEPI and b) ENI database.

a) The ViDEPI (*Visibilità dei Dati di Esplorazione Petrolifera in Italia*, Visibility of Petroleum Exploration Data in Italy) project is designed to make all the documents concerning Italian oil exploration easily accessible. The documentation concerns expired, and therefore public, mining permits and concessions, filed since 1957 with UNMIG, National Mining Office for hydrocarbon and geothermal energy of the Ministry for Economic Development. Oil exploration in Italy is subject to the Law n. 6 of 11 January 1957, which, among other things, regulates the foundation of UNMIG, National Mining Office for hydrocarbon and geothermal energy, Directorate-general for mineral and energy resources, based at the Ministry for Economic Development with branch offices in Bologna, Rome and Naples. Current regulations establish that operating oil Companies shall provide UNMIG with progressive technical reports on the activities carried out on their permits and concessions including copies of exemplifying documents, such as geologic maps, structural maps, final well logs, seismic lines, etc. The law establishes that the filed documents shall become available to the public a year after the permit has expired.

The project, proposed and managed by the Italian Geologic Society (*Società Geologica Italiana*) has been made possible by the Ministry of Economic Development, which has provided the data, and by *Assomineraria* (Italian petroleum and mining industry association) which has financed it. The project realization has been carried out in several phases: 1) retrieval of documentation filed by the various national and regional Mining Authorities; 2) classification and scanning of the documents; 3) geo-referentiation of the

55

seismic lines (commonly referred to as "ministerial lines"), wells and areas of expired mining permits and concessions; 4) web loading of the entire data set, with alphanumeric and geographical search; 5) publication of updates after closure of the project (12/31/2007). All the paper documents acquired in the project have been entrusted to the scientific-technologic Library of Rome University Tre (BAST-*Biblioteca di area scientifico tecnologica*), according to agreements made with the Ministry of Economic Development, where they are consultable.

MCS profiles and wells belonging to the Italian Commercial Zone *C* and *G*, which represent the Italian continental platforms pertaining to the Sicily Channel, were downloaded from the Ministerial database. Based on these data, the work integrates the results obtained from previous studies (MECCARIELLO, 2014; MECCARIELLO et al., 2014).

b) Thanks to courtesy of ENI multinational company, a brief research period was conducted in May 2015 at ENI headquarter in San Donato Milanese (Milan) in order to view and obtain part of the accessible better-reprocessed data. The provided data set consists of multi-channel seismic reflection profiles already processed and rasterized.

The two data sets (ViDEPI and ENI) provide large-scale geological-structural information as they allow to display structures down to a depth of 7-8 km. The difference between the two data sets concerns the resolution. ENI profiles provided a better visualization of seismic reflectors and allowed a precise localization of the structures that deform them. In addition, the high-resolution profiles made it possible to finely characterize the structural features recognized in ministerial profiles.

Data interpretation was performed using the GeoSuite AllWorks software package distributed by Geo Marine Survey System. The software manages data using project files. Projects allow you to correlate heterogeneous

geo-referenced data to create a comprehensive geological / geochemical database of the area of interest.

The software can read the most used formats in seismic (.segy, .xtf), edit them to improve the graphic return of profiles and finally interpret them creating multiple layers (horizons). The latter mark surfaces like as the bottom sea, stratigraphic discordances between different depositional sequences, fault planes or folding axes.

The utility of this program lies in the fact that working in the GIS (Geographic Information System) environment, allows to plot and/or import information such as: sampling points (wells or drillings data) with associated stratigraphic description; DTM; raster images; epicentres of earthquakes with magnitudes; isopach maps; etc. Once the database with all navigation lines is created, a specific tool for editing profiles is attached to the program.

For all the seismic data, the UTM (Universal Transverse Mercator) WGS84 33N was chosen as the geodetic reference system.

3.2 Well-log data analysis

3.2.1 Well-log database

The first step of the study dealt with stratigraphic reconstruction of the study area through the analysis of well-log information downloaded from ViDEPI database. The analysed wells are 47 in total (Fig. 3.1), of which 43 offshore (Alfa, Carla, Corvina mare, Egeria, Nada, Naila, Nanda, Narciso, Nausicaa, Nella, Nerina, Nettuno, Nilde, Nilde3, Nilde4, Nilde5, Nilde6, Ninfea, Niobe, Noemi, Norma, Nuccia, Nunzia, Olga, Onda, Orione est, Orlando 001, Orlando 002, Oscar ovest, Pamela, Pamela bis, Paola est, Piera, Pina, Samantha, Santuzza, Sirio, Sofia, Tania, Tullia, Vallo, Venere, Zagara) and 4 on-land (Biddusa, Campobello, Contrada Triglia, Marinella 003).
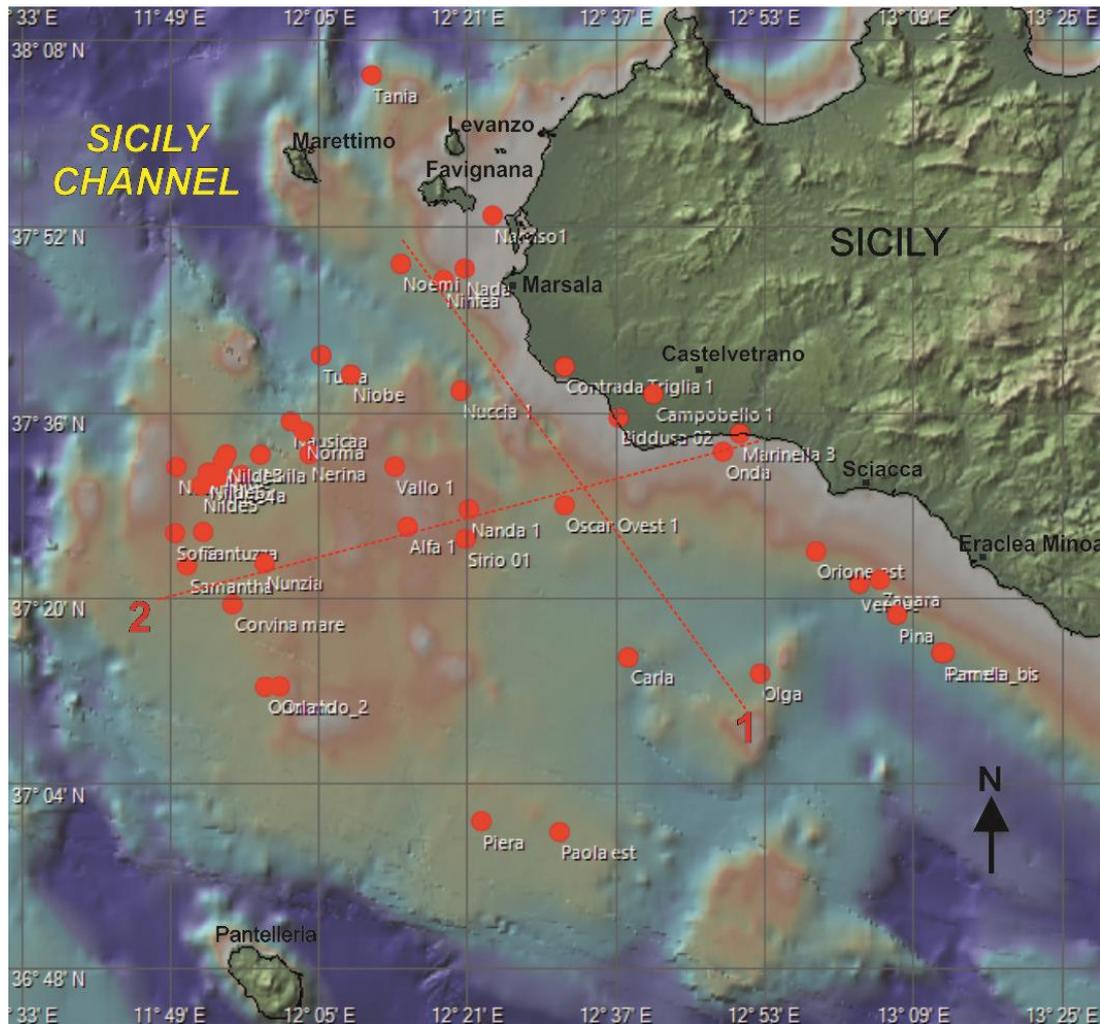
Fig. 3.1 – Bathymetric map of analyzed portion of Sicily Channel with location of analyzed wells.

The stratigraphic information derived from the study of well-logs were synthesized in tables, which consist of 11 columns:

1) rotary depth (m) measures the distance between rotary table and sea level. The rotary table instrument is positioned on the base of drilling rig. The large gap in the centre of the rotary bushings, named bowl, is where the slips are set to hold up the drill string during connections and pipe trips as well as the point the drill string passes through the floor into the wellbore.

2) Sea bottom under rotary table (m) measures the seafloor depth respect with rotary table.

3) Sea bottom (m): this value represents the correction of the previous parameter and is obtained by the difference between 1) e 2).

4) Basal depth under rotary table (m). Whereas the first value corresponds to the depth of start recording, the successive measures are relative to the basal depth of each chrono-stratigraphic interval.

5) Basal depth (m) is the correct value basal depth of each chrono-stratigraphic interval computed from difference between 4) e 3).

6) Thickness (m) is the value of each chrono-stratigraphic interval calculated by the difference between 5) and 3).

7) Total thickness (m) is the sum of thickness values of chrono-stratigraphic interval pertaining to the same formation.

8) Lithology: this column describes the lithology of the different stratigraphic intervals.

9) Formation: it gives the name of the described formation.

10) Chronostratigraphic interval: it defines the geological time necessary to deposition of formation.

11) Criteria of attribution: this column describes the fossiliferous content that characterizes the formation.

The selected wells were imported in the GeoSuite software for spatial analysis.

For this work, a new project was created in which the wells, with known geographical coordinates, have been plotted. In the technical documentation, the coordinates are expressed in terms of longitude Monte Mario for onshore wells and longitude Greenwich for offshore wells. Therefore, for the former a correction was required, consisting in addition of 12° 27' 08" to the coordinates in order to return the measurements in the geographic coordinate system WGS84 (World Geodetic System 1984) with cartographic projection UTM (Universal Transverse Mercator).

For each well the software allows insertion of the following parameters: colour, age, depth, name, lithology and velocity (whose determination is

described in the paragraph 3.3.1). All this information was automatically saved in a GTW (GeoSuite Wells) binary file format.

A .kmz file representing the bathymetric map of the area derived from GeoMapApp (http://www.geomapapp.org/) was also imported.

3.2.2 Lithostratigraphic units recognized in wells and comparison with on-land equivalents

- *Mesozoic-Paleogene pre-orogenic carbonate units*

These units include platform carbonate and silic-carbonate, with platform, slope and basin facies. They belong to the following formations: Amerillo, Bonifato, Buccheri, Corleone, Hybla, Inici, Lattimusa, San Cipirello, Ragusa and Sciacca.

The term **Sciacca** was first used by stratigraphers of AGIP to indicate the oldest carbonate platform unit which represents the substrate of Panormide, Trapanese, Saccense and Hyblean Mesozoic successions. The unit was described in the wells as white, hazelnut, brown, pink or grey dolomite with a medium to coarse grain at the top, and fine and compact with an average thickness of 250 m at the bottom. It is often fractured and intercalated with dolomitic limestone and clay. There are sometimes chert nodules and pyroclastic levels, traces of pyrite and anhydrite.

Because the formation is similar to those of the Hyblean sector (Noto and Gela fms., Fig. 3.2), the term Sciacca was used to refer to the Triassic deposits of different sectors.

Inici was first described in the 1960s, identified on the homonymous mount as a type section. It is also known with the synonyms of Contrada Triglia and Villagonia.

In the wells, it has a maximum thickness of 482 m and is described as alternation of grey, fossil, intraclastic, locally dolomitized packstone and grey, green, compact, locally dolomitized and recrystallized mudstone often passing to whitish, green-grey and rose fine grain dolomite locally calcareous,

intraclastic and fossiliferous with intercalation of green marl and red clay. Intercalations of green hard clay are frequent.

The deposit is attributed to the Liassic for the presence of Paleodasycladus biozones.

The term was also used to refer to the equivalent open marine deposits of Tunisian and Hyblean sectors, namely Siracusa and Streppenosa formations (Fig. 3.2).

The Jurassic **Buccheri** formation, historically known as "Red Ammonitic", consists of grey, red mudstone / wackestone locally clay, dolomitized at the base, with levels of green marl and brown-red clay, sometimes cherty and with an average thickness of 80 m. In the wells, it is also indicated with the synonymous term of Giardini.

Lattimusa was the term used by quarryman who worked this stone with typical milky colour. The unit, informally known as "Calpionella limestone", was described by RIGO and BARBIERI (1959) as a Busambra member of Alcamo fm. corresponding to the Chiaramonte (Hyblean sector) and Sidi Kralif (Tunisian domain) formations (Fig. 3.2).

In the wells, the formation exhibits a maximum thickness of 354 m and consists of grey locally clayey or chalky mudstone and wackestone with occasional cherty nodules and some green-grey marl intercalation at the top.

The presence of calpionellides associations has allowed to date the formation to the Tithonian-Valanginian.

Hybla term was used to designate the deposits of a member included in the Alcamo formation, called with the term "Fahdene" in the Tunisian sector. PATACCA et al. (1979) elevated it to the rank of formation.

It is a grey, hard, compact, fossiliferous mudstone / wackestone, with intercalation of green-grey, soft and hard, fossiliferous marl or of dark grey to green clay. Levels of vulcanites and traces of pyrite and dehydrated quartz in clayey and marl levels are frequent. It is also present as alternation of green-

grey schists with rare lignite, pyrite, brown and grey limestone, mudstone-wackestone with bioclasts. The average thickness is around 170 m.

In the wells, we do not find cherty nodules as described by BASILONE (2012) for the on-land formation.

The presence of planktonic foraminifera (e.g. Ticinella and Hedbergella) allows to date the deposit to the Aptian-Albian.

RIGO & BARBIERI (1959) were the first to use the term **Amerillo** to define a member of Alcamo formation recognized in the type section of Amerillo Valley. PATACCA et al. (1979) elevated it to the rank of formation based on the study of buried sequences in the Hyblean sector.

The formation embraces calcilutite and calcisiltite with chert, white and grey-red marly limestone and green, plankton rich marl. Microscopically, they appear as mudstone-wackestone with planktonic foraminifera and with a maximum thickness of 300 m.

BASILONE (2012) identifies different litofacies from bottom to the top: alternation of calcilutite, marl and marly limestones covering the Late Cretaceous - Early Eocene interval; Middle-Upper Eocene white calcilutite with chert; Lower Oligocene alternation of calcilutite and clay intercalated with calcarenites. However, along the Hyblean succession, levels of mafic volcanic rocks have been recognized. Examples of these are also found in the succession of studied wells. As it can be read from an extract of Orlando 001 well-log there are "from 2790 m to 2812 m very altered pyroclastic rocks, greenish, with thin levels of white carbonate-clay sandstone, marl and silty grey clays".

The unit was dated to Late Cretaceous-Early Oligocene based on the distribution of microfossils. Among the foraminifers, the Rotalipora biozone marker identify the Cenomanian, the globotruncanides (including Globotruncana stuartiformis and Globotruncana Iapparenti) indicate the Santonian-Maastrichtian. Instead, Morozovella velascoensis and Morozovella aragonensis biozone markers identify the Paleocene-Eocene range.

In the wells, the formation is also found as equivalent formations Abiod, Aleg, El Haria and Souar, indicating a deep marine facies in the Tunisian area adjacent to the Trapanese domain.

Bonifato was the unit introduced by SCHMIDT DI FRIEDBERG in 1962 with reference to the succession of Carrabazzi pit.

It is only found in two wells: in Olga is described as a "fossiliferous, arenaceous and glauconitic packstone" and in Orione Est as "green clays, sometimes slightly silty, brown-grey, clayey, silty-sandy packstone, with intercalations of green clay". In both the wells it is dated to the Miocene and exhibits a thickness of 24 m and 167 m, respectively.

On land, the formation was described as shallow marine open platform deposit consisting of an alternation of grey-white calcarenites rich in benthonic foraminifers and grey-green marl with quartz and glauconite granules. The limestones are white, compact and layered.

Ragusa formation was proposed by RIGO & BARBIERI (1959) who studied the succession in San Leonardo deep valley, north of Ragusa.

It is found only in the Carla well as a "grey fossiliferous packstone with rare levels of clay" with a thickness of 85 m, dated to Lower Miocene for the presence of Globigerinoides biozone.

The formation is divided in two members, Leonardo and Irminio, which cannot be distinguished in the well. These are present on the ground as white, marly limestone alternated with marl (Leonardo) and as fine-grained, yellow-grey marly calcarenites intercalated with marly limestone (Irminio).

The **Corleone calcarenites** appear in the Corleone town, recognized as type area. These are fossiliferous, clay calcarenites, with quartz clusters, with an average thickness of 137 m. Microscopically, they are grey, fossiliferous, clayey, compact packstones with intercalations of marl and green-grey clay with planktonic foraminifera and fragments of macro-foraminifera, coralline algae, bryozoans and echinoids; they pass to grey-brown mudstone / wackestone with spathic calcium veins, with grey silty clay levels and to white

mudstone with chalky porosity at the bottom. In some wells, the formation is made of light grey carbonate, clayey and siliceous quartz sandstones, with medium to fine grain. Sometimes pyrite and glauconite are present.

The age attributed to the formation is Lower Miocene due to the presence of planktonic foraminifers such as Globigerinoides trilobus and Praeorbulina biozones attributed to Burdigalian-Langhian.

In the wells, it appears also with the chrono-equivalent Fortuna and Ain Grab terms, which indicate clastic deposits sedimented on the western side of the Adventure Bank and separated from coastal deposits of Corleone formation by the Sciacca high.

San Cipirello marls represent a formation that takes its name from the type section located in the homonymous town.

These are clays and marls with glauconitic granules and widespread presence of pyrite, sometimes intercalated with light grey, intraclastic, fossiliferous, micro-vacuolate, locally clayey packstone. The average thickness reaches 160 m.

The formation ranges from Langhian to Serravallian and is chrono-equivalent to the Nilde and Mahmoud formations, representing carbonate-pelagic platform deposits.

- *Miocene-Pliocene syn-orogenic units*

They are formed by clastic, carbonate and evaporitic sequences that fill the Miocene thrust top basins of the Sicilian chain, and are partly involved in Late Pliocene tectonic.

The deposits, which embrace the time interval between the Late Serravallian and the Early Messinian (pre-evaporitic), belong to the Castellana Sicula and Terravecchia formations, representing the delta and slope environments related to the emplacement of the tectonic sheets towards the foreland

Baucina and **Tripoli** formations, not present in the studied wells, mark the beginning of the Mediterranean closure and evaporitic sedimentation which consists of the Messinian calcareous-solfiferous and chalky deposits with intercalation of chalky marls and chalky clays and potassium salts. The evaporitic phase ended at the beginning of Pliocene with sedimentation of pelagic deposits of the Trubi formation, when open marine conditions re-established.

Castellana Sicula has the name of the outcrop located near the homonymous town in southern Madonie.

BASILONE (2012) described the formation as a green-grey or blue-grey and yellow, rarely fossiliferous, sandy pelites and pelites, with lenticular intercalations of sandy. The planktonic foraminifers attributed a Serravallian-Tortonian age to the deposits.

The formation is only found in the onshore well Biddusa, with a thickness of 132 m and described as " green-grey, sometimes silty, clay with a sandy level between 1876 m and 1882 m" and is attributed to the Lower Miocene. Nevertheless, the sedimentary unit is present in the other wells merged into Terravecchia formation. In fact, in the seismic profiles described in the following paragraphs a transparent seismic facies pertaining to the formation was identified.

Terravecchia formation was introduced by SCHMIDT DI FRIEDBERG (1962). It consists of a predominantly terrigenous succession with a huge thickness, sometimes exceeding one thousand meters, with abrupt lateral variations. The presence of different granulometric deposits allowed to divide the unit into three homogeneous parts: a conglomeratic member, a sandy member and a pelitic-clay member. The first two fall into the Late Tortonian, the latter in the Early Messinian. Conglomerates are reddish, yellowish with carbonate, siliceous and crystalline elements with sandy matrix and stratified in banks. The passage to the sandy member is signed by a discordance surface which separates the previous deposits from yellowish, sometimes grey for the

higher clay content, clay sandstone and sandstone. The lens-like conglomerate intercalations become increasingly smaller upwards. Towards the top, grey marly-clay sandstone appears. The uppermost member consists of marly-sandy clays and sandy marls.

In the analysed wells, sandy and pelitic-clay members predominate. They are described as grey and greenish-grey clay, locally silty, soft, with intercalation and banks of fine quartz sand. Traces of pyrite and glauconite are frequent.

As regards the chronostratigraphic attribution, while the presence of Globigerinoides dates the formation to the upper part of Tortonian, the Globorotalia conomiozea biozone to the pre-evaporitic Messinian.

The equivalent term in the Hyblean sector is Tellaro, in the Tunisian sector is Oum Douil and indicate more marly deposits.

The "**gessoso-solfifera**" series was proposed by SELLI in 1960 to indicate the complex of deposits corresponding to the Messinian age and representative of paleo-oceanographic events know as Messinian salinity crisis.

During the classification of formations for the CARG project, the *gessoso-solfifera* series was elevated to a Group and divided in two units, Cattolica and Pasquasia, which in turn consist of numerous members. Among these Arenazzolo is the only one present in the analysed wells, and precisely in Pina well. In the other wells, the evaporitic sediments are only indicated as belonging to the old *gessoso-solfifera* series.

Cattolica formation, related to basinal areas, is made up of solfiferous calcareous lithotype (*Calcare di base* member), selenitic gypsum (*selenitico* member) and potassic salts with local intercalation of clays (*salifero* member).

Pasquasia formation, indicative of marginal areas, is represented by: gypsum arenites member, marly-gypsum member, member of Congerie limestone, fanglomerates member and Arenazzolo Member (from Sicilian dialect "*rinazzolu*", hypocoristic name of "*rina*" that means sand).

In the wells, the series appears as whitish, microcrystalline, translucent gypsum with clay intercalation or as whitish-grey, hazel, sometimes clayey, fine-coarse grained sandstone with quartz, carbonate passing to clay sands with clay intercalations. Traces of pyrite and glauconite are frequent.

In Pina well, Arenazzolo member consists of greyish, fossiliferous, intraclastic, locally clayey packstone, with a thickness of 37 m.

Trubi term derives from the Sicilian dialect "*trubbu*" that means whitish soil, widely used in geological literature and today considered as the formal name of Traditional Units.

In the wells, the formation is described as greenish-grey, plastic, fossiliferous clay, passing to marl at the base. Microscopically, it is characterized by whitish, locally clayey, fossiliferous, intraclastic packstone / grainstone with frequent traces of pyrite and glauconite.

However, on the ground it appears as an alternation of limestone and marly limestone, sometimes sandy, greyish-white to yellowish-white, well stratified with a rich planktonic content and grey or yellowish biocalcarenites.

The unit belongs to the period between Zanclean and Early Piacenzian and exhibits a thickness range of 47-173 m.

- *Upper Pliocene-Pleistocene units*

They are chrono-equivalents terrestrial and clastic-carbonate deposits identified in three main sedimentation areas. In the Belice valley, western Sicily, the formation is known as Belice marly-arenaceous formation. In central Sicily, the Enna-Caltanissetta Basin consists of: clastic-carbonate formations and marly clays of the Marne di Enna formation; Capodarso Calcarenites and Geracello marls. Southern Sicily, between Gela and Agrigento, is characterized by marly-pelitic lithotypes of Narbone formation followed by the discordant, fossiliferous calcarenites of Agrigento formation (**Ribera group**). Initially, the term Ribera was used to designate Plio-Pleistocene deposits subsequent to Evaporative sedimentation, which closed

the stratigraphic column, consisting of Arenazzolo, Trubi, Narbone and Agrigento members. With the new lithostratigraphic classification, the Ribera formation was elevated to the rank of Group, including the only formation of Mount Narbone and Agrigento.

Monte Narbone formation, of Gelasian (Late Pliocene age according to the old stratigraphic nomenclature), appears on the ground as marl with planktonic foraminifera followed by sandy-silty marls and grey and dark grey clays and sandstones to the top. In other cases, it appears as an alternation of marly clays and silty sands with calcareous-arenaceous banks passing to organogenic calcarenites.

In the wells, the formation is described as grey and green-grey, soft, fossiliferous clay locally sandy-silty and sandy, with frequent traces of pyrite. The thickness is between a minimum of 33 m and a maximum of 2009 m.

The **Agrigento** formation is attributed to the Pleistocene. It consists of calcarenites and fossiliferous sands. Microscopically, they are white, dark grey, fossiliferous packstone / wackestone, with fragments of coral, coralline algae, briozoi, macrophoram, and echinoids. The thickness is variable between 240 m and 428 m.

In Biddusa and Campobello wells, alluvium of fluvial origin is found at the top with limited thicknesses (20 m). These Quaternary deposits are grouped in the Capo Plaia synthem, which embraces all the clastic or carbonate sediments of continental, coastal and marine environment.

3.2.3 Well-log stratigraphic correlations

A stratigraphic correlation among stratigraphic units in the analysed wells was performed. The lateral extension of the logged layers was traced along different directions. Obviously, closer wells with more homogeneous lithofacies afford a better correlation.

The choice of stratigraphic series to correlate depended on the necessity of obtaining indication on the stratigraphic variability of the whole area. To

this aim, Samantha, Alfa, Sirius, Oscar West, Onda and Marinella wells were correlated to highlight the lithological changes transversely to the coast line (Fig. 3.4), and Ninfea, Nuccia, Vallo, Contrada Triglia, Biddusa, Oscar West, Carla and Olga to show lithological variations parallel to the coastline (Fig. 3.5). For the location of the wells, see figure 3.1, where two lines (parallel and transversal to the Sicily coast), along which lithological variations have been evaluated, were drawn.

Moving from SW to NE along line 1, i.e. from the offshore well Samantha to the onshore well Marinella, and along line 2 of fig. 3.1, i.e. from Ninfea to Olga wells arranged in a NW-SE direction, the lateral thickness changes of formations are apparent.

It is worth to note the lack of the Gessoso-Solfifero Group in the Alfa well (fig. 3.4) and also in the Ninfea, Nuccia, Vallo, Contrada Triglia, Biddusa and Olga wells (fig. 3.5). This absence is indicative of an erosion surface. During Messinian age, the whole Mediterranean area was affected by climate change and the creation of a morphologic threshold that completely cut the relationship between the Mediterranean and the Atlantic. Critical temperature conditions (arid climate) and concentration of Mediterranean waters established, promoting the deposition of evaporitic sediments (HSU et al., 1977) as stated by well-log information gained by analysis of Oscar W, Carla, Samantha, Sirio, Onda and Marinella wells.

Oscar West well exhibits the smallest thickness of Terravecchia fm., whereas the older formations exhibit minor thickness (Amerillo, Hybla, Lattimusa) except for Sciacca fm. that shows a locally higher thickness. In fact, the normalized stratigraphic series to the top of Terravecchia fm. evidence the presence of a structural high of Miocene age nearby Oscar W well, which inverted a pre-existing low which persisted during the Trias-Oligocene time (Fig. 3.6).

While the structural high described above was again inverted from the Messinian becoming a basin as documented by thickening of Plio-Pleistocene

sediments when open marine condition re-established, the NW sector occupied by the Adventure bank underwent an opposite process that led to the uplift of the areas, as documented by analysis of Ninfea, Nuccia, Vallo, Contrada Triglia and Biddusa wells.
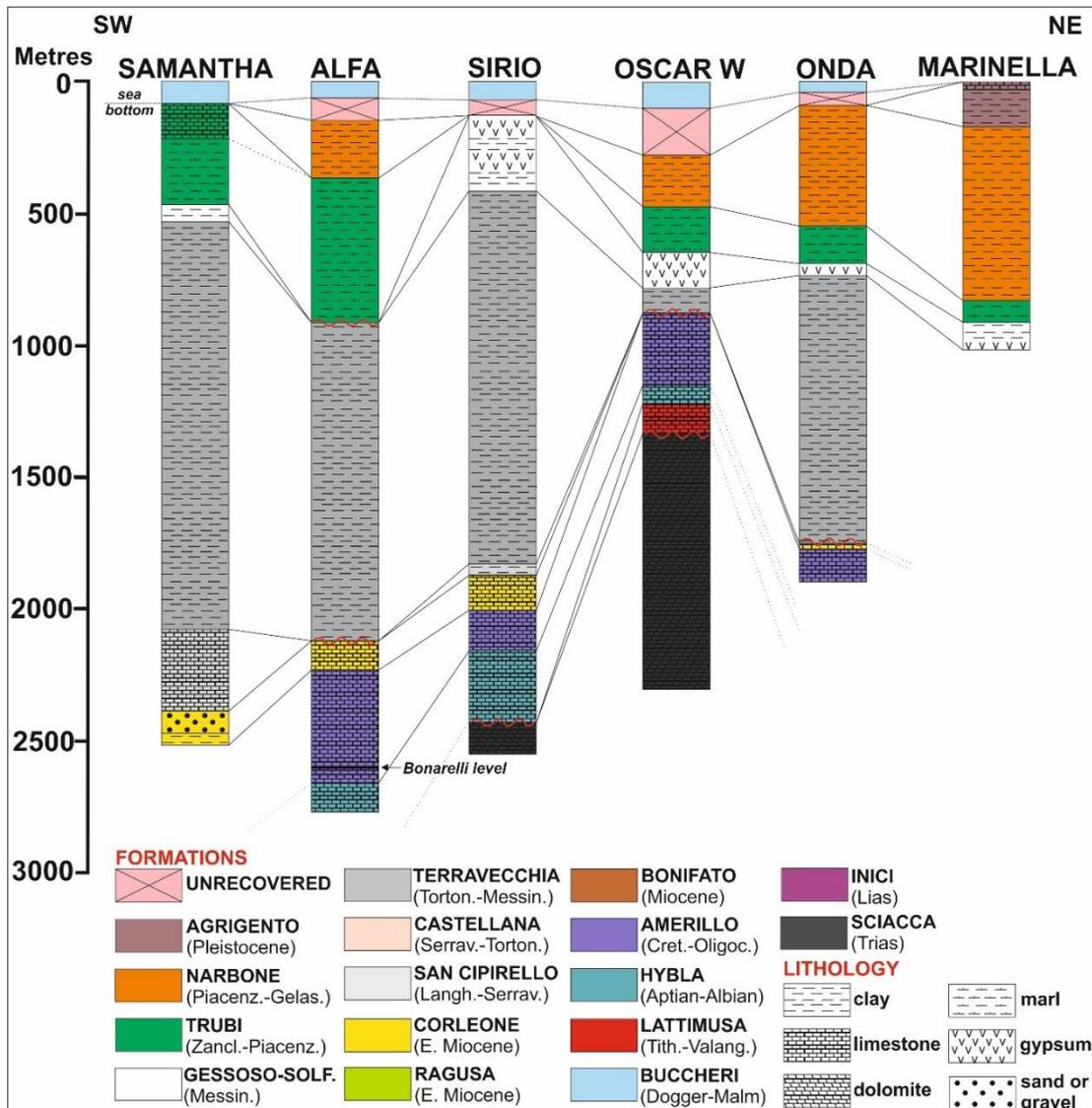

Fig. 3.4 – NW-SE trending stratigraphic correlation between different successions from Samantha, Alfa, Sirio, Oscar West, Onda and Marinella wells, as shown by line 1 in Fig. 3.1.

Since the Quaternary, the latest tectonic movements of Apenninic orogenesis led to the exposure and partial erosion of the Messinian deposits, which are absent or exhibit minor thickness in the wells.

From the observation of Figure 3.5, another important information can also be obtained. The NW-SE directed wells reveal the transition from Trapanese to Saccense domain in correspondence of Contrada Triglia well.
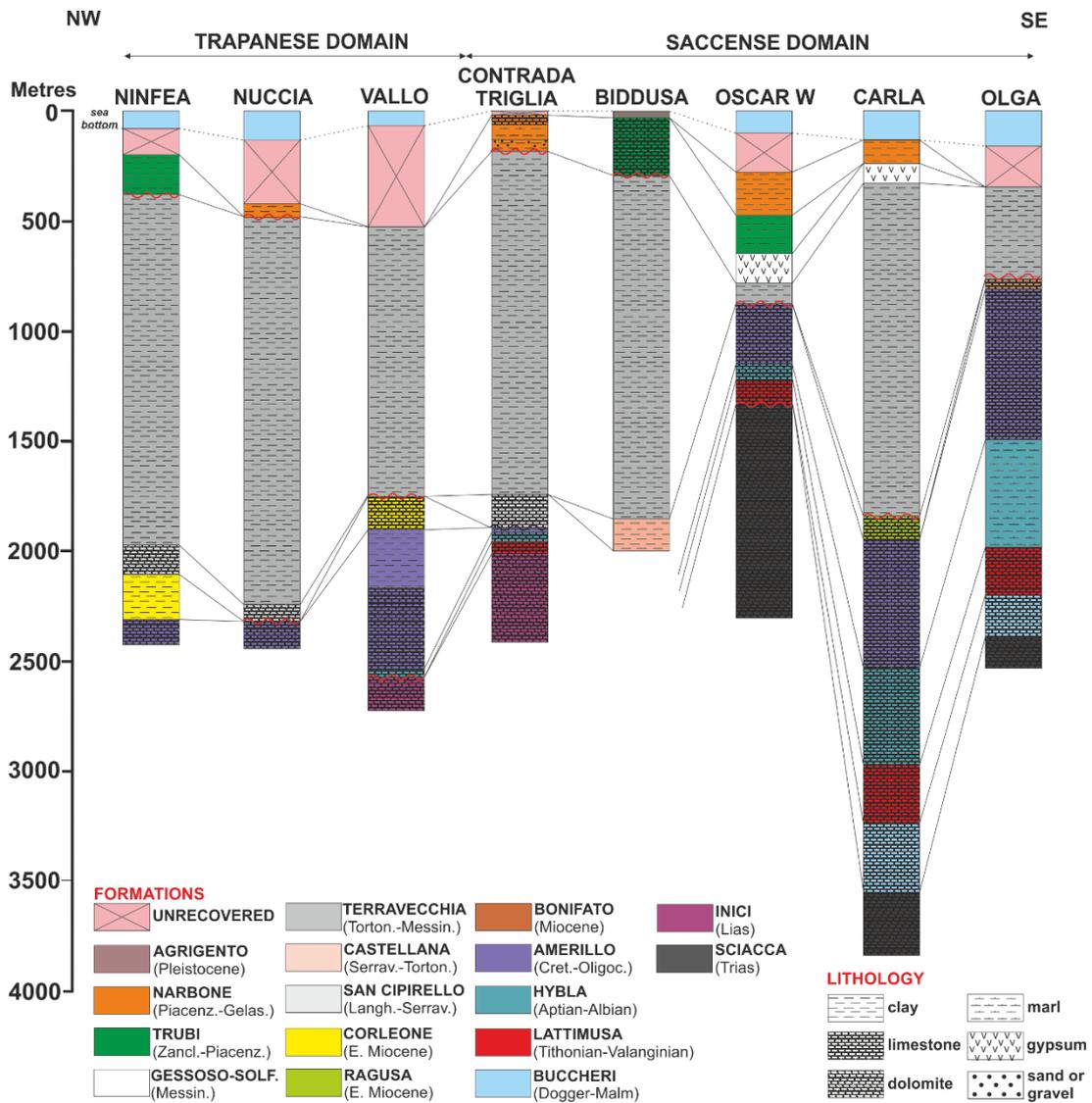

Fig. 3.5 – Stratigraphic correlation between successions from Ninfea, Nuccia, Vallo, Contrada Triglia, Biddusa, Oscar West, Carla and Olga wells, located parallel to the coast line, as shown by line 2 in Fig. 3.1.

In order to highlight the thickness variation of formations older than Oligocene time, the position of stratigraphic series was normalized to the base of Amerillo fm. (Fig. 3.7). This operation has allowed to visualize a thickness increase of Hybla, Lattimusa and Buccheri fms. from NW toward SE.

71

Whereas the same formations don't exhibit great thickness changes in Carla and Olga wells, the reduction of these to NW reveals the transition to the Trapanese domain, characterized by the presence of Inici fm., absent in Saccense domain that instead is marked by high thicknesses of Hybla fm.
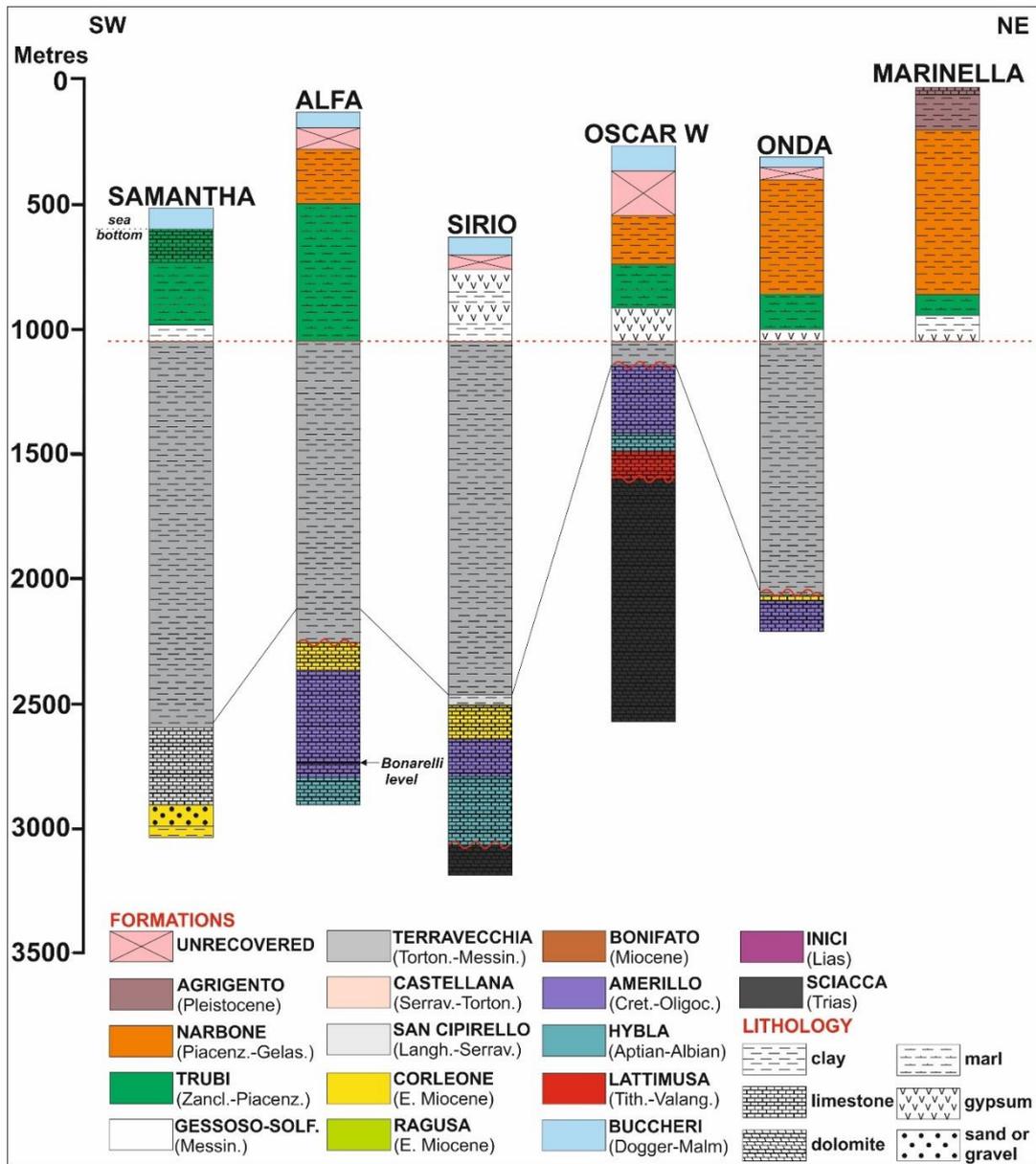

Fig. 3.6 – Stratigraphic correlation of wells of Fig. 3.4 normalized at the top of Terravecchia fm. in order to highlight the thickness variations of the Terravecchia foredeep.
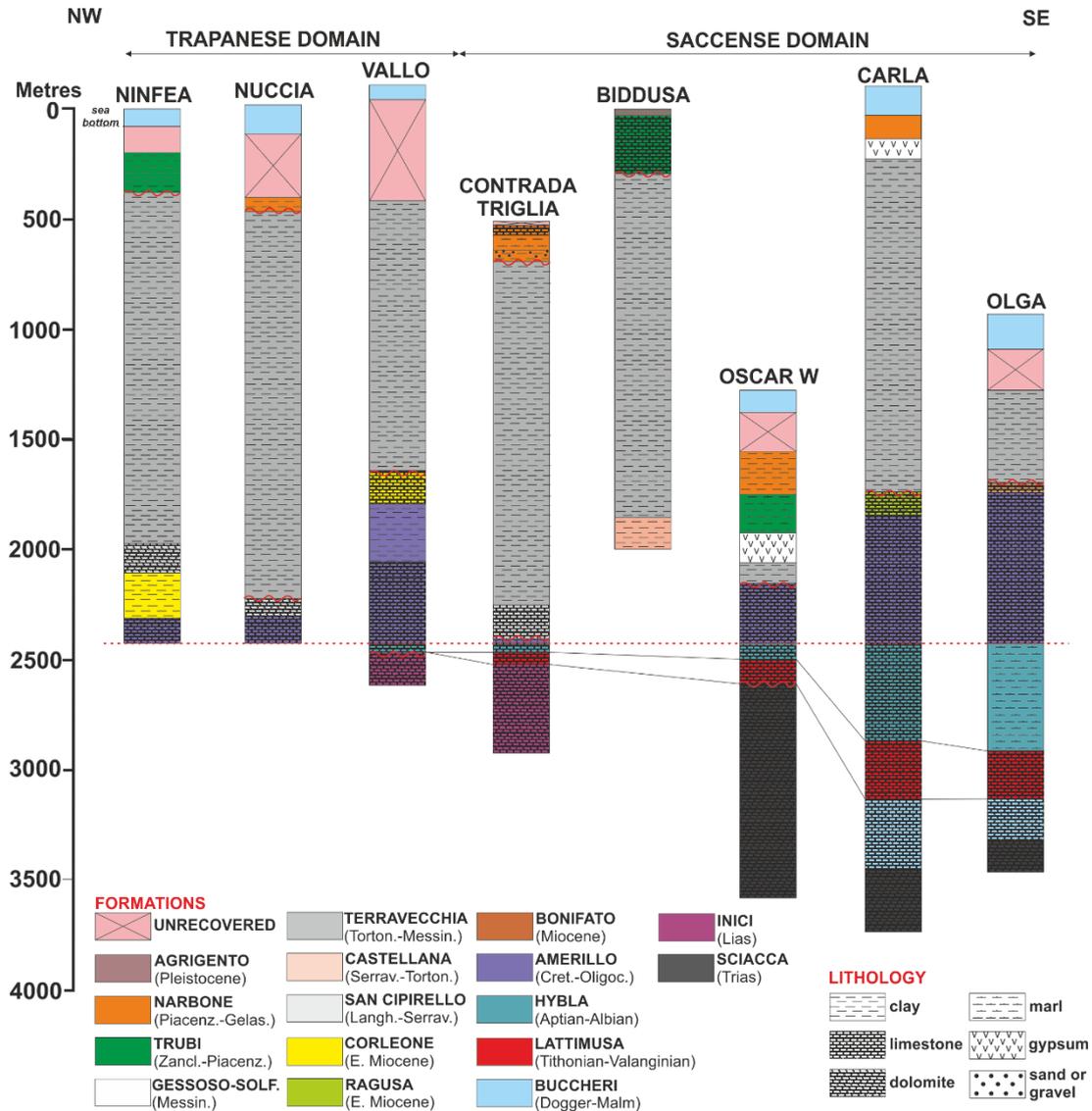
Fig. 3.7 – Stratigraphic correlation of wells of Figure 3.5 normalized with respect to the base of Amerillo fm., in order to highlight the thickness variations of Hybla, Lattimusa, Buccheri, Inici and Sciacca formations.

All of these considerations are related to the geological history of the two domains both documented by offshore and onshore studies (ANTONELLI et al., 1988; CATALANO et al., 2000). The Trapanese domain is characterized by widespread submarine unconformities. It arose as a carbonate platform, then fragmented during the Dogger rifting phase associated with the opening of the Neo-Tethys. Instead, the Saccense domain suffered a gradual foundering, which did not involve very intense fracturing and tilting phases as in the case of the Trapanese platform. This different evolution allowed a larger

sedimentation in the Saccense domain, especially during the Oligocene. Therefore, it can be stated that the Mesozoic paleo-topography envisaged the presence of a structural high (Trapanese domain) and a low (Saccense domain), such that some formations attained different thickness in the two domains.

3.3 Multi-channel seismic reflection profiles analysis

3.3.1 Methods

The raster format MCS profiles available from ViDEPI website are grouped into Zone C and G, which are part of reconnaissance seismic campaigns progressively acquired by AGIP, on behalf of the State, accordingly to Law July 21th 1967, n. 613, at the moment of the opening of the various offshore areas to the petroleum exploration. The analysed data set includes also seismic lines acquired in expired mining permits and concessions and the seismic lines granted by ENI.

Lines editing was developed in different phases. First of all, it was used an image editing program (Photoshop) to merge the sections in which the same profile was subdivided and to enhance the graphic aspect in terms of brightness and contrast. Then, each profile was transformed into a .segy file thanks to the geographical coordinates of start and end points of line acquisition, and finally imported into GeoSuite. In such a way, a grid of profiles was created that cover the entire interested area (Fig. 3.8).

Each seismic profile was processed by means of various operations through the software, which is able to read and edit multiple seismic formats, allowing to improve the graphic return of the profiles and to interpret them by creating multiple layers (such as sea bottom, boundary of formation, fault planes, etc.).

Finally, by assigning velocity values to the recognised formations mapped during lines interpretation, a depth conversion was made to highlight the real geometries.
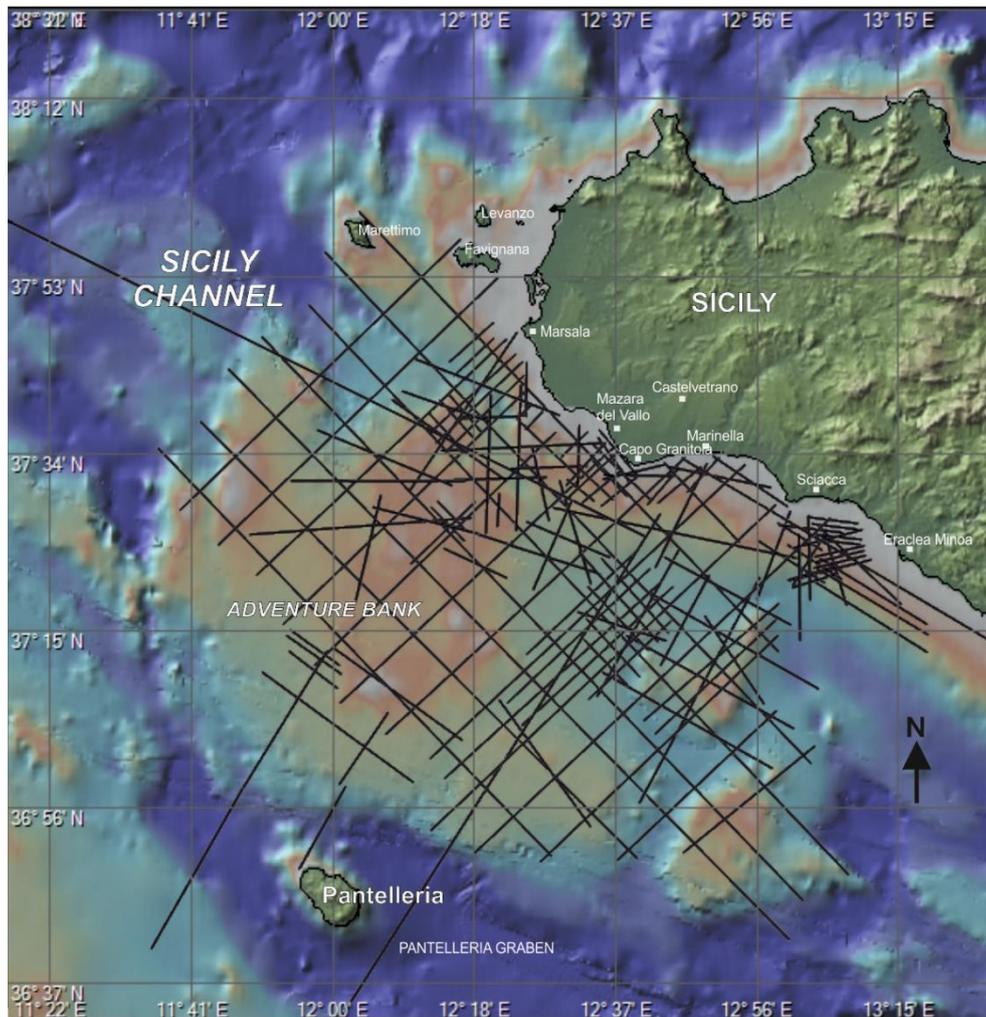

Fig. 3.8 – Bathymetric map of the study area with location of analyzed MCS reflection profiles.

3.3.2 Seismic velocities

The first step in the interpretation was the building of a seismo-stratigraphic reference framework. To this aim, an appropriate velocity value was assigned to the different formations (Fig. 3.9) based on those proposed by different authors (BELLO et al., 2000, CATALANO et al., 2000; GHISETTI et al.,

2009 and CIVILE et al., 2014) and here calibrated with well-log lithostratigraphic information.

SEQUENCE AGE	STAGE AGE	FORMATION	LITHOLOGY	VELOCITY (m/s)				VELOCITY (m/s) (this work)
				Bello et al., 2000	Catalano et al., 2000	Ghisetti et al., 2009	Civile et al., 2014	
Pleistocene	Calabrian-Santernian	*Agrigento / Marsala synthem*	clay, sand			2000 (top)-2600 (bottom)		2200
Upper Pliocene	Gelasian	*M. Narbone / Belice marly-arenaceous*	clay			2600 (top)-2800 (bottom)		2550
	Piacenzian			2500				
Lower Pliocene	Zanclean-Piacenzian	*Trubi*	clay, marl			2800 (top)-3200 (bottom)		2750
Upper Miocene	Upper Messinian	*Gessoso-Solfifera*	gypsum limestone and clay			3200 (top)-3400 (bottom)		3300
	Lower Messinian-Upper Tortonian	*Terravecchia*	clay, sand		3000		2150	2800
Middle Miocene	Lower Tortonian-Upper Serravallian	*Castellana Sicula*	clay, silt			3400 (top)-3500 (bottom)	2500	3000
	Lower Tortonian-Upper Langhian	*S. Cipirello*	marl, clay					3300
Lower Miocene	Langhian-Aquitanian	*Corleone - Ain Grab*	calcarenite, clay, marl					3400
Middle-Upper Oligocene-Lower Miocene	Burdigalian-Chattian	*Ragusa*	marly limestone, with chert		3500		2750	3500
Eo-Oligocene	Rupelian-Ypresian	*Upper Amerillo*	claystone, marl					3500
Upper Cretaceous	Maastrichtian-Cenomanian	*Lower Amerillo (Alcamo)*	lime marl		4000		3100	3600
Lower Cretaceous	Berriasian-Albian	*Hybla*	mudstone, marl	5500 (Hyblean Foreland Unit)				4000
Lower Cretaceous-Upper Jurassic	Albian-Oxfordian	*Lattimusa*	cherty mudstone, chalk		4500	3500 (top)-6000 (bottom)		4700
Middle-Upper Jurassic	Callovian-Hettangian	*Buccheri*	clay mudstone-dolostone				3200	4700
Lower Jurassic	Toarcian-Hettangian	*Inici*	limestone-dolomite		5000			5400
Upper Triassic	Rhaetian-Carnian	*Sciacca*	dolomite				3350	5800

Fig. 3.9 – Seismo-stratigraphic diagram of formations recognized by well-log analysis based on the velocity values proposed by GHISETTI et al. (2009); BELLO et al. (2000); CATALANO et al. (2000) and CIVILE et al. (2014).

BELLO et al. (2000) took up a structural reconstruction of eastern Sicily by producing regional geological sections through the interpretation of seismic profiles supported by well data, surface geological surveys, and gravimetric and magnetometric information.

The derived model describes the eastern Sicily chain as made up of a stack of sheets which can be divided in three large structural units separated by two major levels of detachment. A SE vergent imbricate thrusts system to the North, a back-thrusts region in the centre and a series of S verging thrusts to the South characterize the Imerese and Sicanian allochthonous structural units. This structural framework was connected to a Late Oligocene-Lower Miocene tectonic event which caused allochthonous units to thrust upon autochthonous Hyblean units, and to a Mio-Pliocene tectonic event which involved the Hyblean units and modified the previous geometry of the allochthonous units.

The authors distinguished five stratigraphic horizons to whom a velocity value was assigned (Fig. 3.10). Among these values, we selected those assigned to the Late Tortonian-Pliocene succession and to Hyblean foreland units. In the Sicily Channel, the former velocity (2500 m/s) corresponds to the set of Monte Narbone, Trubi, Gessoso-Solfifera and Terravecchia formations. Instead, the second value (5500 m/s) refers to the set of Amerillo (Upper and Lower Members), Hybla, Lattimusa, Buccheri, Inici and Sciacca units.

Stratigraphic unit	Velocity used for time-depth conversion (m\sec)
Late Tortonian-Pliocene succession	2500
Internal Numidian Flysch Unit	2800
Argyle Variegate Unit	3000
Gagliano Unit	3500
Imerese-Sicano basinal Unit	4500
Hyblean Foreland Unit	5500

Fig. 3.10 – Average speeds of stratigraphic units, identified in the profiles, used for time-depth conversion. (From BELLO et al., 2000).

While BELLO et al. (2000) analysed eastern Sicily, CATALANO et al. (2000) rebuilt the deep structural asset of the central-western Sicily-chain, through the analysis of depth-converted seismic profiles using average velocities obtained from logs of wells drilled in continental Sicily (Fig. 3.11). The authors highlighted a continuous migration of chain-foredeep system toward the foreland with allochthonous units showing duplex geometries and clockwise rotations.

Carbonate platform successions: Trias-Lias	5000 m/s
Dogger-Oligocene	4500 m/s
Basin and slope to basin carbonate successions	4000 m/s
Upper Oligocene-Lower Miocene Numidian deposits	3500 m/s
Serravallian-Messinian deposits	3000 m/s
Pliocene-Pleistocene deposits	2000 m/s

Fig. 3.11 – Average speeds of stratigraphic units, recognized in the profiles, used for time-depth conversion. (From CATALANO et al., 2000).

They divided the tectonic edifice in structural levels bounded by sub-planar discontinuities. The lower level is a 8-9 km thick thrust wedge formed of Trapanese and Saccense carbonate platform imbricates, detached from their basement. The intermediate level consists of 1-3 km thick thrust sheets pertaining to Sicanian and Imerese domains. The top structural levels are represented by a tectonic wedge of Numidian and Sicilide deposits. Upper Miocene molassic deposits, Messinian evaporites, lower Pliocene limestone and Plio-Pleistocene clastic carbonate deposits fill large synthetic depressions.

Based on the different acoustic characteristics, six sedimentary bodies were recognized:

1. Cretaceous-Liassic carbonate platform deposits;

2. Dogger-Oligocene carbonate platform deposits;

3. Basinal carbonate and slope to basin deposits;

4. Late Oligocene-Lower Miocene Numidian deposits;

5. Messinian-Serravallian deposits;

6. Plio-Pleistocene deposits.

Through well-log calibration the authors associated a velocity value to each sedimentary body (Fig. 3.11).

A comparison between the above units with those of the Sicily Channel was made. By matching the available information, the Cretaceous-Liassic carbonate platform succession should correspond to Sciacca and Inici formations; the Jurassic and Cretaceous limestones to Buccheri, Lattimusa and Hybla formations; the basal and slope to basin sequences to the Lower Amerillo formation. Instead, Numidian deposits are equivalent to Oligo-Miocene formations of upper Amerillo and Ragusa. The units ranging between Serravallian and Messinian correspond to the chrono-equivalent formations Corleone, San Cipirello, Castellana Sicula, Terravecchia and Gessoso-Solfifera. Plio-Pleistocene deposits embrace Trubi, Monte Narbone, Agrigento and alluvial and marine deposits.

As already described in chapter I, GHISETTI et al. (2009) investigated the Gela Nappe, the outermost and youngest thrust sheet of the Sicilian chain through the analysis of M23A seismic line, which is part of the *CROP-MARE* project and intersects the Nappe along a NW-SE direction, highly oblique to the SW-transport direction of the nappe. The GN was progressively transported above the Pelagian foreland as testified by the southern migration of basins, which were inverted during the Late Miocene-Pleistocene (GHISETTI et al., 2009). The presence of fold interference pattern was emphasized thanks to the analysis of both on-land outcrops and the seismic profile.

The processing and depth conversion of the profile performed by GHISETTI et al. (2009) revealed multiple imbricates and drapes in the foreland allochthonous units through the identification of six horizons listed in figure 3.12. The authors constructed a velocity model by:

1) manual removing of stacking effects to avoid vertical layer repetition;

2) assigning initial velocity based on geological knowledge and previous analysis of seismic lines in the Apennines;

3) vertical and lateral smoothing of velocity values to remove discrete changes;

4) picking a finely spaced grid of interval velocities through the entire data set.

The values of velocity obtained by GHISETTI et al. (2009) for the top and bottom of seismic sequences (Fig. 3.12) were inserted in Fig. 3.9 and compared with the formations selected for this study.

Layer	Velocity at Top (m/s)	Velocity at Bottom (m/s)
Ocean	1500	1500
Seafloor to base of Pleistocene clays	2000	2600
Base of Pleistocene clays to top of Trubi Formation	2600	2800
Top of Trubi Formation to top of Messinian evaporites	2800	3200
Top of Messinian evaporites to top of upper to middle Miocene claystones and mudstones and Licata Formation	3200	3400
Top of upper to middle Miocene claystones and mudstones and Licata Formation to top of Pelagian carbonate substratum	3400	3500
Top of Pelagian carbonate substratum to base of section (10 s)	3500	6000

Fig. 3.12 – Velocities at the top and bottom of successions recognized in profiles, used for time-depth conversion. (From GHISETTI et al., 2009).

CIVILE et al. (2014) reconstructed the seismic-stratigraphic setting of the Adventure Plateau by analysing 2D multichannel seismic profiles and well data. The authors created synthetic seismograms to calibrate real seismic data reflections with the corresponding stratigraphic discontinuities observed on the wells using Gardner's relation (q = Ca1/4, q = density, a = compressional velocity) for providing approximate densities and velocity values using the Dix equation. The resulting used velocities are: 1500 m/s for water, 1900 m/s for Pliocene-Quaternary succession, 2150 m/s for Tortonian-Messinian succession, 2500 m/s for Aquitanian-Serravallian succession, 2750 m/s for Paleogene succession, 3100 m/s for Cretaceous succession, 3200 m/s for Jurassic succession, 3350 m/s for Triassic succession.

Based on all the above velocity, a value was estimated for each recognized formation taking into account local variations in terms of lithology and thickness, briefly reported in the figure (Fig. 3.9). The selected values

were imported into the GeoSuite well data sheets. This operation was necessary for the following time-depth conversion of seismic profiles.

3.3.3 Seismo-stratigraphic interpretation

The seismo-stratigraphic interpretation of MCS profiles was firstly carried out on the time sections. The first step was picking the seismic horizons.

Six horizons, namely A, B, C, D, E, M (Fig. 3.13) that embrace five depositional sequences, S1 (between the sea bottom, A, and horizon B), S2 (between B and C), S3 (between B and M), S4 (between M and D), S5 (between D and E), were recognized.

The recognition of each horizon in the profiles was based on three criteria. The first criterion is the identification of index horizons, which exhibit similar seismic characteristics (very good lateral continuity, high reflection coefficient, high amplitude). In detail, these are represented by horizons M and D. Horizon M is easily recognizable being the first important seismic discontinuity, correlated with the Gessoso-Solfifero Group, which generates strong reflections respect to the overlaying deposits characterized by lower seismic velocities. Also, D is easily identifiable because of the presence of a transparent sediment package above it.

The second criterion uses the well log information imported into the software. It is obvious that the smaller is the distance between seismic lines and wells, the better is the correlation.

Finally, the third criterion exploits a software utility, based on the intersection between different seismic lines. It allows to display on a profile the intersections with the other profiles and to compare horizon depths or to help to trace a horizon starting from the intersection point when it results difficult (either because of lack of wells attached to the line or because of poor acquisition resolution).

The first horizon (A) representing the sea bottom was easily recognized since it is the first encountered reflection.

B and C horizons, characterized by low amplitude and high frequency reflections with good lateral continuity, are generated by Plio-Pleistocene marly and sandy-clay successions, which produce seismic facies with a simple layered and parallel configuration. While B marks the base of Agrigento fm. (sequence S1), C represents the base of Monte Narbone fm. (sequence S2).
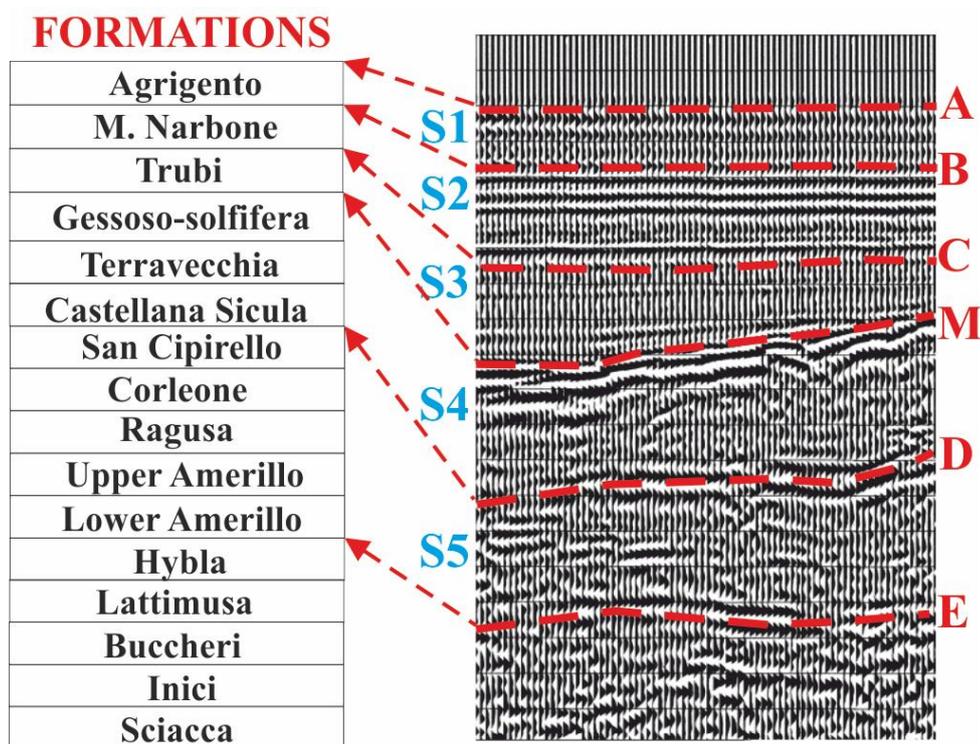

Fig. 3.13 – Sketch of a seismic profile where horizons, in red, correlated to formation boundaries can be observed. The depositional sequences between different seismic horizons are in blue. For the ages of the formations refer to Fig. 3.9.

Sequence S3 is bounded at the base by horizon M (FINETTI & MORELLI, 1973; MALINVERNO et al., 1981), which is represented by very continuous reflectors with high amplitude and strong acoustic impedance. Thanks to its clear characteristics, the reflector was identified within all the profiles, and separates the Upper Miocene units of the Terravecchia fm. or sometimes

Messinian evaporites, from Plio-Quaternary sediments. In some cases, especially in strongly deformed areas, it is an evident erosional surface.

The S3 sequence has easily recognizable seismic facies characterized by high frequency and low amplitude reflections with good lateral continuity, forming a transparent body, which is associated to marly limestones and marls of Trubi fm. The seismic facies is identified as a basin fill in concordance or discordance with underlying reflectors.

Horizon M bounds at the top the silty-clay deposits of Terravecchia fm. (sequence S4), depicted by moderately continuous, high frequency reflections with medium to high amplitude and with complex layered, sigmoidal, and sometimes divergent geometry. The complex geometry of reflector typifies the westernmost sector of the Channel pertaining to the Trapanese domain (Figs. 3.13, 3.14). This geometry ensues from the tectonic history of the Terravecchia fm. after its deposition, characterized by compression that altered its nature of layered deposit. The location at the front of the Maghrebide chain of the most deformed portion of foredeep supports the contention of a Middle-Late Miocene activity of the front.

Towards the eastern foreland, the Terravecchia is replaced by the silico-marly deposits of the coeval Tellaro formation, which appears in the profiles with layered geometry and almost transparent between horizons M and D in figures 3.13 and 3.14.

The Terravecchia fm. overlies the Middle-Lower Miocene deposits. In the Trapanese area (Figs. 3.13, 3.14), it is expressed by a layered seismic facies alternating to transparent intervals. The latter facies was calibrated with well litho-chrono-stratigraphic data, and corresponds to the predominantly clayey Castellana Sicula fm. The seismic facies is interpreted as a distal ramp of Castellana Sicula fm. deposited in the early stages of the foreland flexural subsidence. Because of the impossibility of tracing horizons in all profiles, the facies attributed to the Castellana and Terravecchia were grouped in the same seismic unit S4.
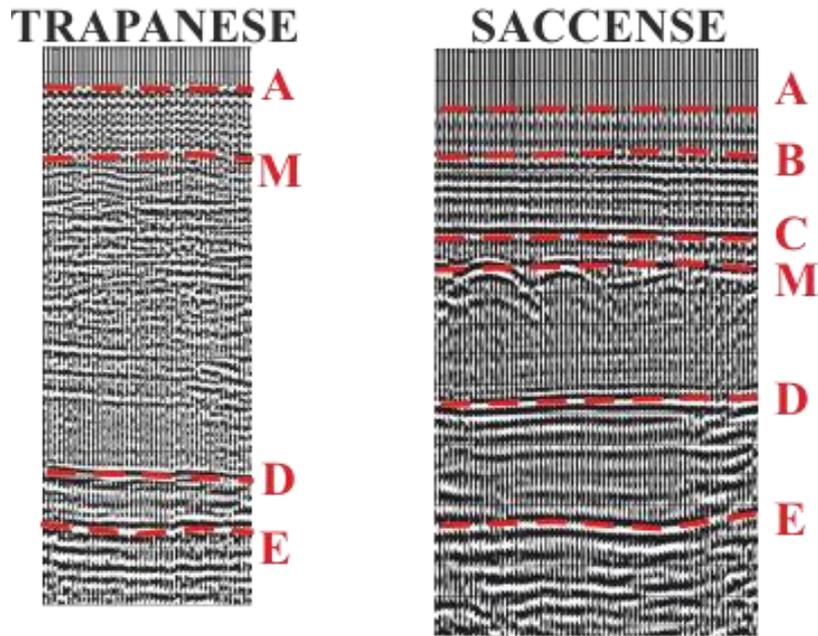
Fig. 3.14 – Comparison of the seismic facies identified in the profiles belonging to the Trapanese (area 1) and Saccense (area 2). Notice how the thickness of the package between M and D increases towards west (Trapanese unit) marking the thickening of the Middle-Late Miocene. Conversely, the thickness of the package between D and E decreases towards west.

The fifth horizon (D) has very continuous, sub-parallel, fairly homogeneous, high amplitude and high frequency reflections (Fig. 3.13). Except for some areas affected by strong tectonic activity, the horizon was easily identified, especially in the Adventure Bank.

D is considered to be a lithologic marker corresponding to the boundary between the top of pre-orogenic carbonate units and the base of Middle-Upper Miocene syn-orogenic silty-clay deposits. Horizons D and E identify the sequence S5 at the top and bottom, respectively. By calibrating wells on seismic lines, it was possible to define the depositional gap associated to unconformity D across the areas. Below the horizon, the sediment age rises from west to east, marking the transition from the Miocene calcarenites of Corleone fm. (Trapanese domain) to the Eocene carbonate units of Amerillo fm. (Saccense domain). The eastward progressively deeper erosion could be associated with the presence of a peripheral bulge (ARGNANI et al., 1986).

The last recognized and traced horizon (E) has similar characteristics to the previous one (D), characterized by strong acoustic impedance and good lateral continuity (Figs. 3.13, 3.14). As D, E is an unconformity surface that overlaps deposits with different ages, which spans between Jurassic and Cretaceous, alternately marking the top of the Hybla, Lattimusa or Buccheri formations.

Horizon E is traced more easily in the seismic profiles crossing the Adventure Bank area compared with those located in the offshore of Sciacca-Agrigento. Such a difference is related to the different pertinence domain of stratigraphic units, Trapanese and Saccense respectively. In fact, the seismo-stratigraphic analysis (Fig. 3.14) revealed well-stratified and continuous reflectors for Saccense platform and structurally more complex facies for the Trapanese platform, probably due to pre-orogenic tectonics related to the early decomposition of the platform (CATALANO et al., 2000).

3.3.4 Main structural lineaments

The seismo-stratigraphic analysis of MCS reflection profiles calibrated with well-logs allowed to recognize the main structural lineaments and to build a structural map of the NW Sicily Channel. The novelty of this map is that it shows not only the structural trends, but also the age of fault last activity (Fig. 3.15).

The tectonic structures were identified along the profiles and projected in map through the software GeoSuite and redrawn with the graphic software CorelDRAW X7 to provide a better visualization.

Three main deformation zones can be distinguished: mainly compressive in northern-western part in the offshore area between the Egadi islands and Mazara del Vallo (ETS, Egadi Thrust System, and ATS, Adventure Thrust System); transcurrent in the southern-eastern part covering the offshore zone between Capo Granitola and Sciacca (SELFB, Selinunte Fault Belt, and SFB, Sciacca Fault Belt); and normal in the Pantelleria rift system (Fig. 3.15).
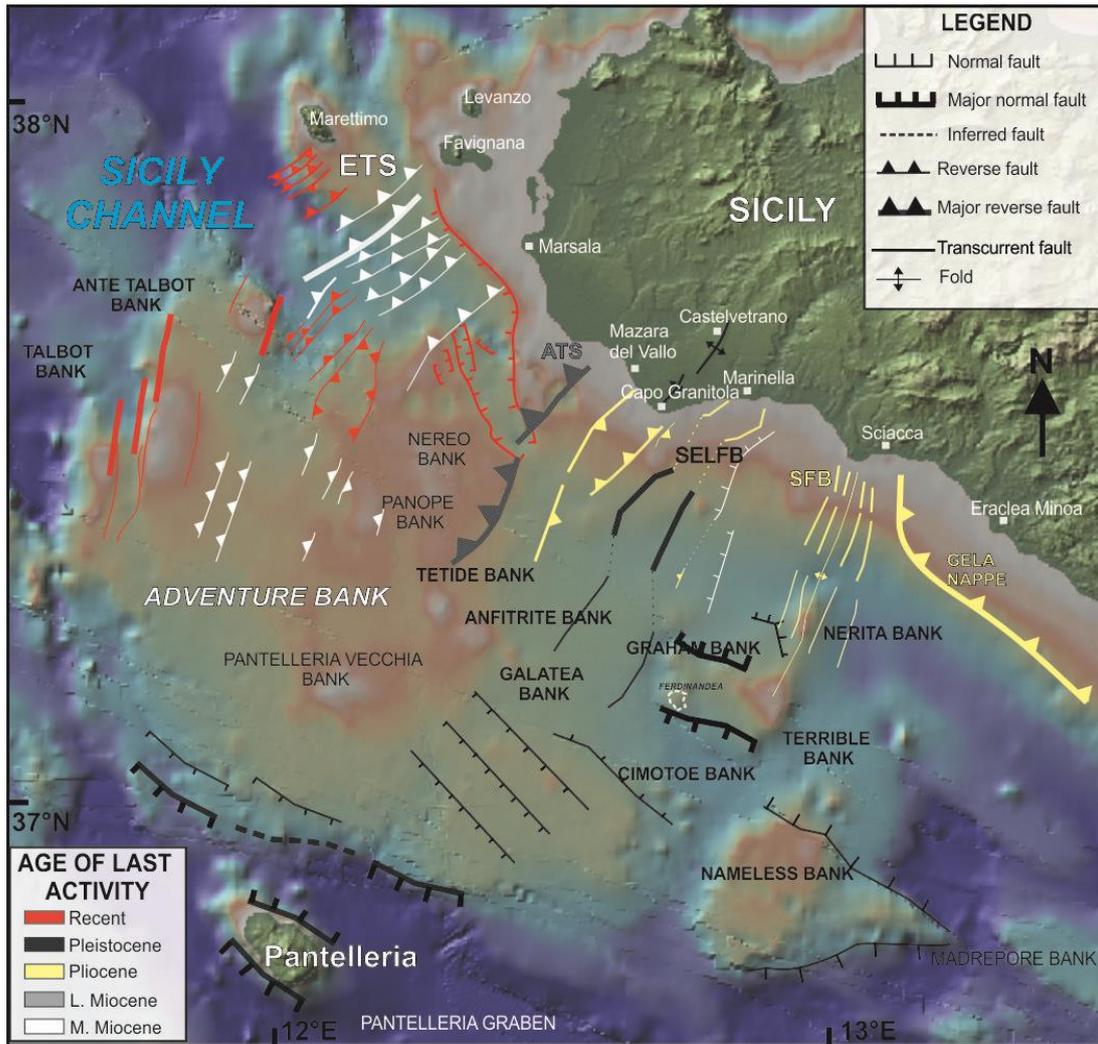
Fig. 3.15 – Structural map of the NW Sicily Channel showing the structural trends and the age of last activity of fault systems. The Neogene tectonic evolution is modulated by different stress regimes, mainly compressive in northern-western part (ETS, Egadi Thrust System, and ATS, Adventure Thrust System); transpressive in the southern-eastern part (SELFB, Selinunte Fault Belt, and SFB, Sciacca Fault Belt) and normal in the Pantelleria rift. The trend of fold onshore western Sicily is after BARRECA et al. (2014).

A detail description of the above mentioned tectonic lineaments is given in the following paragraphs.

3.3.4.1   *Egadi thrust system*

The westernmost sector of the study area is represented by the Egadi Islands offshore, where the Egadi Thrust System (ETS, Figs. 3.15, 3.16) is located, west of the Adventure Bank.

This sector of the Channel is more strongly deformed as documented by Tania well (Fig. 3.1), the only located in the area north of the Levanzo Island. The well shows ~ 100 m of allochtonous units represented by Oligocene-Early Miocene quartzose flysch of Numidian type overlying a Triassic-Jurassic prevalent dolomitic sedimentary sequence (equivalent to Sciacca and Buccheri fms.), attributed to the Pre-Panormide domain, and underlying Pliocene marls pertaining to Trubi fm.
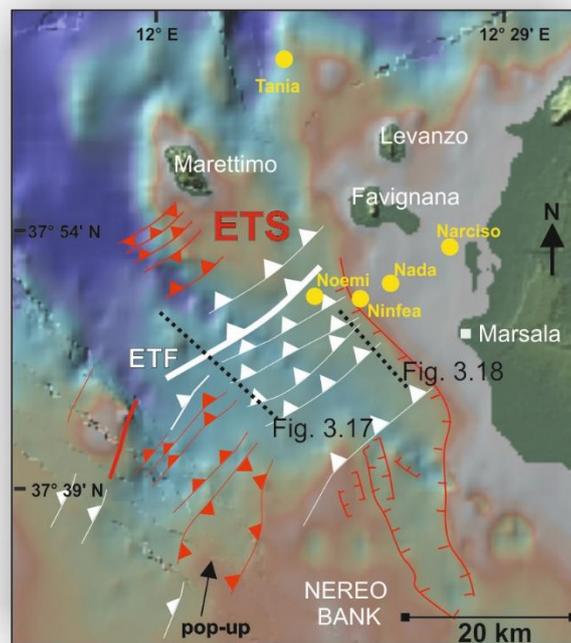

Fig. 3.16 – Zoom of westernmost sector of Figure 3.15 focusing on ETS. Yellow points represent the wells. For the key to structural symbols, see fig. 3.15.

The seismic images highlight two different seismic facies west and east of a thrust ramp which represents the Egadi Thrust Front (ETF; Figs. 3.16, 3.17). Based on the analysis of Tania and Narciso-Noemi-Ninfea-Nada wells and of the seismic signal, we distinguish two lithotectonic assemblages, the Pre-Panormide and Trapanese-Saccense (Fig. 3.17), respectively. On the western side of the thrust, the facies attributed to the Pre-Panormide domain based on Tania well calibration is chaotic and the seismic horizons M and D

recognized on the eastern side are not visible (Fig. 3.17). Hence, the ETF represents the thrust system separating the two paleogeographic domains. The thrust front is imaged by a SE-vergent thrust with a dip angle of ~ 40° and exhibits a listric geometry flattening at ~ 3.5 s (corresponding to ~ 6 km) of downdip penetration.
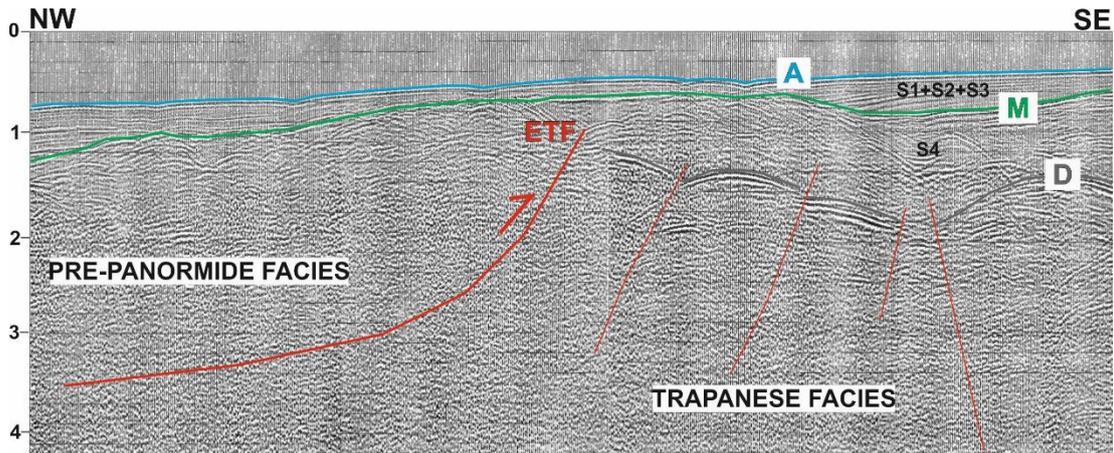

Fig. 3.17 – Sketch of profile C-1009 showing the difference between pre-Panormide and Trapanese facies. The horizonal scale shows the shot points, while the vertical scale shows depths in second (TWT). For location see figure 3.16.

East of the ETF, we mapped an array of thrusts with a ENE-WSW trend changing to NE-SW in the south and deforms an area of 1140 km^2 (Fig. 3.16). On seismic images, they appear as SE-vergent thrusts with a dip angle variable between ~ 40° and ~ 70° and minor antithetic faults (Fig. 3.18). The faults can be traced for up to 7-8 km of length, and produce antiforms with a wavelength of up to ~ 4 km (Fig. 3.18). Because most of the faults cut horizon D and deform S4, but not the overlying reflectors, the timing of regional deformation is Middle-Late Miocene.
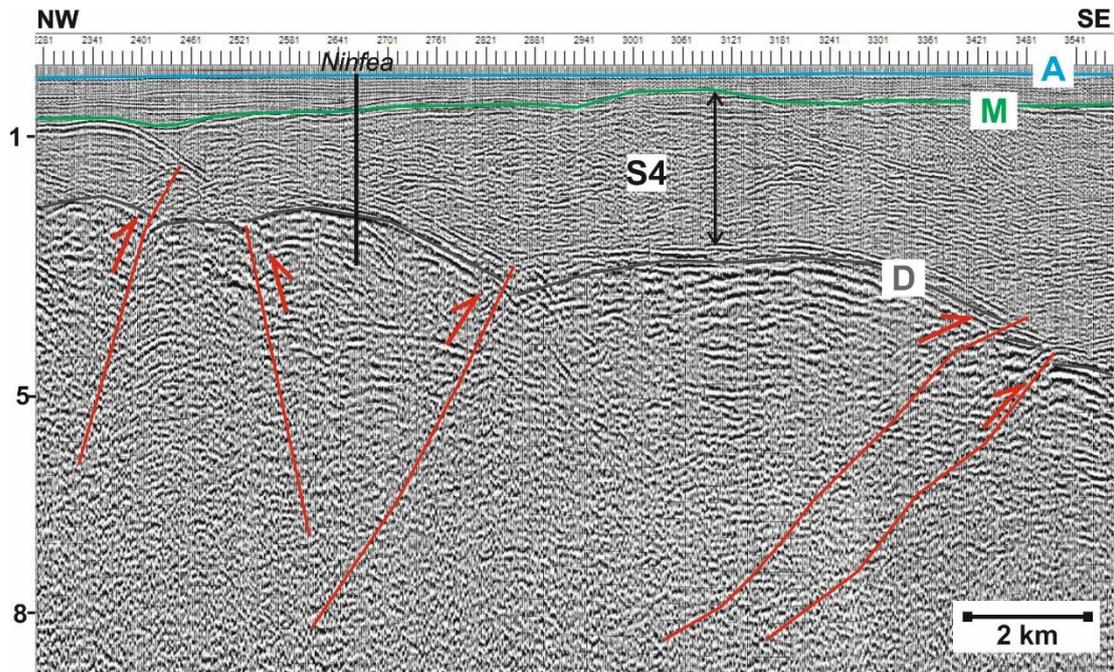
Fig. 3.18 – Sketch of profile C-1007 located in the offshore of Egadi Island and calibrated with Ninfea well (for a description of the well log see Fig. 3.5) showing the deep-seated thrusts associated to the ETF. The horizontal scale indicates the shot points, and the vertical scale shows depths in kilometers. For location see figure 3.16.

However, some of the structures cut up to the sea floor (Fig. 3.16). A pop-up structure detectable on various profiles (Figs. 3.19, 3.20) is highlighted on the Adventure Bank, west of Nereo bank.

The structure is limited by ~ 7 km long high-angle reverse faults which acted during the Miocene and until the present, as they deform both horizon D and the sea bottom (Fig. 3.20). The crest of the anticline, with a height of ~ 3 km above the relatively undeformed horizon D toward south-east, is cut by two normal faults probably connected to a gravitational collapse. The chaotic seismic facies of the core of the pop-up is attributed to fluid rising that partly obscure the seismic signal.

On the north-western side of the Adventure bank, three ~NNE-SSW trending minor banks (Talbot, Ante Talbot Bank and the bank north of Ante Talbot, NAT) are present (Fig. 3.19). They are characterized by a ~ 8° azimuth angle and differ in orientation from the above pop-up structure of ~ 10° CCW.
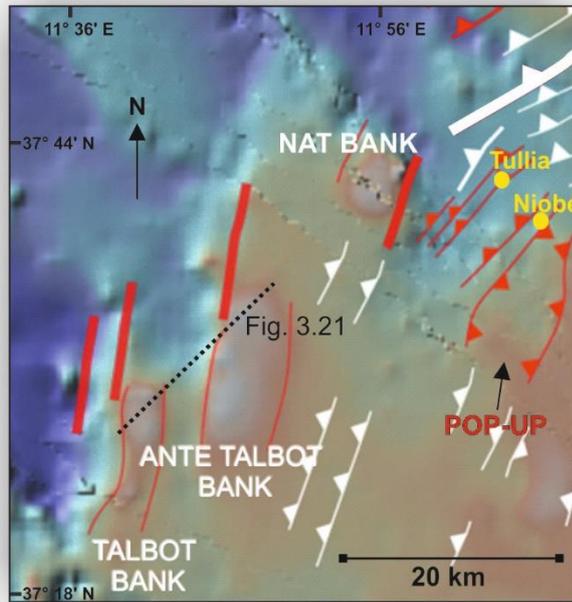
Fig. 3.19 – Zoom of Figure 3.15 focusing on the north-western sector of Adventure bank showing the Talbot, Ante Talbot banks and bank north of Ante Talbot (NAT). For the key to structural symbols, see fig. 3.15.

The two structural highs Talbot (~ 3 km wide) and Ante-Talbot (~ 6 km wide) are separated by a relatively deep (~ 300 m) and narrow (~ 4 km) channel developing in a ~ N-S aligned direction (Fig. 3.21). The banks were affected by folding and faulting of the sedimentary succession started in the Middle-Late Miocene and by minor normal faults during the Plio-Pleistocene. The structural highs are bounded by high-angle faults with a reverse sense of motion which cut the sea bottom generating morphological scarps and the central basin. The bank north of Ante Talbot arises from a fault escarpment of ~ 800 m (Fig. 3.20). The fault activity is deduced by the onlaps within seismic units above horizon D suggesting growth during the Late Miocene-Recent time (Fig. 3.20). The recent reactivation of the associated structures is highlighted by transpressive structures (Fig. 3.21) and by new generation back-thrust reverse faults in the Egadi offshore (Fig. 3.22), which, as seen for the pop-up on the Adventure Bank, cut the sea-floor.
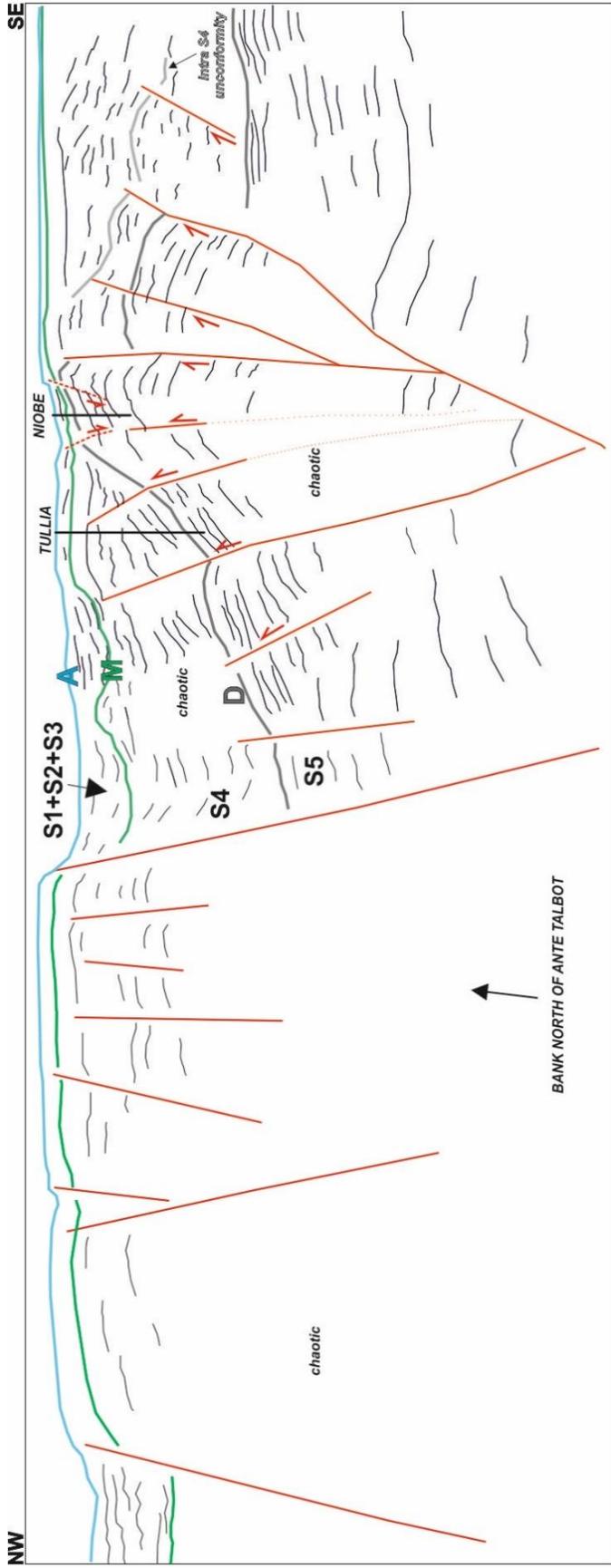
Fig. 3.20 – Line drawing of a seismic line from ENI database. In the NW, the profile evidences the bank north of Ante Talbot bounded by high angle faults that produce a fault escarpment of 800 m on the south-eastern flank. Toward the SE, a push up structure which deforms the seismic horizons, calibrated with Niobe and Tullia wells, and also the seafloor is visible. The exact location of the profile cannot be shown for reasons of confidentiality.
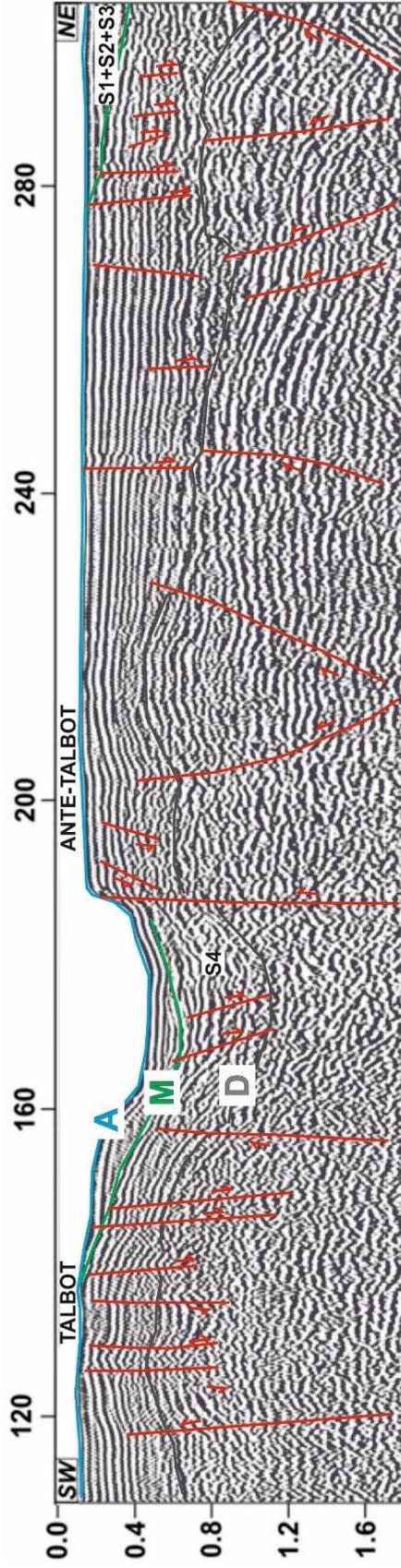
Fig. 3.21 – Sketch of profile C-1002 showing the Talbot and Ante-Talbot banks. Modified from Civile et al., 2015. The horizontal scale indicates the shot points, and the vertical scale shows depths in seconds (TWT).
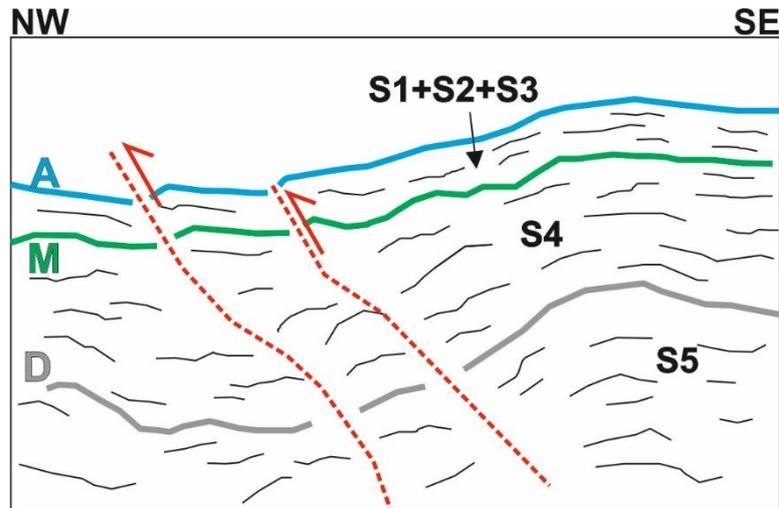
Fig. 3.22 – Line drawing of a seismic reflection profile from ENI database. Back-thrusts, locally cutting the sea-floor, are interpreted in the profile. The exact location of the profile cannot be shown for reasons of confidentiality.

3.3.4.2   *Adventure thrust system*

The Adventure Thrust System (ATS, Figs. 3.15, 3.23) is represented by an ~ 40 km long tectonic lineament with a NE-SW trend extending on the eastern side of the Adventure bank in the offshore of Mazara del Vallo. Toward the south, the ATS tends to be masked by the extensional structures and magmatic intrusion related to Anfitrite bank.
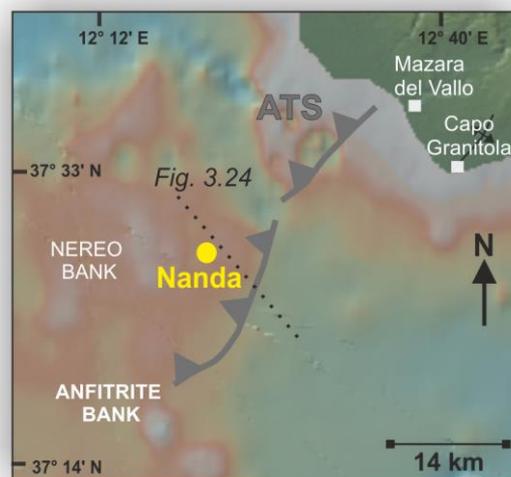

Fig. 3.23 – Zoom of Figure 3.15 focusing on ATS on the south-eastern side of Adventure bank. For the key to structural symbols, see fig. 3.15.

On the seismic profiles, the ATS is imaged by a NW-dipping reverse fault cutting horizon D and responsible of deformation of seismic sequence S4 (Fig. 3.24).

The fault activity was deduced by the analysis of a prominent high amplitude reflector, here labelled T, included between D and M, and recognised in the profiles acquired offshore between Mazara del Vallo and Capo Granitola (Figs. 3.24, 3.25).
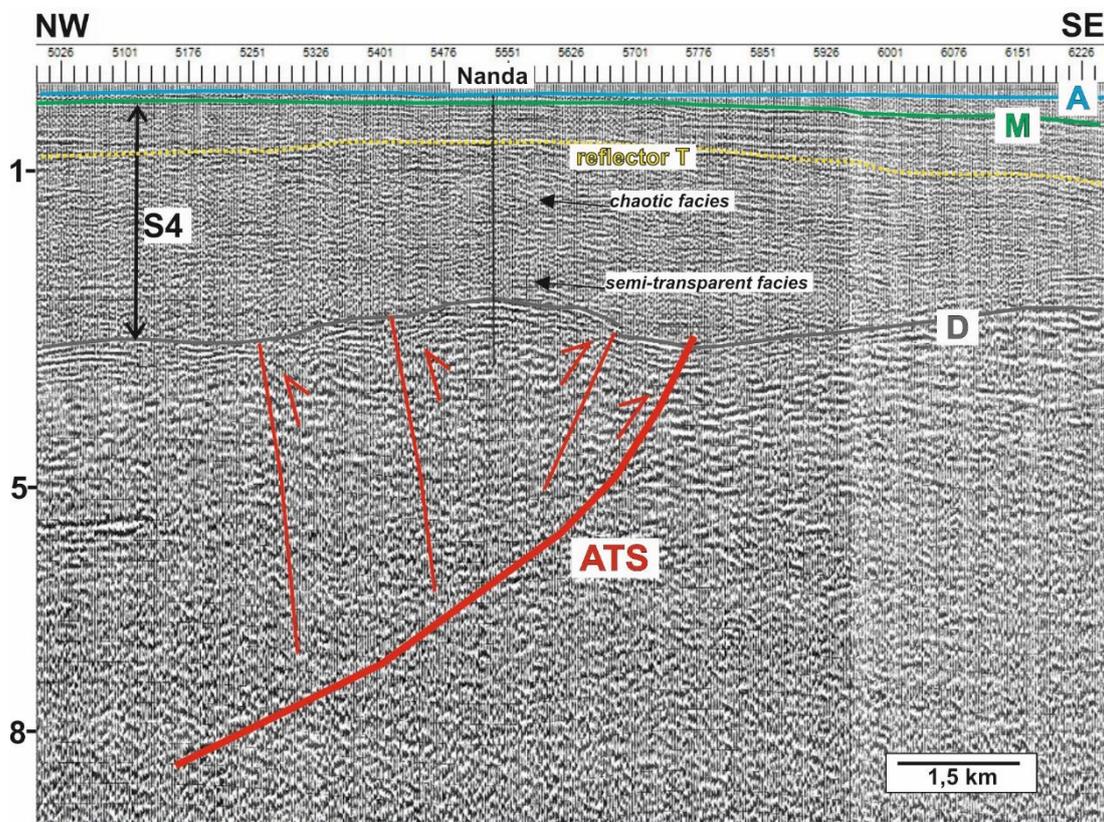

Fig. 3.24 – Sketch of profile C-1009 showing the ATS. The horizontal scale indicates the shot points, and the vertical scale shows depths in kilometers. For location see figure 3.23.

The seismic facies above horizon D is characterized by a semi-transparent basal package, by discontinuous, high amplitude, high frequency reflectors in the middle part, occasionally chaotic in more highly deformed zones, and by continuous, with low-middle frequency and low-middle amplitude reflectors at the top. These three seismic facies were assembled in

seismic sequence S4. In the Adventure Bank S4 reaches the major thickness (depocenter) and is characterized by toplap terminations (Fig. 3.24), whereas its thickness decreases toward SE where the seismic unit shows a prograding geometry (Fig. 3.25).
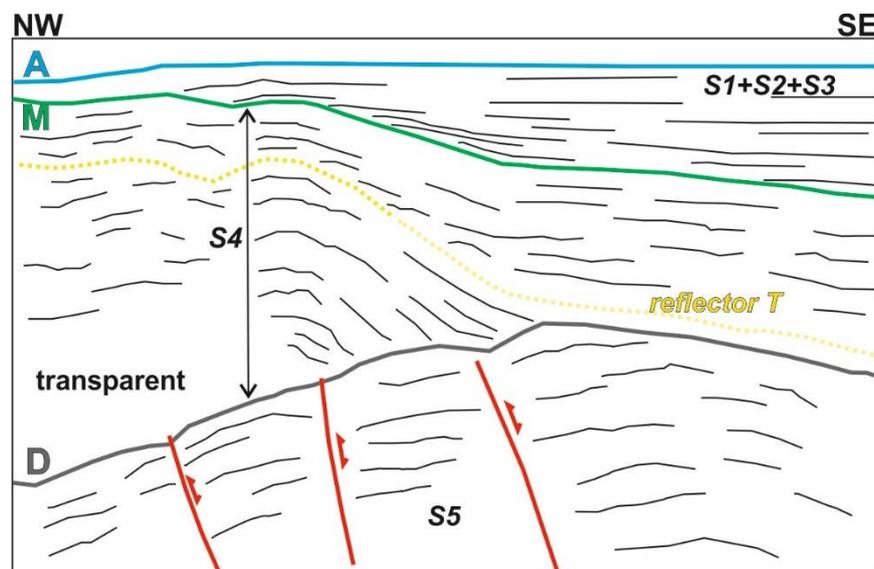

Fig. 3.25 – Line drawing of a seismic reflection profile from ENI database. The downlap geometry of the reflectors pertaining to the middle-late Miocene Terravecchia foredeep broadly ends at a reflector (yellow) that marks the passage to the sandy member of the formation, and is roughly 8 Ma old. The Miocene foredeep has been subsequently deformed by the growth of an antiform in the pre-orogenic units under horizon D. The faults are interpreted as normal faults inverted during the orogenic process. The exact location of the profile cannot be shown for reasons of confidentiality.

Whereas the interpolation of the seismic line with the closer profiles allowed to assign the basal package to the Castellana fm., the calibration with Nanda well suggested to associate the upper seismic bodies to the conglomeratic and sandy-pelitic members of Terravecchia fm., respectively (BASILONE, 2012). In the well-logs covering the area of interest, the Terravecchia fm. is characterized by a basal green-grey clay member with prevalence of *Globorotalia acostaensis*, dating to Tortonian age, and by an upper sandy member with prevalence of *Globorotalia conomiozea*, dating to Messinian. Terravecchia and Castellana Sicula formations are interpreted to be

the proximal and distal facies, respectively, of the Miocene foredeep formed during the Serravallian-Tortonian (BASILONE, 2012).

Through the well-log calibration, reflector T was associated to the passage from the conglomeratic to the sandy-pelitic member within the Terravecchia fm., dated to ~ 8 Ma, i.e. Tortonian, (BASILONE, 2012). At this time, the activity of ATS ended (Fig. 3.25).

3.3.4.3   *Transcurrent belt*

The south-eastern sector of the study area corresponding to the offshore between Mazara del Vallo and Sciacca is affected by a transcurrent belt that represents the link between the western and eastern segment of the SFTB (ARGNANI et al., 1986; ANTONELLI et al., 1988; ARGNANI, 1990, 1993a, b; GRASSO, 2001), redefined as a transfer zone by CIVILE et al. (2014). We maintain this terminology to design the ~ N-S trending tectonic features recognized in this area (Figs. 3.15, 3.26), but we present a partly different interpretation.

The area is characterized by an intense Miocene extensional deformation expressed by ~ 7 km long, NNW and SSE dipping normal faults, with a dip of ~ 80°. These faults (MF1 and MF2, Fig. 3.27) dissected the Mesozoic-Paleogene Trapanese carbonate succession creating accommodation places completely filled by seismic sequence S4.

The high amplitude reflector T (~ 8 Ma), previously described, marks the onset of MF1 and MF2 fault inversion within the Mesozoic-Paleogene Trapanese bedrock (see also Fig. 3.25). The extensional activity of the faults was most contemporaneous to the emplacement of the ETS and ATS; during the Tortonian-Early Pliocene they were reactivated as reverse faults producing a mild basin-wide inversion (Fig. 3.27).
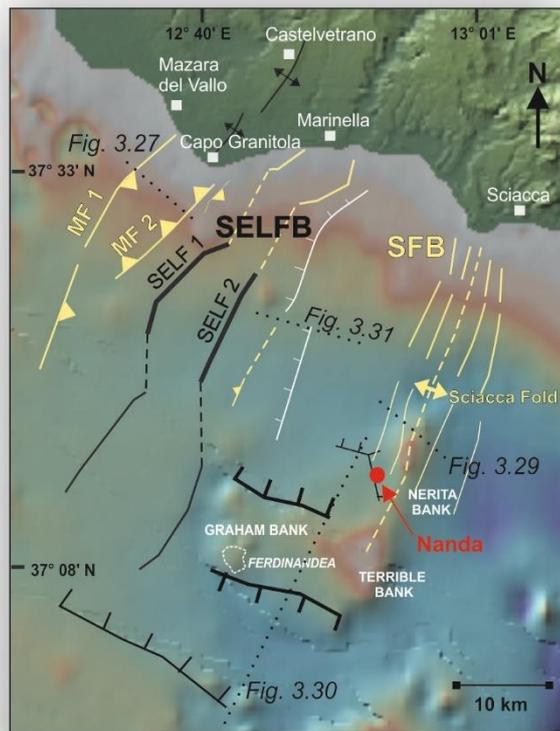
Fig. 3.26 – Zoom of Figure 3.15 focusing on SELFB and SFB. For the key to structural symbols, see fig. 3.15.
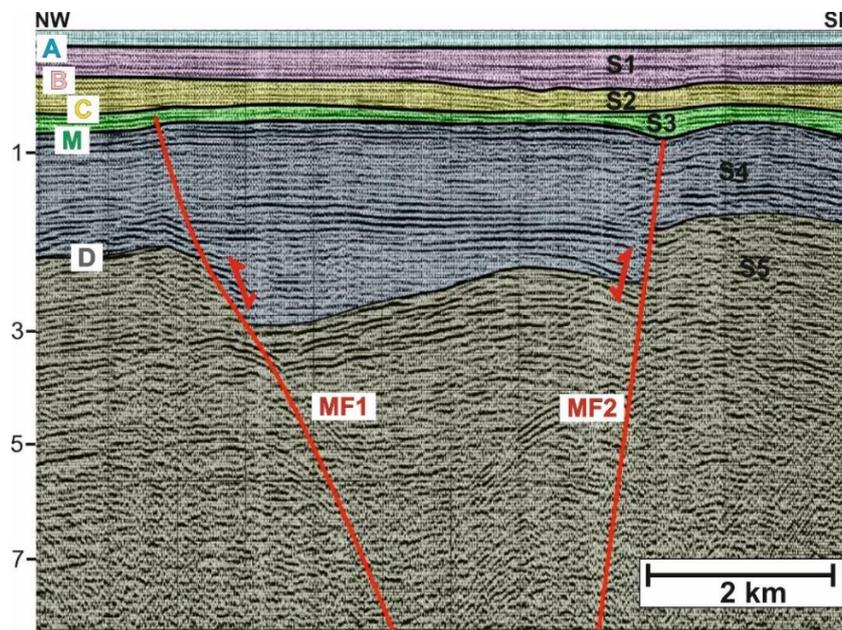

Fig. 3.27 – Sketch of profile ZC-106 showing Miocene normal faults which inverted their movement during the Late Miocene-Pliocene. The vertical scale indicates the depth in kilometers. For location see figure 3.26.

Toward the south-east, the fault reactivation occurred during the Pliocene-Pleistocene, and can be associated to two structural arrays: SELFB (Selinunte Fault Belt) and SFB (Sciacca Fault Belt) (Figs. 3.15, 3.26).

- *SELFB*

SELFB is represented by two arrays of transpressional faults (SELF1 and SELF2) with a NNE-SSW trend extending from offshore Marinella to the western side of Graham bank, and limited to the south by the extensional faults of the Pantelleria system (Fig. 3.26). Each array is characterized by three fault segments that are arranged en echelon with a left step-over pattern. In detail, the arrays have a cumulative length of ~ 50 km (SELF 1) and ~ 55 km (SELF 2), and a spacing variable between ~ 5-13 km. The fault system becomes less evident toward the south and vanishes on approaching the extensional structures of Pantelleria rift (Figs. 3.15, 3.26).

The main structural expression of the SELF is found in the vicinity of Capo Granitola coast, where a remarkable positive structure is present. The structural high is bordered by the two faults expressed in the profiles as high angle reverse faults with a length of ~ 7-8 km (Fig. 3.28).

The observation that S4 thickens within the high respect to lateral sides where thickness decreases, supported by calibration from Carla well that documents ~ 1600 m of Miocene deposits in the central high, suggests that the high was a Miocene graben bounded by extensional faults, where S4 accumulated. The basin was then inverted creating the positive structure. The inversion started during the Pliocene as documented by growth of reflectors pertaining to S3 (Fig. 3.28), producing a ~ 5 km wide anticline. However, the resulting feature is characterized by faults that retain net extension at depth and show net contraction associated with anticline growth in the upper portions. Such feature indicates partial structural inversion of faults, along which the contractional movements were arrested or decelerated, and did not balanced the previous extensional slip (WILLIAMS et al., 1989).
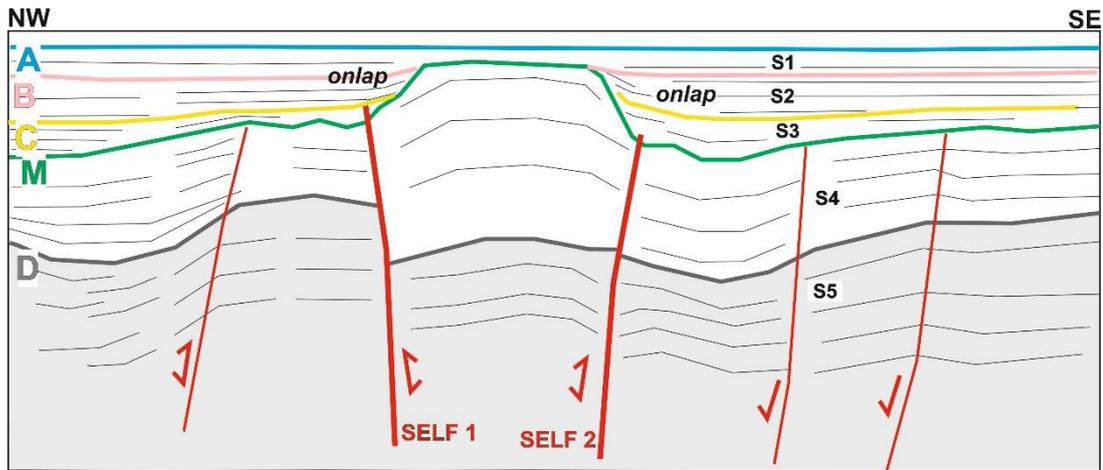
Fig. 3.28 – Line drawing of a seismic reflection profile from ENI database showing the inverted push-up structures. The exact location of the profile cannot be shown for reasons of confidentiality.

As suggested by well-log analysis, the SELF is also responsible of separation between the Trapanese and Saccense domains (see paragraph 3.2.3). Hence, by calibrating seismic profiles with information gathered by well-log, we distinguished in the Terravecchia foredeep a proximal shelf facies in the NW from a distal ramp facies in the SE. The former facies shows higher thickness and is imaged by chaotic seismic facies varying to more regular, high amplitude, low frequency at the top and semi-transparent at the bottom (Figs. 3.14, 3.24). The ramp facies is expressed by relatively minor thickness and by regular and parallel reflections (Figs. 3.14, 3.29).

• *SFB*

The Sciacca Fault Belt is a NNE-SSW trending array, which extends in the offshore of Sciacca toward the Nerita bank. The array is characterized by en echelon folds and faults for a length of ~ 27 km and a width of 6 km (Figs. 3.15, 3.26).

Positive flower structures associated to the fault system (Figs. 3.29, 3.33) are characterized by fan-like, rather steep faults converging at depth into a single, sub-vertical fault which represents the main fault (the stem). The seismic profiles image a shallow antiform displaced by the upward diverging

strands of a wrench fault with reverse separations (Fig. 3.29). The upward-diverging faults exhibit a convex upward geometry.
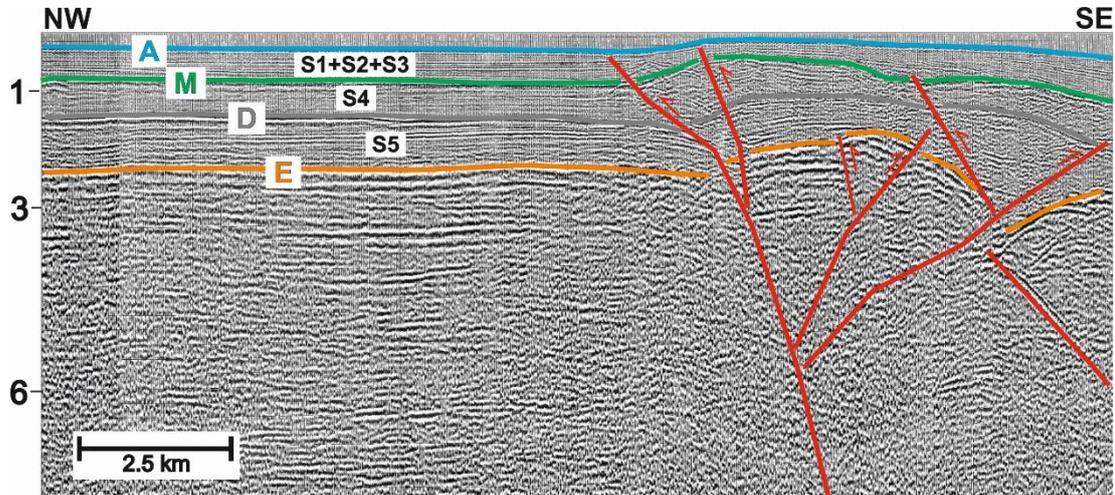

Fig. 3.29 – Portion of profile C-1007 showing a positive flower structure pertaining to SFB. The vertical scale indicates the depth in kilometers. For location see figure 3.26.

Nearby Nerita and Terrible banks the flower structures are less evident because of the interference with negative structures related to the Pantelleria rift (Fig. 3.26, 3.30) becoming predominant south of the banks. The extensional faults are associated to widespread fluid ascent and occasionally to volcanic centres (Fig. 3.31). The volcanism is predominant in the Graham and Nameless bank, whose structural evolution cannot be detailed as seismic images are obscured by presence of volcanic materials. Nevertheless, the WNW-ESE trending bank-bounding faults with a normal component of the movement are visible (Fig 3.30).

As for SELFB, we speculate the SFB derives from reactivation of inherited normal faults, suggested by the fact that during the Miocene the area was affected by extensional faults that at places gave rise to magma ascent. As documented by growth strata in sequence S3, these faults were reactivated as transcurrent during the Pliocene-Pleistocene (Fig. 3.29).
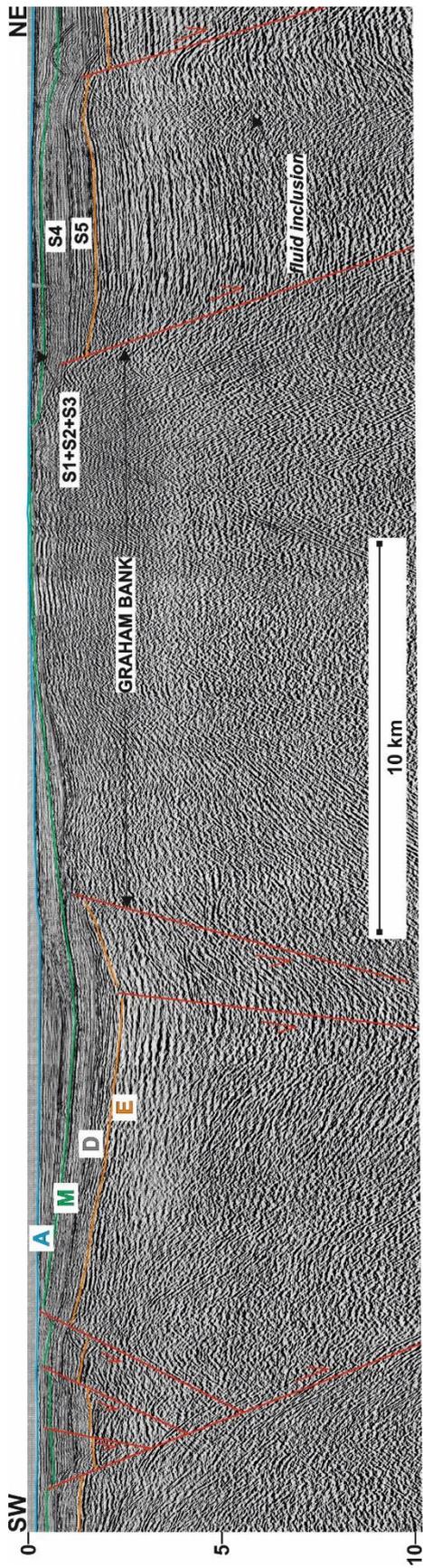
Fig. 3.30 – Sketch of profile G-140 showing the Graham Bank and the negative structures related to Pantelleria rift. For location see figure 3.26.

101
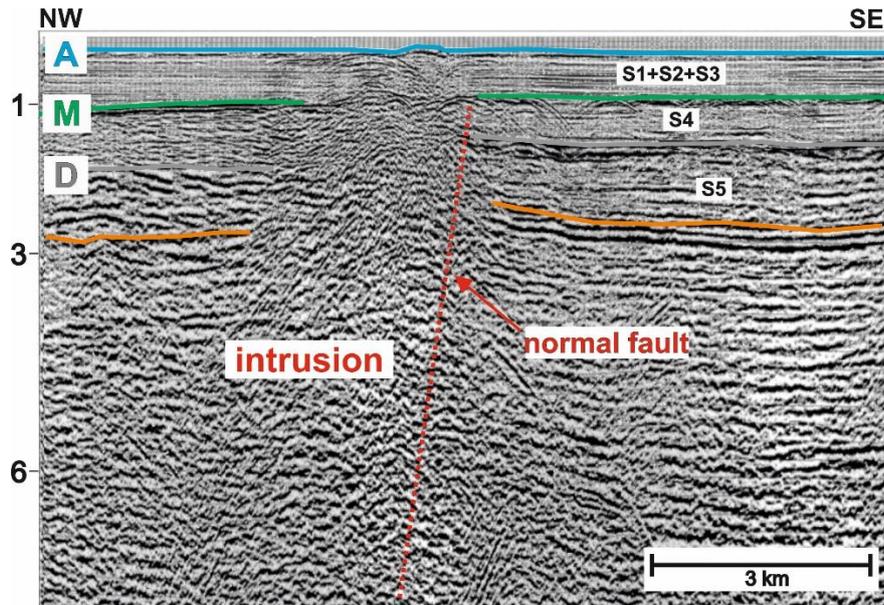
Fig. 3.31 – Sketch of profile G-140 showing magma ascending in the offshore between Capo Granitola and Sciacca along a normal fault. The offset of horizon D and the presence of magmatic materials in sequence S3 date fault activity to Miocene. The vertical scale indicates the depth in kilometers. For location see figure 3.26.

3.3.4.4   Gela Nappe

East of the SFB, the SW-vergent Gela Nappe (GN) extending ~ 10 km offshore Sciacca-Eraclea Minoa coasts, is present (Fig. 3.15, 3.32). The analyzed part of the GN (its northwestern part, ~ 30 km long) shows an arcuate shape in map, with a N-S trend near Sciacca and with a NW-SE trend toward the south-east.

The GN represents the most external and youngest thrust front of the SFTB, and the analysis of ENI profiles allowed to perform its detailed location and characterization.

The seismic images depict a convex wedge-shaped body thickening northward where shows a maximum thickness of ~ 2 km, resulting from processes of tectonic accretion. The internal reflection pattern of GN is represented by a chaotic geometry marked by discontinuous reflections of variable amplitude, interpreted as imbricated thrusts limiting packages of folded and disrupted deposits. Well-log calibration (Zagara, Venere, Pina wells projected on the seismic line of Fig. 3.33) suggests a Miocene age of the

deposits that were detached from their substrate and transported toward the SW during the Plio-Pleistocene (Argnani et al., 1986; Argnani ,1987; Antonelli et al., 1988).
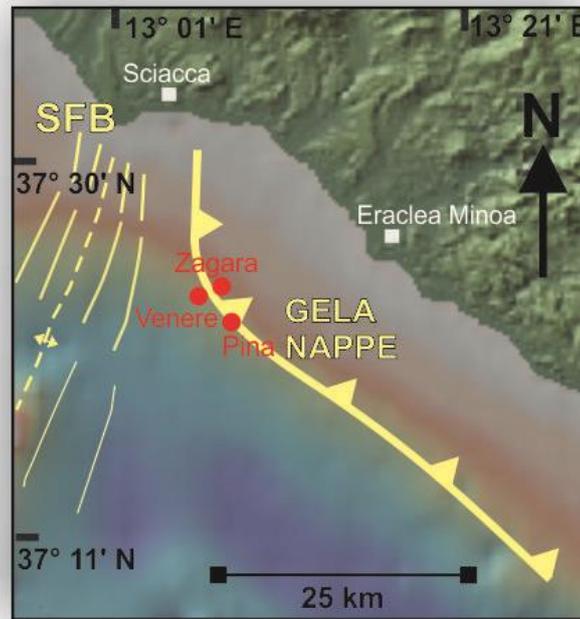

Fig. 3.32 – Zoom of of Figure 3.15 focusing on GN. For the key to structural symbols, see fig. 3.15.

The base of the allochthonous body has been picked at the boundary between nonreflective and reflective units and maintaining a maximum thickness of ~ 2 km in the central part consistent with log information (Ghisetti et al., 2009).

The GN is faced seaward by a foredeep basin (Gela Foredeep, GF) that shows a maximum thickness of 3000 m (Fig. 3.33). The Plio-Pleistocene infilling of the basin is associated to the emplacement of GN as suggested by the growing wedge-shaped geometry with an increasing thickness and divergent fanning strata down to the dip slope of the tilted fault blocks (Fig. 3.33). Further, the folded geometry and the lateral detachment of shallow landslides of S3 and S2 at the top of the GN (Fig. 3.33) suggest that tectonic

movements took place during the Pliocene-Pleistocene. Thus, emplacement of the GN is largely coeval to activity of the SFB and probably the westward propagation of the nappe was driven by the presence of a structural low related to SFB.
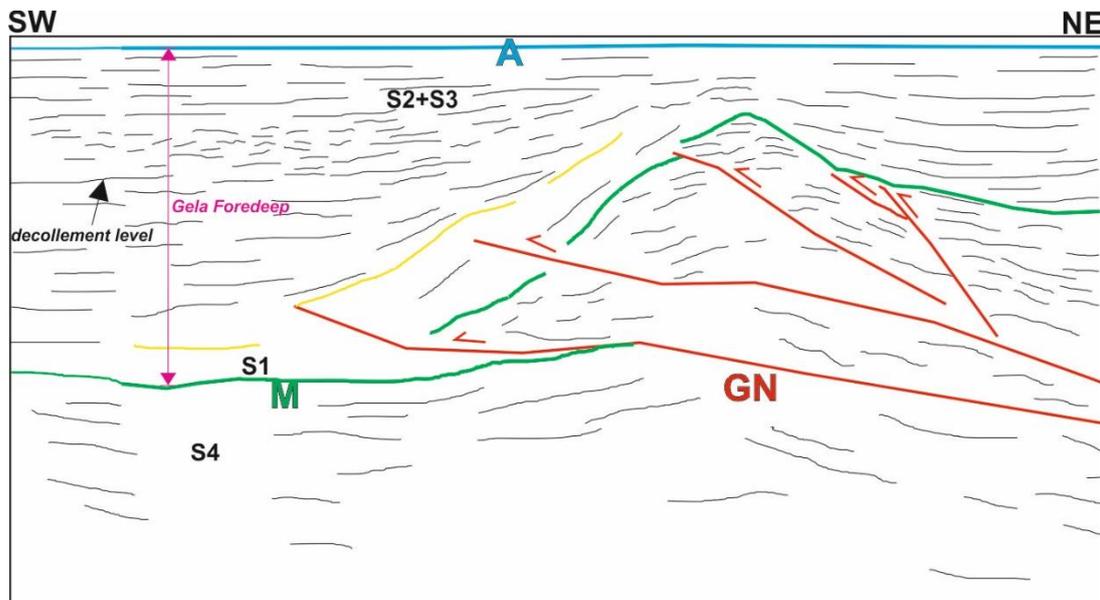

Fig. 3.33 – Line drawing of a seismic reflection profile from ENI database showing the Gela Nappe. The exact location of the profile cannot be shown for reasons of confidentiality.

3.3.4.5 *Extensional faults of the Pantelleria rift*

The southernmost sector of the study area is occupied by the Pantelleria rift (Fig. 3.15, 3.34). Deformation of this area was only analyzed on three seismic lines by ENI. The goal was to describe the main structural features responsible of the extensional basin formation.

The seismic data point out an asymmetric through with a width of ~ 7 km and a depth of ~ 800 m below the sea level north of Pantelleria (Fig. 3.35) becoming ~ 20 km wide and with a depth of ~ 1 km south of the island (Fig. 3.36).

In figure 3.35 the north-eastern flank of Pantelleria Island is visible in the left, bordered by a NE dipping fault. This fault together with antithetic SW-dipping faults toward the NE limit a V-shaped half-graben basin filled by Plio-

Pleistocene deposits. The faults show a domino-style configuration with half-grabens separated by modest NW-trending lineaments and with variable offset between ~ 300 m and ~ 1 km.

Shallow and widespread magmatic bodies mask the base of the Plio-Quaternary succession within the central part of the graben (Figs. 3.35, 3.36).
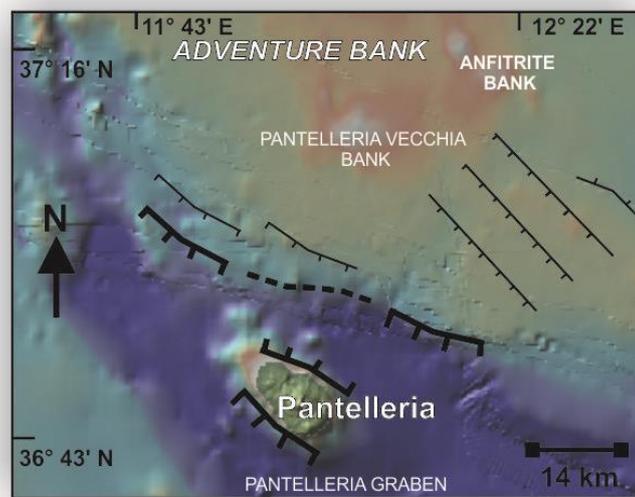

Fig. 3.34 – Zoom of Fig. 3.15 showing the Pantelleria rift system.
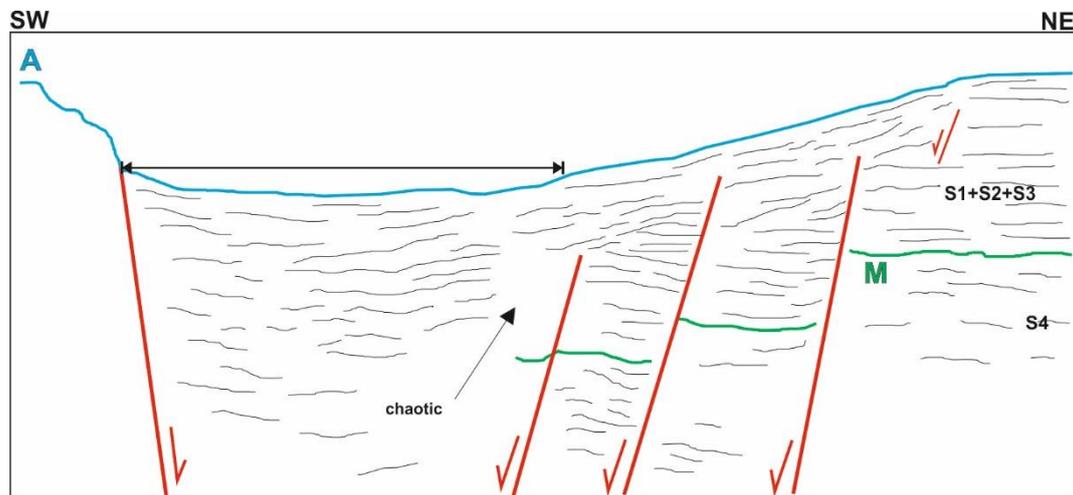

Fig. 3.35 – Line drawing of a seismic reflection profile from ENI database showing the north-eastern flank of Pantelleria affected by extensional faults which originate a V-shaped half graben. The exact location of the profile cannot be shown for reasons of confidentiality.
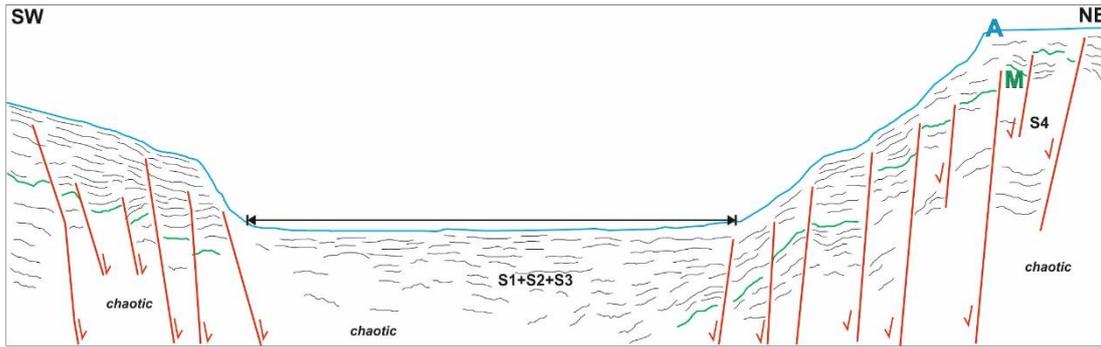
Fig. 3.36 – Line drawing of a seismic reflection profile from ENI database showing the central part of the Pantelleria graben where the Plio-Pleistocene strata are masked by magmatic bodies characterized by chaotic seismic facies. The exact location of the profile cannot be shown for reasons of confidentiality.
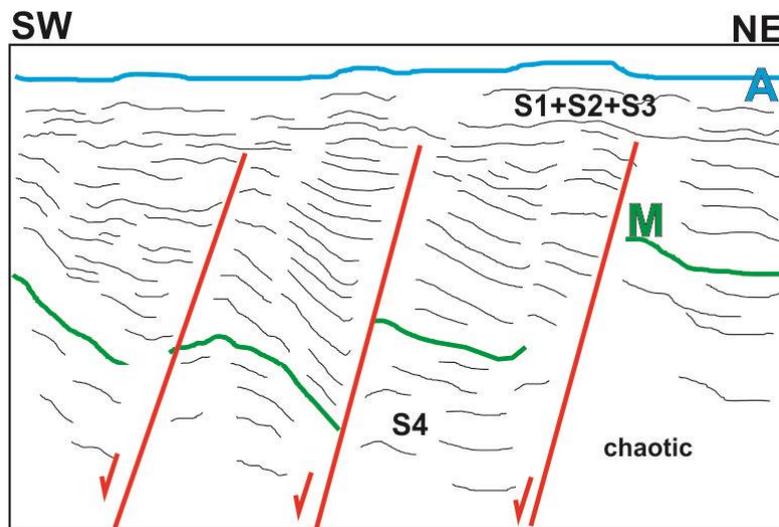
Fig. 3.37 – Line drawing of a seismic reflection profile from ENI database showing the normal faults of Pantelleria rift system and strata growth in the seismic sequence S3. The exact location of the profile cannot be shown for reasons of confidentiality.

Growth strata in sequence S3 (Figs. 3.35, 3.36, 3.37) supports an Early Pliocene age for commencement of fault activity. Within the basin we distinguish: a succession, corresponding to the Terravecchia Formation, defined by sub-parallel reflectors that have been tilted by normal faults; a syn-rift sequence, mostly represented by the acoustically semi-transparent Early Pliocene deposits, and showing fault-related thickness changes (a growth wedge-shaped geometry); a late-rift to post-rift succession, probably Late

Pliocene–Quaternary in age, characterized by sub-parallel reflectors that drape the morphology below.
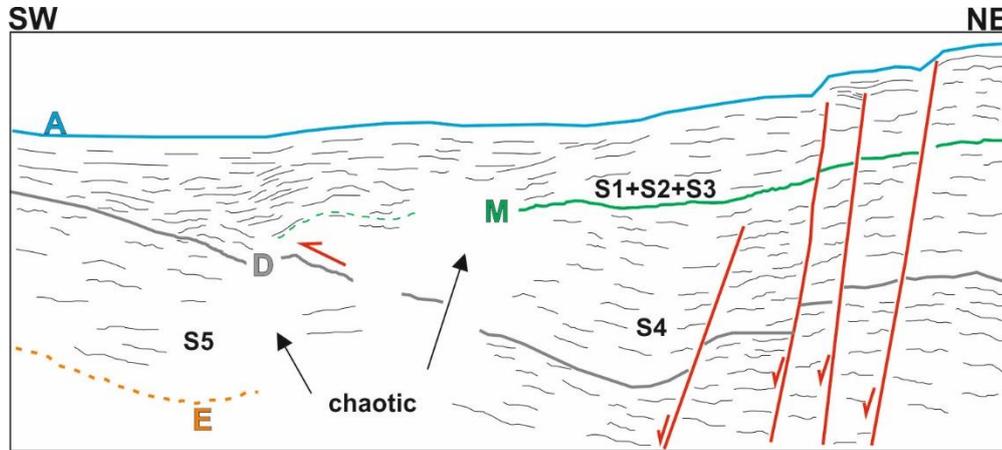
*Fig. 3.38 – Line drawing of a seismic reflection profile from ENI database showing the extensional faults of Pantelleria system with a rollover anticline shaped by horizon D. A reverse reactivation of the Plio-Pleistocene sequence is also visible. The exact location of the profile cannot be shown for reasons of confidentiality.*

South of Pantelleria, SW-dipping faults and anticlines are also present (Fig. 3.38). The seismic sequence S3 is segmented by NE-dipping normal faults in the footwall block where a gentle antiformal geometry is also recognized (Fig. 3.38), and probably arising from a local reverse reactivation of normal faults.

3.3.5 Structural analysis

A structural analysis of the lineaments (folds and faults) located in the offshore between Capo Granitola and Sciacca was made in order to estimate fold and fault parameters. This analysis will be then integrated with that performed using high resolution single-channel seismic data (see chapter IV).

3.3.5.1   Selinunte Fault Belt

The analysis computed for faults SELF 1 and SELF 2 was based on the measurements of fault displacement, dip angle, length and trace length (Tables

107

3.1, 3.2). Fault displacements recorded by offset reflectors were measured for horizon M in order to evaluate post-Miocene deformation. Dip angles were estimated using the linear tool of GeoSuite obtained by tracing the fault and reading the automatic calculated value. The fault length (also known as downdip length or width) corresponds to tip-to-tip straight-line distance, calculated as the difference from the maximum and minimum depth at which the fault appears in each profile. Hence, the fault length is the longest dimension along the fault plane. The fault trace length is the exposed fault length on an arbitrary (sub)-horizontal plane (KIM & SANDERSON, 2005), and was estimated using a graphic method explained later. In addition, the last deformed seismic sequence was annotated.
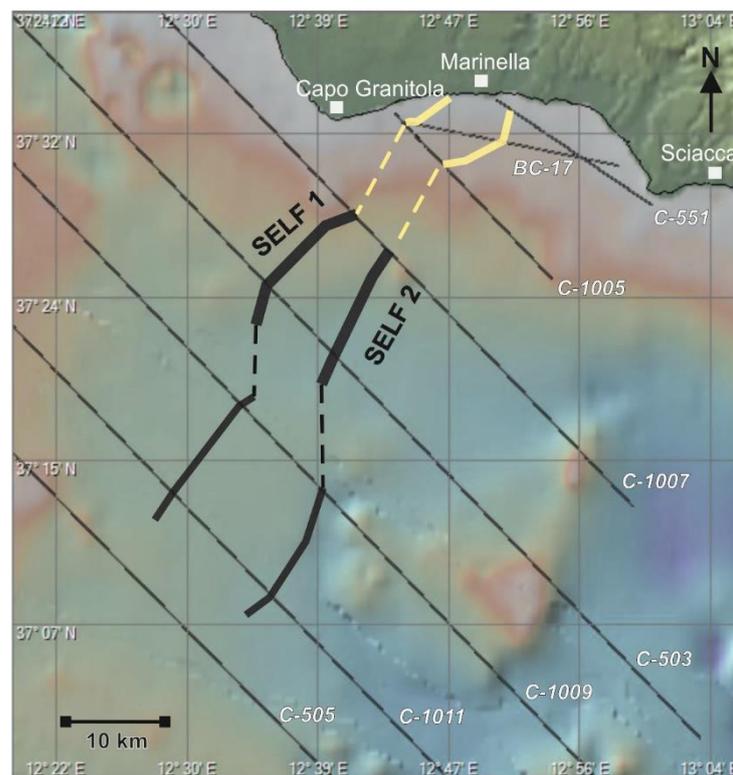

Fig. 3.39 – Bathymetric map with location of SELFB and crossing profiles.

Our estimations rely on seismic images recording up to 5 s TWT on average, the resolution of the seismic horizons offset is generally good down to ~ 5 km, and tentatively traced up to 9 km.

The listed displacement values were plotted in the graphs of figures 3.40, 3.41, 3.43 with respect to the distance from the coast of the seismic lines imaging the analysed faults (Figs. 3.39, 3.42). Thus, we are computing displacements along the trace length of the faults and not normal to the faults, focusing on the extent of the structure rather than on the spatial dimension across the fault where displacement accrues.

TABLE 3.1

| Id_line	Displacement (m) *Horizon M*	Min depth (m)	Max depth (m)	last deformed seismic sequence	dip (°)	Fault length (m)	Distance from the coast (km)
BC-17	126	1280	9000	S3	279°	7720	4,4
C-1005 ext	142	1430	9000	S3	279°	7570	13,83
C-1007	221	620	9000	S3	284°	8380	22,3
C-503	200	812	9000	S3	280°	8188	32,9
C-1009	90	953	9000	S3	277°	8047	42,7
C-1011	50	340	9000	S3	298°	8660	53,3
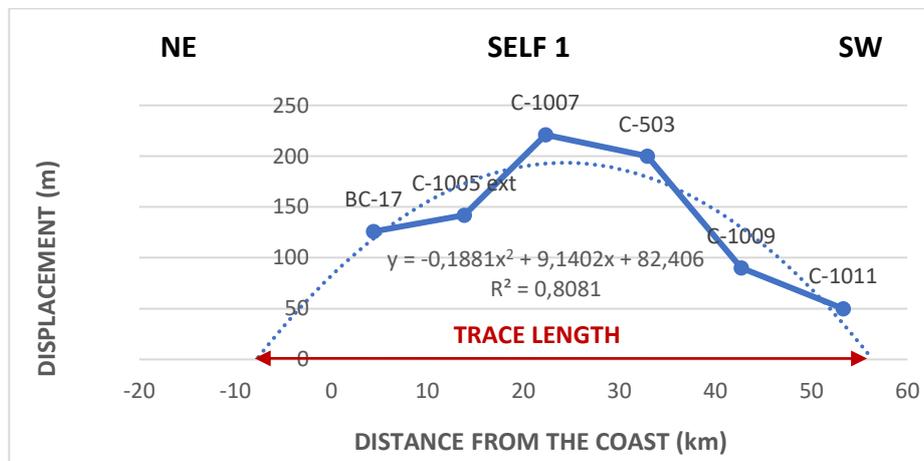
Fig. 3.40 – Graph of displacement vs. distance from the coast for horizon M relative to SELF1.

In general, the graphs depict a data distribution with a bell-shaped curve, meaning that displacement is greatest at or near the centre of the fault and decreases toward the fault tips. This geometry is predicted by COWIE & SCHOLZ'S (1992) model of faulting. In particular, the maximum value of

displacement in the central part of SELF1 and SELF2 is recorded on lines C-1007 and C-503.

The graph of figure 3.40 shows the fault displacement measured along horizon M for fault SELF1. The bell-shaped curve is not complete, because not all the fault has been sampled by available profiles. We used the 2nd order polynomial trendline automatically generated in Excel starting from plotted data to obtain a prediction of real fault length (dashed line in Figs. 3.40, 3.41). Hence, the trendline should approximate the complete bell-shaped curve. The end members of the curve where the values are equal to zero should correspond to the fault tips, so that the scaled distance between them would represent the fault trace length. The derived trace length of the fault measured from the tips (Fig. 3.40) is ~ 60 km.

The trace length of fault SELF2 derived from the analysis of fault displacement measured along horizon M (Fig. 3.41) is equal to ~ 55 km.

TABLE 3.2

Id_line	Displacement (m) *Horizon M*	Min depth (m)	Max depth (m)	last deformed seismic sequence	dip (°)	Fault length (m)	Distance from the coast (km)
C-551	53	1590	9000	S3	285°	7410	4,4
BC-17	45	1130	9000	S3	280°	7870	7,22
C-1005	50	1170	9000	S3	292°	7830	12,743
C-1007	88	960	9000	S3	279°	8040	22,293
C-503	80	1140	9000	S3	276°	7860	32,923
C-1009	48	570	9000	S3	276°	8430	42,713
C-1011	20	531	9000	S3	293°	8469	53,313
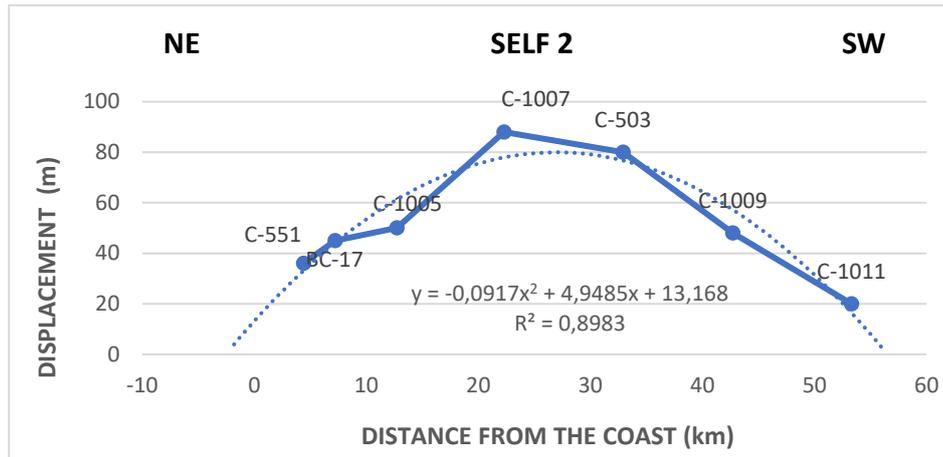
Fig. 3.41 – Graph of displacement vs. distance from the coast with respect to horizon M relative to SELF2.

The above graphs reveal that the two faults should continue of few km toward north-east and south-west. More in detail, SELF1 and SELF2 should be up to ~ 3-4 km longer toward the south-west in direction of the central part of the Channel. However, this continuance cannot be detected by profiles because this would require a distance minor than of that of the closer crossing profile which is ~ 7 km away (Line C-505 in Fig. 3.39). Instead, a ~ 5-10 km north-eastern prolongation toward Sicily mainland can be estimated for both faults.

The R^2 parameter that expresses the coefficient of determination of the 2nd order polynomial regression, depicted by the trendlines (figs. 3.30 and 3.31), is positive and ranges from ~ 0.5 to ~ 0.9. Taking into account limitation of data frequency and resolution, our R^2 parameters are acceptable, because values approaching the unit suggest a good data correlation.

3.3.5.2   Sciacca Fault Belt

The structural analysis dealt with the measure of maximum elevation recorded in the uplifted antiformal area associated to the positive flower structure visible along the seismic profiles in the offshore of Sciacca (Fig. 3.29). The fold amplitude was measured by taking the distance along the axial plane from the anticlinal hinge to the surface enveloping the two adjoining

synclinal hinges. The measures are relative to horizon M in order to obtain an estimation of post-Miocene deformation.

The measured values were listed in Table 3.3 and projected on a graph (Fig. 3.43) as a function of distance from the coast.
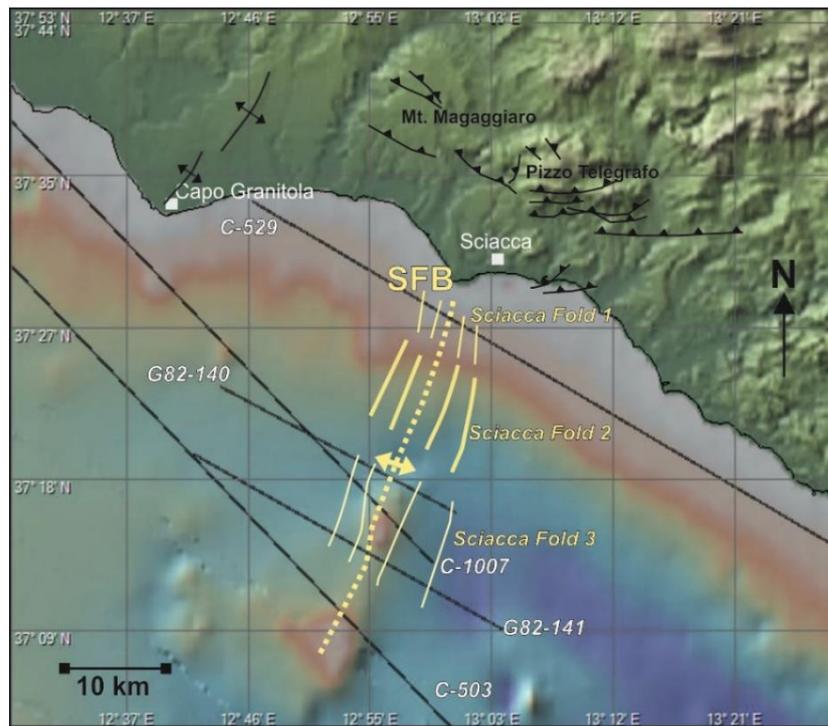
Fig. 3.42 – Bathymetric map with location of SFB and crossing profiles. The on-land structures near Sciacca are also reported (from MONTANARI et al.,2015).

Table 3.3

SCIACCA FOLD		
Id_line	Fold amplitude (km)	Distance from the coast (km)
C-529	1,4	3,71
C82-111	1,1	4,6
CNW 103 01	0,7	5,23
CNW 103 02	0,9	8,55
CNW 103 03	1,1	10,51
G82-140	0,5	21,19
C-1007	0,6	23,83
G82-141	0,8	29,09
C-503	0,4	34,99
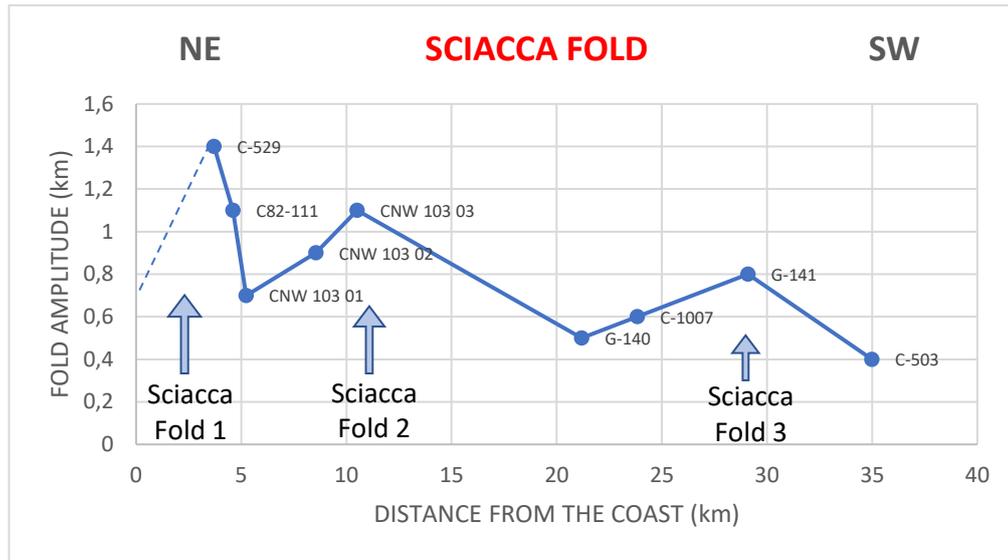
Fig. 3.43 – Graph fold amplitude vs. distance from the coast for Sciacca Fold.

In the case of a fault, the bell-shaped curve highlights fault amplitude with a maximum central value located near the middle of the underlying fault plane, and the minimum at both tips (SCHWARZ & COPPERSMITH, 1984). Similarly, in the case of a fold, the longitudinal variation of fold amplitude can be used to estimate the fold trace-length, based on the assumption that when the curve is not complete, the fold is not completely sampled and should continue outside the investigated area.

The results evidence a curve characterized by three longitudinally parallel folds named Sciacca Fold 1, Sciacca Fold 2 and Sciacca Fold 3 (Fig. 3.43), showing two complete (SF2 and SF3) and one undersampled (SF1) bell-shaped geometries. In the segment to the NE (SF1), only one side of the bell-shaped feature is present. This may suggest a north-eastward prolongation of the structure, not detected because of lack of further seismic profiles approaching the coast. The fact that the folds have bell-shaped longitudinal profiles suggests the existence underneath of laterally defined fault segments of broadly the same trace length. Based on this assumption, the lateral change in fold amplitude allows to estimate the corresponding variation in deformation accommodated on individual fault segments and to search for the

position of segment boundaries. The comparison shows a south-westward reduction of fold amplitude.

If we consider Sciacca Fold 2 and Sciacca Fold 3, the amplitude difference between folds is of 0.3 km. Assuming the same value for the amplitude difference between Sciacca Fold 1 and Sciacca Fold 2, 1.4 km (which corresponds to maximum recorded value) can be considered as the maximum value of fold amplitude among the three folds.

Taking into consideration this analysis, we can attribute to the three folds the meaning of en echelon arranged folds. In this perspective, the two minor values recorded among the three folds may represent the locus of separation between two adjoining fault segments.

Nevertheless, it could be also probably that the transpressive system is incompletely sampled if compared with Capo Granitola system. In this case, the system should continue for about 35 km in the NE beneath Magaggiaro-Pizzo Telegrafo in Sicilian mainland (Fig. 3.42).

3.3.5.3   *Isopach maps*

An isopach map is a map showing the spatial distribution of a unit thickness. In the case of a map generated by seismic horizons, the map enhances the visualization of geomorphologic and depositional elements of specific paleo-depositional or erosional surfaces. If the interpretation of seismic reflections is correct, these horizon slices should be very close to time lines, providing a snapshot of past depositional environments (CATUNEANU, 2006). Such maps yield the best image of the complete depositional system adding important information regarding the subsidence-uplift history and the structural style of the studied area.

Picking of seismic horizons which bracket homogeneous seismic facies allowed to generate isopachs maps. The GeoSuite software supports the definition and visualization of isopach maps calculated from the horizons defined in the project, by choosing the first and second horizons of interest. By

computing depth differences of two selected horizons, the thickness distribution of the intervening seismic facies is given. The interpolation principally depends on the distance between seismic lines used to map the horizons: the greater is the distance, the lesser is the accuracy of the reconstruction.

We built two isopach maps (Figs. 3.44, 3.45) relative to the seismic facies bracketed between horizons M-D and A-M in order to evaluate the thickness changes of Serravallian-Messinian (Middle-Late Miocene) and Plio-Pleistocene deposits, respectively. We choose these two intervals because they represent the timing of the building up of the chain, which started during the Miocene in the NW part of the study area, and persisted in the Plio-Pleistocene in the central and the SE part.

Finally, we built a third isobath map by using as input horizons A and D (Fig. 3.46). Hence, the map reveals the thickness of the entire package of seismic sequences bracketed between the two horizons. It images the depth of Paleogene basement as horizon D marks the base of Miocene sediments. The Paleogene basement represents the pre-orogenic carbonate units underlying the syn-orogenic clastic rocks. Hence the map offers a quick view of the structural frame resulting from the deep-cutting faults. We are aware that several non-rigid formations occur between the Lattimusa fm. and the base of the Terravecchia fm. (such as San Cipirello fm.), we have nonetheless incorporated them in the bedrock map construction. In fact, with the existing well calibration and the marked lateral variations in thickness of these formations as evidenced in the paragraph 3.2.3, we were forced to group them with the underlying rigid carbonate bedrock.

The maps, automatically generated by the software, were smoothed and redrawn using the graphic software CorelDRAW X7. The constraints are represented by punctual well-log information.
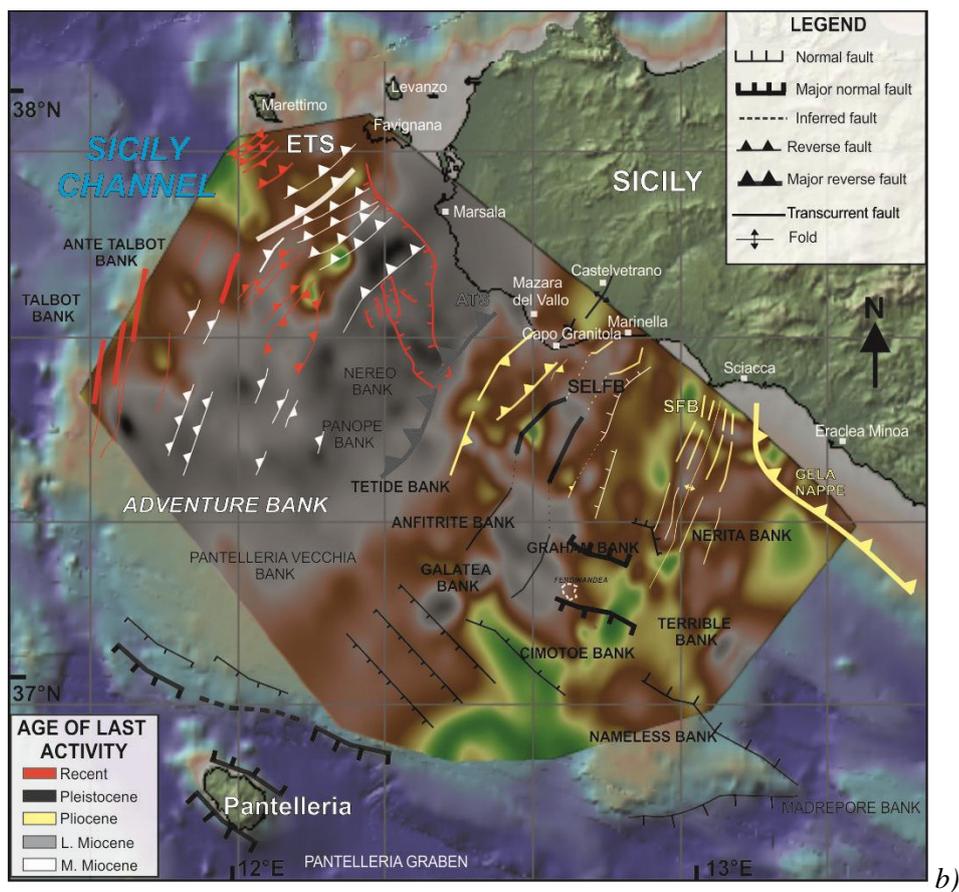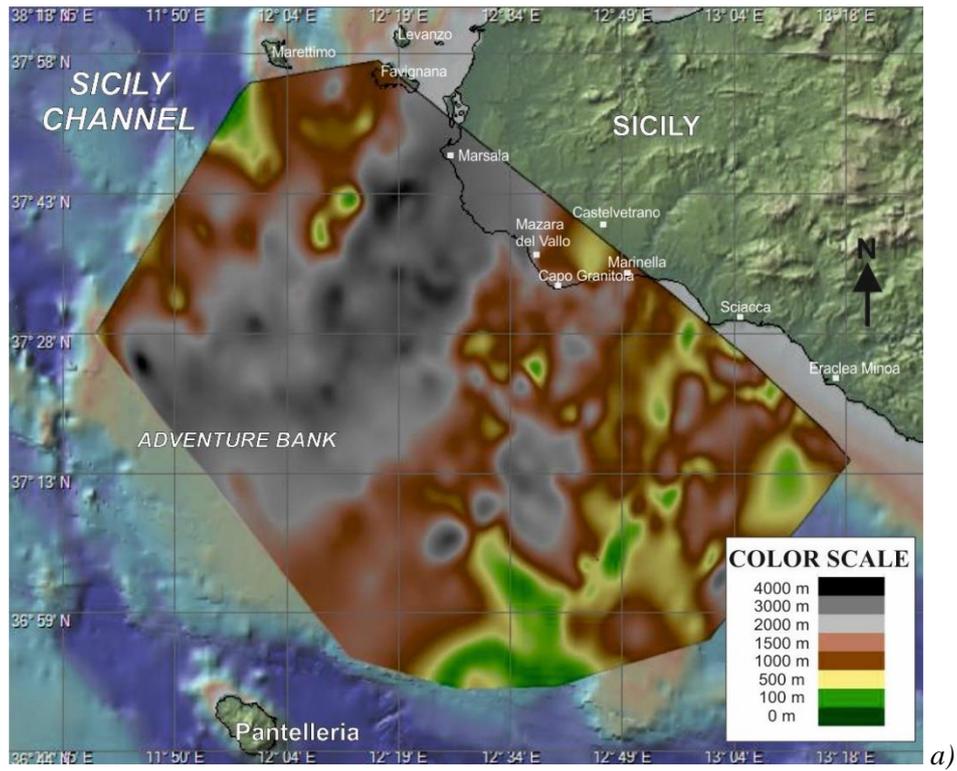
Fig. 3.44 – a) Isopach map of the Miocene sediments b) with overlaps of structural features of Figure 3.15.

116
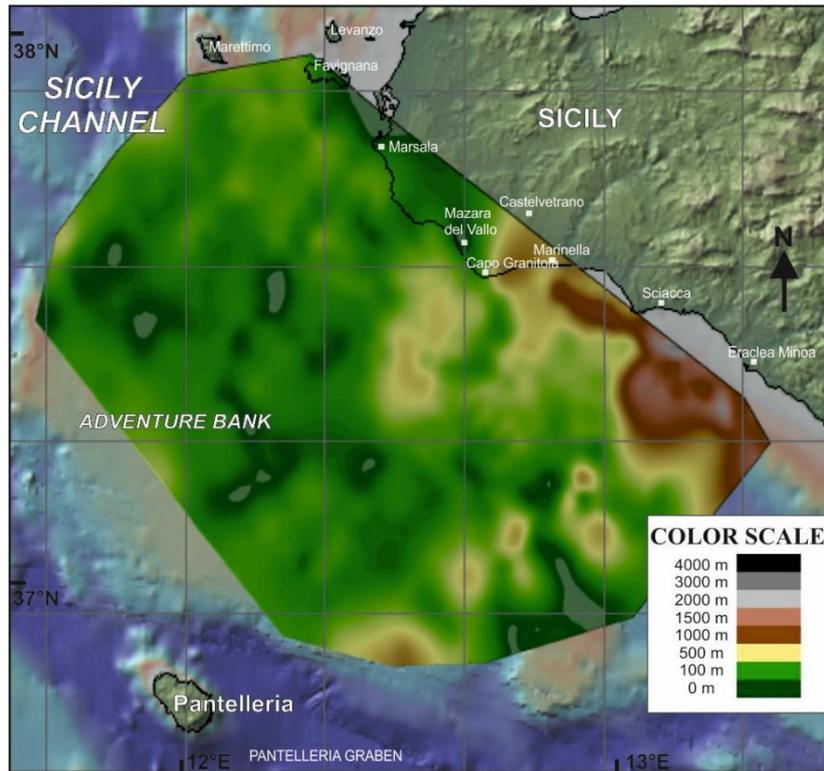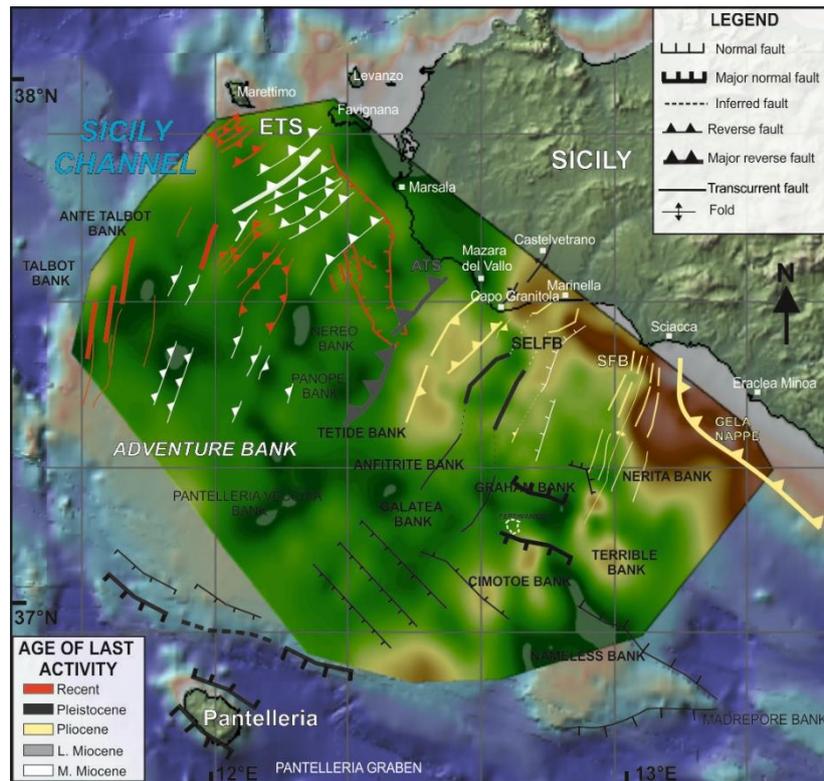
Fig. 3.45 – a) Isopach map of the Plio-Pleistocene sediments b) with overlaps of structural features of Figure 3.15.

Figure 3.44 shows the thickness distribution of seismic sequence S4 which embraces Serravallian-Tortonian sediments pertaining to Castellana Sicula, Terravecchia, and Gessoso-solfifera formations (Figs. 3.9, 3.13).

Starting from the north-western sector of the Channel, areas of low thickness are visible highlighting the presence of structural highs above which minor deposition of Middle-Upper Miocene sediments occurred. This distribution is related the compressive activity of the ETS (figure 3.15). Conversely, in the adjacent area, the seismic unit exhibits the maximum thickness of up to ~ 3500-4000 m.

The NE-SW trending depocenter extends on the Adventure bank from Marsala to Mazara del Vallo offshore and is associated to the Miocene foredeep of SFTB, as proposed by ARGNANI et al. (1986).

Toward the south-east, the Upper Miocene sedimentary body decreases in thickness as already evidenced by well-log analysis (Fig. 3.5). However, locally in the area between Capo Granitola and Eraclea Minoa, secondary basins of Miocene sediments are individuated. These basins are bounded by structures that show a Plio-Pleistocene activity.

Taking into account the thickness distribution of the Pliocene-Pleistocene deposits of figure 3.45, an inversion of previous depocenters and highs can be noted. The area of the Channel floored by the Adventure bank, which formed the depocenter of Miocene syn-orogenic deposition, is characterized by minor deposition during the Pliocene-Quaternary. Thus, the bordering faults of Miocene basins were re-activated in compression during the Pliocene-Pleistocene, as documented by seismic images. In general, the thickness of the Pliocene-Pleistocene sediments, grouped in seismic sequences S3, S2 and S1, remains quite constant (about 100-200 m) except for the offshore area between Sciacca and Eraclea Minoa where the thickness reaches values of 2000 m. This increment is related to the presence of the Gela foredeep ahead of the GN (Fig. 3.15).

Moreover, also toward Pantelleria there are increments in the thickness of deposit reaching ~ 1-1500 m (Fig. 3.45), that are related to the infilling of Plio-Pleistocene grabens of Malta, Linosa and Pantelleria.

The map of the pre-Miocene bedrock (Fig. 3.46) shows maximum and minimum values in the same areas of Figure 3.44a, except for the Sciacca offshore zone where the isobaths increase their depth. Even if they are similar, the two maps give different information. While the map of Figure 3.44a indicates the thicknesses of the Miocene foredeep basin, the map of Figure 3.46 images the depth of the entire sedimentary succession from Recent to Miocene sediments with respect to the sea bottom, i.e. the depth at which the Paleogene sediments appear.

The maxima and minima distribution has a good spatial coincidence with the structures inferred from seismic interpretation, underlining that this marine zone is strictly controlled by the tectonics and associated phenomena. In particular, we note the control exercised on pre-Miocene bedrock uplift in the ETS area by Miocene thrust faulting; the control exercised in the SE by Miocene-Pliocene extensional faults; the striking limit represented by the Sciacca Fault Belt on the eastern side of a N-S trending bedrock ridge, which separates the ridge from the deep bedrock low in front of the Gela Nappe. Comparison between the bedrock and the Miocene isopach map indicates that the structural framework of this part of the Chanel shaped during Miocene interplay between extensional, contractional, and transpressional tectonics. Pliocene-Pleistocene deformation of the pre-Miocene bedrock was particularly vigorous south of Sciacca and in front of the Gela nappe.
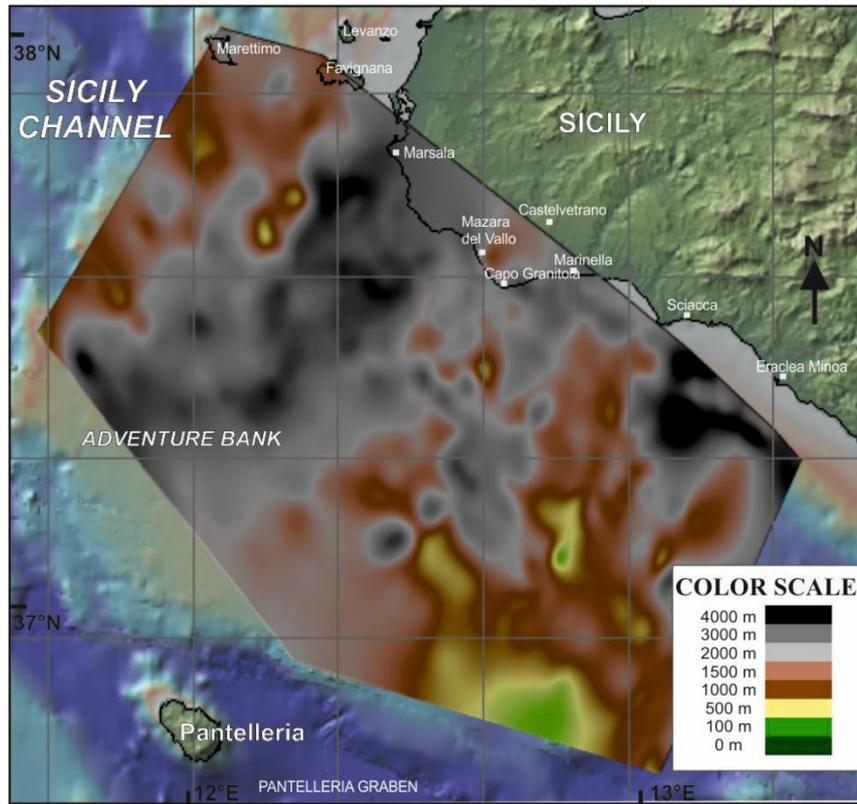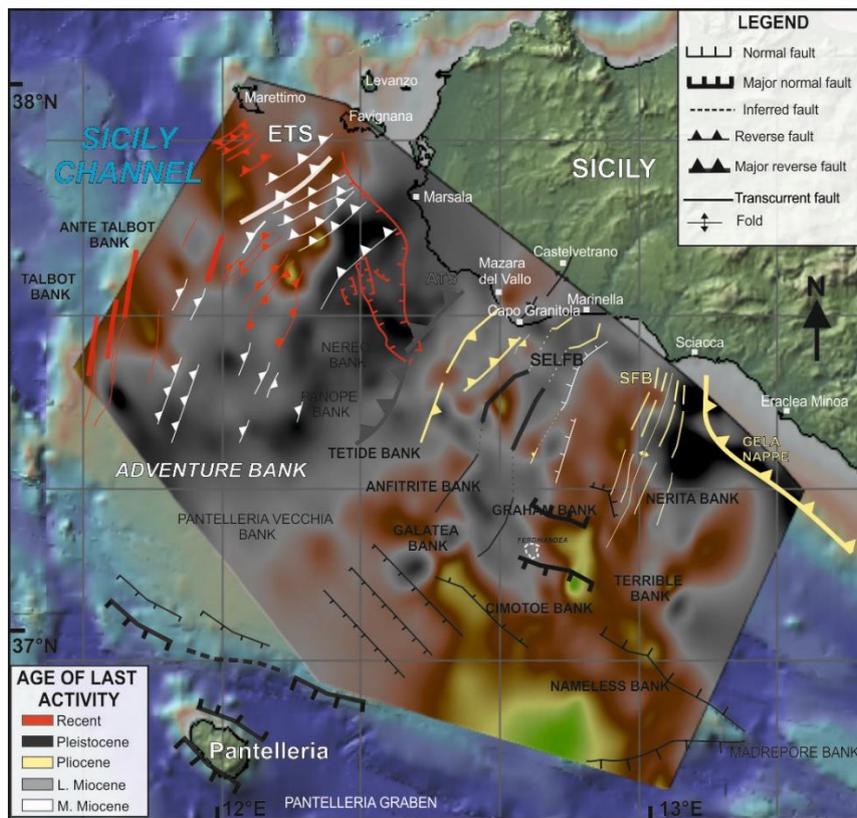
Fig. 3.46 – a) Isobath map relative to the top of Paleogene basament b) with overlaps of structural features of Figure 3.15.

CHAPTER IV

4. HIGH RESOLUTION, SINGLE CHANNEL SEISMIC REFLECTION PROFILES

4.1 Data acquisition

An irregular, but locally dense grid of single-channel seismic (SCS) reflection profiles (Fig. 4.1) was collected in the offshore area between Torretta Granitola and Eraclea Minoa during two oceanographic cruises. The profiles were acquired using the Geomarine survey instrumentation (http://www.geomarinesurveysystems.com/).
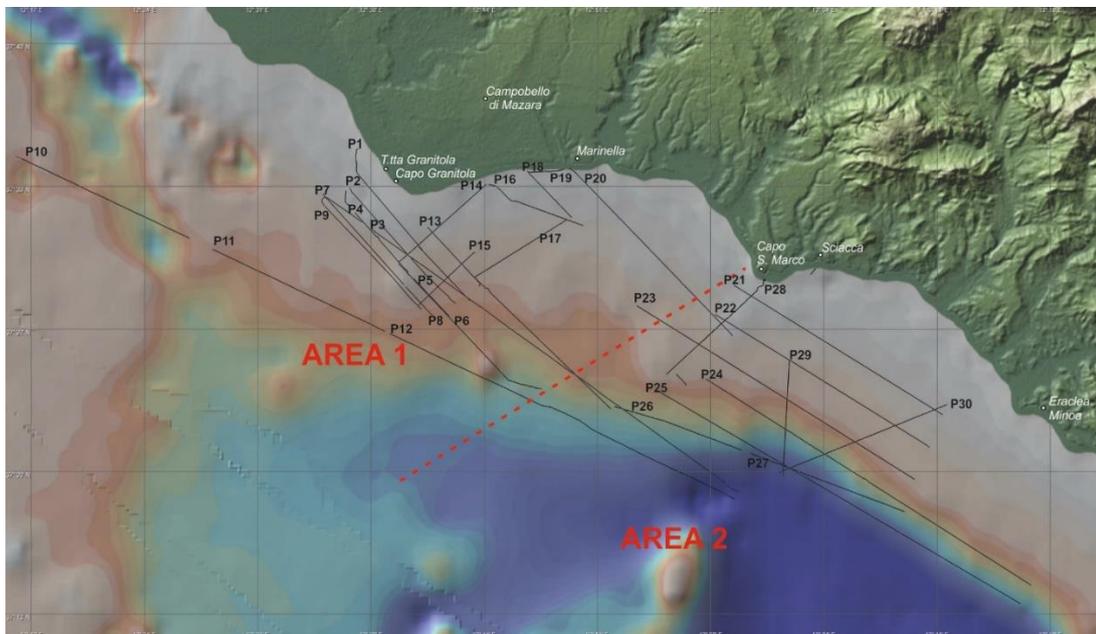
Fig. 4.1 – Bathymetric map of the study area with location of SCS profiles. The red dotted line offshore from Capo S. Marco separates the SCS profiles in areas 1 and 2.

The first survey (August 2013) was targeted in the offshore of Capo Granitola. The objective was to define the offshore prolongation of a SW–NE tectonic line outlined by previous studies between Campobello di Mazara and Castelvetrano (CCA, see chapter I). The survey was conducted on board of the Neptune 1 PE 1275 (Fig. 4.2), a small boat 6,33 m long that allowed to collect data in shallow water and with a distance from the coast up to 500 m.

The acoustic source used during seismic prospecting was a 1 kJ Sparker power supply with a multi-tips Sparker array, which lacks ringing and has a base frequency of around 800 Hz, fired at a time interval of 1.5 s. Data were recorded using a single-channel streamer with an active section of 2.8 m, containing 7 high-resolution hydrophones. The marine sub-bottom was imaged for 0.5 s. two-way time (t.w.t.) at a 10 kHz (0.1 ms) sampling rate. Positioning was controlled by a Differential Global Positioning System. The vertical resolution is ∼ 1 m near the sea floor.

Fig. 4.2 – Neptune1 PE1275 boat used for data acquisition during August 2013.

On September 2015, additional profiles were acquired during the oceanographic cruise SoTyBe (Southern Tyrrhenian Belt) on board the R/V Minerva Uno (Fig. 4.3). The cruise was funded by the IAMC-CNR (Napoli), and involved personnel from the former institution and from the ISMAR-CNR (Bologna), INGV (Roma), DISTAR (Università degli studi di Napoli "Federico II") and DISTeM (Università di Palermo).

The research vessel is 41m long and is equipped with DGPS (Differential Global Positioning System) and SEAPATH positioning system, single beam

and multibeam depth sounder, marine and water column sediment sampling equipment and geophysical and oceanographic data acquisition instrumentation (e.g. ADCP, CHIRP SBP, and other sonar sensors).

In the survey areas, high resolution seismic reflection profiles were obtained using a water gun S15 Sodera seismic source and a Geometrix-GeoEel digital streamer (Fig. 4.4) provided by the ISMAR-CNR (Bologna), together with sub-bottom Chirp and multibeam data. Part of these data are described and analysed in this doctoral thesis.

Fig.4.3 – Minerva Uno research vessel in the Napoli harbour.

Fig. 4.4 – Details of the S15 Sodera water gun seismic source and of the Geometrix-GeoEel digital streamer.

4.2 Data processing

Seismic data processing was performed using the Geo-Suite AllWorks software. A new project file was created to process the single channel seismic data and separate them from the multi-channel ones.

The following mathematical operators were run:

- *IIR FILTER MODULE.* Several filters are available: band-pass, low-pass, high-pass, notch and custom. The first four are implemented as IIR (Infinite Impulse Response) filters and are optimized to attenuate edge effects. Custom filters are implemented as FIR (Finite Impulse Response) filters. With these filters, the user can specify the shape of the frequency response of the filter to address circumstances. IIR Filter module can be used to attenuate undesired frequency content of the signal spectrum (e.g. electrical low frequency noise).

- *A.G.C.* Automatic gain control compensates the signal attenuation by scaling the data such that the average absolute value of the amplitudes within a specified window will be a certain value. The user can specify the window length and the desired output average level. With this AGC routine the user can also control the way near zero values can affect the computation of the scaling factor. If the window contains too many near zero values, the previous scaling factor is used, to prevent the P-breaks to be over scaled (and thus, clipped). Two parameters can be used to control this effect: 1) *Dead values in a window*: indicates the maximum number of near zero samples that can be found in a window before using the previous scaling factor; 2) *Dead level (mV)*: indicates the near zero threshold level (e.g. a value of 100 mV means that every sample whose absolute value is less than 100 mV is considered a near zero value). The *Percent AGC* parameter can be used to soften the effect of the AGC operator: 100% means that the signal will be scaled completely using the AGC scaling factor; values less than 100% will reduce the scaling factor.

- *GAIN* module is used either to apply a constant gain to the entire profile or a simple linear TVG. The option "Start at seabed" will vertically shift the TVG curve trace by trace depending on the seabed position. The slope is not altered by this option. Please note that this option has no effect if the seabed picking line is not available.

- *TVG*. With this operator, the user has full control on the gain curve applied to the data. The curve can be defined manually, by clicking on the plot and dragging the modal points or editing the values displayed in the TVG curve table. Each point can be defined in terms of *absolute gain* (dB) or *slope* (db / sec). Like for the simple gain operator, the Start at seabed option can be used to shift the TVG curve trace by trace so that 0 ms in the TVG curve will correspond to the seabed position.

- *DECONVOLUTION* operators are used to reverse the effects of convolution processes which take place during data acquisition. Source and surface multiples, for instance, can be modelled as the output of a linear system which is cascaded to the acquisition system. The goal of deconvolution techniques is to compute an inverse system which attenuates those undesired effects. Signature deconvolution operator is a powerful tool to recover true data resolution and attenuate source – surface multiples. The operator needs an estimate of the source signature in order to compute a matched filter to perform deconvolution. A source signature estimation can be computed from the data itself using the "Signature tool", available in the "Tools" toolbar of the 2D profile window. This tool computes the source signature wavelet from the seabed reflector. Therefore, seabed line must be digitized to proceed. The data window section allows the user to select the portion of the profile to use to extract the seabed reflector wavelet. Start time and end time parameters are relative to the seabed line. That is, a start time of -5 ms means that the wavelet is calculated with data starting 5 ms before the seabed line event. In the preview panel the resulting wavelet, as well as its frequency spectrum is displayed. Once the desired wavelet has been computed, you can save your

results in a signature file, to be later used with the deconvolution operator. Once the source signature is available, the deconvolution can take place. The deconvolution operator needs three parameters to operate: 1) the signature file, previously created with the Signature tool; 2) the output wavelet central frequency; 3) the FIR operator length (in samples), the operator will compute a matched filter to transform the input wavelet (the source signature) into an ideal wavelet (the Ricker wavelet in this case). The output central wavelet should match the central frequency of the source.

The FIR operator length is used to attenuate edge effects that may arise, depending on the data. Increasing this parameter will result in a more accurate yet sharp filter; lowering this parameter will generate a less accurate yet smooth filter.

- *INVERT POLARITY*. Sometimes it is necessary to correct the polarity of the signal. The following operators can be applied for this purpose. Use this operator to invert the polarity of the signal.

- *BURST NOISE REMOVAL.* This filter is used when data are contaminated by burst noise, detecting the burst peaks and then replacing the samples affected with an average value. Three parameters affect the behaviour of the filter: the traces window, the burst threshold and the override threshold. The traces window parameter specifies the number of traces to use to compute a moving average of the absolute values of the current sample. If this value is more than N times higher than the value of the absolute average of the whole profile, where N is the burst threshold parameter, the current sample is marked as burst noise and filtered. The override threshold prevents the filtering of low amplitude samples. That is, bursts samples with an absolute amplitude lower than the average amplitude by the factor specified by the override threshold will not be filtered.

- *MUTE*. This module mutes the water column of the current seismic profile. It is also possible to stop the muting operator before the actual seabed

by entering the desired interval in ms. This will prevent the muting operator from affecting the seabed reflector.

- *TRACE MIXER* mixes adjacent traces. This is equivalent to applying a low pass filter in the k domain. The application of this operator will reduce the horizontal resolution of the processed profile, so it is recommended only in case of spatial aliasing (when the horizontal resolution is low and artefacts like strong discontinuities in adjacent traces are noticeable). In the Options panel, you can set the proper rate for the computation of the average values to assign to each sample of the current trace based on the previous and the next traces.

- *SWELL FILTER* performs the swell filtering on the seismic data, using the seabed line previously picked.

As described in the following section, following the seismic facies analysis, the SCS lines were depth-converted using velocity intervals of 1500, 1600, 1700 and 1800 m/s for the water column, Holocene, Middle-Late Pleistocene and Lower Pleistocene sedimentary units, respectively.

4.3 Seismo-stratigraphic analysis

The analysed dataset resulting from the different campaigns in the offshore area of SW Sicily (Fig. 4.1) consists of 45 SCS reflection profiles. The profiles have been grouped in two spatial data sets, labelled Area 1 and Area 2, located west and east of Capo San Marco near Sciacca, respectively (Fig. 4.1).

The sparker lines acquired with NW-SE and NE-SW trends are oriented parallel to regional dip and strike, respectively. The seismic profiles image the first 2-300 m of sediments below the sea floor.

The bathymetric range from the coast toward the offshore is between 10-150 m, so it includes the average sea level oscillation range during the last glacial period, namely the Marine Isotopic Stage (MIS) 2 corresponding to the "Wurm" (18000 years ago, ~ 120-130 m below the current sea level). In this

way, it is possible to recognize in seismic images the discordance surface produced during the MIS 2.

The seismo-stratigraphic analysis of the SCS reflection profiles allowed to detect 5 seismic units, labelled from the highest to the lowest, MD, A, B, C, D, bounded by unconformities, and characterized by different types of reflections. Each unit is identified based on internal configuration such as amplitude, reflection continuity, frequency and on external shape. Each seismic facies unit has been associated to a series of sedimentary units based on correlation with well-logs and outcrops (see paragraph 4.4).

Two major erosional surfaces (ES1 and ES2) have been detected because of their evident seismic character that makes it possible their identification. Where identification of the ES is doubtful due to either noise of acquisition or tectonic disturbs, the Geosuite software allows to pick horizon by means of a utility that displays the depths of the same horizon traced in the cross-profiles.

4.3.1 Unit MD

Unit MD (Figs. 4.5, 4.6) is detected in the profiles thanks to its morphological features. It is a mound-shaped unit showing irregular and discontinuous internal reflection patterns. Underneath the mound structures, the seismic signal is characterised by irregular to chaotic, mostly discontinuous, moderate- to locally high-amplitude reflections.

The presence of acoustic wipeout zones, the high reflectivity, and the velocity change are the criteria for distinguishing mound structures. A wipeout zone is an area on the seismic section where the reflections from stratigraphic layers are deteriorated such that the primary reflections are either absent or very weak.

Depending on the presence or not of sedimentary cover overlying unit MD, active mounds are distinguished from buried mounds.
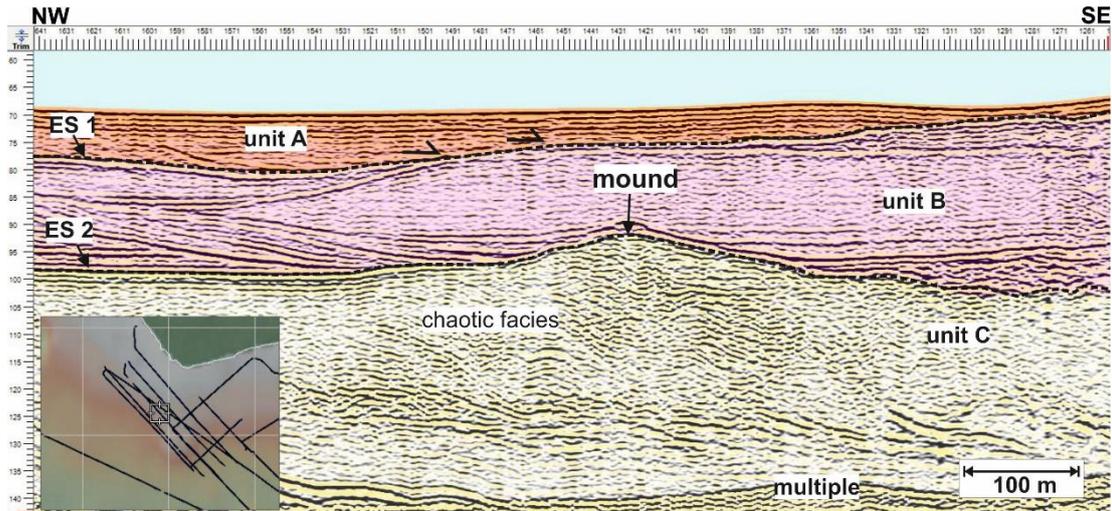
Fig. 4.5 – Sketch of profile P4 located in the Area 1 in which a buried mound is visible. The horizontal scale indicates the shot points, while vertical scale shows depths in milliseconds.
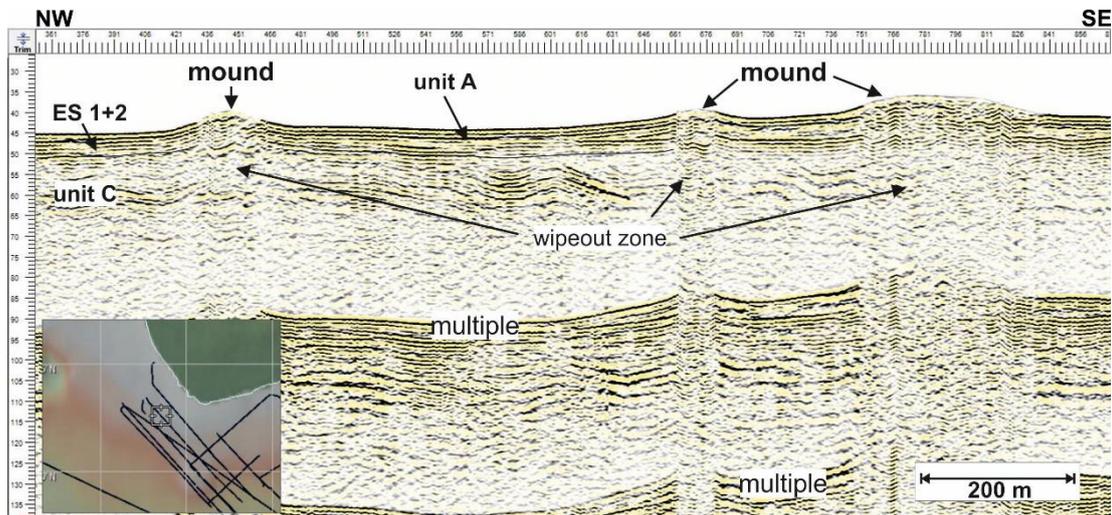
Fig. 4.6 – Sketch of profile P2 located in the Area 1 showing active mounds. The horizontal scale indicates the shot points, while vertical scale shows depths in milliseconds.

4.3.2 Unit A

Unit A (Figs. 4.7, 4.8) is limited at the top by the seafloor and at the bottom by unconformity ES1. It can be seismically subdivided into two sub-units named A1 and A2. Sub-unit A1 exhibits slightly seaward dipping, well-defined, high-amplitude and laterally continuous reflections with parallel geometry draping the underlying units. Sub-unit A2 onlaps the basal unconformity ES1. A conformable, downlap surface (MFS) separates the retrograding strata of sub-unit A2 from the prograding strata of sub-unit A1.
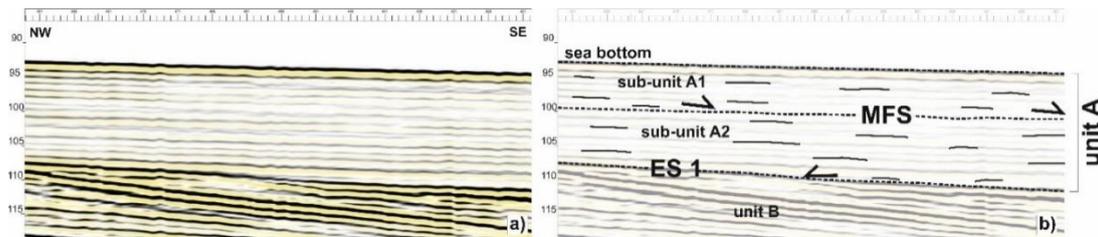
*Fig. 4.7 – Sketch of a profile within Area 1 showing the unit A. The horizontal scale indicates the shot points, while vertical scale shows depths in milliseconds.*
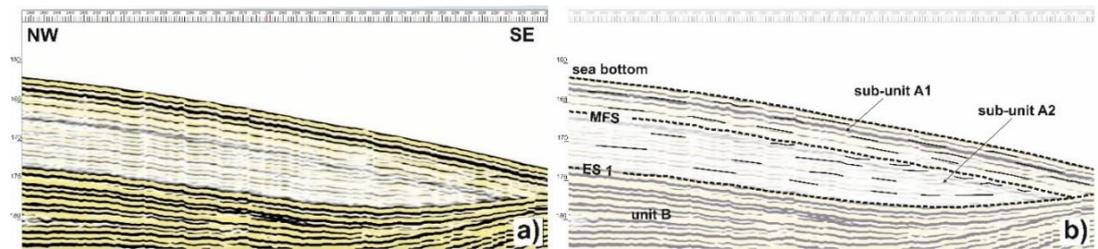
Fig. 4.8 – Sketch of a profile within distal part of Area 1 showing the truncation of sub-unit A2 by MFS. The horizontal scale indicates the shot points, while vertical scale shows depths in milliseconds.

In Area 1, unit A reflectors show parallel geometry and high acoustic impedance in the upper part, and low reflectivity downward. The thickness changes among the profiles with a range commonly of ~ 1.5–10 m (~ 2-13 ms). In some cases, it reaches a maximum value of ~ 20 m (Fig. 4.9), probably because of an increment of sediment supply associated to the vicinity of fluvial courses.

It is worth to note that the thickness of sub-unit A1 is quite constant in the shelf, except for areas affected by deformation (see following paragraphs 1.7, 1.12) where it drastically decreases down to ~ 4 m (~ 5 ms). In these areas unit A, which elsewhere onlaps unit B reflectors, often directly overlies unit C.

In Area 2, seismic unit A is thicker than in the Area 1. The maximum value reaches ~ 40 m. Toward the south, the unit and the underlying strata pertaining to unit B are separated by a conformity surface indicating an undisturbed relationship between adjacent sedimentary strata that have been deposited in orderly sequence (Fig. 4.10). This relationship is not visible in

Area 1 because of the low bathymetric depth (lesser than 100 m) of seismic profiles acquisition.
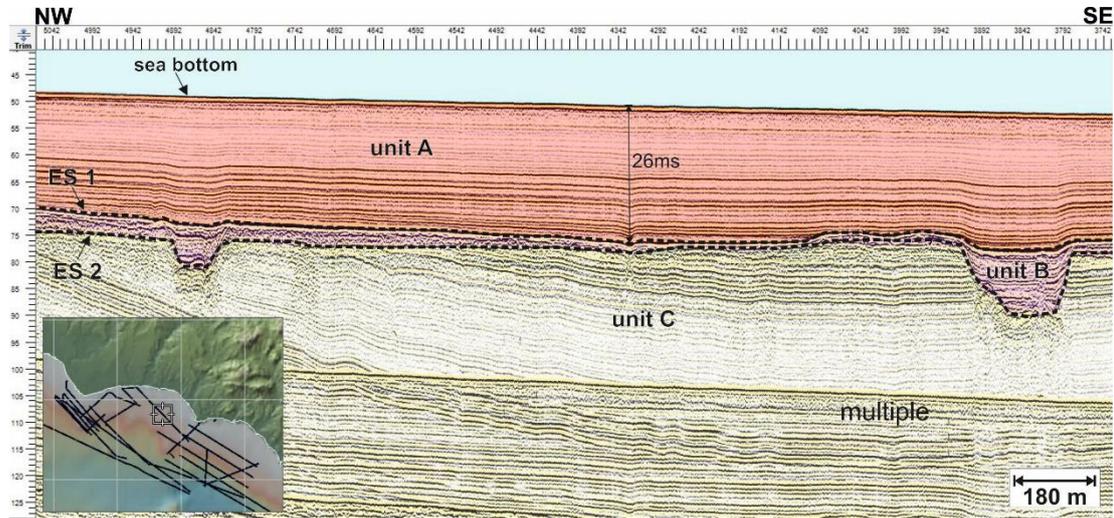
Fig. 4.9 – Sketch of profile P20 located next to the Sicily coast, west of Capo S. Marco. Unit A exhibits high thickness (26 ms = ~ 20 m) probably due to vicinity of river deltas. The horizontal scale indicates the shot points, while vertical scale shows depths in milliseconds. The inset in the lower left corner is a basemap box that allows to visualize the current position along the analysed profile.

Based on its seismic facies and stratigraphic position, unit A is associated with the Upper Pleistocene-Holocene deposits, formed during the transgressive and highstand stages of the last sea level rise, overlaying the well-developed surface ES1. Sub-unit A2 is interpreted as reflecting the transgressive sequence of the Late Pleistocene. The unconformity MFS represents the Maximum Flooding Surface or maximum transgressive surface or final transgressive surface (CATUNEANU, 2006 and references therein), which marks the end of shoreline transgression during base-level rise, when sedimentation rates outpace the rates of base-level rise.

Only in distal parts of the shelf, the MFS truncates the underlying strata (Fig. 4.8) suggesting that in these parts the sediment supply is overcome by the sea-level rise. Finally, sub-unit A1 is interpreted as reflecting the regressive highstand sequence of the Late Holocene.
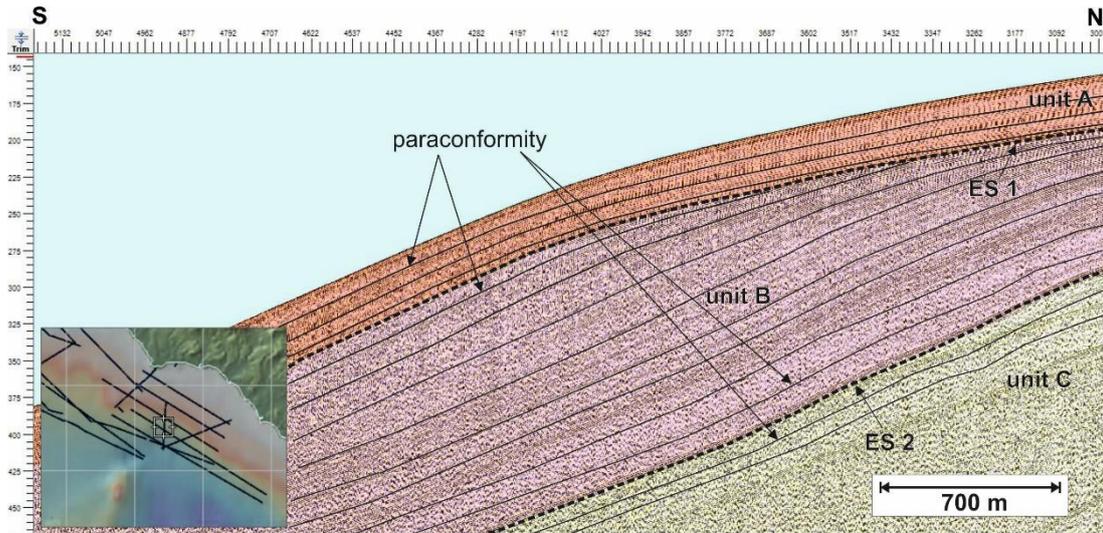
Fig. 4.10 – Sketch of profile P29 located in the Area 2 showing unit A in paraconformity with the basal part of unit B. The horizontal scale indicates the shot points, while vertical scale shows depths in milliseconds. In the lower left corner, the basemap box is shown.

4.3.3 ES1

ES1 (Fig. 4.11) is easily recognised thanks to its high reflection coefficient. It is a high-amplitude and well-defined laterally continuous event interpreted to represent a subaerial erosional surface. It depicts a sub-horizontal regional unconformity, which cuts the underlying sequences on the shelf, and traceable seaward in paraconformity with the lower strata on the slope only in the Area 2 (Fig. 4.11, 4.12). The correlative conformable seismic reflector and the associated rollover point (the morphological break in slope at the topset-foreset transition that in margin-scale clinoforms coincides with the shelf edge) are less evident than of them pertaining to ES2, probably because of the higher grade of erosion.

Based on its stratigraphic position at the base of the most recent sedimentary cover and overlying unconformably above units B or C, ES1 is interpreted as the surface carved during the Last Glacial Maximum (LGM), aged at ~ 18-23 ka, when the sea level was ~ 120-130 m below the current level.

133
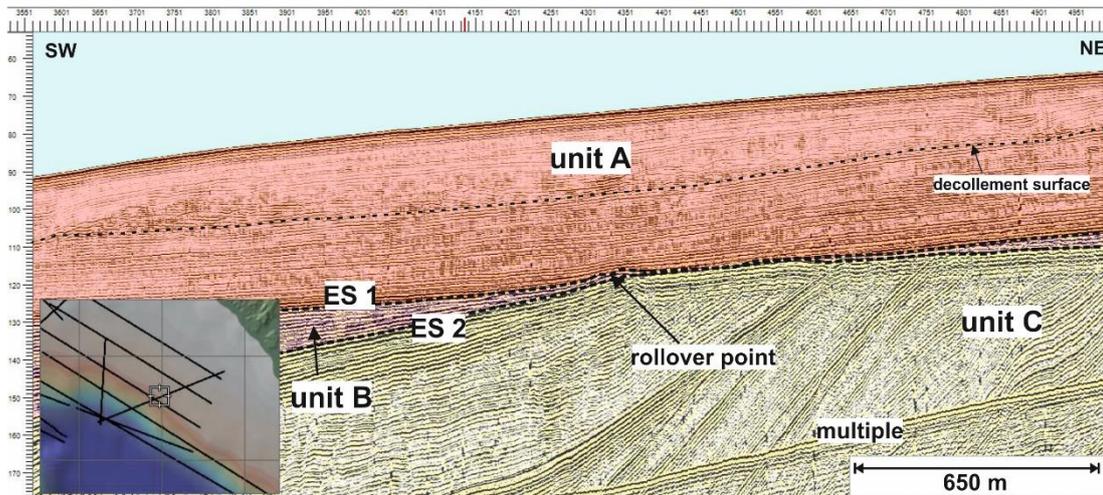
Fig. 4.11 – Sketch of profile P30 located in the Area 2 showing the ES1 unconformity which separates unit A from unit B. Its rollover point is also visible. The horizontal scale indicates the shot points, while vertical scale shows depths in milliseconds. In the lower left corner, the basemap box is shown.

4.3.4 Unit B

Unit B shows different facies in the study area. At the bottom, the unit is characterized by onlapping, well-stratified, seaward dipping, high-frequency and high amplitude reflections of good lateral continuity lying above unit C by means of an unconformity (ES 2) or a paraconformity surface (Figs. 4.10, 4.11, 4.12). Moving upward, an alternation of high amplitude, high frequency and sub-parallel reflections and of chaotic reflections separated by unconformities and limited to the top by ES1 (Fig. 4.5).

Seismic unit B is interpreted as being formed by an alternation of regressive and transgressive units deposited during the Middle-Late Pleistocene sea-level changes. Because the sea-level oscillations had broadly comparable amplitudes (WAELBROECK et al., 2002), the different ESs formed during this time span cannot be traced in unit B because it is characterized by a very thin and reworked (condensed) section, where erosion processes likely outpaced deposition.

134

4.3.5 ES2

ES2 (Fig. 4.12) is a well evident reflector characterized by continuous, high amplitude reflections which separates the overlying transgressive-regressive sequences grouped in unit B from the underlying, often inclined strata pertaining to unit C. The surface exhibits large variability along strike as documented by its variable geometry generating irregular topographic relief due to differential erosion. At local scale, ES2 is carved by gullies and valleys (Fig. 4.9).
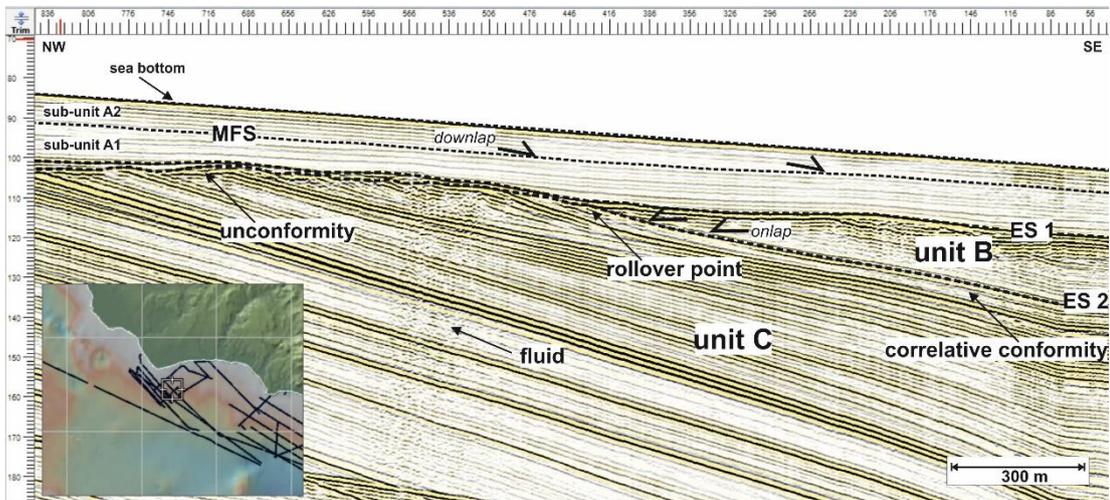
Fig. 4.12 – Sketch of profile P13 located in Area 1 showing seismic units and the bounding ESs. The focus is on ES2 that is an unconformity in the NW and becomes a paraconformity toward the SE. The two surfaces, ES1 and ES2, are separated by the rollover point positioned at ~ 110 ms. The horizontal scale indicates the shot points, while vertical scale shows depths in milliseconds. In the lower left corner, the basemap box is shown.

Its erosional character progressively vanishes in the distal and deeper part of the Channel, where the surface tends to become a correlative conformity, whose timing corresponds to the end of base-level fall at the shoreline, and the distinction between unit B and C is less clear. Where erosional processes fully eroded and/or obstructed the sedimentation of deposits pertaining to unit B, the ES2 merges with ES1. In these cases, the resulting composite sub-horizontal surface separates unit A from unit C (Fig. 4.12).

135

4.3.6 Unit C

Unit C (Figs. 4.9, 4.11, 4.12) is limited to the top by ES2 and/or ES1 and is characterised by a thick succession of well-stratified, seaward dipping, high-frequency, and medium- to high-amplitude reflections of good lateral continuity, with parallel (the distal portion) to oblique and tangential (the proximal portion) internal configuration with apparent dip direction toward the SW.

The unit is affected by numerous faults and folds which produce different deformation. It is partially affected by gas, locally making up difficult to distinguish the internal geometry and seismic facies.

4.3.7 Unit D

Unit D (Figs. 4.13, 4.14) is the lowest and oldest stratigraphic unit, not recognizable in all the profiles but visible only in Area 1 albeit it is often partly obscured by multiple reflections.
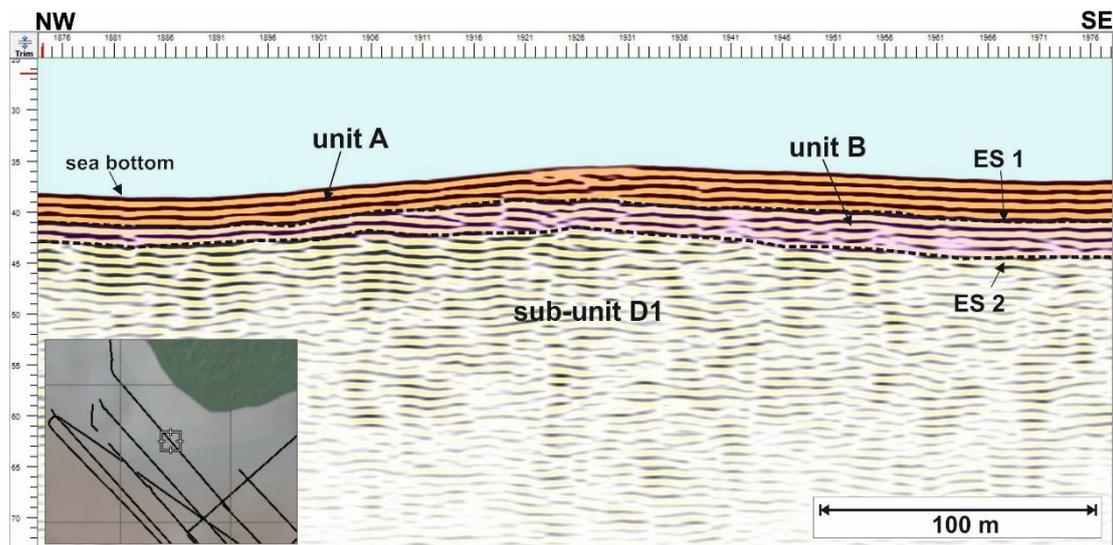
Fig. 4.13 – Sketch of profile P1 located in Area 1 showing chaotic facies of sub-unit D1 underlying a thin vein of reflectors pertaining to unit B. At the top unit A. The horizontal scale indicates the shot points, while vertical scale shows depths in milliseconds. In the lower left corner, the basemap box is shown.

The unit shows different facies as a function of its stratigraphic position, and can be divided in two sub-units. Sub-unit D1 is recognised at shallow depths (~ 45 ms), and is characterized by free or chaotic reflections (Figs. 4.13, 4.14). Oppositely, sub-unit D2 (Fig. 4.14) is present at variable depths ranging from 150 ms to 420 ms and shows a succession of stratified, high amplitude, medium to high frequency and discontinuous to local continuous reflections.
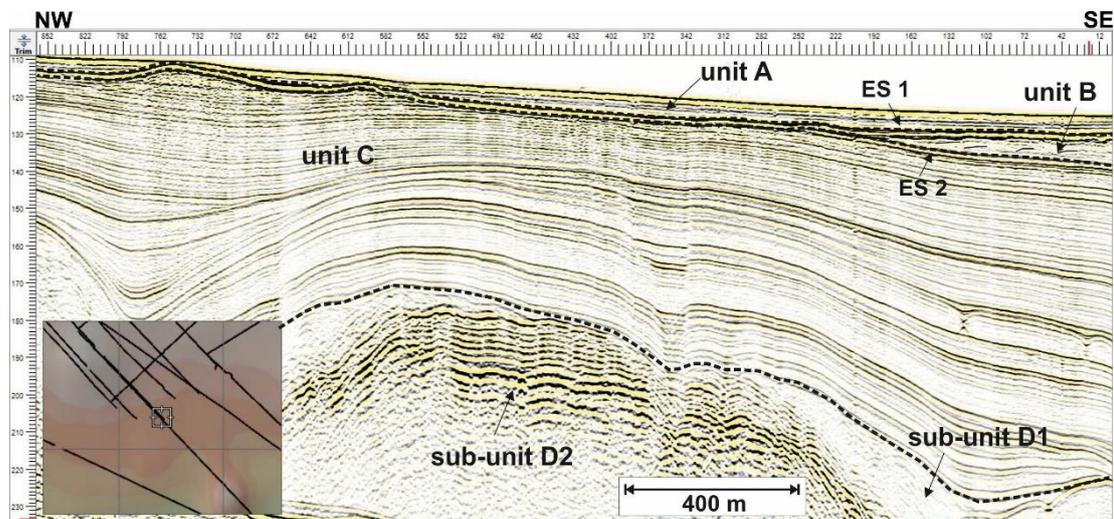
Fig. 4.14 – Sketch of profile P5 located in Area 1 showing chaotic facies of sub-unit D1 overlying the high amplitude, locally stratified sub-unit D2. All the seismic units and ESs are visible. The horizontal scale indicates the shot points, while vertical scale shows depths in milliseconds. In the lower left corner, the basemap box is shown.

4.4 Calibration of seismic profiles using well logs and on-land outcrops

Because of the lack of direct information on sediment age, a correlation between the seismic facies seen in the high-resolution profiles and outcrops on land has been performed in order to place constraints on the age of seismic units. In addition, information from the upper part of offshore and onshore deep exploration wells is used to calibrate the seismic units, and to extrapolate at depth the outcrops, respectively.

4.4.1 Well-log analysis

A detailed analysis has been made of onshore wells Biddusa and Marinella, and of offshore wells Oscar Ovest, Onda, Orione est, Venere, Zagara, Pina, Pamela bis (Fig. 4.15), located on the shelf and located close by the analysed SCS profiles. These wells are also used to calibrate the MCS reflection profiles from ViDEPI and ENI database (see chapter III).
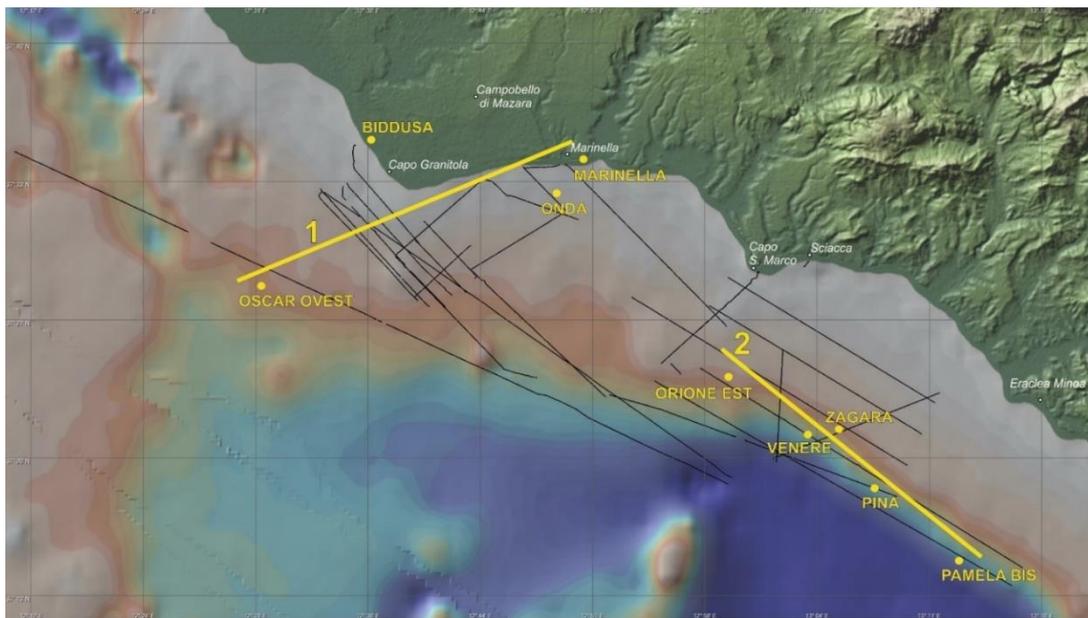
Fig. 4.15 – Location of deep exploration wells calibrated with SCS reflection profiles. The yellow lines 1 and 2 indicate the direction along which lithological and thickness variations of the logged formations were analysed.

The above wells have been imported in Geosuite AllWorks. Through a specific utility of the software, they have been projected into nearby seismic lines. Figures 4.16 and 4.17 show correlation of the Pliocene-Quaternary formations among the wells projected along two NE-SW and NW-SE trending lines (Fig. 4.15) for the offshore area of Capo Granitola and Sciacca, respectively. The lines 1-2 in figure 4.15 illustrate the direction along which lithological and thickness variations of the logged formations have been considered. The stratigraphic series are in scale, drawn with different symbols and colours for each lithology and stratigraphic interval.
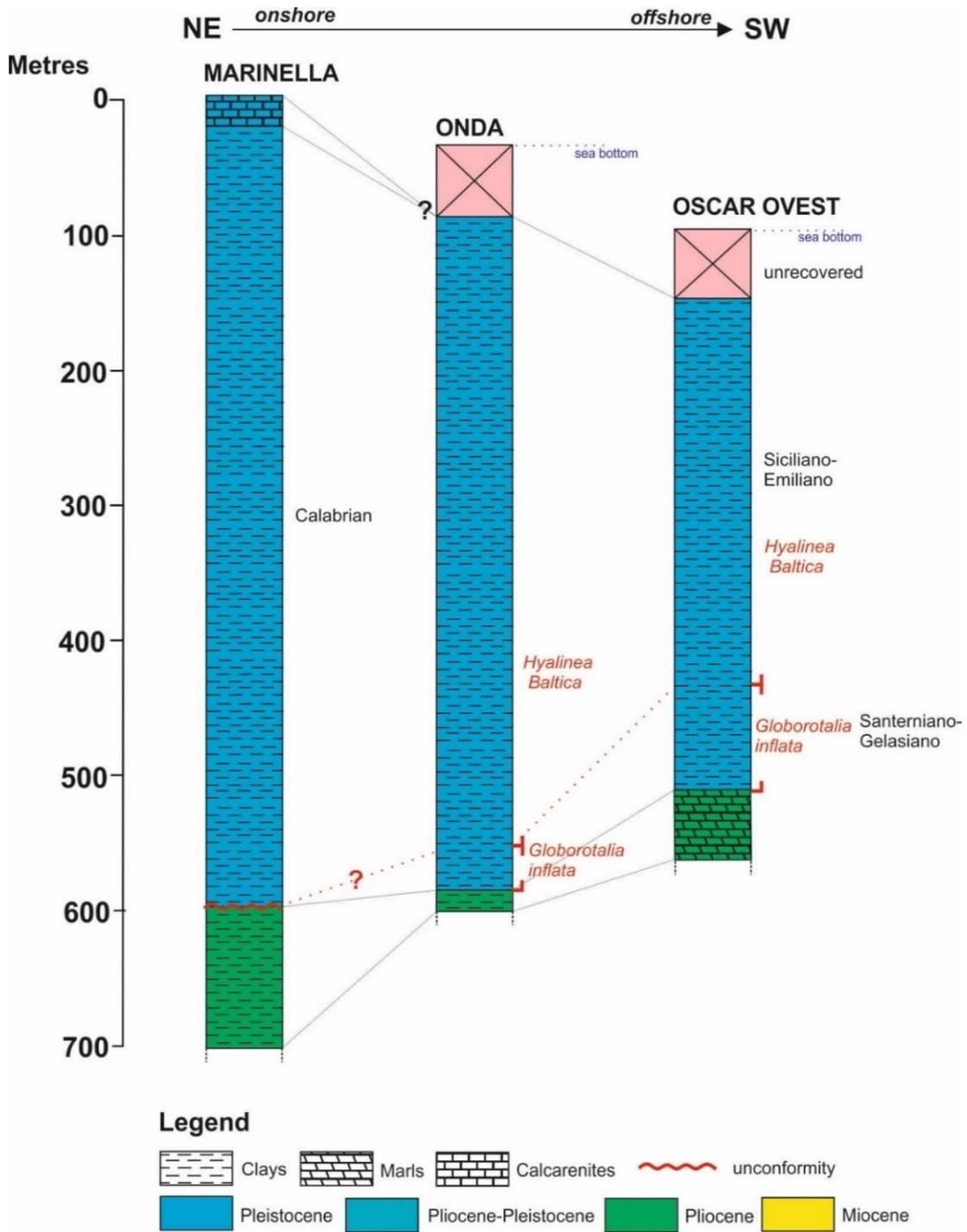
Fig. 4.16 – Correlation among the well-logs projected along line 1.
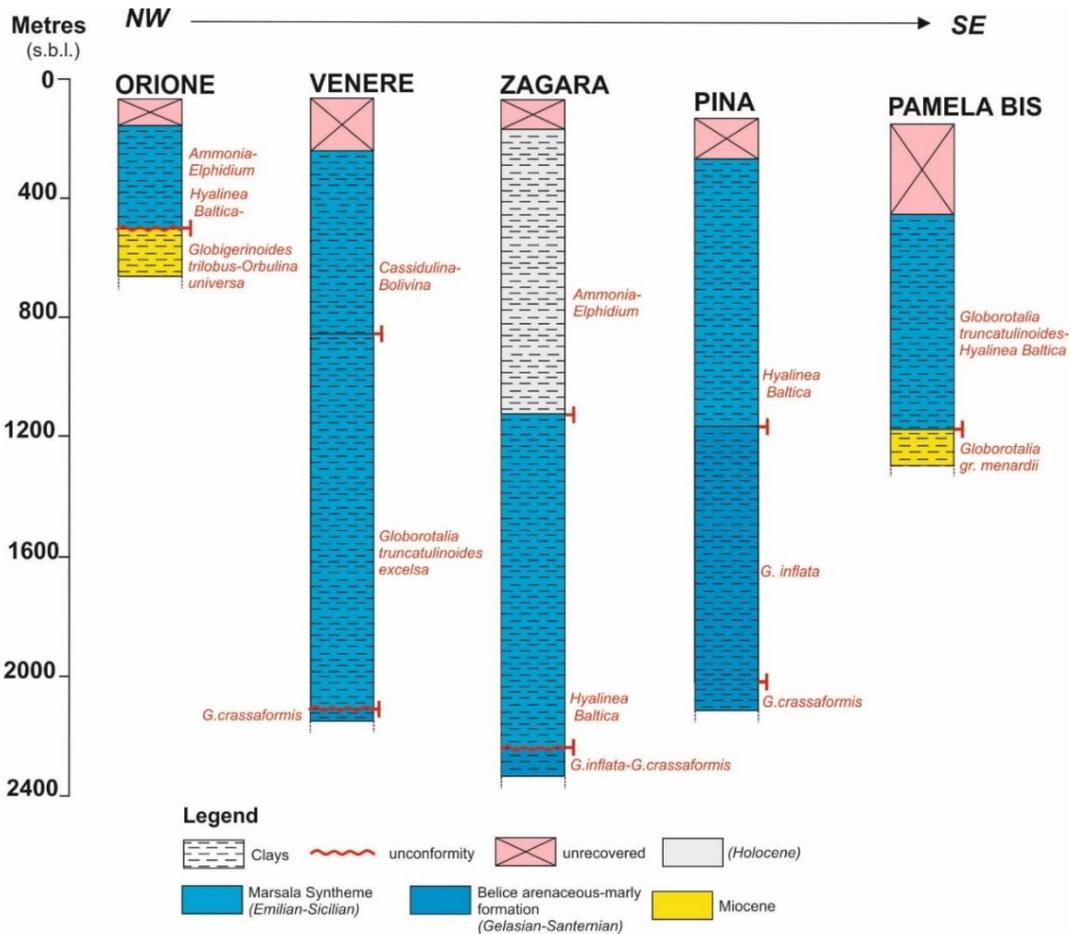
Fig. 4.17 – Correlation among the well-logs projected along the line 2.

Beneath the unrecovered upper part of the logged sedimentary section, the well-logs show green-grey fossiliferous slightly silty clays with sandy intercalations assigned to the Pleistocene epoch, except for the onshore well Biddusa that shows 20 m of Quaternary alluvium (*Fig. 4.18 on the right*). Further down-section, the wells have drilled through Lower Pliocene sediments (Trubi Formation), in turn overlying older sediments.

The logged deposits have been distinct based on bio-events and biozones.

In Marinella well, the shallower lithology consists of calcarenites which overlie a package of clays. The calcarenites
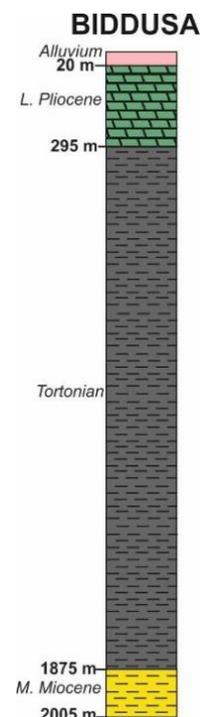
likely reflect a regressive event that established shallow water conditions in the area around the well. The lack of Gelasian sediments indicates the presence of an unconformity between the Calabrian and Pliocene sediments.

Moving from land toward the sea (Fig. 4.16), the lithological thickness of the Pleistocene clays decreases from 600 m (Marinella) to 338 m (Oscar Ovest). The minimum thickness detected in Oscar Ovest highlights the decreasing sediment supply with distance from the coast but also the presence of a high around the well (see chapter III).

The occurrence in Pleistocene sediments of the planktonic foraminifer *Globorotalia inflata* and of the benthic foraminifer *Hyalinea baltica* reveals deposits belonging to Gelasian(-Santernian?) and Emilian-Sicilian sub-stages, respectively (*Fig. 4.19 on the left. Timescale correlation of plankton and benthic zones and of Plio-Pleistocene litho-stratigraphic successions of SW Sicily. On-*land studies remark these fossils as characteristic of the Belice marly-arenaceous (Marnoso-
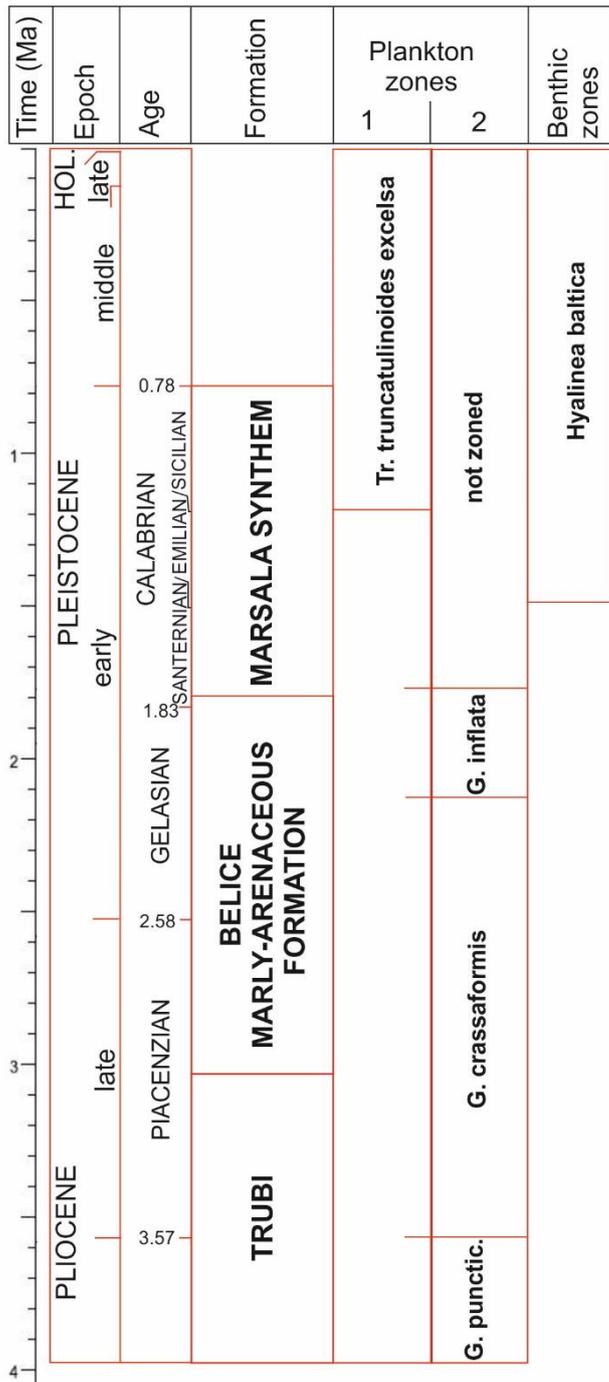
Arenacea del Belice) formation and of the Marsal synthem (BASILONE, 2012), respectively.

The well-logs in figure 4.17 are projected parallel to the coast and show a strong thickness increase of the Pleistocene sediments, which overcome the 1000 m, with respect to the wells in figure 4.16. We have distinguished the different stratigraphic formations in the logs based on the occurrence of planktic and benthic foraminifers (in particular, *Globorotalia gr. menardii, Globorotalia crassaformis, Globorotalia inflata, Hyalinea baltica, Globorotalia truncatulinoides excelsa, Ammonia, Elphidium, Cassidulina, Bolivina*).

The *Ammonia-Elphidium* association reveals that sedimentary deposition occurred in shallow and low salinity water (epi-neritic zone) and are considered as being characteristic of Holocene sediments. Whereas, the "northern guest" *Hyalinea baltica* indicates slightly deeper depositional settings (infra-neritic zone), which appeared in the Emilian sub-stage and still persists. The planktonic foraminifers *Globorotalia truncatulinoides excelsa* appear from the Sicilian upward to the present and occur in the Marsala synthem.

In view of the above, Zagara and Pina wells exhibit complete stratigraphic sequences. The remaining wells show unconformities in the stratigraphic columns.

From NW to SE, it is evident a thickness variability of the Pleistocene sediments. In Orione and Pamela wells, the Pleistocene deposits, lying unconformably on those of Miocene age, exhibit a very small thickness with respect to the others, but comparable to the wells in the north (line 1). These wells indicate a location on relative topographic highs. Venere, Zagara and Pina wells show the largest Pleistocene thickness outlining a subsiding area.

Considering that the wells are often located very close to the seismic lines, which have a depth penetration of ~ 400 ms (t.w.t.) equivalent to ~ 300 m, the calibration between wells and seismic facies highlights that seismic

units B and C correspond to Pleistocene sediments (A, as already stated, is composed of uppermost Pleistocene-Holocene sediments). Whereas, unit D may locally image the pre-Pleistocene as documented by the projection of Biddusa well-log into the closer profiles (Fig. 4.20). In fact, there is a good fit between the seismic facies change and the lithostratigraphic transition in the well-log from the Quaternary to the Lower Pliocene sediments, which occurs at a depth of ~ 35-40 m. The calibration highlights at this depth a change from quite continuous, high amplitude, medium-high frequency reflectors (unit A) to discontinuous, high amplitude, medium-high frequency reflectors assigned to the unit D. The latter semi-transparent seismic facies (unit D) in NW sector is considered as the seismic response of the Pliocene clays of Trubi Formation.
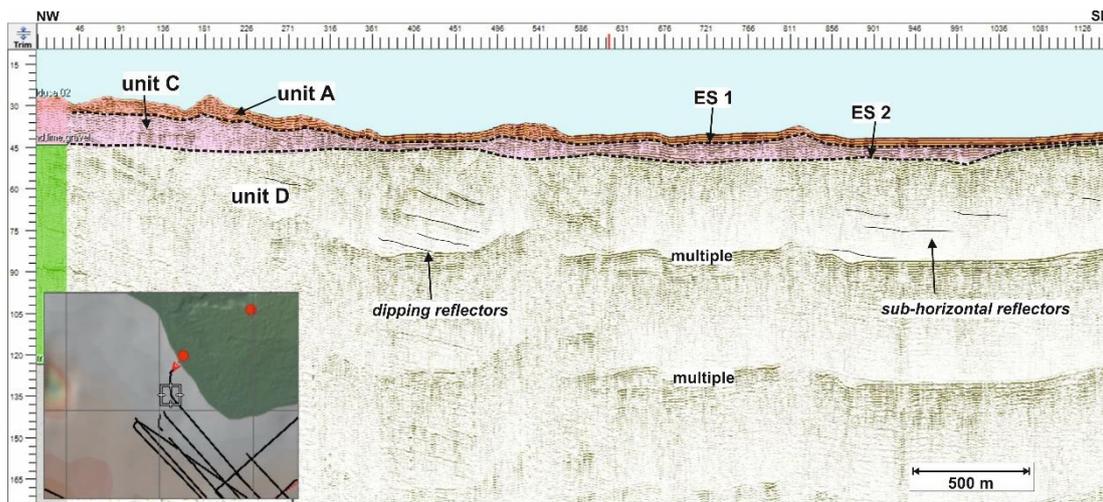
Fig. 4.20 – Biddusa well used for calibrating seismic units in P1. The distinction of unit A and C is not based on the well log information (for description see Fig. 4.18) but on seismic signal and interpolation with intersecting profiles. The horizontal scale indicates the shot points, while vertical scale shows depths in metres.

4.4.2 Correlation with on-land outcrops

Correlation between the wells and land exposures in the coastal region of the studied offshore sector supports the seismic unit attribution described above and provides information for a sequence stratigraphic interpretation of the seismic images. The correlation has been performed with outcrops in the

Marsala-Marinella area, where there are published reports (D'ANGELO & VERNUCCIO, 1994; 1996), and has been corroborated by direct observations in the frame of an ongoing research project on the Quaternary evolution of the area (FERRANTI et al., 2016).

The onshore of the study area is characterized by the widespread occurrence of Quaternary sediments. The Middle-Late Pleistocene system is composed by a regressive suite of terraced coastal deposits, which results from the interplay between eustatic and tectonic sea level changes (D'ANGELO & VERNUCCIO, 1996). This system includes wave-cut platforms with minor terraced deposits, punctuated by submarine bars evolving to back-shore dunes (FERRANTI et al., 2016).
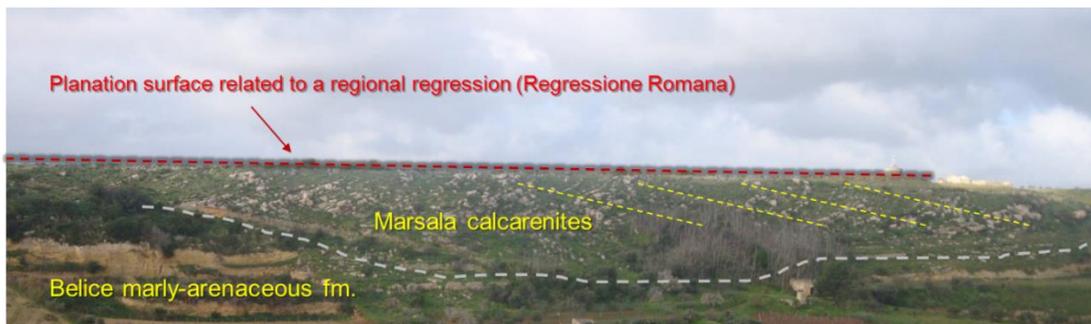
Fig. 4.21 – Seaward prograding calcarenites of the Lower Pleistocene pertaining to Marsala synthem, overlaying Belice marly-arenaceous fm. and outcropping in the area of Borgata Costiera (Mazara del Vallo).

Lower Pleistocene marine sediments (Marsala synthem) are widespread, and consist of bio-clastic calcarenites and calcirudites (Fig. 4.21; RUGGIERI et al., 1977; D'ANGELO & VERNUCCIO, 1992; 1996). The lithostratigraphic features and fossiliferous content of this deposit indicate a shoreface setting (BASILONE, 2012), where sediments were transported and deposited by wave action forming a long-lasting highstand prograding system (DI MAGGIO et al., 2009).

The synthem sediments unconformably overly that of the Belice marly-arenaceous formation (RUGGIERI et al., 1973; VITALE, 1990), formed by a

Plio-Quaternary sequence of sandstone and calcarenites with clay intercalation. The sedimentary unit is typical of deltaic-turbiditic setting. Further, the thickness changes and the thinning toward the south reveal a syn-sedimentary tectonic control of the basin (VITALE, 1990).

Down in the stratigraphic column, marly calcilutitic pelagic deposits of Lower Pliocene pertaining to Trubi formation, the sediments of Messinian evaporitic group unconformably resting on conglomeratic and /or sandy marly clay deposits of Terravecchia formation.

4.5 Stratigraphic interpretation

Based on the correlation with wells and on-land outcrops, the stacked seismic units imaged by the SCS profiles are attributed to the Pliocene-Holocene interval. In summary, considering their vertical position:

- unit A is assigned to the latest Pleistocene-Holocene;

- unit B, owing to its position between ES1 and ES2, spans the middle-late Pleistocene and is correlative to the terraced coastal deposits on-land;

- unit C, is related to the Lower– Middle Pleistocene silty clays (Marsala Synthem and older sediments exposed on-land); it is not excluded that in Area 1 (Capo Granitola sector), unit C includes well-cemented prograding calcarenites as detected in Marinella well.

- unit D is assigned to the Pliocene substratum (Belice marly-arenaceous and Trubi formations);

- unit MD is locally recognised only above the unit C, so its age is younger than unit C, either buried by unit B or A and at the sea bottom.

4.6 Adopted seismic velocities

Lacking direct measure of velocities, a seismic velocity analysis was made by considering the calibration performed using borehole data and geological outcrops from the areas surrounding the studied offshore zones.

TABLE 4.1

UNIT	SEISMIC FACIES	AGE	SEISMIC VELOCITY (m/s)
Water column	*transparent*	*/*	**1500**
MD	*irregular to chaotic, mostly discontinuous, moderate- to locally high-amplitude reflections*	*Recent or Middle-Late Pleistocene*	**1600**
A	*seaward dipping, well-defined, high-amplitude and laterally continuous reflections with parallel geometry (A1) and onlapping reflectors (A2)*	*Late Pleistocene-Holocene*	**1600**
B	*onlapping, well-stratified, seaward dipping, high-frequency and high amplitude reflections of good lateral continuity or an alternation of high amplitude, high frequency and sub-parallel reflections and of chaotic reflections separated by unconformities*	*Middle-Late Pleistocene*	**1700**
C	*well-stratified, seaward dipping, high-frequency, and medium- to high-amplitude reflections of good lateral continuity, with parallel (the distal portion) to oblique and tangential (the proximal portion) internal configuration*	*Lower–Middle Pleistocene*	**1800**
D	*free or chaotic reflections (D1) and a succession of stratified, high amplitude, medium to high frequency and discontinuous to local continuous reflections (D2)*	*Pliocene*	**2500**

Table 4.1 shows the average velocity values assigned to each seismic unit taking into account the seismo-stratigraphic information derived from the analysis of MCS profiles as no constraints are available for the velocities (see chapter III). The latter were used as a loose starting value and were modified

on the base of punctual stratigraphic data from well-logs, lithologies and the seismic signal response.

An average velocity of 1500 m/s was considered for the water column. For seismic units A, B, C, D, values of 1600 m/s, 1700 m/s, 1800 m/s and 2500 m/s, respectively, were used. The SCS profiles were depth-converted using such values. The estimated velocities are broadly similar to those adopted in surrounding areas of the Sicily Channel and Sicily land (BELLO et al., 2000; CATALANO et al., 2000; 2002; GHISETTI et al., 2009; CIVILE et al., 2014) and overall in the central Mediterranean Sea (PEPE et al., 2010; 2014; FERRANTI et al., 2014).

The uncertainty in seismic velocities estimates implicit in this approach has no consequences on the geological interpretation because they were used for the time-depth profile conversion.

4.7 Structural analysis

4.7.1 Evidence of syn-tectonic sedimentation in the SCS profiles

Several tectonic structures (fault planes and fold axes) as well as structures attributed to gravitational processes have been detected in the SCS reflection profiles. The criteria used to distinguish a fault plane are: offset terminations (fault cut-offs) of a previously continuous horizon; sub-vertical reflection-free lineaments; tilts of horizontal reflectors and abrupt dip increase of inclined reflectors; diffraction hyperboles.

The analysed fault planes are generally high-angle. Sometimes, they form larger fault zones up to 30 km wide in Area 2, showing pervasive small-scale faulting offset of reflectors and diffuse wipe-out or reflection-free zones, related to fluid ascent to the seafloor and/or tectonic disturbance. Folds are affected by high-angle fractures, commonly associated to narrow wipe-outs likely related to fluid ascent.

In order to illustrate the structural framework of the study area 5 SCS profiles are shown. These profiles are representative of the structural deformation of Areas 1 and 2.

The NW-SE trending profile P1 (Fig. 4.1) is the closest to the Capo Granitola coast and derives from the junction of two adjacent seismic lines, for a total length of 17,75 km. The seafloor has a depth between ~ 20 m to the NW and ~ 85 m to the SE.

The NW side of the profile has been calibrated with the onshore Biddusa well-log (Fig. 4.20), described above. Considering the well-log stratigraphic information and the calibration with the seismic signal, the passage from Quaternary sediments (unit A) to Pliocene clays (unit D) is visible at a depth of ~ 35-40 m. The change of seismic facies of unit D from discontinuous, high amplitude, medium-high frequency reflectors (before the shot 618) to free or chaotic reflections (after the shot 618) is due to a different direction of line acquisition near parallel and normal to the strata dip, respectively (Fig. 4.20).

As predicted by well-log analysis (par. 4.4), unit D should be encountered at ~ 600 m in Area 1 and at ~ 2000 m in Area 2. So, the occurrence of the unit at shallower depths in the NW is owing to tectonic uplift related to folding. Uplift of unit D testified by the well is responsible of the formation of a tectonic escarpment (Capo Granitola -CG- escarpment, Fig. 4.22) of ~ 30 m height (between 35 m and 62 m depth) evidenced by the ES2 and separates unit D from slumping and tilted younger deposits of unit C that show bottomset and foreset internal configuration produced by the regional uplift. Such feature is mapped also along profiles parallel to P1. Above the escarpment and below ES1, a wedge-shaped seismic unit is characterized by oblique downlap pattern between 33-50 m; this is considered as a lowstand prograding wedge.

Towards the SE, unit D is partly obscured by multiple reflections and is topped by discontinuous, high amplitude, low frequency reflectors (sub-unit D2) that appear at the minimum depth of 270 m (shot 1200) and maximum of

430 m (shot 182) producing folding in the unit above (unit C; Fig. 4.23). A series of high angle faults cut the reflectors of unit C and B with a maximum relative offset of 100 m with a progressive decrease upwards, implying sin-depositional deformation (Fig. 4.23). The reflector pattern allows to infer a Lower-Middle Pleistocene age to the two structures CG1 and CG2 (see Fig. 4.25) responsible of unit D uplift; the analysis of thickness change of reflector packages, i.e. the presence of growing strata (see Fig. 4.25), evidences that the two structures acted together during the Pleistocene even if with different rates of deformation, greater for CG1.
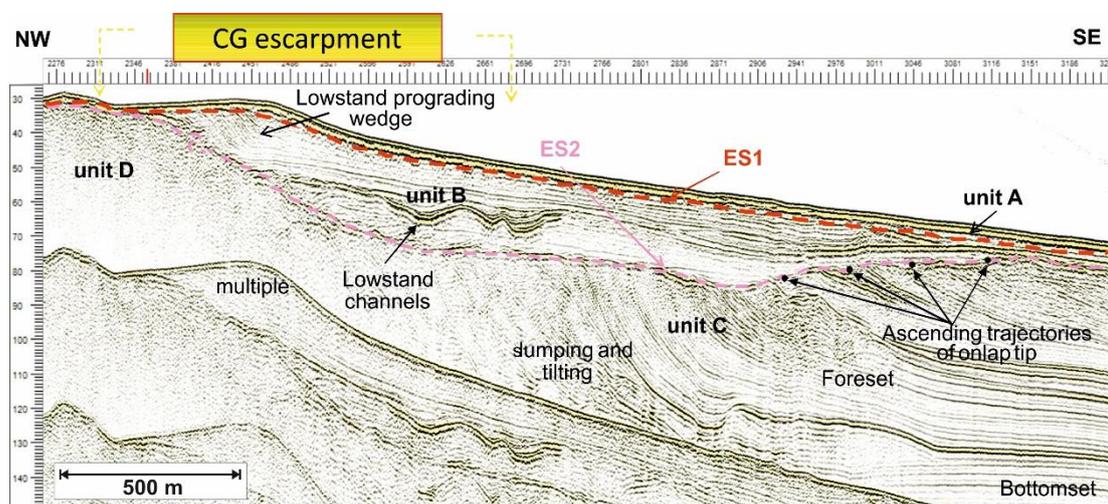
Fig. 4.22 – Sketch of P1 in which the deformed units C and D, juxtaposed along the CG escarpment are visible. Toward SE the ascending trajectories of onlap tip is attributed to unit C aggradation during a period in which rates of accumulation were greater than rates of uplift. The horizontal scale indicates the shot points, while vertical scale shows depths in metres.

Unit C is the most widespread in the profile. It is topped by ES2 which lies at a minimum depth of ~ 35-40 m where it preserves an erosional character; seaward of the rollover point (at a depth of ~ 72 m), it becomes a correlative conformity detectable at a maximum of ~ 175 m.

Toward the NW, ES1 merges with ES2, and this is interpreted as related to folding.

After shot 2887, the onlap tip of the reflectors (the foreset, the transition from topset to bottomset) takes on an ascending trajectory (Fig. 4.22). As documented elsewhere (MELLERE et al., 2002; BULLIMORE et al., 2005; HELLAND-HANSEN and HAMPSON, 2009), this occurrence is probably due to aggradation during a period in which rates of accumulation were greater than rates of uplift. On this basis, we can infer that the fold activity decreased at the end of Middle Pleistocene.
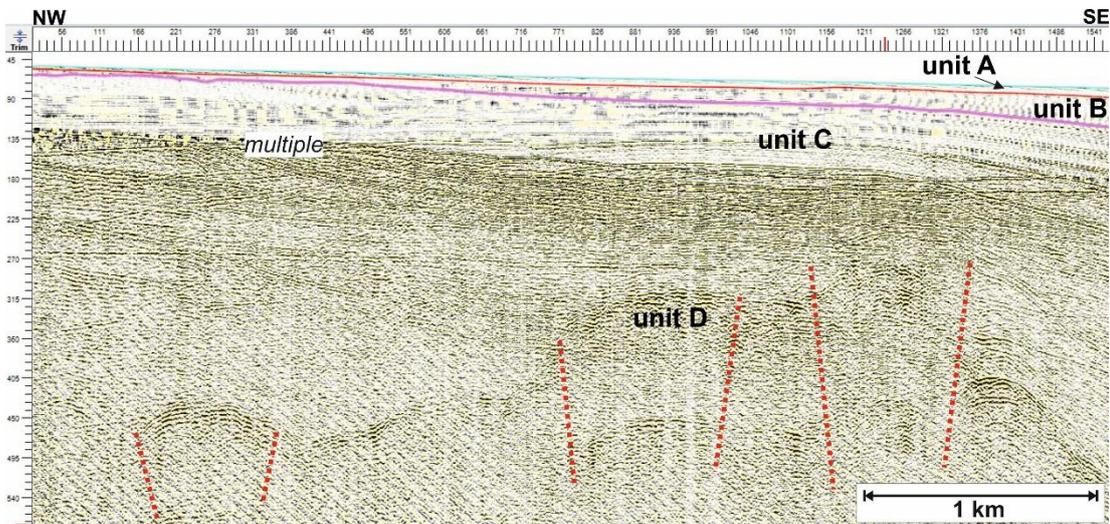
Fig. 4.23 – Sketch of P1 in which high angle faults deforming unit D and C are visible. Rollover point is located at a depth of 75 m. The horizontal scale indicates the shot points, while vertical scale shows depths in metres. Vertical exaggeration 4:1.

Many escape fluids pervade the units giving rise to a mound-shaped unit (MD) with irregular and discontinuous reflections. The lack of sedimentary cover above the mounds reveals a recent building activity.

The second imaged NW-SE trending transect (P4 and P6) is located ~ 6 km from Capo Granitola coast with a total length of 15 km and was acquired at 20-130 m bathymetric depths. The sea bottom is between 37 m and 110 m below the sea level.

In the NW part of the profile, unit A exhibits a mound-shaped internal geometry typical of sediments affected by bottom-water circulation (i.e. contourites; REBESCO et al., 2014), with a core thickness of ~ 8 m (Fig. 4.24).

The bottom-current sediments are also present within unit B showing a complex geometry of thin packages of reflections separated by continuous and high amplitude reflectors that mark secondary unconformities (Fig. 4.24).

From shot 1388 up to shot 6273 a ~ 3 km wide mound above a zone of wipe-outs interpreted as due active fluid flow, responsible for building up of the mounds, is visible. The fluids seem to arise from unit C in which wide wipe-out zones are visible and probably associated to the presence of faults along which fluids go up. The ascending fluids pervade unit B and A and originate both active and buried mounds (Fig. 4.5).
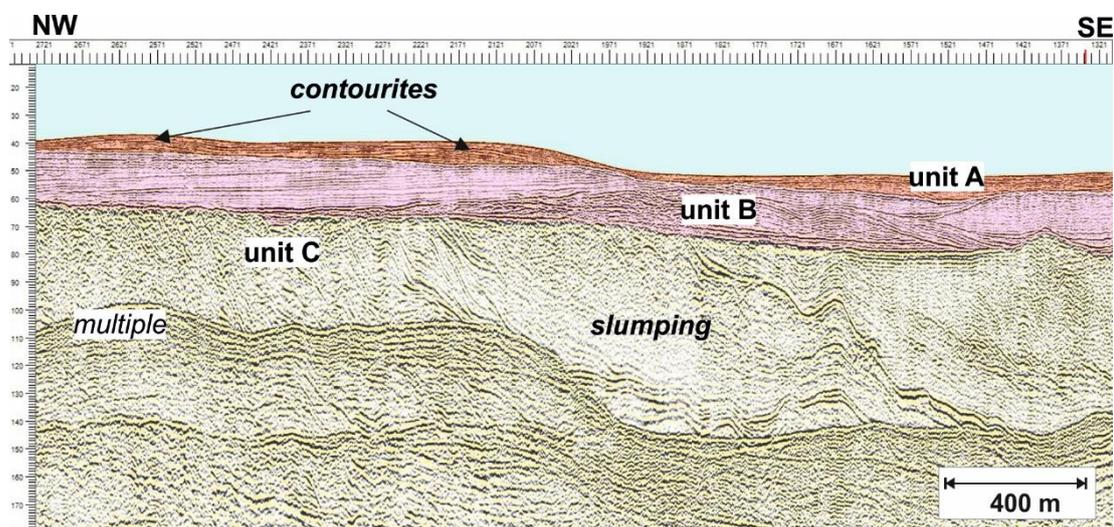
Fig. 4.24 – Sketch of P4 showing slumping within unit C produced by tectonic movements responsible of unit D uplift visible in Fig. 4.22. Unit B is characterized by complex geometry related to secondary unconformities. Unit A exhibits a mound-shaped internal geometry typical of contourite deposits. The horizontal scale indicates the shot points, while vertical scale shows depths in metres. Vertical exaggeration: 9:1.

As in P1, toward NW unit C is affected by slumping and tilting associated to unit D uplift, even if this unit is not visible in this part of the transect and the fault escarpment is less evident along ES2 (Fig. 4.24). Toward SE, the reflectors are more continuous and parallel, deformed by a series of faults that originates two main anticline folds (CG1, CG2) whose activity over time is deduced from reflectors geometry (Fig. 4.25). The structures are more evident than P1 and are responsible of unit D uplift that is highly

discontinuous. Along CG1 and CG2, unit D is topped by a semi-transparent/chaotic body probably related to fluid escapes through the faults (Fig. 4.25).
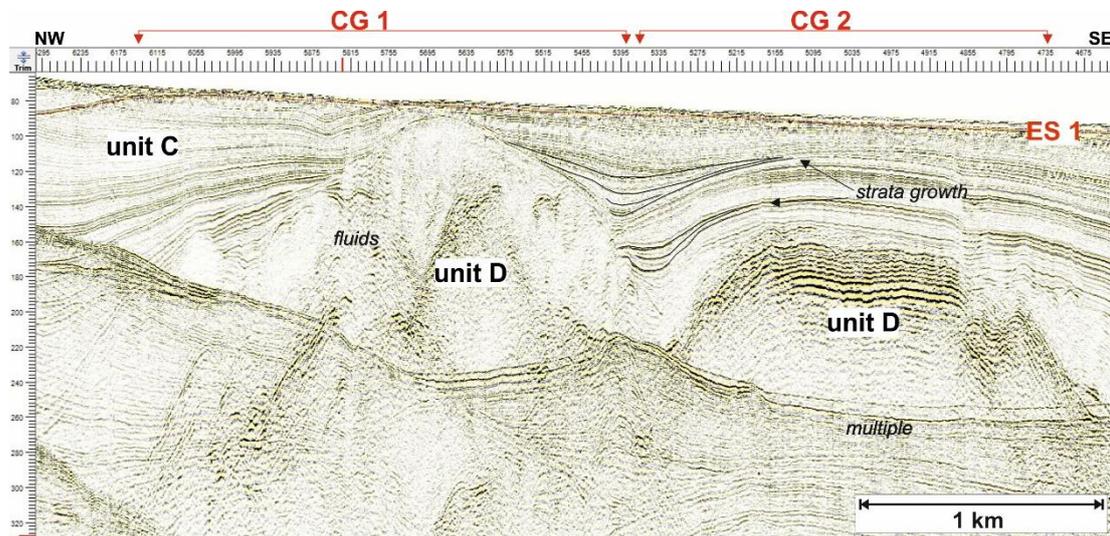
Fig. 4.25 – Sketch of P6 showing CG1 and CG2 responsible of unit D folding and faulting along which fluids escape. The overlying unit C is deformed: strata growth indicates more intense Pleistocene tectonic activities. The horizontal scale indicates the shot points, while vertical scale shows depths in metres. Vertical exaggeration: 7:1.

The profile P20 ubicated between Marinella and Capo San Marco for a length of 20,7 km shows a NW-SE direction. Along the profile the ES2 presents a very high acoustic impedance and is carved by numerous channel connected to Sicilian rivers (Fig. 4.5). Among these, a 1,19 km width channel with levees at a depth of 33 m represents the seaward prolongation of Belice river valley.

The ES2 truncates the folded reflectors pertaining to unit C (Fig. 4.9). The latter are deformed by two gentle anticlines, the first of which is visible only at half, separate by a syncline. The reflector geometry fixes the right limb of the NW anticline whose hinge could be out of the analysed area next to Sicilian coast between Capo Granitola and Marinella as evidenced by close profiles. Conversely, the hinge of the second anticline is visible.

The profile P23 is located in Area 2 at ~ 8 km from Capo San Marco. It was acquired along a NW-SE direction at a bathymetric depth of ~ 60-70 m. The sea bottom is between 60 m and 88 m below the sea level.

Along the seismic line, unit A exhibits a thickness ranging between 9 m and 46 m from the NW to the SE, respectively. Toward SE the unit is characterized by décollement surfaces associated to gravitational collapses which can be due to tectonic structures, indicating a Holocene age for the fold activity (Fig. 4.11). In fact, the underlying unit C is clearly deformed. At the northern-western sector of P23, high frequency folds are visible within unit C which are part of a major deformational system (Fig. 4.26).
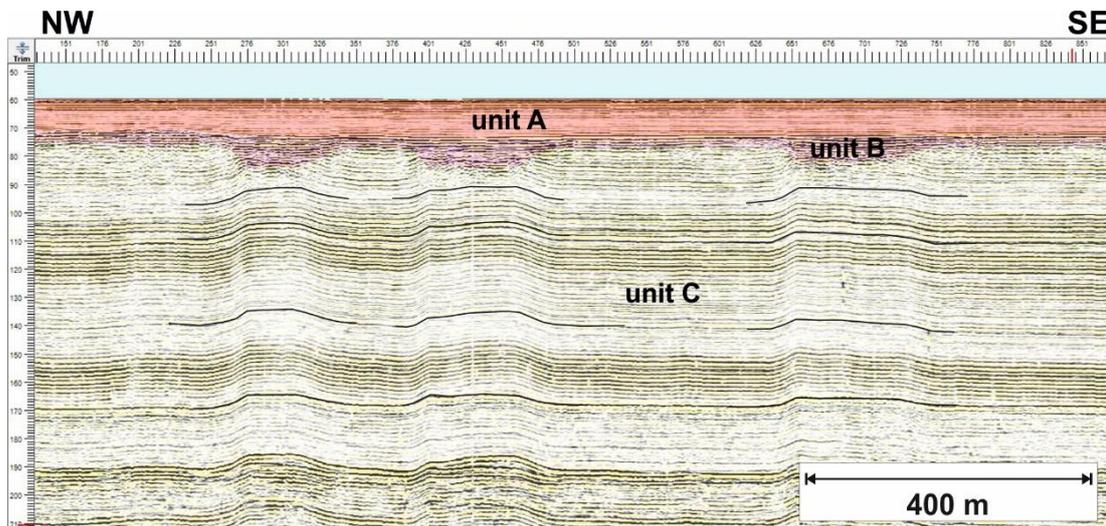
Fig. 4.26 – Sketch of P23 showing high frequency folds within unit C. The horizontal scale indicates the shot points, while vertical scale shows depths in metres.

Wipe-out zones, chaotic facies alternating to SE dipping reflectors separated by faults characterize the profile between the shot 4831 and 5981. A feature resembling Christmas tree structures related to a diapir is also visible (see figure 4.38). The fault zone is ~ 3 km wide and can be approximated to a broad anticline fold (SC1) that deforms also ES2. The associated synclinal is visible in the central part of P23 followed by a second anticline (SC2). Along the left limb of the fold, parasitic folds are recognized.
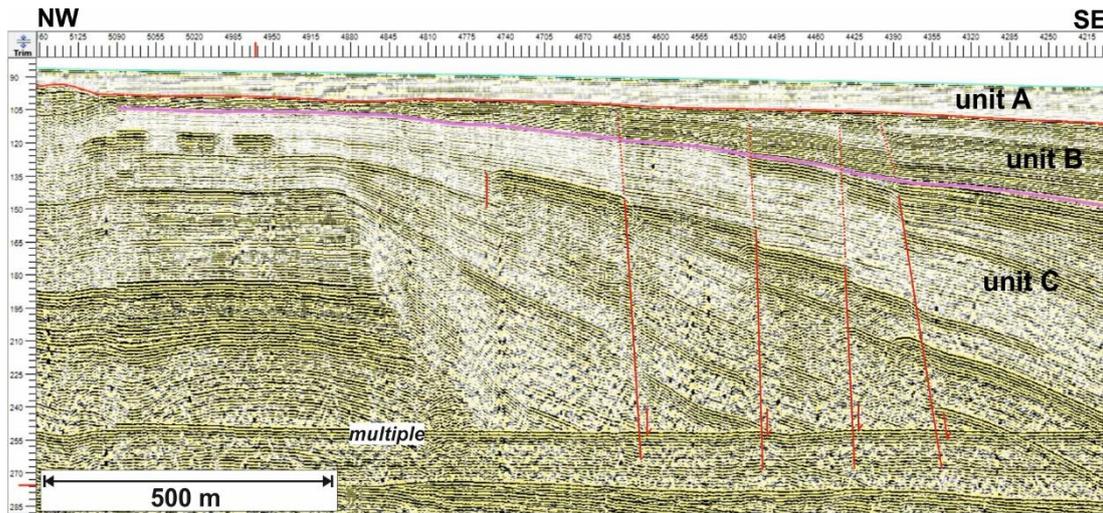
Fig. 4.27 – Sketch of P24 in which a series of high angle faults which deform unit C and B is highlighted. The horizontal scale indicates the shot points, while vertical scale shows depths in metres.
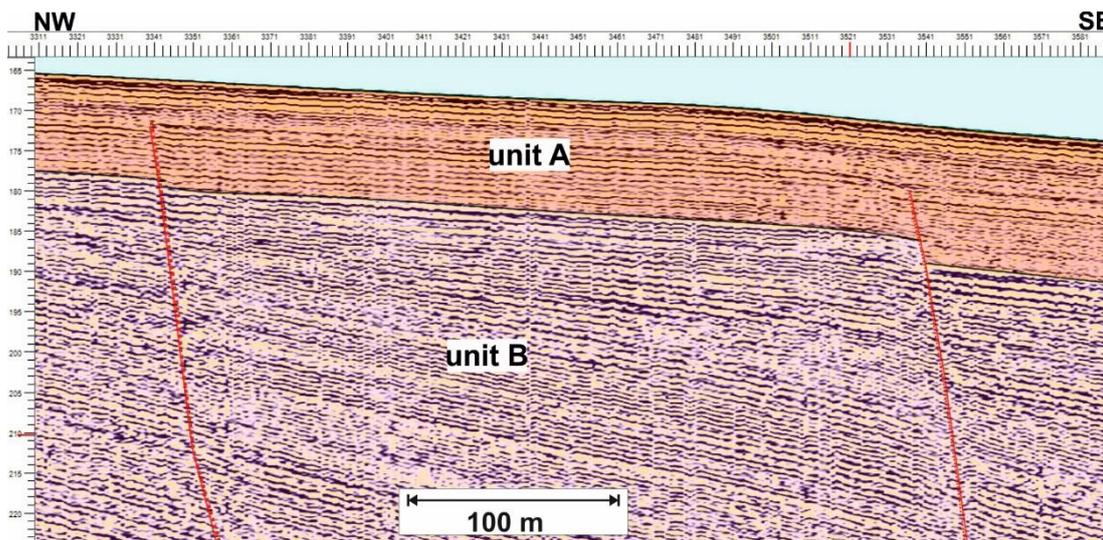
Fig. 4.28 – Sketch of P26 in which two fault deforming unit A are visible. The horizontal scale indicates the shot points, while vertical scale shows depths in metres.

Figure 4.27 shows a sketch of NW-SE trending profile P24, parallel to P23, where it can be noted the basal unit C deformed by high angle faults which are part of the fault zone associated to SC1. The faults exhibit a maximum offset of 20 m and seem to be active in the Holocene (Fig. 4.28). Locally, they constitute the preferential path for fluid escapes (e.g., Fig. 4.25).
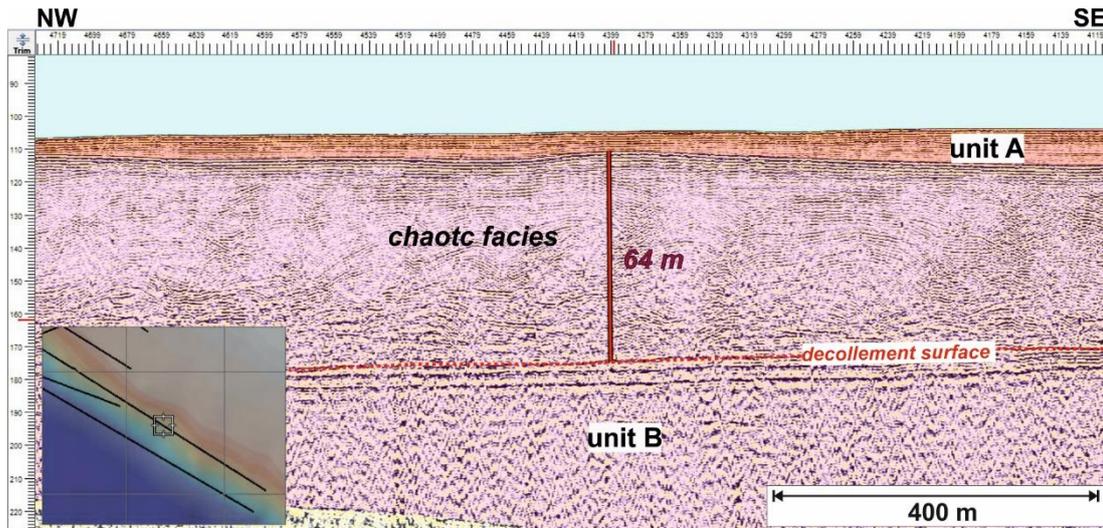
Fig. 4.29 – Sketch of profile P25 showing a chaotic seismic body with a maximum thickness of 64 m limited at the base by a decollement surface. The horizontal scale indicates the shot points, while vertical scale shows depths in metres. In the lower left corner, the basemap box is shown.

An important tectonic feature is visible in the profile P25 (Fig. 4.29), and is represented by a 10,87 km long seismic body characterized by a chaotic facies with a central maximum width of 64 m decreasing to zero toward SE and wedge-shape ending to NW. The body topped by ES1 and is limited down by a decollement surface which separates the chaotic body from the undisturbed seismic package pertaining to unit B.

4.7.2 Tectonic control on the depositional pattern of unit C

As described above, unit C reflectors are characterized by a seaward-prograding clinoform geometry both in the studied offshore area and on-land. This pattern is evident in all seismic profiles, but clearly only apparent dips can be calculated in a profile. Intersections of SCS lines with variable trend were used to calculated the true dips of the seismic reflectors attributed to unit C through a graphic method (RANUCCI & MONTI, 1963). This analysis on unit C reflectors is particularly useful to the purpose of this work, because it allowed us to characterize dip direction changes and correlate with growing

fold structures on one hand, and to merge information from on-land and offshore.

The graphic method is based on the knowledge of the apparent dip of a reflector within two intersecting lines. To achieve this information, the linear measurement tool of the Geosuite software was used. It allows to obtain the dip of a specific reflector by clicking on it to set a start point and again to set the end point, thus defining the distance over which the dip is measured. The apparent dip was measured along distances which vary among profiles on the base of the extent of the local deformation. The longer is the distance, the more accurate is the value of dip. In light of this, the linear segments were traced for distances ranging between 80 m-200 m.
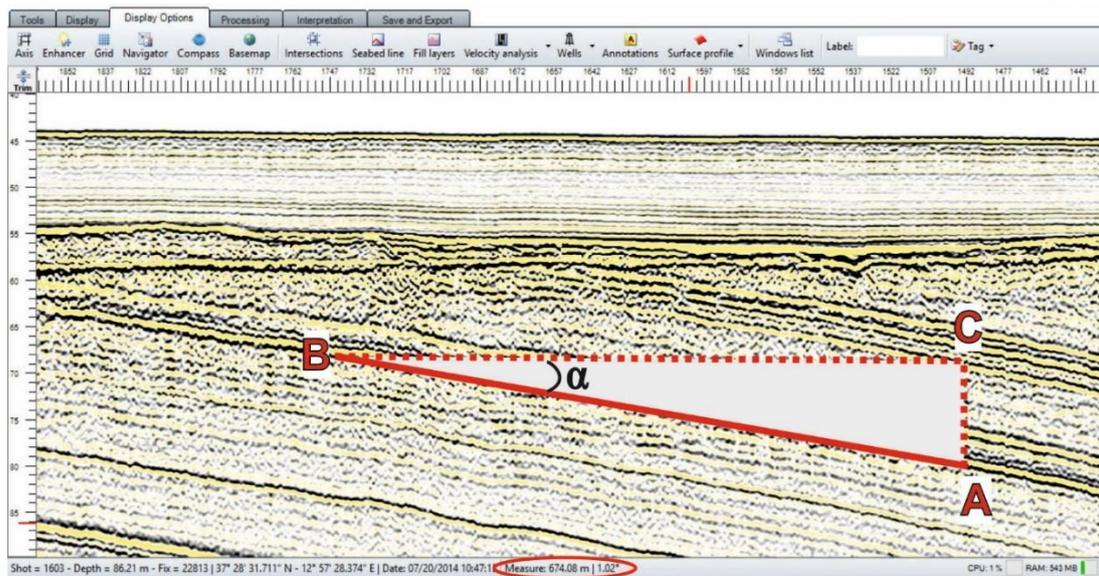
Fig. 4.30 – $\overline{\text{AB}}$ i*ndicates the traced segment along which dip value was measured and represents the hypotenuse of ABC triangle. α is equal to the dip angle calculated with the trigonometric method.*

Various quality checks were made using a simple trigonometric approach. Here, an example is presented (Fig. 4.30).

A 674,08 m ($\overline{\text{AB}}$, Fig. 30) long segment was traced between depths of 68,25 m (B, Fig. 30) and 80,22m (A, Fig. 4.30). This segment represents the

hypotenuse of a right triangle whose legs were drawn adjacent to the right angle (Fig. 30). The segment $\overline{AC}$ length derives from a difference between A and B and is equal to 11,97 m. By the Pythagorean theorem, the sum of the squares of the lengths of the legs is equal to the square of the length of the hypotenuse. So, $\overline{BC}$ can be calculated:

$$\overline{BC} = \sqrt{\overline{AB}^2 - \overline{AC}^2} = \sqrt{674,08^2 \ m^2 - 11,97^2 \ m^2} = 673,97 \ m$$

The α dip angle is equal to:

$$\alpha = arctg \ \frac{\overline{AC}}{\overline{BC}} = arctg \ \frac{11,97 \ m}{673,97 \ m} = 1,02°$$

The calculated value of α is equal to that obtained with Geosuite linear tool (red circle in Fig. 4.30). This equivalence represents the proof of the good quality of the linear measurement tool.

Each value of dip measured at profiles intersections is listed in Table 4.2. Then, a polar coordinate system was used in which each point on a plane is determined by a distance from a reference point and an angle from a reference direction. The reference point (analogous to the origin of a Cartesian system) is called the pole, and the ray from the pole in the reference direction is the polar axis. The distance from the pole is called the radial coordinate or radius, and the angle is called the angular coordinate, polar angle, or azimuth.

Each profile was drawn considering its direction respect to the North (azimuth) from the origin point O (Fig. 4.31). Starting from O and in direction of apparent dip of the checked reflector, segments indicative of the tangent of dip angle were drawn to scale. From each ending point a normal segment was traced. The resulting segment $\overline{OH}$ gives the direction of the maximum dip, whereas its length is proportional to the α tangent.

When the dip is equal to zero in a profile, the direction of maximum dip coincides with the trend of the intersecting line, i.e. it was acquired along the maximum dip.
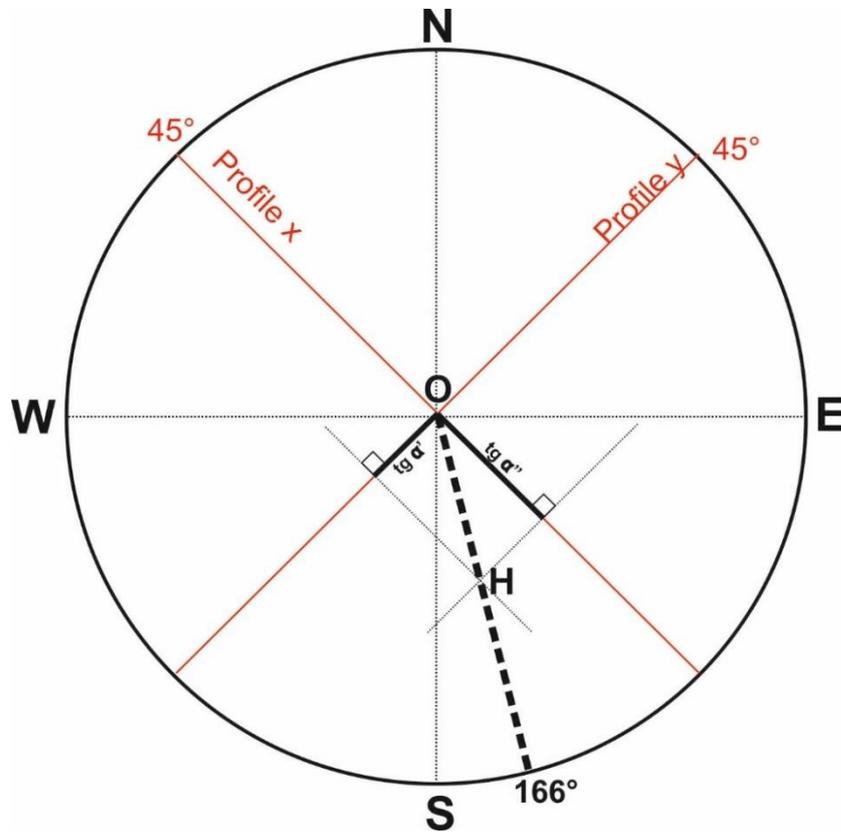
Fig. 4.31 – Example of dip direction and dip angle determination starting from apparent dip. The red lines indicate the profiles directions respect to the North. Starting from O in direction of apparent dip of the checked reflector, two segments indicative of the tangent of dip angle were drawn to scale (tg α' and tg α''). From each ending point of the two segments, normal segments were traced. These segments cross in a point, H. The length of the traced $\overline{OH}$ segment is proportional to the α tangent and its projection on the polar circle gives the direction of the maximum dip.

This graphic method was used for the computation of true dips of reflectors pertaining to unit C located at an average depth of ~ 100 m. The computed angles and dip direction listed in the Table 4.2 are reported in a map (Fig. 4.32). The dip direction shows a general trend toward the S, but trend and inclination values locally differ. In Area 1, south of Capo Granitola coast,

the dip angles have a wide range up to 8.7°. Dip directions are variable from N 110° E to N 251° W.

TABLE 4.2

	P15	**P13**	**P15**	**P1**	**P15**	**P2**	**P15**	**P5**	**P15**	**P8**
APPARENT DIP	0,41°	1,53°	0°	0,22°	0,71°	0,35°	0,78°	1,63°	0,5°	0°
MAXIMUM DIP (TRUE ANGLE)	1,6°		0,22°		0,87°		1,75°		0,5°	
DIP DIRECTION	S 151° E		S 137° E		S 251° O		S 110° E		S 227° O	

	P14	**P13**	**P14**	**P1**	**P14**	**P2**	**P14**	**P4**	**P14**	**P16**
APPARENT DIP	4,7°	1,5°	3,1°	2,5°	5°	7,2°	3,6°	1,9°	1,32°	1,02°
MAXIMUM DIP (TRUE ANGLE)	4,9°		4,4°		8,7°		4,1°		3,7°	
DIP DIRECTION	S 219° O		S 182,5° O		S 172° E		S 201° O		S 159° E	

	P28	**P21**	**P28**	**P22**	**P28**	**P20**	**P28**	**P23**
APPARENT DIP	4°	0,65°	2,4°	1°	1,9°	1,9°	2,6°	0°
MAXIMUM DIP (TRUE ANGLE)	4,3°		2,9°		2,7°		2,7°	
DIP DIRECTION	S 203° O		S 192° O		S 180° 0		S 212,5° O	

	P29	**P22**	**P29**	**P23**	**P29**	**P24**	**P29**	**P25**	**P29**	**P27**
APPARENT DIP	1,3°	2°	1,7°	0,6°	1,4°	0,3°	3°	1°	3°	0°
MAXIMUM DIP (TRUE ANGLE)	2,1°		1,85°		1,28°		3,1°		3,2°	
DIP DIRECTION	S 132° E		S 193° O		S 201° O		S 193° O		S 201° O	

	P30	P21	P30	P22	P30	P23	P30	P24	P30	P25
APPARENT DIP	0°	0,2°	2,15°	1,2°	0,95°	0,1	2°	0°	2°	2°
MAXIMUM DIP (TRUE ANGLE)	0,3°		3,95°		1,32°		2,5°		4,6°	
DIP DIRECTION	S 158° E		S 193,5° O		S 207° O		S 211,5° O		S 186° O	

P30	P27	P30	P29
0,84°	1,1°	1,96°	3,4°
2,7°		3,5°	
S 177 E		S 192° O	

	P17	P13	P17	P16
APPARENT DIP	0,1°	1,2°	3,5°	1,51°
MAXIMUM DIP (TRUE ANGLE)	1,25°		6°	
DIP DIRECTION	S 145° E		S 186° O	

	P1	P3	P26	P19	P18
APPARENT DIP	2,61°	0,29°	0,6°	0,2°	1,12°	3,86°
MAXIMUM DIP (TRUE ANGLE)	4°		0,79°		6,5°	
DIP DIRECTION	S 226° O		S 186° O		S 187° O	

Based on observations on the outcropping Marsala formation next to the coasts of Capo Granitola and Marinella (black arrows, Fig. 4.32), the predicted average value of the offshore zone should be around N 200° W for the direction and around 4° for the dip angle. Thus, the large departures from the average values can be attributed to syn-depositional tectonics.

Dip directions and angles differ in Area 2 offshore between Sciacca and Eraclea Minoa even if with a lesser discrepancy with respect to Area 1, probably due to the greater distance among the profiles that not allows to detect dip variations. Nevertheless, the value of 4,3° near Capo San Marco disagrees with the closer values highlighting a strain zone.

The spatial orientation of unit C shown in the map of figure 4.32 has been compared with the structures visible in the profiles and above described (see par. 4.7; Figs. 4.22 to 4.27). It can be argued that the locally observed anomalies in dip values in the area south of Capo Granitola are influenced by the folds that caused uplift of unit D and controlled unit C deposition. The spatial control exerted by active fold growth on unit C is discussed in next paragraphs.
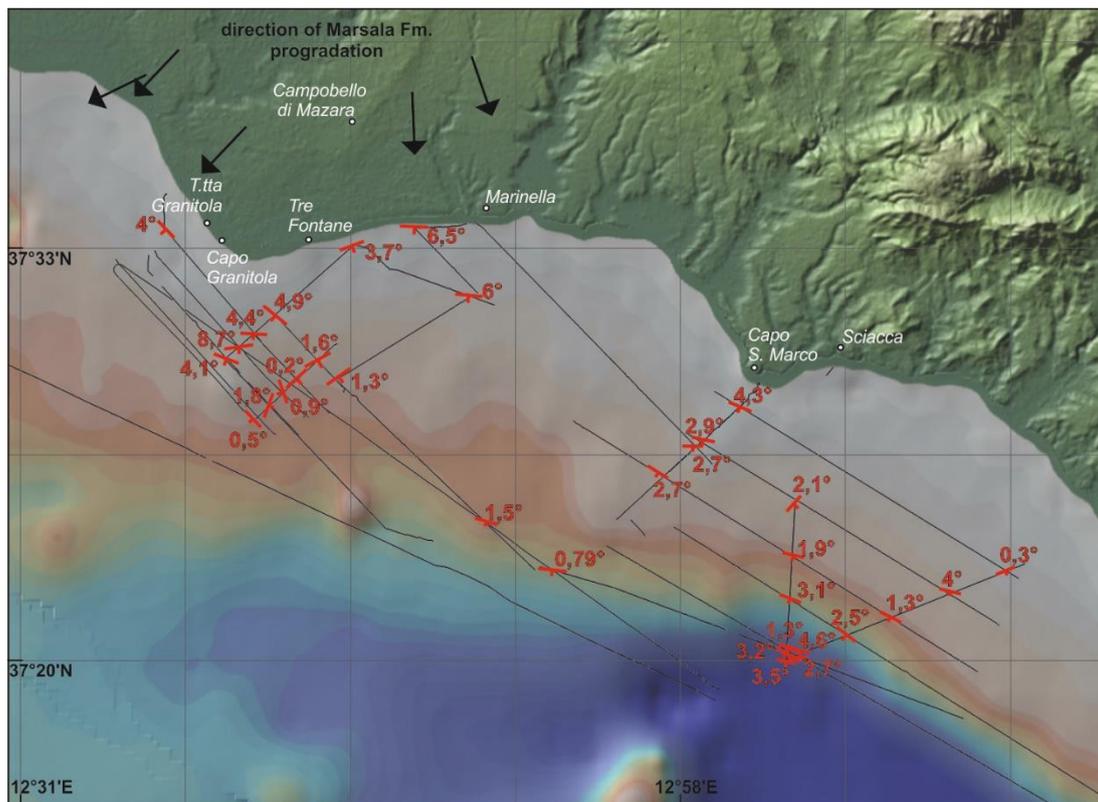
Fig. 4.32 – Dip directions and dip angles computed for a horizon within unit C, through the method described in the text.

4.7.3 *Mound and fluid distribution*

The seismo-stratigraphic analysis of SCS profiles allowed to highlight seismic signal anomalies related to fluid seepage. A distinction was made between seepages with no morphologic expression and seepages associated to mound-shaped features. The former show no dislocation of erosional surfaces or of the overlying horizons, but only evidences of deformation and blanking zones. The mound-shaped features can be convex, plane or buried. As introduced in the paragraph 4.3, these positive structures are characterized by irregular and discontinuous internal reflection patterns and have been grouped in seismic unit MD. These structures are tentatively interpreted as representative of "Cold Seeps".

The seepage of fluids from the seafloor into the water column is a widespread phenomenon in the world's oceans (SUESS, 2010). Cold seeps are defined as localities of low temperature fluid escape from the seafloor (TALUKDER, 2012) with a lower emission rate respect to "Hot Vents", which on the contrary are fluids heated in close vicinity of magma chambers within the oceanic crust spreading centres. Convergent plate boundaries, and particularly subduction zones, form a preferred area for cold seeps. The dewatering of the underlying plate and the methane production in the accretionary wedge provide fluids for seafloor seepage. The pressure created by the plate convergence further facilitates upward fluid migration and the formation of pathways such as fault splays. The prerequisites for evolution of seafloor methane seepage include the abundant presence of organic matter to allow methane to form and the geological features to facilitate methane migration towards the seafloor. Most of cold seeps occur in coastal and continental margin settings due to the maximum of terrigenous organic input by river deltas and marine fans. Seepage sites in the deep oceans are generally related to drift deposits incorporating organic material of terrigenous origin (JUDD & HOVLAND, 2007).

Sub-marine morphological expressions of cold seepage include a wide variety of different features ranging from build-ups (such as mud volcanoes, carbonate mounds) to depression (pockmarks). Mud volcanoes are extrusion points of solid material and fluids that show a positive topography at the seafloor or beneath it. Whereas, diapirs are intrusion of fluids within the sedimentary cover and are not associated to material extrusion. When a diapir reaches the seafloor, it generates a mud mound which is different from a mud volcano because of the lack of conduit.

In the Mediterranean Sea, many mud volcanoes were discovered. In the offshore of SE Sicily, they are ~ 3-4 km in diameter and 400 m in height with a total volume of 11.4 km^3 (HOLLAND, 2003).

MILKOV (2000) individuated the common features of mud volcanoes: the presence of a plastic clay level within the sedimentary succession; generally, they are associated to overpressured Tertiary sediments and hydrocarbon, especially methane; seismicity of the area; they generally form within passive margin where there is a high rate of sedimentation or within zones affected by tectonic compression.

We used evidence of seepage in seismic profiles to build the map of figure 4.33. The seepages are classified on the base of areal dimension measured along one direction and interpolated in two dimensions by assuming a cylindric model.

Buried mounds are mostly observed on the continental shelf in front of Capo S. Marco, at a distance from the coastline ranging from 6 to 12 km, and at a depth between ~ 50 and 80 m. They show chaotic or transparent seismic facies, cut adjacent reflectors and are topped by a high amplitude reflector. These structures are sealed by more recent deposits (unit A), have a horizontal width between 50 m and 300 m and rise from the erosion surface ES2 or ES1 for ~ 4 m. Some of them cross the ES2 and the above reflectors (Fig. 4.34), instead others deform the erosional surfaces and surrounding reflectors without crossing them (Fig. 4.36).
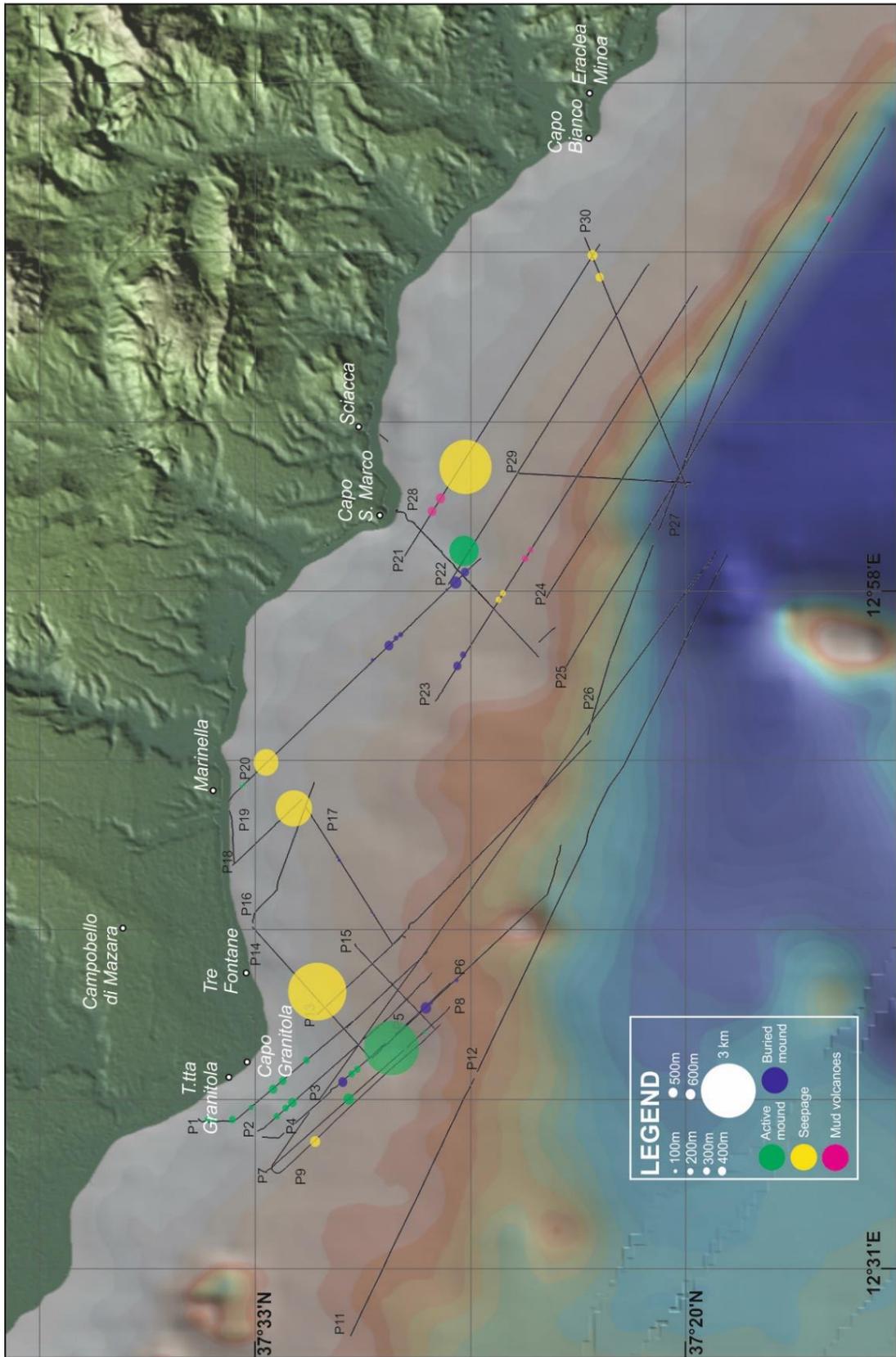
Fig 4.33 – Mound and fluid distribution.
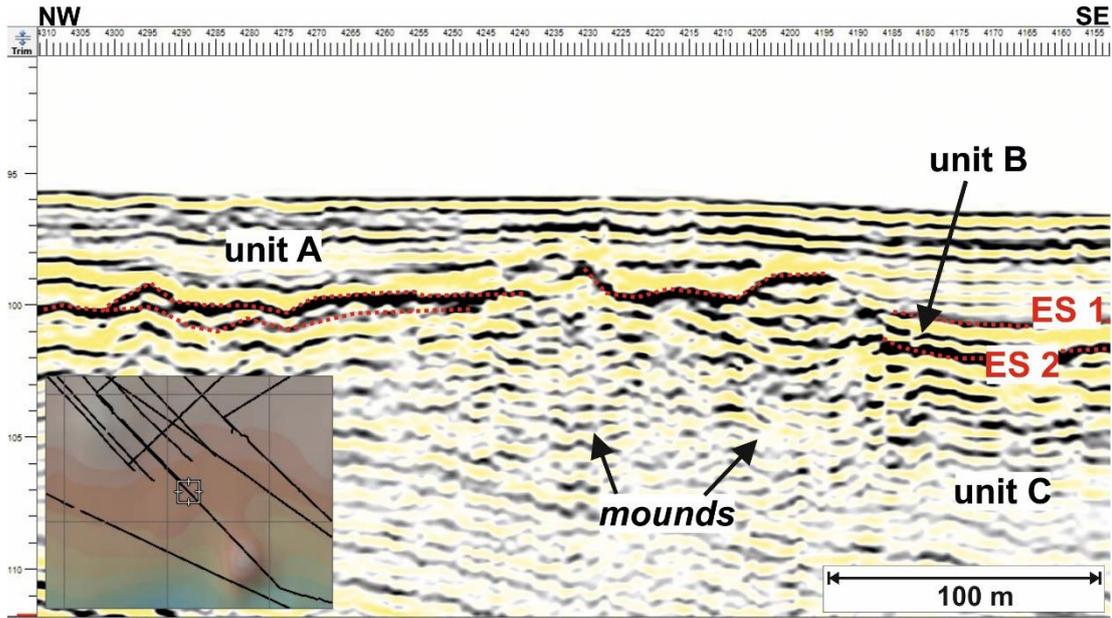
Fig. 4.34 – Sketch of profile P6 showing buried mounds that cross the ES1 and ES2. The horizontal scale indicates the shot points, while vertical scale shows depths in metres. In the lower left corner, the basemap box is shown.

Active mounds (Fig. 4.35) were recognized exclusively on the continental shelf at depths between ~ 20 m and 130 m. They range from 100 m to 3,5 km in width and rise up to 15 m in height. These structures show internal facies from chaotic to transparent and dome-shaped form, locally with a central depression, and deform adjacent reflectors.
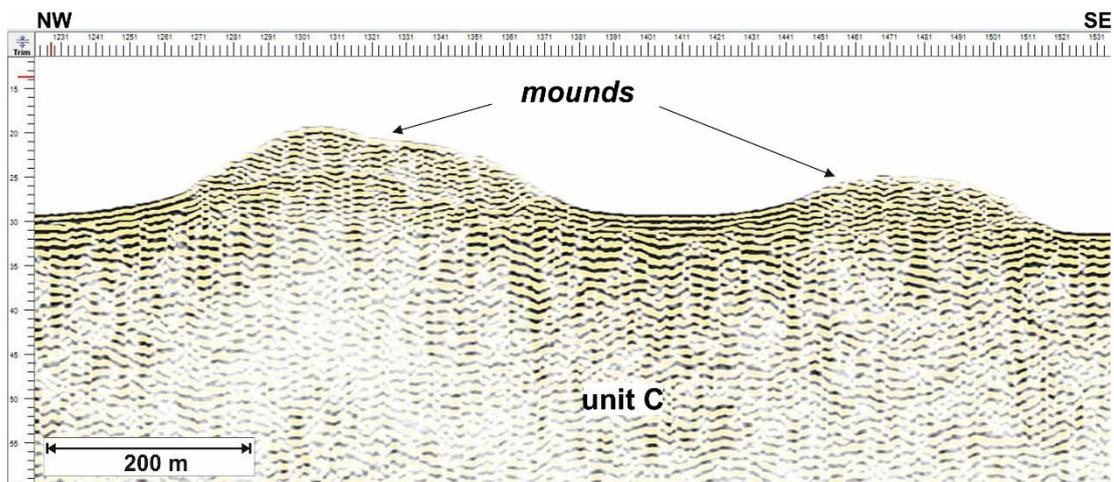
Fig 4.35 – Sketch of profile P1 showing active mounds. The horizontal scale indicates the shot points, while vertical scale shows depths in metres.

The zones affected by seepage without morphological expression in the seismic images (Fig. 4.36) were recognized based on the occurrence of wipe-out zones and reflector amplitude anomalies. In some cases, no large parabolic reflection cones are observed in seismic images at wipe-out zones and reflections remain significantly lower in amplitude. Thus, the acoustically transparent zones signify high attenuation and not out of-plane reflections, as if caused by a physical offset (faulting) of sediments.

The wipe-out zones occur underneath seafloor craters, formed by episodic but violent gas blowouts, and mud or carbonate mounds (Figs. 4.35, 4.36, 4.37, 4.38). Such anomalous seismic pattern might result from processes that promote mobilization of fluids through layers and may indicate, more than a discontinuity zone, areas where upward migration of gas-fluids most likely occurs or has occurred (SIMONETTI et al., 2011). In general, the distribution of fluid seeps is controlled by buried underlying features such as faults and erosional surfaces.
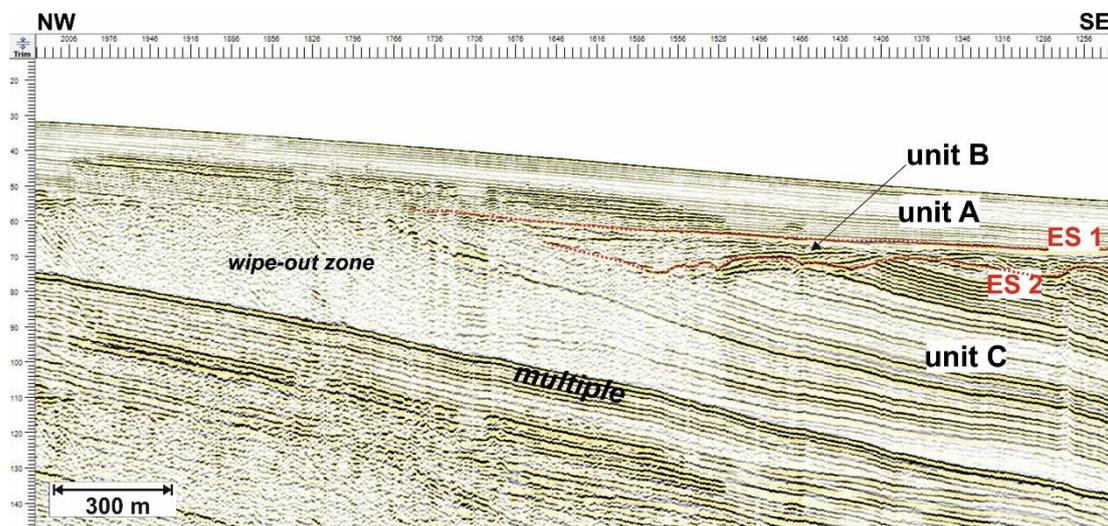
Fig. 4.36 – Sketch of profile P13 showing fluid seepage without morphological expression. The horizontal scale indicates the shot points, while vertical scale shows depths in metres.

The acoustically-transparent zones are also found in correspondence of high-angle fractures or secondary faults of minor, often undetectable offset

(Figs. 4.37, 4.38). In some case, larger faults are expressed as fault escarpments and extend beyond the penetration depth of the Sparker signal.
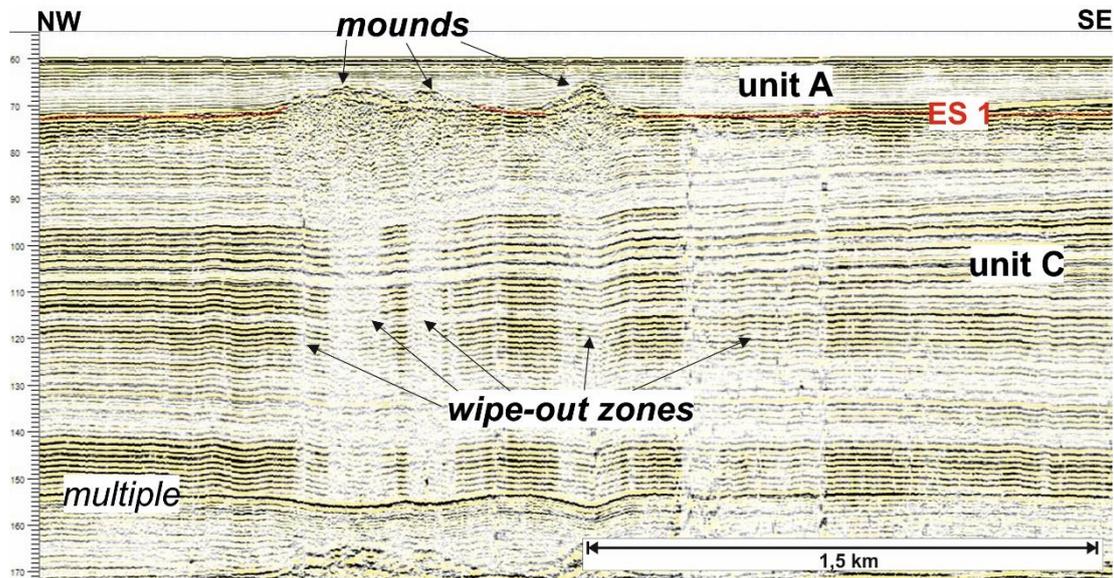
Fig. 4.37 – Sketch of profile P23 of Area 2 showing wipe-out zones associated to fractures. The horizontal scale indicates the shot points, while vertical scale shows depths in metres.

High permeability faults probably act as primary conduits for fluids, and the acoustically transparent zones likely represent lower permeability sediments located adjacent to the faults either charged with gassy fluids or affected by cementation and diagenetic processes. Similar acoustically-transparent features are frequently observed in seismic data collected in hydrate provinces and are interpreted to result from (1) attenuation of acoustic signals by gas bubbles, (2) seismic blanking caused by grain cementation via gas hydrate formation, (3) loss of sediment grain-to-grain contact created by high pore-pressure, or (4) authigenic carbonate formation. Regardless of the mechanism, acoustically-transparent sediments below seeps are typically taken as evidence for past or ongoing fluid migration (HORNBACH et al., 2007 and references therein).
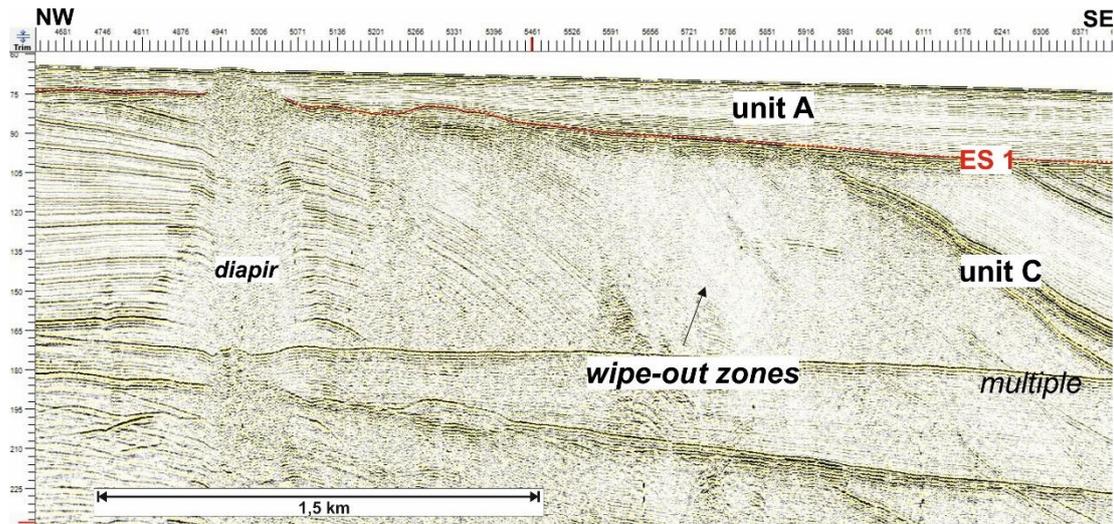
Fig. 4.38 – Sketch of profile P23 in which diapir and fluid seepages related to faults are visible. The horizontal scale indicates the shot points, while vertical scale shows depths in metres.

4.7.4 Structural framework

The seismo-stratigraphic analysis of SCS reflection profiles calibrated with well-log data and land outcrops, as described in the previous sections, has allowed to reconstruct the structural framework of the shallowest part of the studied offshore area. The morpho-bathymetric evolution seems to be governed by the growth of compressive structures (folds and fold scarps), characterized by locally different geometries. Scarps and folds recognized along individual profiles were projected in map (Fig. 4.39) through utility of the Geosuite software. The map of figure 4.39 shows axes of anticline and syncline folds recognized in the SCS profiles. Specifically, within Area 1, a prominent tectonic scarp (here named the "CG Escarpment"), described in subparagraph 4.7.1, and three major folds ("CG1" to "CG3") are recognized. Three main folds are mapped within Area 2 (folds "SC1" to "SC3").

The geometrical parameters: offset or amplitude (i.e., the distance along the axial plane from the median surface to the hinge), distance from the coast and wavelength (i.e., the distance between two successive anticlinal or synclinal hinges), of the scarp CG and of folds CG1, CG2, SC1 and SC3, extracted from each profile, are summarized in Tables 3 and 4, respectively.

168
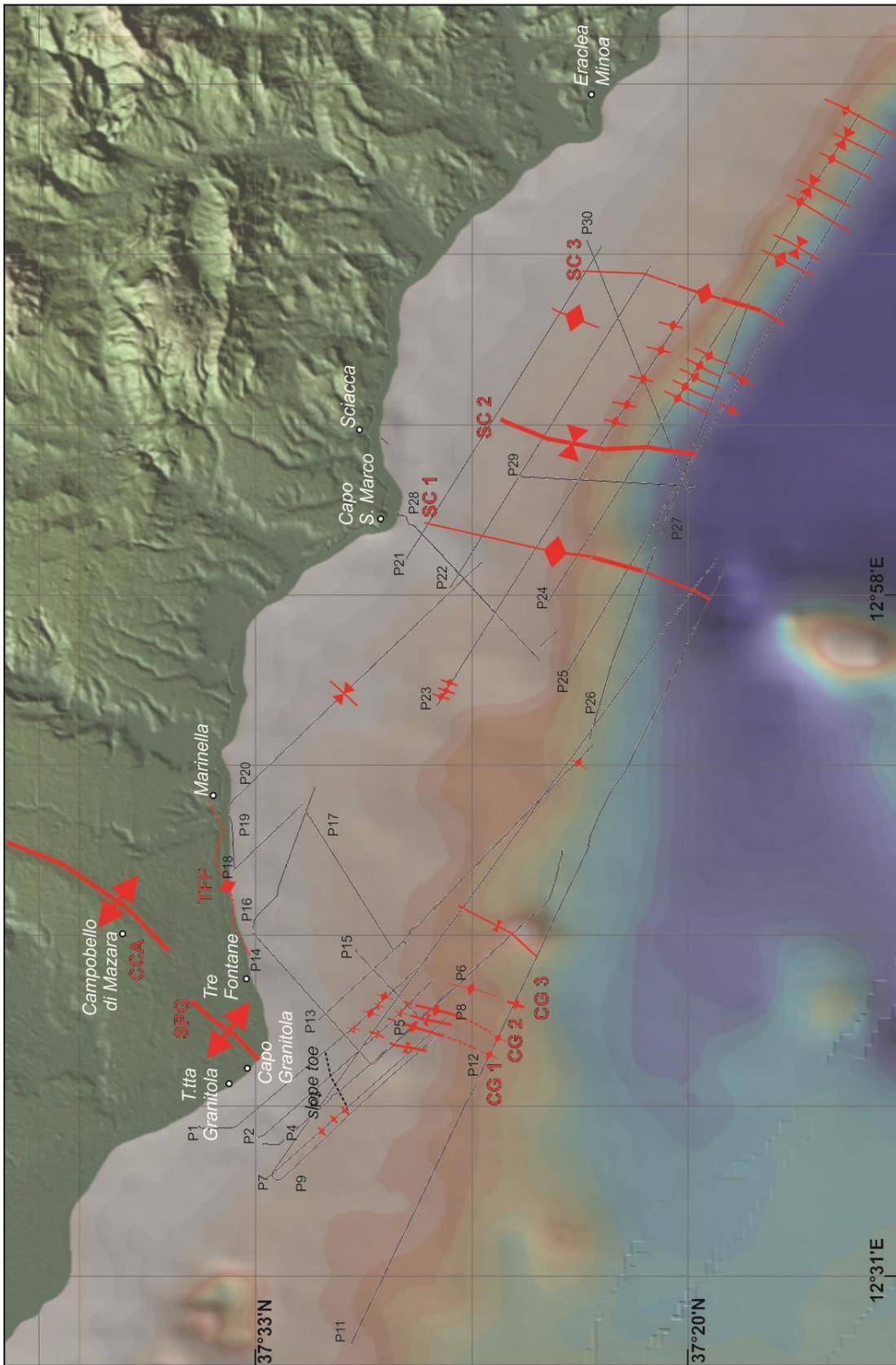
Fig. 4.39 – Structural map of the study area.

TABLE 4.3

CG Escarpment		
LINE	**ES2 offset (m)**	**DISTANCE FROM THE COAST (km)**
P1	30	2,3
P2	33	3,6
P3	20	4,5
P4	13	4,67
P7	16	5,85
P9	16	6,35

TABLE 4.4

CG 1			
LINE	**AMPLITUDE (m)**	**DISTANCE FROM THE COAST (km)**	**WAVELENGTH (km)**
P1	20	4,410	0,74296
P2	64	6,410	1,48
P6	87	7,541	2,35
P8	125	8,496	2,29
P9	118	8,846	1,62
CG 2			
LINE	**AMPLITUDE (m)**	**DISTANCE FROM THE COAST (km)**	**WAVELENGTH (km)**
P1	6	4,410	4,18
P2	27	6,410	2,86
P5	35	7,470	2,47
P6	36	7,541	9,32
P8	47	8,496	0,861
P9	24	8,846	1,61
SC 1			
LINE	**AMPLITUDE (m)**	**DISTANCE FROM THE COAST (km)**	
P21	46	2	
P22	44	5	
P23	69	8	
P24	182	10,24	
P25	218	13,24	
P26	121	14,24	
P3	170	19,14	
P12	158	20,27	

SC 3		
LINE	AMPLITUDE (m)	DISTANCE FROM THE COAST (km)
P21	18	2
P22	42	5
P23	60	8
P24	103	10,24
P26	202	10,82
P25	156	12,68

On the base of the fold geometrical properties, different styles of deformation can be attributed to Area 1 and Area 2, respectively.

Within the NW sector of Area 1, the height of the fault escarpment changes along its trend, as recorded by profiles with varying distance from the coast (Table 4.2). Similarly, the offset of horizon ES 2 along the escarpment, has a maximum value (33 m) visible in profile P2 at 3.6 km away from the coast; this height decreases toward both the south-west and north-east. This structural feature is here interpreted to be associated to a blind fault which caused folding and uplift of unit D (Fig. 4.22) and considered as the offshore prolongation of the on land SPG (Straglio-Punta Granitola) fold described in the chapter I (Fig. 1.6). Toward the SW, the uplift decreases and contemporary unit A thickness increases moving to the offshore from ~ 3 m in P1 to ~ 30 m in P7. Three small folds are recognized in profile P7, which in our interpretation represent a local effect of deformational system related to uplift of unit D, visible in the parallel profiles (P1, P2, P4) closer to the coast.

The central part of Area 1, south of Capo Granitola, is affected by three main anticline folds, CG1, CG2, CG3, with different amplitude and wavelength as evidenced by figures 4.22, 4.23, 4.25 and Table 4.4. The folds are part of a ~ 3 km wide and ~ 8 km long deformation zone.

The anticlines CG1 and CG2 produce the maximum deformation of unit C strata along profile P8, ~ 8 km from the coast, laterally decreasing in adjacent profiles along a NNE-SSW direction, which is the mapped fold trace.

Conversely, fold CG3, which is visible in profile P6, where the deformation is very small, shown an increase in amplitude (33 m) toward the south in the profile P12.

The near offshore area between Tre Fontane and Marinella is controlled by a fold (TFF; Fig. 4.39) whose hinge is not visible in the profiles but tentatively drawn in the map according to changing stratal dips. Probably, it represents a secondary folding related to the main CCA-SPG folds.

The Area 2 is characterized by two main anticlines, SC1 and SC3, separated by syncline SC2, all of which showing a NNE-SSW trend. These folds are associated to a deformational pattern characterized by blanking and semi-transparent fault zones (Fig. 4.38). SC1 and SC3 show the maximum amplitude within P25 and P26 at 12,68 and 10,82 km from the coast, respectively. At ~ 10 km from the coast the amplitude exceeds the 200 m (Table 4.4). The minor anticlines between SC2 and SC3 are parasitic folds highlighted along parallel profiles (Fig. 4.39). Nevertheless, because of the limited extension of these folds a correlation of geometrical parameters across parallel profiles cannot be made.

Furthermore, the lack of profiles in the shelf next to Eraclea Minoa does not allow a complete description of the folds located to the south-east of SC 3.

4.7.5 Analysis of fold geometries

By using the values of amplitude and distance from the coast listed in Tables 4.3 and 4.4, a series of graphs (Figs. 4.40 to 4.46) has been constructed to illustrate the changes in displacement magnitude along the described structures, and to readily identify sectors with relatively higher tectonic activity. The almost regular 1 km spacing between profiles resulted in a homogenous distribution of individual value estimates.

We seek here to show how the amplitude, the trace length and the wavelength change both among and within individual structures.

We analysed the structures benchmarking them against a standard bell–shaped curve typical of fault growth, as we made for the geometrical analysis of Sciacca Fold explained in chapter III. We used the curve showing the longitudinal change in amplitude to estimate the length of the structure measured along the trace (trace-length, to avoid confusion with wavelength). In the case that the structures are not completely sampled by our profiles, we computed an estimated trace length by projecting the observed part toward coasts or further offshore (dashed in Figs. 4.41 to 4.46).

Figure 4.40 shows the pattern of CG escarpment computed along profiles by measuring the height difference of the ES2 reflector. The visible trace length of fault escarpment, measured from P1 to P4, is about 2 km. We consider the offset (uplift) of ES2 from P4 to P9 as not being caused by the tectonic escarpment but by a more regional process. Thus, we propose that the CG scarp tends to disappear in the south-western part of Area 1, where the trend line tail shows slightly higher value with respect to the inflection point in P4, possibly due to the presence of fluid seepages visible in the profiles, that affected fault escarpment height.
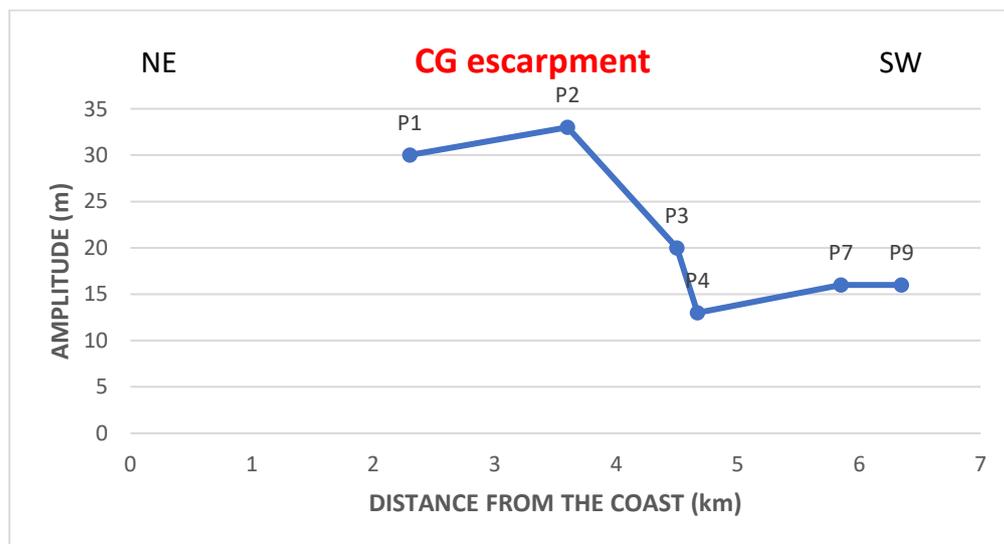
Fig. 4.40 – Graph of amplitude vs. distance from the coast relative to CG escarpment.

Toward NE, because the displacement trend is abruptly truncated, we suggest that the structure is not completely sampled in our analysis. The trend shows only one branch of the bell-shaped curve (here adopted for a fold escarpment). Thus, the truncation indicates that the slope should continue outside the study area and in direction of Capo Granitola coast.

Figures 4.41 to 4.46 highlights the pattern of CG1, CG2, SC1, SC3, computed along the same reflector pertaining to the middle part of unit C, to which a broad early Sicilian age (~ 1 Ma) can be assigned. The profiles show both complete or incomplete bell-shaped curves.
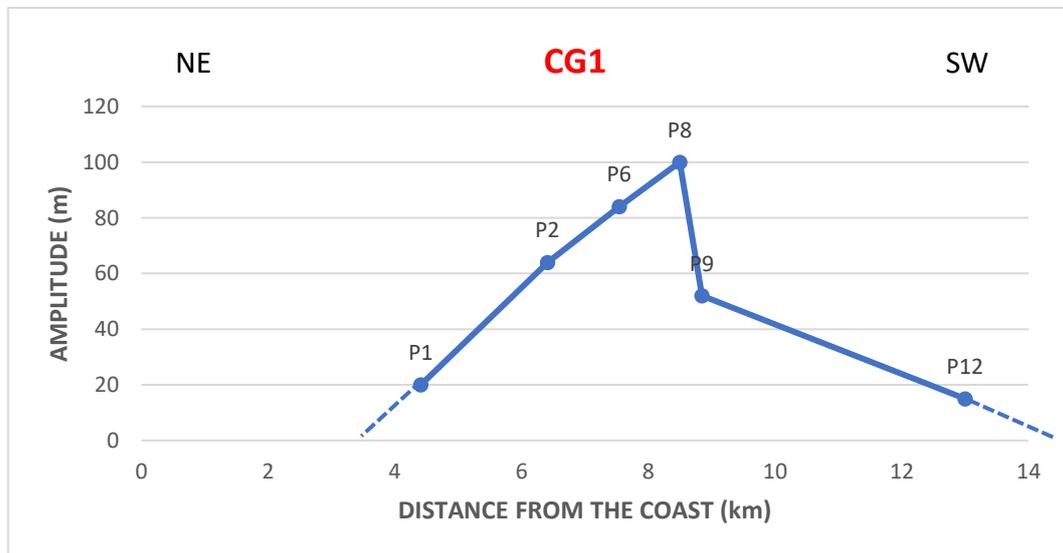
Fig. 4.41 – Graph of amplitude vs. distance from the coast relative to CG1.
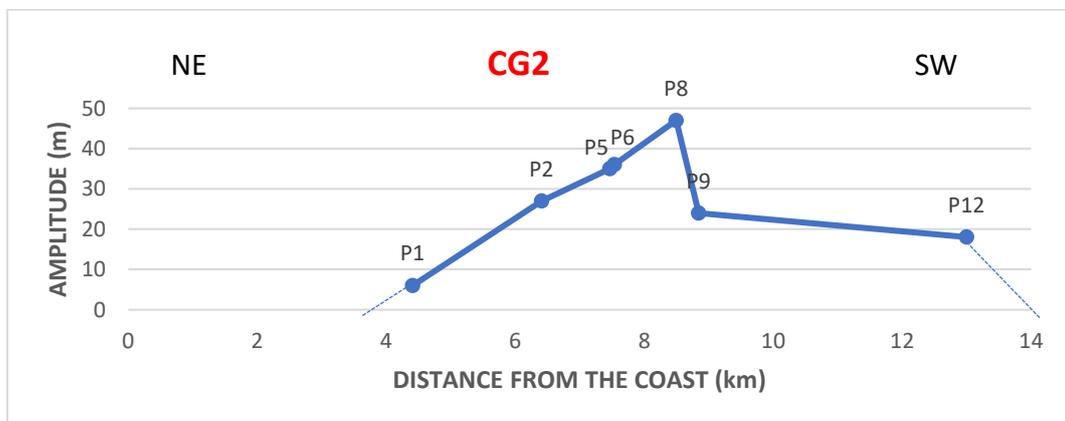
Fig. 4.42 – Graph of amplitude vs. distance from the coast relative to CG2.
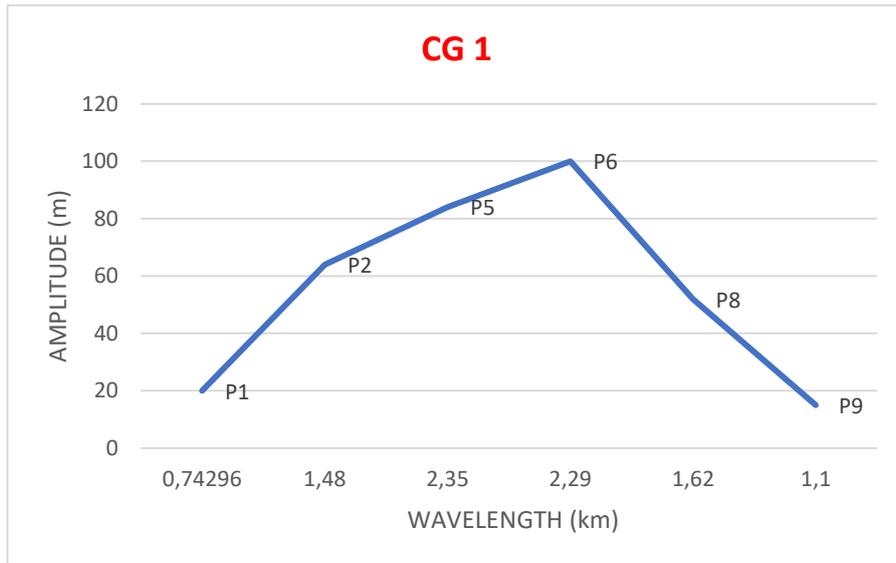
Fig. 4.43 – Graph of amplitude vs. wavelength relative to CG1.
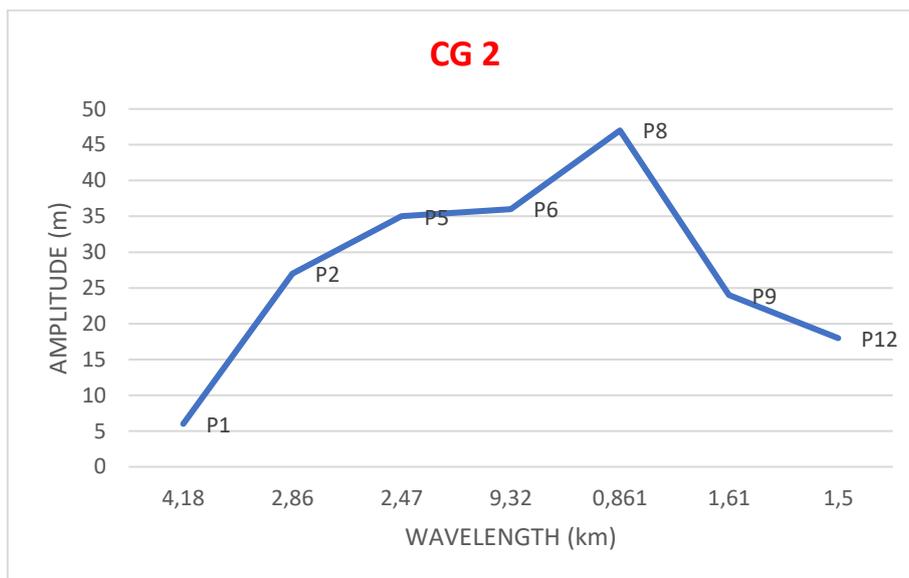
Fig: 4.44 – Graph of amplitude vs. wavelength relative to CG2.

The trend of CG1 and CG2 (Figs. 4.41 to 4.44) exhibits a complete bell-shaped curve revealing that the structures are almost fully detected by the crossing seismic lines. By comparing the maximum values of amplitude, it is evident that CG1 has accrued a larger vertical displacement with respect to CG 2, both being of similar length. Both the folds have deformed a 10 km long

175

area, which correspond to the trace length deduced by the projections of ending points of the curves on the x axis (Figs. 4.41, 4.42).

Conversely, a not complete sampling can be put forth for SC1 and SC3, whose amplitudes should decrease further south-west outside the investigated area.
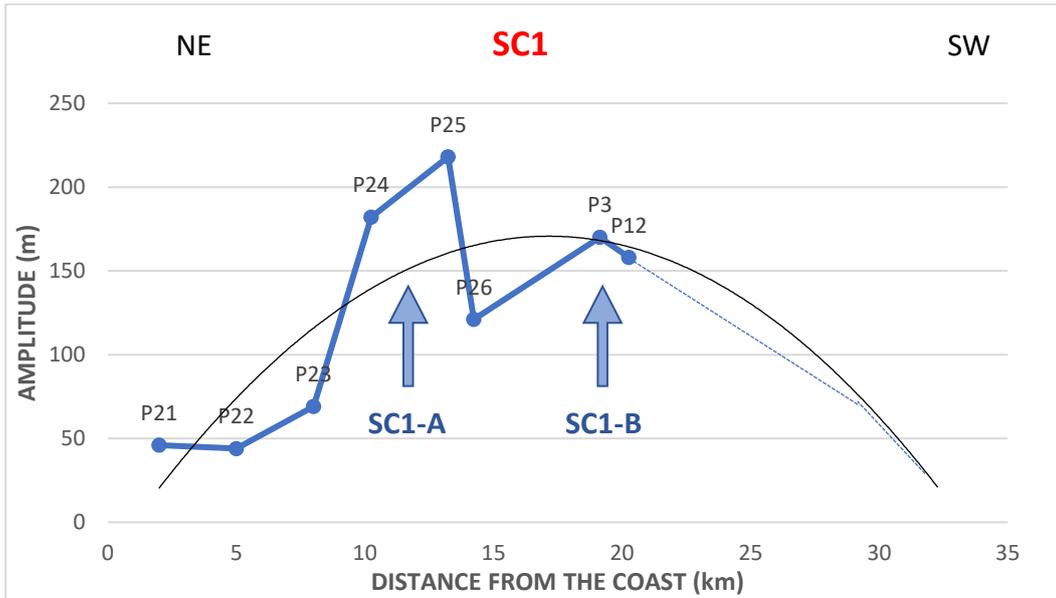
Fig. 4.45 – Graph of amplitude vs. distance from the coast relative to SC1.
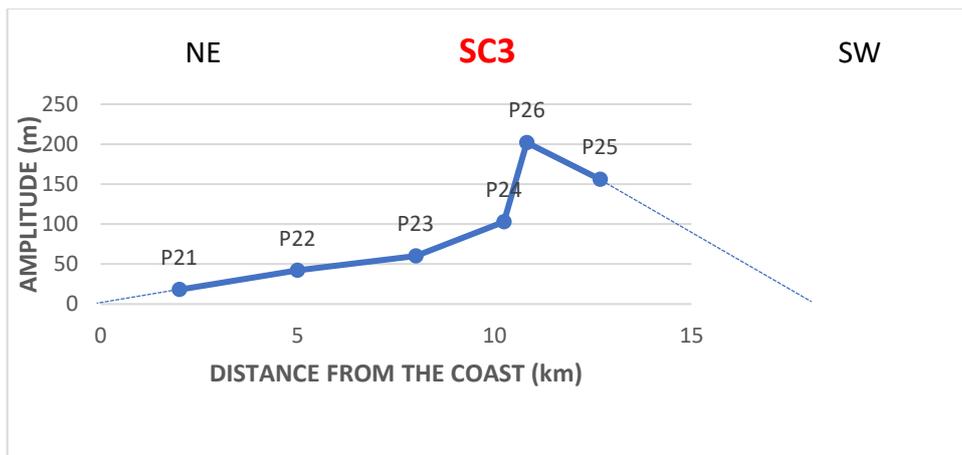
Fig. 4.46 – Graph of amplitude vs. distance from the coast relative to SC3.

As regards fold SC1, figure 4.45 shows two single bell-shaped curves highlighting the presence of two minor folds (SC1-A and SC1-B) of which the

second is not entirely detected as suggested by its shape. The estimated trace length is ~ 21 km.

We regard the two folds as being grown separately until they accrued a vertical displacement of 50 (SC1-B) and 100 m (SC1-A), as estimated from the height difference between their maximum amplitude and the height of the saddle separating them. Afterword, they have probably linked to produce a single deformation profile maintaining their characteristic displacement/length scaling relationship (RODA-BOLUDA & WHITTAKER, 2016 and references therein), with an additional 60-70 m vertical displacement accommodated by the linked structure. So, the re-adjusted profile (black bell shape calculated from a 2nd order polynomial regression, Fig. 4.45) recovers the pre-linkage segments and their segment boundaries, because tip propagation stops after the linkage.

The trend line of figure 4.46 shows the amplitude pattern of SC3. The incomplete bell-shaped curve suggests that the fold should continue further NE for about 7 km as estimated from the maximum at P26, for a total trace-length of 19 km.

TABLE 4.5

Max geometrical parameters values				
STRUCTURE	MAX AMPLITUDE (m)	WAVELENGTH (km)	ASPECT RATIO	TRACE LENGTH (m)
CG escarpment	33			6000
CG 1	100	2,29	0,436681223	9000
CG 2	47	0,861	0,545876887	9000
SC 1	218	13,24	0,164652568	18000
SC 3	202	10,82	0,186691312	17000

A comparison among all the folds is shown in Table 4.5 and in figures 4.47 and 4.48, where the maximum values of amplitude, wavelength and trace length of each analysed fold, listed in Tables 4.3 and 4.4, were reported.
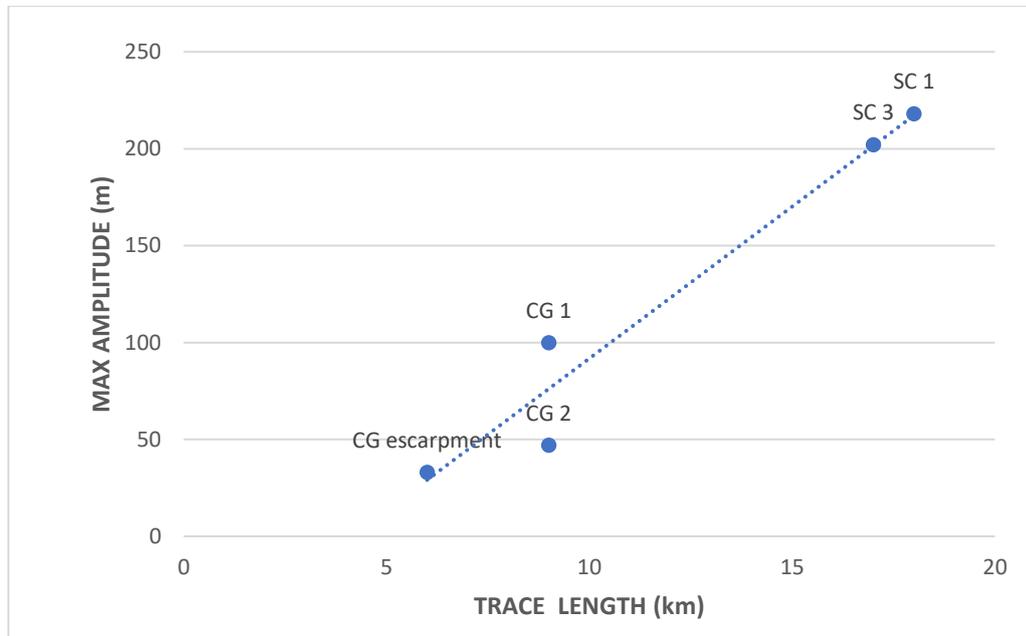
Fig. 4.47 – Graph of max amplitude vs. trace length relative to CG slope, CG1, CG2, SC1, SC3.

The 5 points can be grouped in three classes based on their distribution in the graph. The first class is represented by SC1 and SC3, the second by CG1 and CG2 and the third by CG escarpment. This differentiation supports the contention that there are 2 styles of deformation in the examined areas. The structures associated to folds SC1 and SC2 produce deformation of relatively higher amplitude, wavelength, aspect ratio and trace length. Conversely, folds CG1 and CG2 are positioned in the centre of the graphs, with CG escarpment closely following down the curve (Fig. 4.47, 4.48). In general, the trend line indicates a linear correlation between amplitude and trace length (Fig. 4.47), and similarly between amplitude and wavelength (Fig. 4.48, where CG escarpment is not included).

The folds were also categorized using aspect ratio calculated from fold amplitude vs. wavelength (aspect ratio), and trace length (Fig. 4.49). SC1 and

SC3 are characterized by low aspect ratio and high trace length, whereas CG1 and CG2 show the same value of hinge length but different aspect ratio, lower for CG1. The spatial distribution of the four points in the graph supports a linear correlation between the two parameters, aspect ratio and trace length.
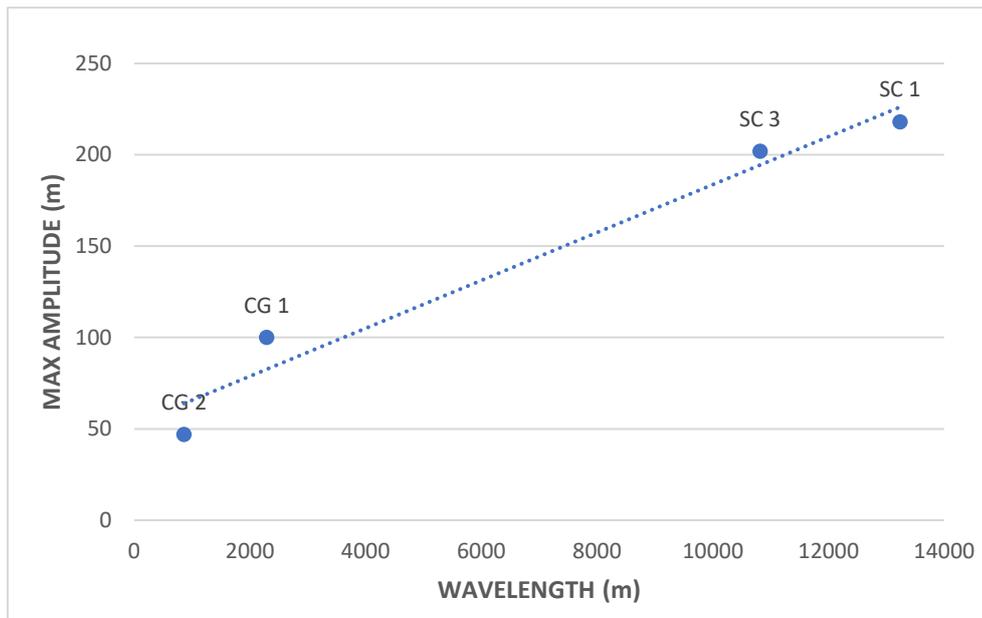
Fig. 4.48 – Graph of max amplitude vs. wavelength the relative to CG1, CG2, SC1, SC3.
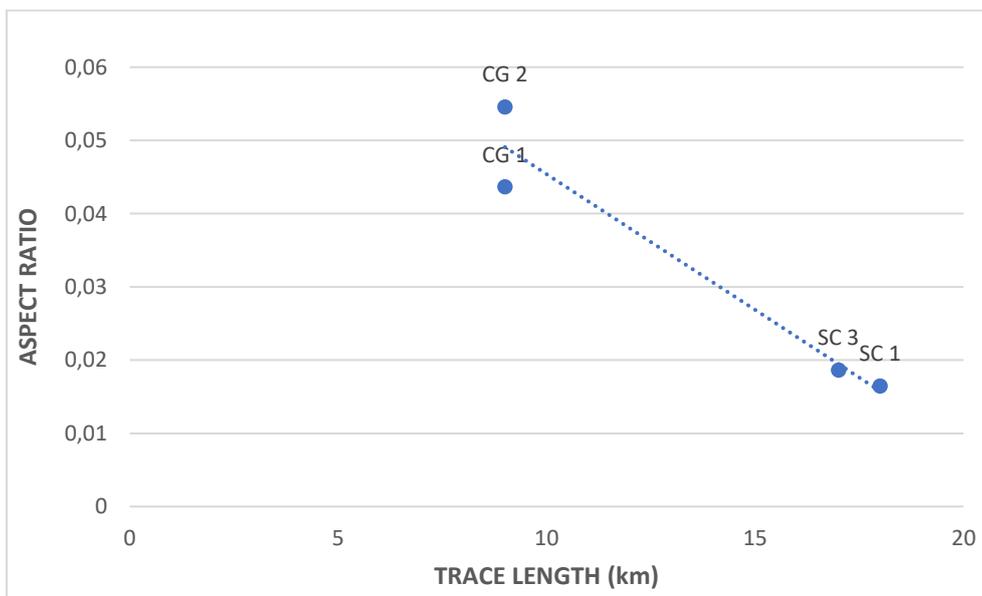
Fig. 4.49 – Graph of aspect ratio vs. trace length relative to CG1, CG2, SC1, SC3.

179

The above information leads to some preliminary conclusions regarding the tectonic framework of the area. Area 1 is characterized by deformation expressed by folds of relatively lower amplitude and wavelength, and of trace length of ~ 10 km; they are associated to slumping and fluid seepages, and are responsible of dip changes of the unit C strata.

Whereas, Area 2 is controlled by high amplitude and high wavelength folds extending for about 20 km and producing major deformation of unit C. They are associated to fluid infiltration along high angle faults that diverge of some degree to the north from the structures of Area 1.

4.7.6 Isopach maps of unit A and B

The identification of erosional surfaces, ES, through the seismo-stratigraphic analysis of SCS seismic lines, has allowed to generate isopach maps (Figs. 4.53 to 4.55). These maps represent the thickness change of a specific unit in the study area. The information derived from the analysis of isopach maps were then compared with the results of the structural analysis (Figs. 4.54, 4,56).

Isopach maps are automatically generated by the software Geosuite that interpolate the picking points of a specific horizon through the profiles.

In general, it can be noticed that the thickness of units thins in proximity of the folds due to pinch-out of depositional sequences and the isopach lines trend presents greater gradients in the areas affected by tectonic uplift. The areas where sediments show increased accumulation (depocenters) migrated in time and space toward the SE, as evidenced by comparing the isopach maps of unit A and B. A likely explanation envisages a syn-tectonic deposition, during the formation of syncline folds.

The thickness of unit A is equal to 5 m in the area affected by CG1 and CG2 folds. Outside the deformed zones, two main depocenters with a maximum of 20 m of Upper Pleistocene-Holocene sediments are present. A third depocenter occupies the offshore zone between Marinella and Capo San

Marco. In the Area 2 a main depocenter between folds SC1 and SC2 is visible. The thicknesses vary from 5 m at the hinge of anticline SC1 to 45 m in the syncline and decrease again to 20 m at the hinge of SC2. High gradients characterize the fold limbs.
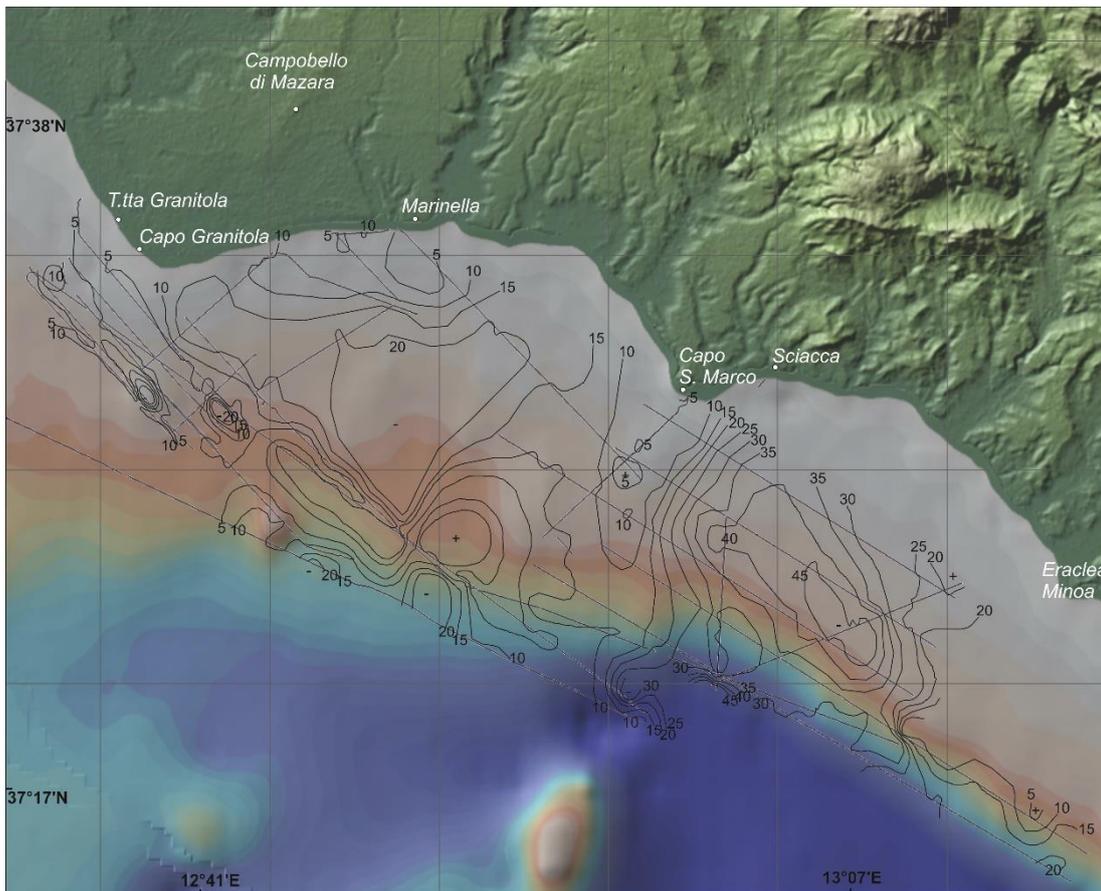
Fig. 4.53 – Unit A isopach map.
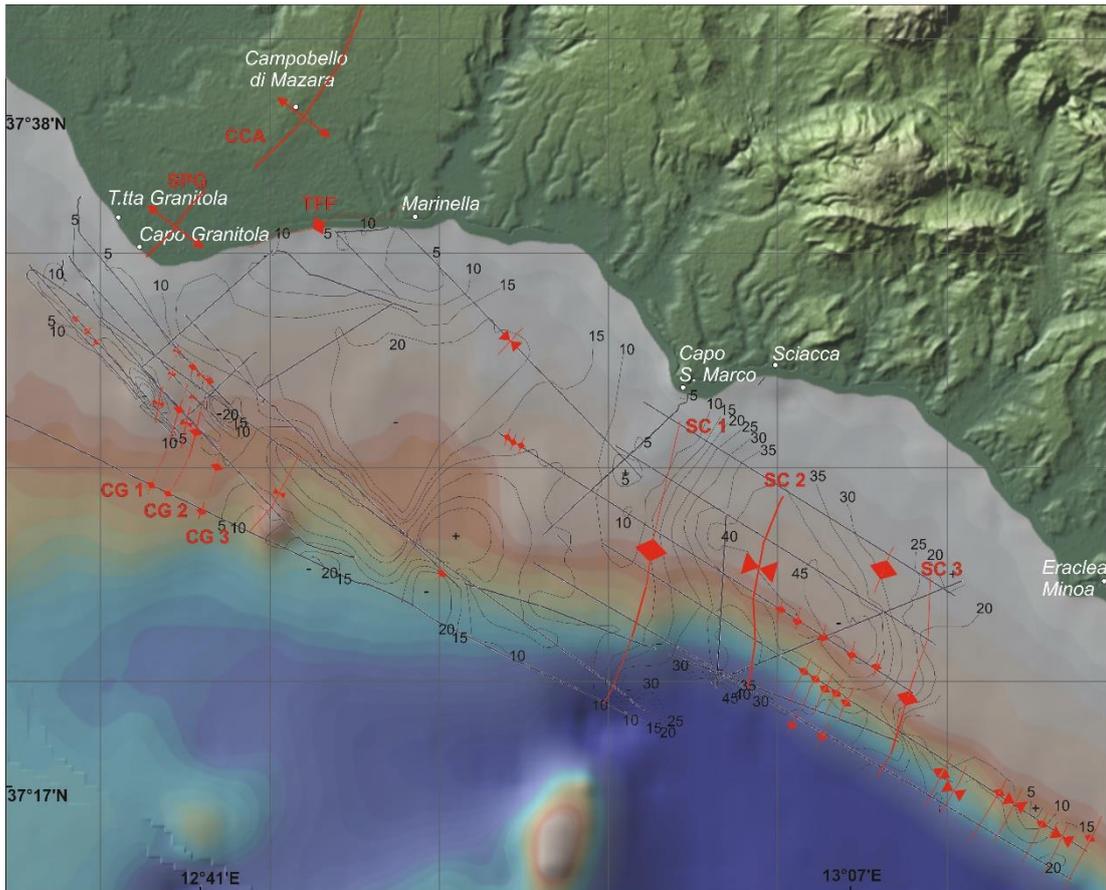
Fig. 4.54 – Unit A isopachs with superimposed tectonic structures of Figure 4.39.

Observing unit B isopach map (Fig. 4.55, 4.56), it is evident an increment of seismic unit thickness in the SE shifted depocenters that record up to 250 m of Middle-Upper Pleistocene sediments.

Finally, the space-temporal distribution of seismic units highlights a major tectonic control on the thickness distribution of unit A, compared to that of unit B, as it better follows the structure trends. So, we can infer that tectonic activity pulsed in the Middle Pleistocene-Holocene.
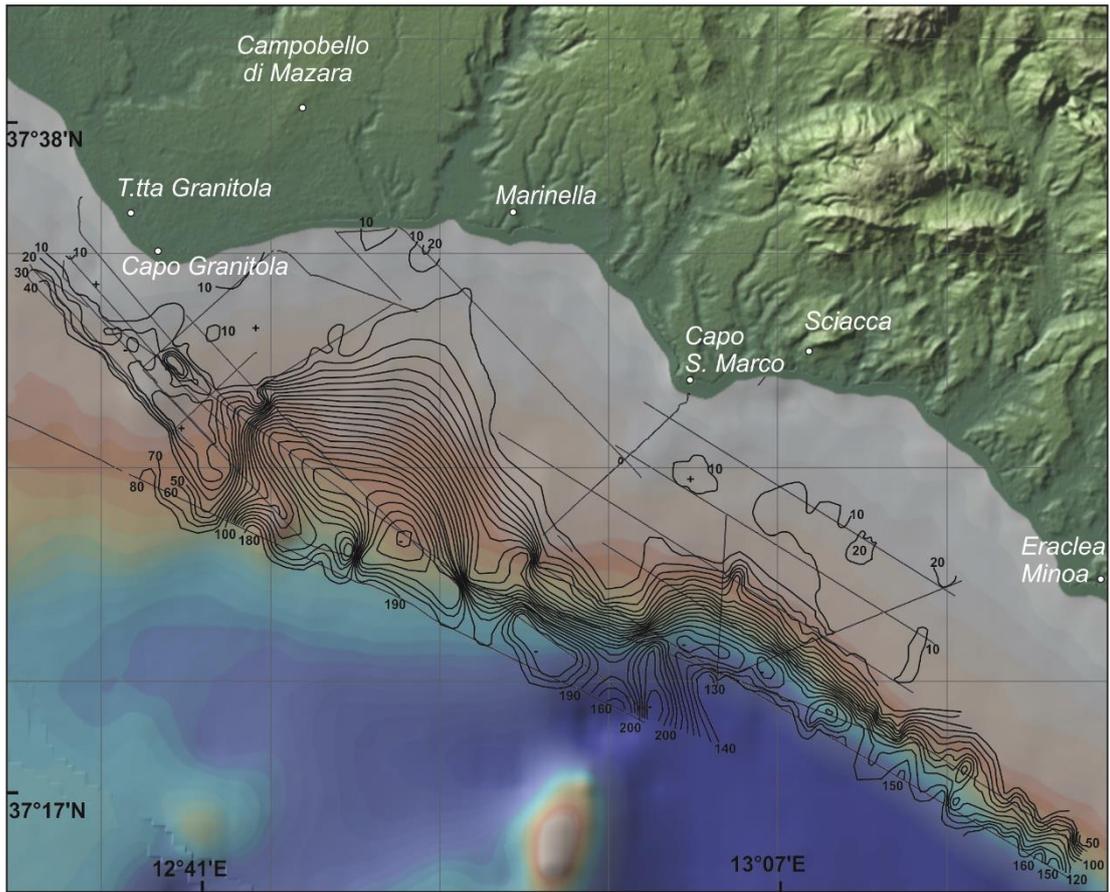
Fig.4.55 – Unit B isopach map.
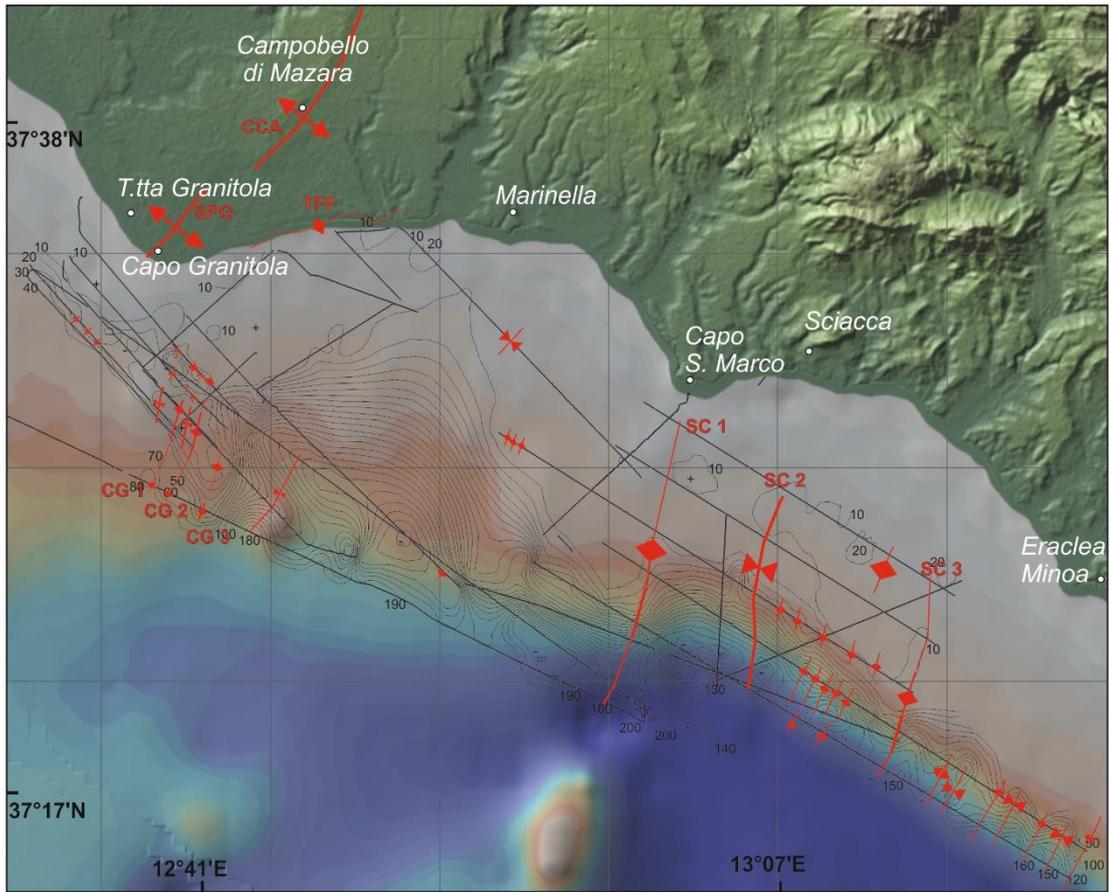
Fig. 4.56 – Unit B isopachs with superimposed tectonic structures of Figure 4.39.

184

CHAPTER V

5. THE LAMPEDUSA PLATEAU

As stated in the introduction, the work regarding the Lampedusa Plateau has been published on the official journal of the Italian Geological Society, named Italian Journal of Geosciences, with the title "*New insights on the tectonics of the Lampedusa Plateau from the integration of offshore, on-land and space geodetic data*" (MECCARIELLO Melania, FERRANTI Luigi, BARRECA Giovanni, PALANO Mimmo, 2017).

The work is based on a joint analysis of different methodologies. I analysed the seismic profiles in order to reconstruct the structural evolution of the Lampedusa-Lampione offshore. The results have been integrated with on-land structural and geodetic data performed by some co-authors and have led to a new tectonic framework for the Lampedusa Plateau.

5.1 Seismo-stratigraphic analysis

A seismo-stratigraphic analysis supported by borehole data was carried out on a grid of seismic reflection profiles (Fig. 5.1), collected in the offshore of Lampione-Lampedusa islands and available from the ViDEPI database (http://unmig.sviluppoeconomico.gov.it/videpi/videpi.asp). The raster images of seismic profiles were converted in *segy* format, georeferenced and imported, together with information gathered from well-log analysis, into a Geodatabase using the Geosuite AllWorks 2.5 software.

Wells Riccio Sud and Remo Nord have drilled an ~ 5 km thick Mesozoic to Quaternary succession (Fig. 5.2). The basal Nara formation is made of Jurassic platform carbonates. These are the deepest rocks known in the area and are overlain by Lower Cretaceous deep-marine limestone and marls of the Sidi Kralif Formation.
The Middle-Upper Cretaceous stratigraphic section is formed by neritic shales and shallow water coarse-grained clastic sediments alternating with carbonates (Gebel Nehal and Sidi Alich Formations), by Aptian carbonates, and by

pelagic marls of the Fahdene Formation. This latter succession marks the onset of a deepening event (TORELLI et al., 1995), which extends into the Late Cretaceous to Early Eocene with open-platform and deep-marine carbonates.
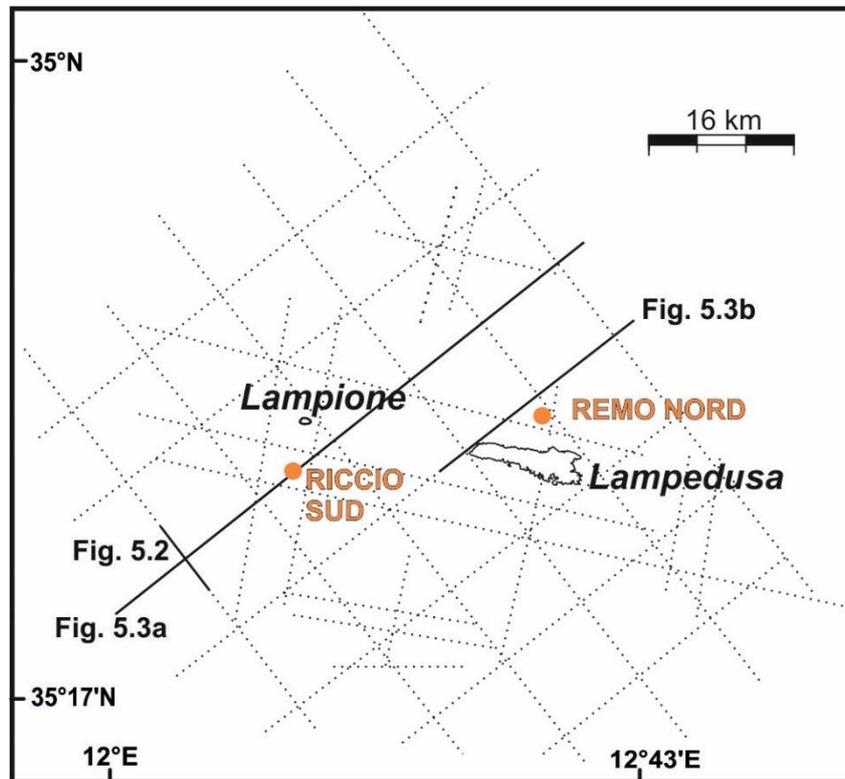
Fig. 5.1 – Location of analysed seismic reflection profiles and well-logs in the studied part of the Lampedusa Plateau.

A thick succession of Upper Lutetian to Priabonian shallow-water platform carbonates forms the Halk el Menzel Formation, which only outcrops at Lampione Island. Well log information indicates that open shallow platform rocks dominate in the lower part of the formation, whereas the upper part is dolomitized and was deposited in a restricted shallow platform environment. Because the wells were drilled on structural highs, the Messinian evaporitic unit is missing in the well log record. For the same reason, the logged Pliocene-Quaternary sediments are only ~ 200-300 m thick.

187
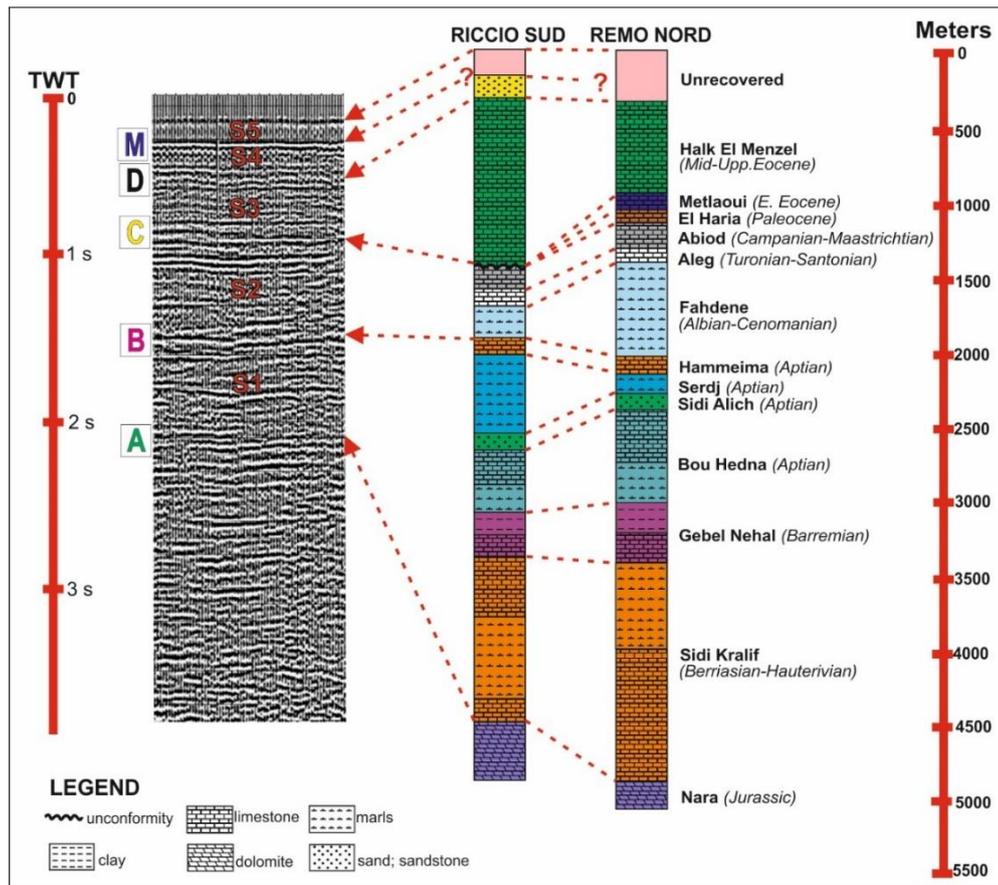
Fig. 5.2 – Seismostratigraphic frame of the Lampedusa Plateau, showing calibration of seismic reflectors using Riccio S and Remo N well logs. S1 to S5: seismic sequences 1 to 5. A, B, C, D, M: horizons traced in the seismic profiles. For description of sequences and horizons see the text.

Joint analysis of well logs and profiles allowed identifying five prominent seismic reflectors (Fig. 5.2), labelled, from bottom to top, A, B, C, D (which broadly correspond to those recognized by TORELLI et al., 1995 and GRASSO et al., 1999) and M. These reflectors were readily identified because of their marked seismic expression, and were mapped in pseudo-3D imaging. The reflectors bound five seismic units (S1 to S5, Fig. 5.2), whose variable seismic facies and lithological characteristics calibrated by well logs testify changes in depositional environments and/or oceanographic conditions.

A seismic velocity value was assigned to each sequence. We used as starting input the reflector calibrations of TORELLI et al. (1995) and GRASSO et al. (1999) based on the velocity survey for Riccio Sud well. Using the

188

lithostratigraphic information drawn from both Riccio Sud and Remo Nord wells, we confirmed or slightly refined the position of these reflectors, which was checked by tracing the selected reflectors along the profiles to ensure the finding of a good seismic signal when it was missing under the wells. We then computed the average velocities by matching the thickness of the different litho-stratigraphic intervals logged by Riccio Sud and Remo Nord wells with the TWT reflector depths in seismic profiles as close as possible to the wells. This resulted sometimes in a different velocity value assigned to the sequences with respect to the values reported in TORELLI et al. (1995) and GRASSO et al. (1999) (Table 5.1). We also list in Table 5.1 the velocities reported by SEBEI et al. (2007) from the AKD-1 well in the Halk el Menzel sector of the Pelagian Block northwest of Lampedusa (Fig. 1.11) for comparison.

Based on the well-log calibration (Fig. 5.2), we traced the marker reflectors in all profiles. We used both closely projected wells and outcrops at Lampione and Lampedusa island (GRASSO & PEDLEY, 1985) as ground-truth points.

The lowermost horizon (A) exhibits reflections with high-amplitude seismic character and good lateral continuity, and it has been assigned to the top of the Nara formation. Seismic sequence S1 generally lies disconformably on the basal reflector A, where low-angle downlap and onlap terminations occur. This unit displays vertical and lateral facies changes from high-amplitude subparallel prograding reflections to transparent and chaotic patterns (Fig. 5.2). The complex seismic arrangement is consistent with the variable litho-stratigraphy of the Lower Cretaceous section documented in wells.

Horizon B shows high amplitude, quite continuous reflections that becomes discontinuous in correspondence of upward convexities (Fig. 5.2). It likely corresponds to the base of the Fahdene Formation. Overlaying seismic sequence S2 consists of alternating transparent and

variable-amplitude seismic packages, often lacking in lateral continuity. A strongly continuous central package of few high-amplitude reflections is often present in the profiles (Fig. 5.2). The uppermost part of the sequence exhibits toplap and erosional truncations. The unit includes shales, marls and limestone deposited during the Albian to Early Eocene.

Table 5.1

EPOCH	LAMPEDUSA SHELF				WESTERN PELAGIAN FORELAND	
	FORMATION	SEISMIC SEQUENCE	VELOCITY (This work)	VELOCITY (Torelli et al., 1995)	Equivalent formation, from Sebei et al., 2007	VELOCITY (Sebei et al., 2007)
Quaternary	UNRECOVERED	S5	2000	1910		
Pliocene					Ain Ghrab	
Miocene		S4			Salammbo	3700
Oligocene						3400
Upp. Eocene	HALK EL MENZEL	S3	4800	5960	Reineche member	3200
Lower Eocene	METALOUI	S2	3900	3130	Bou Dabbous	3900
Paleocene	EL HARIA				El Haria	3890
Campanian-Maastrichtian	ABIOD				Abiod	4100
Turonian-Santonian	ALEG				Aleg	4500
Albian-Cenomanian	FAHDENE					
Aptian	HAMMEIMA	S1	5600	6208		
Aptian	SERDJ					
Aptian	SIDI ALICH					
Aptian	BOU HEDNA					
Barremian	GEBEL NEHAL					
Berriasian-Hautevirian	SIDI KRALIF					
Jurassic	NARA		6000			

Horizon C (Fig. 5.2) displays reflections with variable amplitude and a moderate lateral continuity marking an Eocene erosion surface. Overlying seismic unit S3 corresponds to the Halk El Menzel formation, characterized by a seismic facies with either high-amplitude sub-parallel, or inclined reflections

(Figs. 3a, 3b), which are correlated to Middle–Upper Eocene shallow-platform and to prograding shelf carbonates, respectively.

High amplitude and strong lateral continuity characterize reflections associated to horizon D (Fig. 5.2) underneath the Lampedusa Plateau. Towards the north-east, it loses continuity and displays variable amplitude, and for this reason it can be traced with some uncertainty. The reflector marks the boundary between the Halk el Menzel carbonates, which outcrop at Lampione islet with sub-horizontal attitude (GRASSO & PEDLEY, 1988) and overlying deposits (sequence S4; Fig. 5.2). Beneath the plateau, these younger deposits may be locally represented by Upper Miocene rocks, which outcrop at Lampedusa island (GRASSO & PEDLEY, 1988). In seismic profiles, they exhibit a seismic facies characterized by low-medium amplitude discontinuous reflections. Moving to the north-east, a thicker wedge of onlapping reflectors, which displays high amplitude discontinuous reflections alternating with a transparent facies seismic package, can be traced above horizon D (Figs. 3a, 3b). In the upper part, it shows unconformities and onlapping reflectors, which likely correspond to the outcropping Upper Miocene deposits. The precise age of the lower part of S4 is undetermined; it may include or not the Oligocene, which was a time of regional erosion (TORELLI et al., 1995).

Reflector M (Fig. 5.2) is characterized by a sharp seismic signal, represented by high-amplitude reflections with a good lateral continuity. In the basinal area north-east of the plateau, M is more readily distinguishable (Figs. 3a, 3b), but it is only tentatively identified underneath the shelf. Moving from the north-eastern basin toward the plateau, M truncates progressively older deposits and under the highs drilled by wells it merges with D (Figs. 5.3a, 5.3b). Note that in Figs. 5.3a and 5.3b the wells are projected onto the profiles and thus a thin (~ 50-100 m) layer of S4 is admitted on the highs; this estimate is consistent

with the ~ 100 m thickness of Upper Miocene sediments in Lampedusa (GRASSO & PEDLEY, 1985).

In Riccio Sud and Remo Nord wells, M, that forms a single erosion surface with D, is overlain by a relatively thin (200-300 m) veneer of Pliocene-Quaternary sediments (sequence S5, Fig. 5.2). In the basin to the north-east, M is a prominent reflector, and is overlain by a wedge with low-amplitude, high-frequency continuous reflections, whose lower part has a growing geometry and is marked by transparent reflections (Fig. 5.3b, inset 3). This latter seismic facies is generally attributed to the Early Pliocene (ARGNANI et al., 1987; ARGNANI, 1990; ARGNANI & BONAZZI, 2005), and the upper part of the sequence spans the remaining Pliocene-Quaternary epoch.

Based on the above observations, M is related to a horizon of regional significance, which in the Central Mediterranean Sea is associated with the top of evaporites and clastic sediments deposited during the late Messinian salinity crisis, or with an erosional unconformity formed during the coeval sea level fall (RYAN & CITA, 1978). Available wells in the study region do not record the existence of the evaporite succession (Fig. 5.2) and thus reflector M is most likely an erosional surface, at least on the plateau (Fig. 5.3b, inset 1).

5.2 Structural analysis

The most prominent structural feature under the northern part of the plateau is represented by a regional anticlinorium (LPA) marked by a series of relative highs and lows which have a WNW-ESE trend (Fig. 5.4a). The foremost high in the area is the ~ 40 km long Lampione-Lampedusa High (LLH), which culminates in the two eponymous islands. The position of the hinge of the LLH is constrained by the sub-horizontal attitude of the Halk El Menzel carbonates at Lampione (Figs. 5.4a, 5.4b), which forms the core of the high.

The LLH, as defined by the position of the bounding faults, has width between ~ 8-10 km. Wells Riccio Sud and Remo Nord are located above

secondary structural highs at the southern and northern flank of the LLH, respectively (Figs. 4a, 4b). North of the LLH, all reflectors beneath M depict the rather steep northerly dipping flank of the LPA (Fig. 5.3b). South of Riccio, an additional high is drilled by Ksar well (Figs. 5.4a, 5.4b). Unlike the LLH, which is sharply bounded by steep fault-controlled scarps, the Ksar High is expressed by a broad fold, whose only northern part is imaged by the available seismic profiles (Figs. 5.4a, 5.4b). Because of this limitation, we do not have constraints to place the southern flank of the anticlinorium, which could lie just south of the Ksar High or further south. However, the southerly tilt of reflectors under the Ksar High as opposite to the northern dip under the LLH (Fig. 5.4a) suggests that the two highs could represent the southern and northern limbs of the LPA, respectively.

We tentatively locate the hinge of the anticlinorium in between Riccio Sud and the Ksar High (Fig. 5.4a), where divergence between northern and southern dip of reflectors occurs. This location broadly corresponds to a set of Paleogene folds mapped by GRASSO et al. (1999), as portrayed in figure 5.4a.

High-angle faults with a reverse component of displacement bounds the highs and lows (Fig. 5.3a, inset 1 and 2; Fig. 5.3b, inset 1; Fig. 5.4a). The offset mode of reflectors, and often the basinward-tilted onlaps in the downthrown blocks, suggests a reverse component. Although we are aware that these criteria are not decisive, the association of the faults with the larger anticlinorium is evidence for reverse shear. The faults can be traced down to a depth of ~ 3 sec TWT (roughly corresponding to ~ 8 km) with a steep angle of dip. The estimated displacement is typically of few (~ 0.01-0.05) sec, only locally larger.
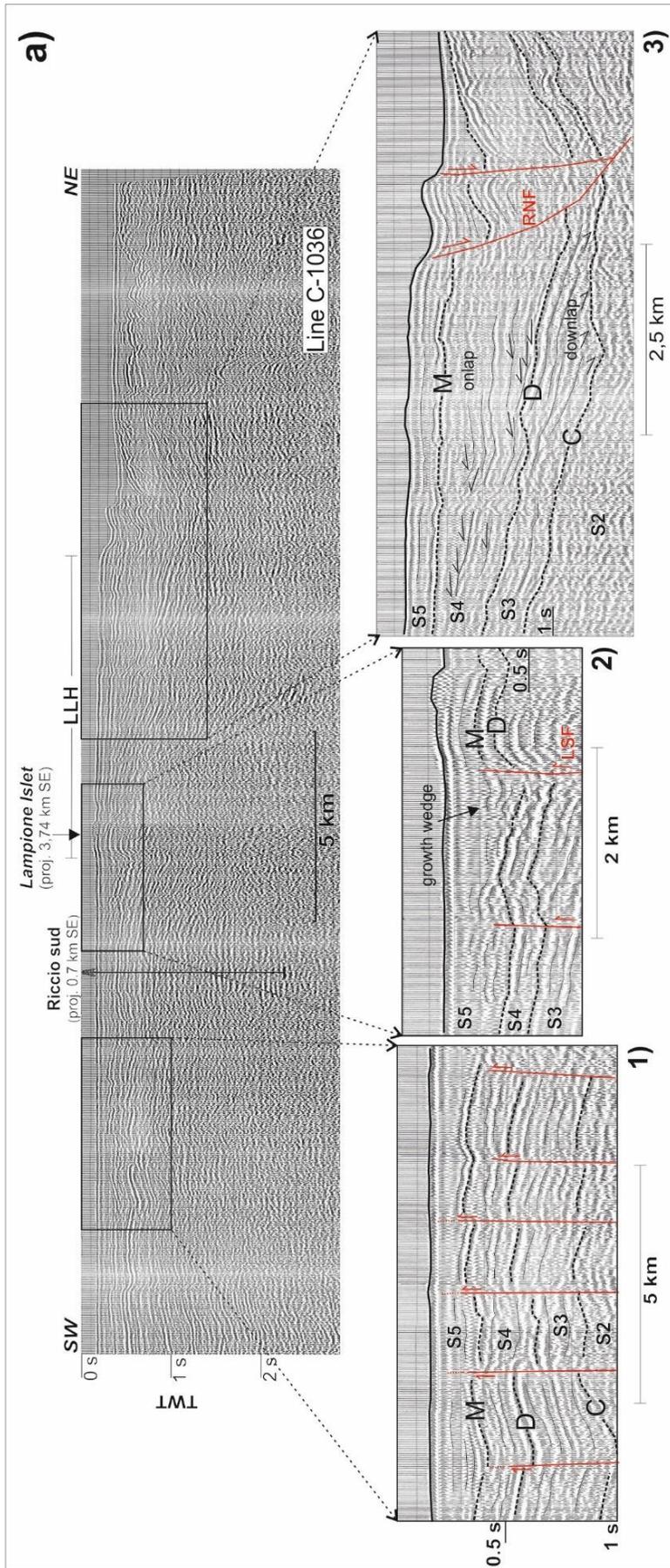
Fig. 5.3 – a) Multichannel seismic profile C-1036 with enlarged frames 1 to 3, showing the folds and related faults with a reverse component of motion underlying the Lampione-Lampedusa and the Riccio highs (drilled by Riccio S well). Towards the NE extensional faults are present. Location of seismic profiles is shown in figure 5.1. Labels are as follows: LLH, Lampione-Lampedusa High; LNF, Lampedusa North Fault; LSF, Lampedusa South Fault; RNF, Remo North Fault.

194
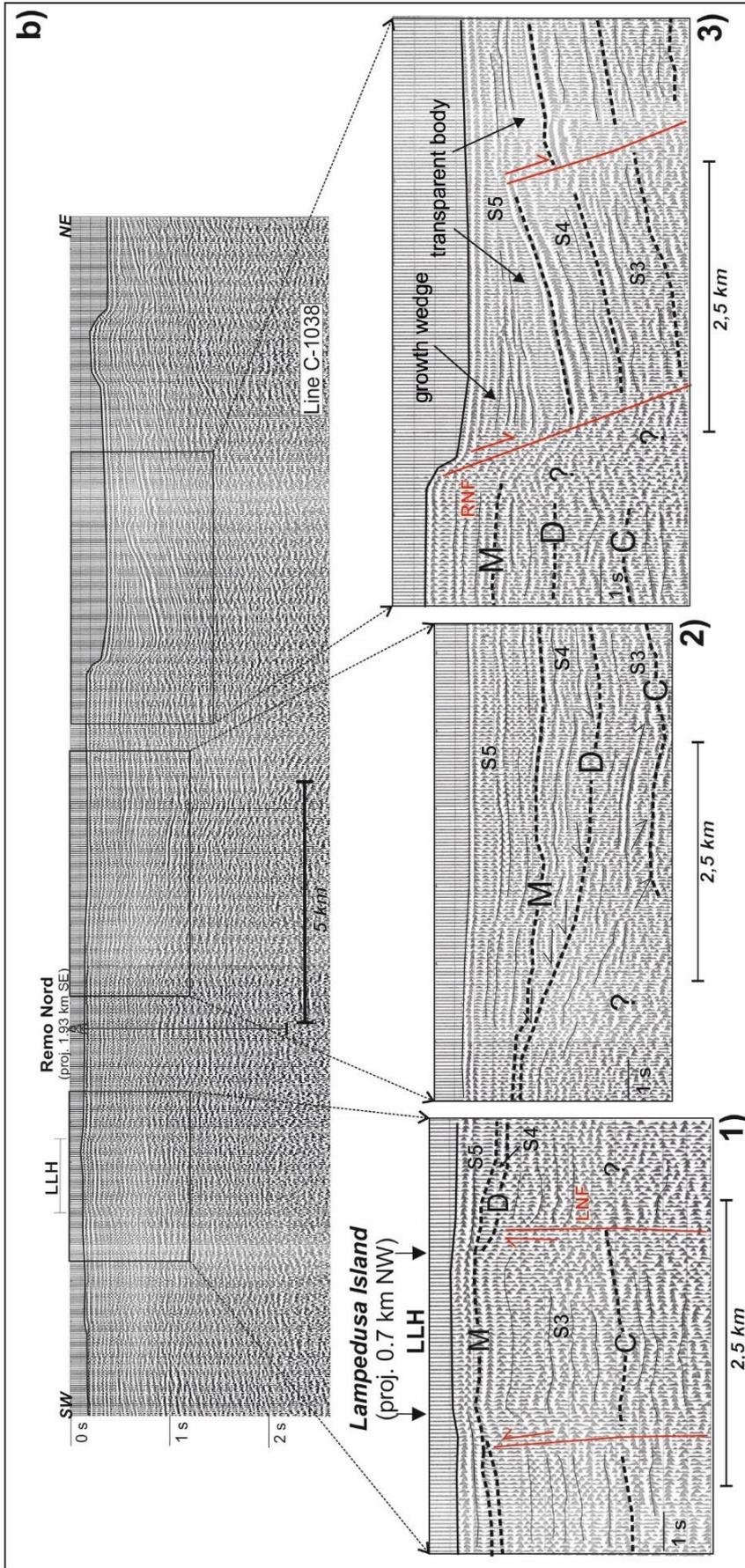
Fig. 5.3 – b) Part of multichannel seismic profile C-1038, showing the narrowing of the Lampione-Lampedusa High compared to profile C-1036. Enlarged frames 1 to 3 show the structures underlying the plateau and the basin to the northeast. Location of seismic profiles is shown in figure 5.1. Labels are as follows: LLH, Lampione-Lampedusa High; LNF, Lampedusa North Fault; LSF, Lampedusa South Fault; RNF, Remo North Fault.

Unlike the rest of the shelf, the region north-east of the plateau is characterized by extensional faults which typically correspond to abrupt steps in the sea bottom (Figs. 5.3a, inset 3; 5.3b, inset 3; 5.4a). A prominent normal fault is located east of Lampedusa (RNF, Fig. 5.3a, inset 3; Fig. 5.3b, inset 3; Fig. 5.4a), and accounts for a ~ 0.3 sec (~ 300 m) vertical throw of reflector M in a ~ 20 km long and <10 km large basin (Lampedusa Eastern Basin, LEB, Fig. 5.4a).

Figure 5.4b shows the isopachs of Middle-Upper Eocene Halk el Menzel carbonates (sequence S3). Here, the LEB extensional feature is clearly lacking, pointing to a later activity of normal faults. However, the dominant trend of the isopachs is WNW-ESE consistent with the trend evidenced in sequence S5 (Fig. 5.4a) and with the mapped structural fabrics (and most notably the LLH). The later extensional faults appear placed on the area where the Eocene deposits had the minimal thickness, although this may reflect in part a paleogeographic control.

5.3 Timing of deformation

Seismic profile analysis indicates a polyphase tectonic history for the growth of the Lampedusa Plateau. Through the analysis of a dense grid of seismic profiles and of Riccio Sud, Remo Nord and Ksar-1 well-logs, GRASSO et al. (1999) proposed that the first contractional structures formed during the Late Cretaceous-Early Paleogene. Effectively, pinch-outs of Middle-Upper Cretaceous formations and hiatuses in the Paleocene-Early Eocene in the well log record (Fig. 5.2) point to early shaping of the LPA was occurring at that time, and that the central area where Riccio Sud is drilled formed the hinge of the anticlinorium (Fig. 5.4a). These structures possibly created the bathymetric conditions where deposition of the Middle-Upper Eocene Halk el Menzel carbonates occurred (Fig. 5.4b). Although regional progradation of these shallow-water sediments is documented toward the southeast off Tunisia (SEBEI et al., 2007) and toward the south under the Lampedusa Plateau

(GRASSO et al., 1999), our analysis shows progradation of the Halk el Menzel both in the trough between the LLH and the Ksar High, and to the northeast of the LLH (Fig. 5.3a, inset 3; Fig. 5.3b, inset 2; Fig. 5.4b). Thus, we propose that Eocene deposition occurred above a pre-existing structure, whose culmination broadly coincides with the LLH. Northeast of the plateau culmination, the Halk el Menzel is covered by sequence S4, of Oligocene (?)-Miocene age. On approaching the high, onlaps are present within S4 (Fig. 5.3a, inset 3; Fig. 5.3b, inset 2), suggesting growth, albeit at a slower pace, during the Oligocene (?)-Miocene.

South of the LLH, horizon M cuts at different stratigraphic levels, and at places merges with horizon D (Fig. 5.3b, inset 1) as documented by Riccio Sud well (Fig. 5.2). Horizon M itself is involved in broader folds and small-displacement faults and, just south of the LLH, is tilted toward the high forming a wedge offset toward the north by a fault with a reverse component (LSF; Fig. 5.3a, inset 1 and 2; Fig. 5.3b, inset 1). The overlying reflectors, Early Pliocene in age as constrained by the correlation with Riccio Sud well, onlap to the south against M and are themselves folded up to ~ 0.1 sec below the sea-bottom (Fig. 5.3a, inset 2). Image resolution does not allow detecting whether the uppermost reflectors are involved in folding. Thus, we conclude that a component of shortening was occurring during Paleogene (in accordance with GRASSO et al., 1999), but continued in the Miocene and locally in the Early (?) Pliocene.
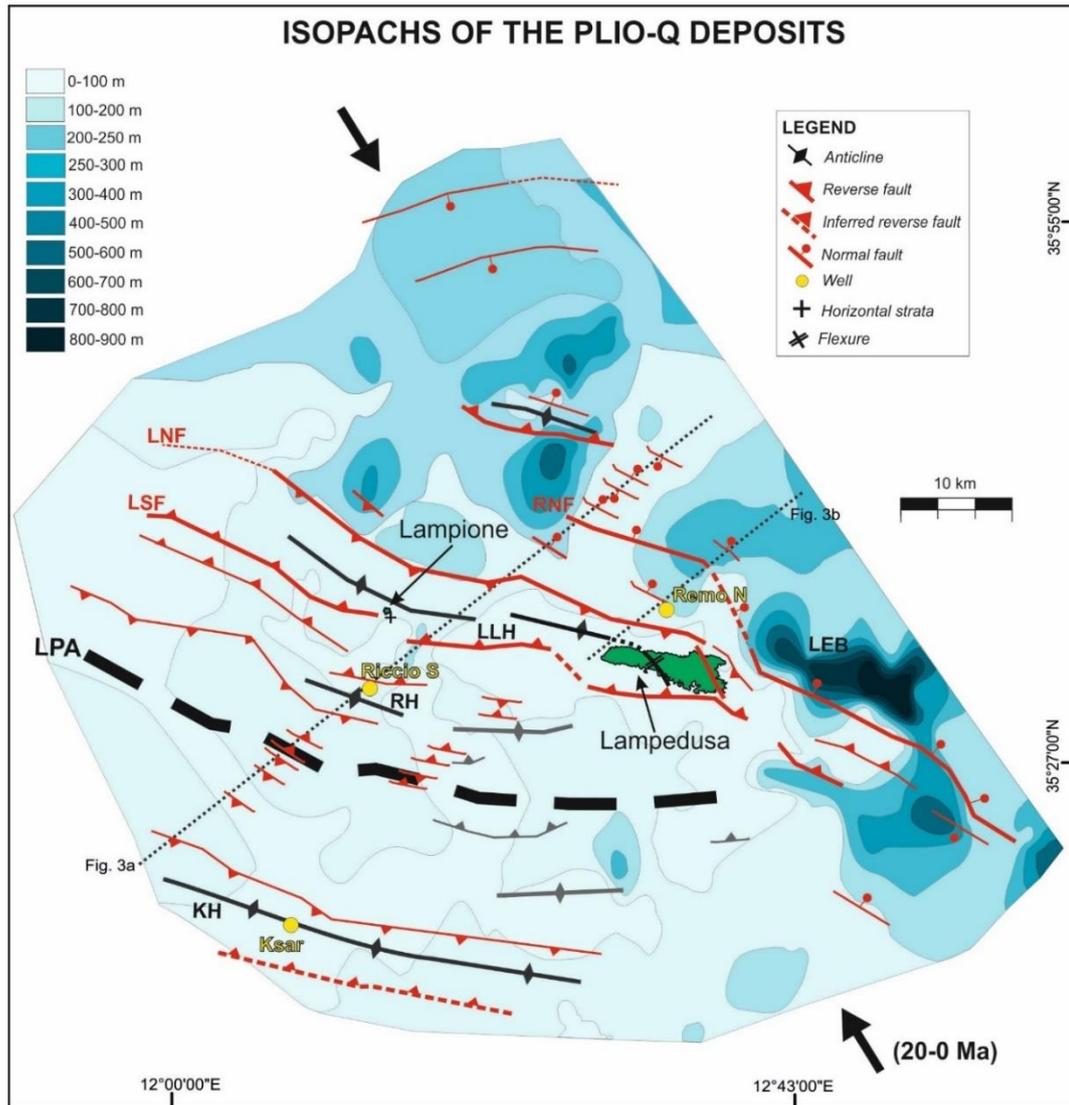
Fig. 5.4a – Isopachs of Plio-Quaternary unit (sequence S5), along with the main folds and faults. The map has been obtained by depth-conversion of TWT seismic profiles using the average seismic velocities listed in Table 5.1. Black arrows are the computed convergence direction between Lampedusa (Nubia) and Eurasia during the last 20-0 Ma. Labels are as follows: LPA, Lampedusa Plateau Anticlinorium; KH, Ksar High; RH, Riccio High; LNF, Lampedusa North Fault; LSF, Lampedusa South Fault; LLH, Lampione-Lampedusa High; RNF, Remo North Fault; LEB, Lampedusa Eastern Basin.
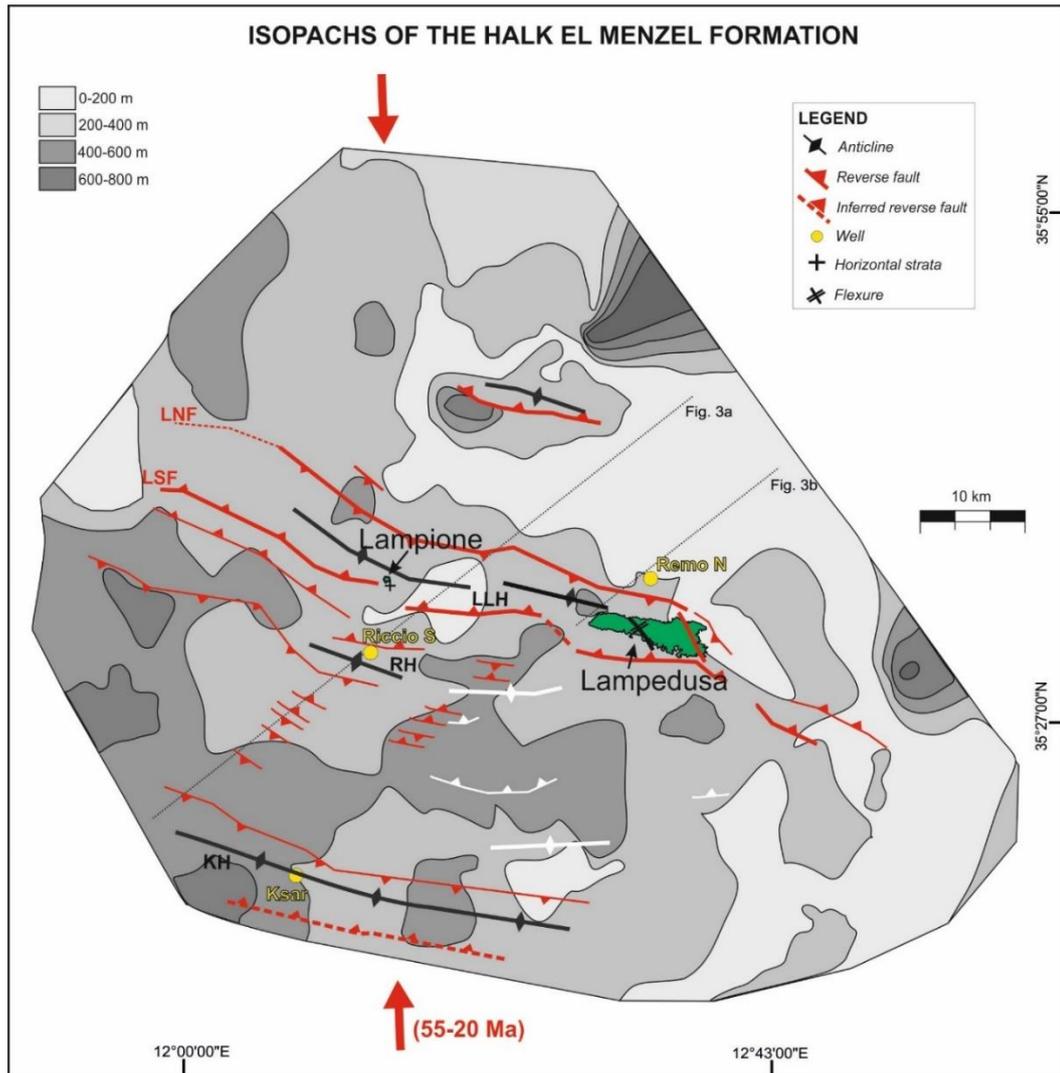
Fig. 5.4b – Isopachs of the Halk El Menzel Formation (sequence S3), along with the main folds and faults. The maps has been obtained by depth-conversion of TWT seismic profiles using the average seismic velocities listed in Table 5.1. Red arrows are the computed convergence direction between Lampedusa (Nubia) and Eurasia during the last 55-20. Labels are as follows: LPA, Lampedusa Plateau Anticlinorium; KH, Ksar High; RH, Riccio High; LNF, Lampedusa North Fault; LSF, Lampedusa South Fault; LLH, Lampione-Lampedusa High; RNF, Remo North Fault; LEB, Lampedusa Eastern Basin.

Northeast of the LLH, reflectors immediately above M diverge toward the RNF and synthetic extensional faults, forming a wedge suggestive of growing relations of sediments and faults in the Early Pliocene (Fig. 5.3b, inset 3). Extension is not clearly documented in younger reflectors (S5). These observations confirm previous findings on

the age of normal faults in the main rift basins of the Sicily Channel (ARGNANI, 1990; ARGNANI & TORELLI, 2001).

5.4 Insights from outcrop and space geodetic data

5.4.1 Structural observations on Lampedusa Island

Lampedusa Island emerges at the eastern terminus of the LLH for a ~ 11 km length and a ~ 3 km maximum width (Figs. 5.4a, 5.4b). The island is floored by Upper Miocene (Tortonian-Lower? Messinian) shallow-water carbonate rocks with minor Quaternary marine and continental cover (GRASSO & PEDLEY, 1985). The structure grades from a tabular mesa in the west, where the youngest sediments outcrop, to a gently undulated plateau in the east. The flexure axis between the two compartments lies in the central part of the island and has a NW-SE trend (Figs. 5.4a, 5.4b).

The stratigraphic evolution and structural pattern of Lampedusa were analyzed by GRASSO & PEDLEY (1985), who documented an intense Tortonian syn-sedimentary strike-slip activity followed, in their reconstruction, by minor extension. Brittle structures are mostly exposed in the eastern part of the island, where a detailed structural analysis has been carried with the aim to unravel the fault kinematic evolution and derive the related displacement field.

We measured kinematic indicators (mainly slickenlines and Riedel shears) on fault planes and trend of fractures within Upper Miocene carbonates offset by the NW-SE striking Cala Creta fault (CCF; GRASSO & PEDLEY, 1985) and by an E-W striking unnamed fault, here baptized Cala Francese fault (CFF; Fig. 5.5)
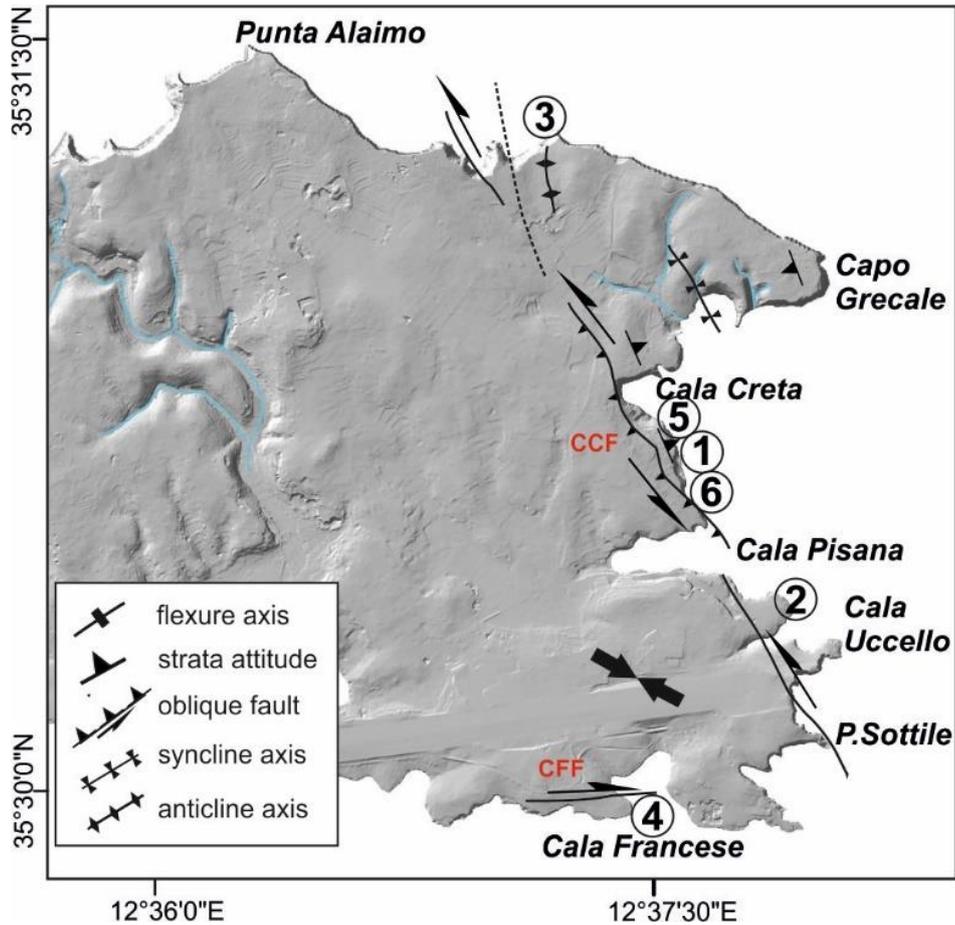
Fig. 5.5 – Map of the eastern part of Lampedusa, showing the trace of main faults and folds, and the sites of structural measurement (circled numbers). Labels are as follows: CCF, Cala Creta Fault; CFF, Cala Francese Fault. The solid thick arrows are the inferred shortening direction.

In the area between Cala Creta and Cala Pisana (station 1, Fig. 5.5), carbonate mudstone of the Capo Grecale member (Lampedusa Formation, Tortonian - Early Messinian?) are deformed by multiple fault segments and by a pervasive set of fractures developed within the CCF deformation zone. Fault segments have an average NW-SE strike (Fig. 5.6a) and dip towards the SW (toward higher local elevations) with inclinations ranging from 45° to sub-vertical (Fig. 5.6a, picture 1).

In detail, these faults show undulated surfaces that give rise, at various scales, to restraining and releasing bend structures according to the fault segments overlap (Fig. 5.6a, picture 3). The main fault planes

exhibit striated surfaces with slickenline rakes between 30° and 60° to the NW (Fig. 5.6a, picture 2) that indicate left-oblique transpression at this site. East of Cala Creta, the Capo Grecale carbonates are deformed by a ~1 km wavelength gentle syncline (Fig. 5.6a, picture 4), whose trend is consistent with the reverse component of motion observed on the fault.

Statistical analysis reveals that fractures at station 1 are mainly distributed along the NW-SE (N120°-130°E) and to a lesser amount along the E-W direction (Fig. 5.6a). Small offset observed along the fractures together with their angular relationships with the major fault planes allow to interpret the main sets as tension (T) and the lesser represented one as synthetic (R) Riedel.

In the area of Cala Uccello (station 2, Fig. 5.5), we have followed the CCF along the same NW-SE trend, whereas GRASSO & PEDLEY (1985) make it swing to the east-southeast and run offshore. Our evidence is based on a close set of fractures and minor faults measured within reef carbonate deposits of the Cala Pisana member (Tortonian) of the Lampedusa Formation. Faults show sub-vertical planes and are distributed along the N120-130E direction. Although establishment of the sense of motion form striations on faults at this site is somewhat ambiguous (question mark in Fig. 5.6b), the distribution of N120°E fractures, interpreted as R-type Riedel, suggests a left-lateral sense of motion, in agreement with results from station 1 (Fig. 5.6a).

On the northern coast of the island, between Capo Grecale and Punta Alaimo, the CCF apparently branches to form a wider deformation zone (station 3, Fig. 5.5). To the east of the fault zone, NW-SE trending mesoscale box-folds and thrust faults have been measured in carbonate mudstones of the Capo Grecale member. Pop-ups at both mesoscopic and macroscopic scale are generated by thrusts and associated back-thrusts (Fig. 5.6c, picture 1). These contractional structures are interpreted as positive flowers developed at a restraining bend of the CCF.

On the southern side, west of Cala Francese (station 4, Fig. 5.5), the E-W striking CFF cuts across shallow-water limestone. The fault is characterized by a transcurrent shear zone oriented N80°E with associated sub-vertical joints and tension fractures (Fig. 5.6d, picture 1). The geometry of outcrop-scale pull-apart basins nucleated at bends and overlaps of fault segments inside the shear zone provide indication of a right-lateral movement (Fig. 5.6d, pictures 2 and 3).

On the southern part of the CCF outcrop, red matrix-supported, uneven-size carbonate breccia assigned to the Late Pleistocene-Holocene (GRASSO & PEDLEY, 1985) seal or locally fill fault planes and fractures associated to the CCF (Fig. 5.6e), establishing a maximum upper age constraint for fault motion.

It is important to remark that many outcrops of the CCF fault surfaces exhibit a morphological expression at the topographic surface, represented by up to 0.5 m high scarplets dipping toward the interior of the island (Figs. 5.6e, 5.6f). In addition, the fault planes and associated striations appear fresh, and the rocks in proximity of the fault are often characterized by crushing related to development of a damage zone (Fig. 5.6a, pictures 1 and 2). These observations suggest that, at the observed sites, the last activity of the CCF is relatively young and affected lithified rocks.
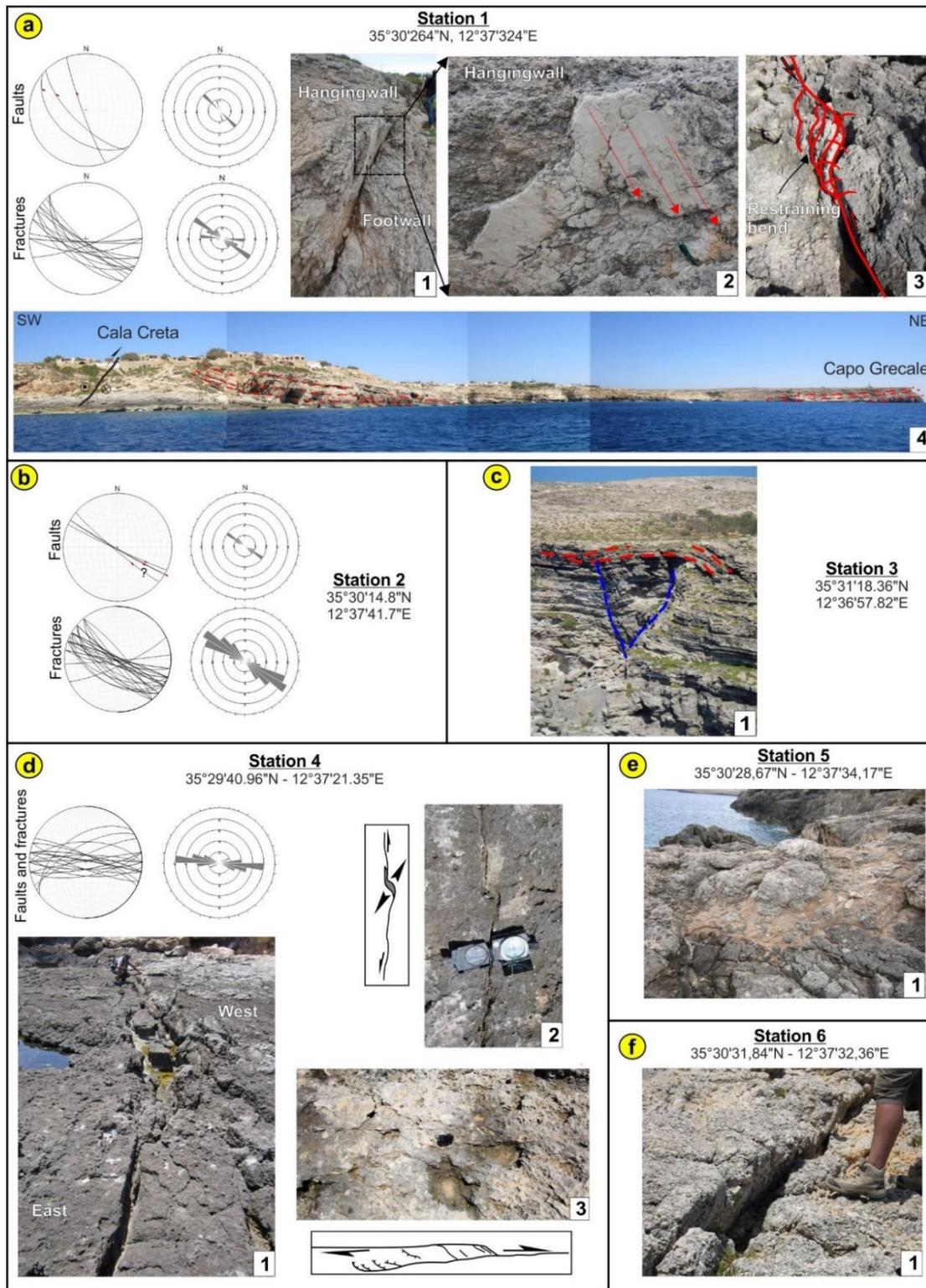
Fig. 5.6 – *Structural measurements and outcrops in the eastern part of Lampedusa Island (see Fig. 5.5 for location of sites). Stereoplots are Schmidt lower-hemisphere projections, showing attitude of fault and fractures, and slip lineations on faults (arrows point to motion of hanging-wall block).*

5.4.2 GNSS data analysis

Geodetic monitoring of the Sicily Channel started in 1991 with the establishment of a not-permanent network in the frame of the TYRGEONET and GEOMODAP projects (ANZIDEI et al., 1995). The monitoring by mean of continuous GNSS stations started in 1999 and in 2005 for Lampedusa (LAMP station) and Pantelleria (PZIN and other 2 stations installed within the caldera), respectively (Fig. 5.7). Previous studies have evidenced as the Sicilian-Pelagian domain is moving independently from the Nubia plate and is subject to crustal stretching along the NE-SW direction and contraction parallel to the Nubia-Eurasia geodetic convergence (see PALANO et al., 2012 for an overview).

Here, taking advantage of the availability of a set of continuous GNSS stations installed along the southern Sicilian on-shore, we propose an improved picture of the current crustal deformation pattern over the investigated area. To this aim, we collected and analysed all available data coming from the permanent GNSS stations installed across the Sicily Channel as well as the southern Sicilian onshore, spanning the 1999.01 - 2015.72 time interval.

Raw GNSS observations were reduced to loosely constrained daily solutions by using the GAMIT/GLOBK software packages (HERRING et al., 2010) and following the approach described in PALANO (2015). The analysed dataset consists of 16 GNSS stations (with more than 2.5 years of observations) belonging to various networks developed in the last two decades for crustal deformation monitoring and commercial applications (e.g. mapping and cadastral purposes). Estimated GNSS velocities, referred to a Nubian-fixed reference frame (SARIA et al., 2013) and associated uncertainties at the 95% level of confidence are reported in Figure 5.7 and Table 5.2.

Within this reference frame, LAMP station shows a SSE-directed residual velocity of ~1 mm/yr, evidencing a small deviation from Nubia.

Stations installed on the Hyblean-Malta block move toward ENE with rates of ~ 2.3 mm/yr, while stations installed on Pantelleria and on SW Sicilian onshore move toward ESE with rates ranging between ~ 2.1 mm/yr (SW Sicilian onshore) and 3.8 mm/yr (Pantelleria).
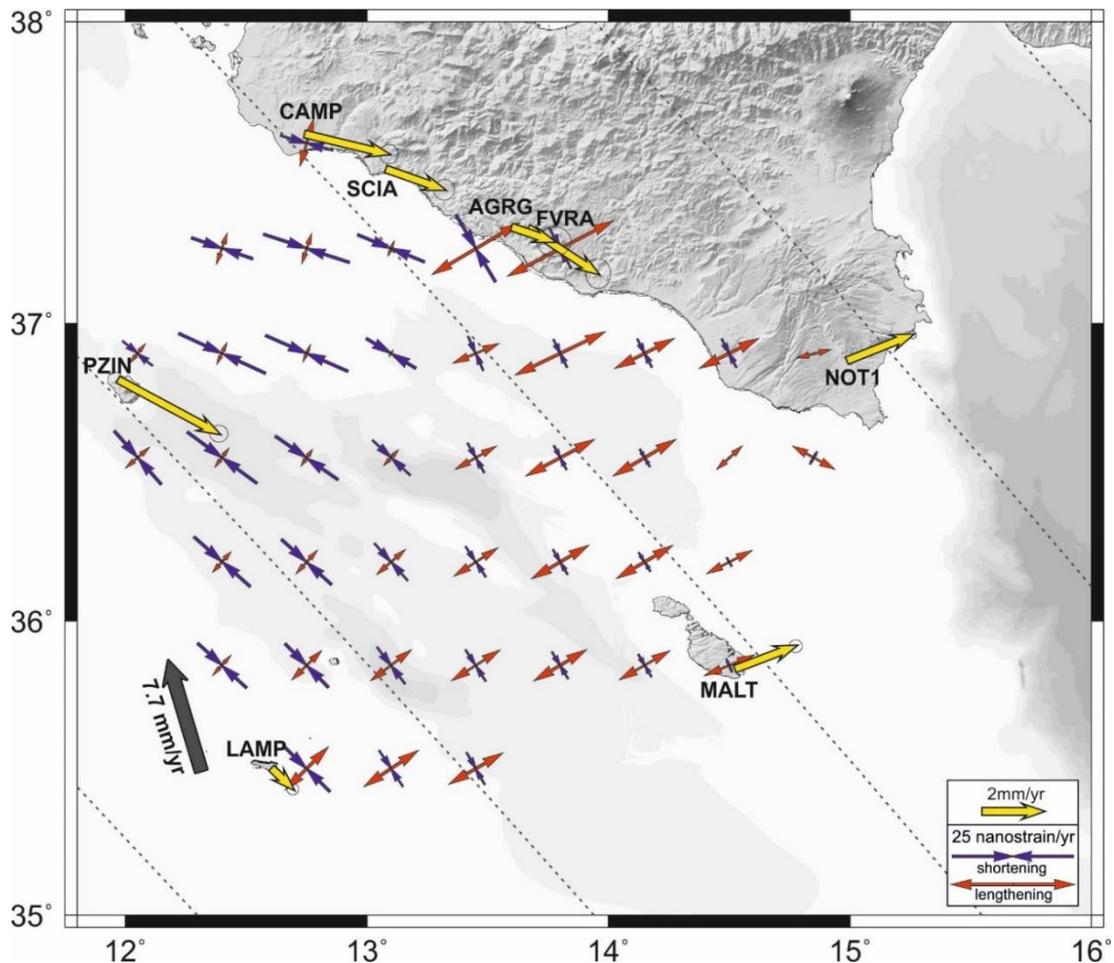
Fig. 5.7 – GNSS velocities (yellow arrows) and 95% confidence ellipses in a Nubian-fixed reference frame (SARIA et al., 2013) for sites in the Pelagian islands and southern Sicily. Estimated geodetic strain-rate is also reported: greatest extensional and contractional horizontal strain-rates are shown as red and blue arrows, respectively. Black dashed lines are parallel to the predicted Nubia-Eurasia geodetic relative motion direction (see PALANO et al., 2015 for details). The gray arrow represents the predicted motion of Nubia relative to Eurasia at 35.5°N, 12.6°E (LAMP GNSS station) according to geological plate motion model MORVEL (DEMETZ et al., 2010).

Table 5.2

SITE_Id	Lat.	Long	V_E (I08)	V_N (I08)	V_E (Nu)	V_N (Nu)	V_E error	V_N error	RHO
FVRA	13.66905	37.31753	21.03	17.62	2.31	-1.52	0.19	0.23	0.006
MALT	14.5262	35.83798	21.19	19.87	1.99	0.76	0.1	0.1	0.017
LAMP	12.60566	35.49978	19.6	18.48	0.7	-0.68	0.09	0.09	0.004
NOT1	14.98979	36.87585	21.23	19.96	2.15	0.86	0.06	0.06	-0.073
PZIN	11.97143	36.81113	21.81	17.38	3.32	-1.79	0.14	0.13	0.004
CAMP	12.74489	37.62926	21.24	18.49	2.77	-0.67	0.14	0.15	0.002
AGRG	13.60117	37.32028	20.1	18.66	1.39	-0.48	0.26	0.23	0.016
SCIA	13.07976	37.5123	20.48	18.47	1.92	-0.68	0.18	0.16	0.004
CAGL	8.97276	39.13591	21.6	16.06	4.27	-3.13	0.07	0.06	0.011
ZIMM	7.46528	46.8771	19.57	16.33	4.67	-2.84	0.05	0.05	-0.021
MATE	16.70446	40.64913	23.3	19.31	4.67	0.28	0.12	0.07	0.006
GRAS	6.92058	43.75474	20.39	16.08	4.73	-3.09	0.05	0.05	-0.029
GRAZ	15.49348	47.06713	21.84	15.77	5.04	-3.30	0.06	0.06	0.011
GENO	8.92115	44.41939	20.59	15.84	4.65	-3.35	0.07	0.06	-0.007
IENG	7.63941	45.01513	20.35	15.57	4.87	-3.61	0.08	0.08	-0.007
MILO	12.58432	38.00817	21.6	18.28	3.25	-0.88	0.15	0.09	0.001

To highlight the crustal deformation pattern over the study region, we computed the 2-D strain-rate tensor following the strategy reported in PALANO (2015). More in detail, by taking into account the observed horizontal velocity field we derived a continuous velocity gradient tensor on a regular 0.2° x 0.2° grid (whose nodes do not coincide with any of the GNSS stations) using a "spline in tension" technique (WESSEL & BERCOVICI, 1998). The tension is controlled by a factor T, where T=0 leads to a minimum curvature (natural bicubic spline), while T=1 leads to a maximum curvature, allowing for maxima and minima only at

observation points. We set T to the value of 0.5 because it represents the optimal value to minimize short wavelength noise. Lastly, we computed the average 2D strain-rate tensor as derivative of the velocities at the nodes of each grid cell.

The estimated strain-rates are reported in Figure 5.7: the arrows show the greatest extensional (ε_{Hmax}) and contractional (ε_{hmin}) horizontal strain-rates, respectively. The strain-rate field is mainly characterized by two different patterns. The western sector is dominated by a prevailing contractional field with ε_{hmin} axes having a WNW-ESE attitude in area comprises between PZIN and CAMP and a NW-SE attitude in area comprises between PZIN and LAMP. The eastern sector is dominated by a prevailing extensional field with ε_{Hmax} axes aligned to the NE-SW direction, coupled with a minor contraction with ε_{hmin} axes having a NW-SE attitude.

5.5 Tectonic evolution of the northern Lampedusa Plateau

Analysis of multichannel seismic reflection profiles shows that the structure of the northern part of the Lampedusa Plateau is characterized by a large-wavelength arch with secondary highs and lows, and associated faults with a reverse albeit minor component of motion. However, because of the wide spacing of the profiles and the locally limited seismic data resolution, a detailed structural analysis to detect the kinematic evolution of the plateau is not possible. Toward this end, we have integrated the seismic profile analysis with plate motion reconstructions and with field observations on Lampedusa Island, which offer a chance to characterize the recent kinematics that has led to the growth of structures buried under the shelf.

In figure 1.10 (see chapter I) we show a reconstruction of the trajectory of the Lampedusa Plateau relative to Eurasia back to 55 Ma. Specifically, the selected point is LAMP GNSS station, which allows to rigorously correlate past and current evolution, as detailed in chapter VI. Being this point located on the northern continental margin of Nubia, the path indicates that plate

convergence was occurring in a broad ~ N-S direction throughout the Eocene-Early Miocene (55-20 Ma). Furthermore, inspection of figure 1.10 (see chapter I) reveals that convergence rates progressively decreased in time, particularly after 35-30 Ma. The 55-20 Ma convergence direction is almost orthogonal to the broad folds and associated faults that represent in our view the dominant structures of the plateau (red arrows in Fig. 5.4b). Consequently, we consider the folding and reverse component of fault motion interpreted in the seismic profiles as an expression of contraction acting across the plateau because of convergence.

These structures certainly had started forming prior to 55 Ma in response to the same processes (GRASSO et al., 1999). This had led to the formation during the Paleocene of the embryonic LPA (see in Fig. 5.4a the spatial correspondence between the Paleogene structures mapped by GRASSO et al., 1999 and the Neogene structures mapped in this work). We remark here that, because plate convergence was continuing during the Eocene, contraction controlled progradation of the Halk el Menzel formation both to the north and to the south of the LLH, and enhanced growth of the inherited structural high (Fig. 5.4b). During the Oligocene-Early Miocene (~ 35-20), slowing convergence rates (see chapter I, Fig. 1.10), coupled to a prevailing global eustatic fall (VAIL et al., 1977) have conspired to produce regional erosion across the plateau (GRASSO et al., 1999) and to cause a diminished expression of folding associated to the LPA.

Plate reconstructions indicate that, after 20 Ma, the plateau moved NNW relative to Eurasia at significantly lower rates (see chapter I, Fig. 1.10). Under the assumption that plate convergence still controlled the kinematics of the plateau, the inherited Paleogene structures were likely reactivated in strike-slip starting from Early-Middle Miocene. Because of

their inherited WNW-ESE trend, they should have also recorded a reverse component of motion.

Structural observations on Lampedusa Island offer the chance to test this latter hypothesis. The CCF and CFF in the eastern part of the island have been active with left and right strike-slip motion, respectively, as documented by analysis of fault slip lineations and Riedel-type fracture association. These faults have moved during the same time span, as documented by growth relation of sediments and by neptunean dykes emplaced at releasing bends (GRASSO & PEDLEY, 1985). Considering that the CCF and CFF have NNW-SSE and E-W trend, respectively, the acute angle formed by the faults is bisected at a ~ NW-SE direction, which is taken as the local shortening direction (Fig. 5.5). Similar conclusions were reached by GRASSO & PEDLEY (1985), who considered small N100°-110° striking normal faults associated to the CCF as extension fractures within a Riedel-type shear zone, and derived a N125°-130°E shortening direction on the base of fracture association. This NW-SE shortening axis is consistent, with only a limited ~ 10° difference, with the predicted convergence between Lampedusa and Eurasia (black arrows in Fig. 5.4a). Thus, the faults were activated obliquely because of the same convergence process, and by assuming the correlation as appropriate for the Lampedusa shelf as a whole, the faults mapped in seismic profiles must be considered as transpressive.

GRASSO & PEDLEY (1985) regarded the CCF as a left-transtensional fault with a down-thrown eastern side. Furthermore, they suggested that, following a Late Miocene peak syn-sedimentary activity, the fault was reactivated as normal during the extension episode associated to rifting in the Sicily Channel. Our field survey indicates that the CCF has several bends with dominant restraining nature, which is responsible for growth of contractional folds and oblique thrust faults (Fig. 5.5). Because these structures are developed in lithified rocks and are associated to brittle fabrics such as cataclasite and striated shear planes (Fig. 5.6e, f), we consider these features as an expression

of a later reactivation of the fault. Thus, we argue that the CCF controlled formation of a local depocenter in its eastern, down-thrown block during the Tortonian-Early Messinian (broadly 12-7 Ma), and was reactivated in transpression since then. This reactivation occurred during progressive growth of the LLH, which possibly caused oversteepening and transpressional reactivation of the previous transtensional fault plane. The transtensional motion suggested by GRASSO & PEDLEY (1985) during Tortonian-Early Messinian deposition cannot be clearly related to regional processes, because of plate convergence at that time (Fig. 5.4a). Thus, it is possible that transtension occurred locally in a more general frame of transpressional-driven uplift.

In addition, we did not find systematic superposition of slip lineations, which would support the notion of reactivation of the fault in later extension. Rather, we consider the locales where the fault has steeply dipping lineations as bends of the main fault trace which were developed during strike-slip displacement. The location where GRASSO & PEDLEY (1985) claimed a reactivation in extension is found on the northern part of the island, which could have been affected by local displacement unrelated to regional tectonics. In summary, Late Miocene transtension followed by transpression occurred at Lampedusa, and pure normal faulting is not documented.

All in all, by considering the seismic profiles, the on-land observations and the large-scale plate reconstructions, we argue that probably after ~ 20 Ma and certainly after ~ 7 Ma the LPA and related structural highs and lows ceased their growth and were affected by relatively minor oblique strike-slip deformation.

Because of the lack of post-Miocene marine deposits on Lampedusa, on-land observations do not allow to detect the upper age limit for strike-slip and transpressional deformation under the plateau. Nevertheless, MCS profiles shows that folds and locally faults deform

the M horizon (Figs. 5.3a; 5.3b), documenting a post-Miocene activity with a reverse component. The Lampedusa South fault on the southern side of the LLH causes shortening of Lower Pliocene and possibly even younger reflectors (Fig. 5.3a, inset 2). As pointed above, these structures have a reverse deformation component also in post-Miocene time because they were inherited with a WNW-ESE orientation from Paleogene shortening. It is likely that Lampedusa (and possibly Lampione) emerged as a result of localized post-Tortonian transpression.

The reconstructed tectonic evolution of the northern Lampedusa Plateau since ~ 55 Ma matches well the protracted positive inversion of pre-existing faults in the Halk el Menzel region west of Lampedusa (SEBEI et al., 2007). This region lies ~ 100 km west of the plateau (Fig. 1.11) and is along-strike with the main structural fabrics described in our study. The structural culmination in the Halk el Menzel area is centred on the homonymous well, where major hiatuses are recorded (SEBEI et al., 2007). We suggest that the Halk el Menzel area and the north-eastern Lampedusa plateau were part of a regional system of structural highs formed in response to intraplate shortening.

Our structural reconstruction modifies previous models in which transpressional faults were only assigned to the Paleogene, and the post-Miocene evolution of the shelf was controlled by extensional faults (TORELLI et al., 1995; GRASSO et al., 1993; GRASSO et al., 1999; ARGNANI & TORELLI, 2001). Rather, we surmise that normal faults only affect the shelf northeast of Lampedusa, and control Early Pliocene deposition in the LEB half-graben (Fig. 5.4a). The fact that basins associated to relatively thick Pliocene-Quaternary deposits and limited by faults which have a clear bathymetric expression are confined to the northeast of Lampedusa suggests that the effects of an extensional pulse during the early part of the Pliocene are expressed only in this sector (BOCCALETTI et al., 1987; CELLO, 1987; CATALANO et al., 1995b; ARGNANI, 1990; CIVILE et al., 2010). Thus, we consider these basins and the bounding normal faults as the southern forefront

of the regional faults bounding the flank of the Linosa rift basin (Fig. 1.11). On the contrary, the consequence of moderate but steady strike-slip with local transpression prevailed on the plateau during that time, and superimposed on previous contractional features.

CHAPTER VI

6. DISCUSSIONS

6.1 Structural setting of the NW Sicily Channel: update of existing models

6.1.1 Timing of deformation

The joint analysis of MCS reflection profiles from the ViDEPI project and the ENI database, supported by a thorough appraisal of well-log data, has permit to reconstruct the structural evolution of the sector of the Sicily Channel between the Egadi Islands in the NW and Eraclea Minoa in the SE. The results of this study, while confirming the known migration of the locus of active shortening associated to the Sicily Fold and Thrust Belt (SFTB) from NW toward SE, refine existing reconstructions (ARGNANI et al., 1986; 1990; ANTONELLI, 1988; CATALANO, 1987; CIVILE et al., 2014) and bring new implications for tectonic models of the area.

The NW Sicily Channel was long recognized as the submarine prolongation of the contractional chain in western Sicily (CATALANO et al., 1985; ARGNANI et ala., 1986). This chain involves a complex system of thrust allochthonous developed as result of the Neogene-Quaternary Africa-Europe collision processes (DEWEY et al., 1989; BEN-AVRAHAM et al., 1990).

In the northern sector of western Sicily, the up to 12 km thick tectonic stack (CATALANO et al., 2002) is made of Mesozoic carbonate platforms (pre-Panormide, Panormide, Trapanese) successions and their Neogene clastic cover, which to the east structurally pass to imbricates of Meso-Cenozoic (Imerese-Sicanian) and Oligo-Miocene basinal rocks. Toward the south, due to less intense and younger deformation, these units are encountered only in wells drilled for oil exploration (CATALANO et al., 1995b; 1998; MONTANARI et al., 2017). Moving from northwest to southeast across western Sicily, the thrust edifice displays three ENE-trending structural highs of the Trapanese–Saccense carbonate platform (Paceco, Montagna Grande and Lippone structures). These highs are separated by two ENE-trending deep depressions

(Mozia and Biddusa–Vita synforms), filled by Miocene (up to Messinian) and Upper Miocene–Pliocene rocks, respectively (Figs. 6.1, 6.2). Northward-dipping ramp imbricates in the buried carbonate layer characterize the antiformal highs. The imbricates are displaced by blind thrusts that are locally associated to development of thin tectonic slices in the overlying Upper Miocene–Pliocene deposits.
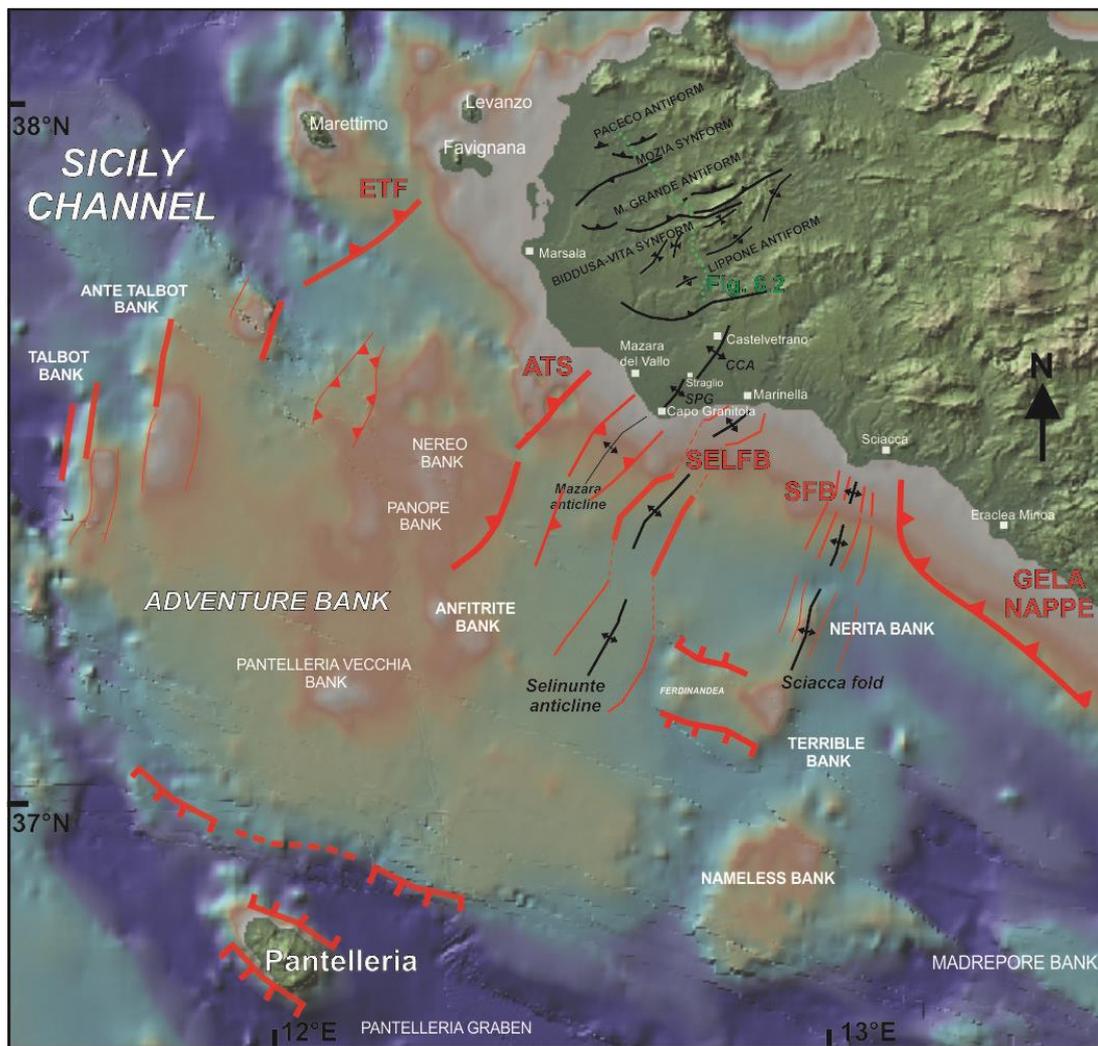
Fig. 6.1 – Bathymetric map of the NW Sicily Channel with location of the main structural lineaments (see chapter III for more details, Fig. 3.15) in the area and in western Sicily (from CATALANO et al., 2002).
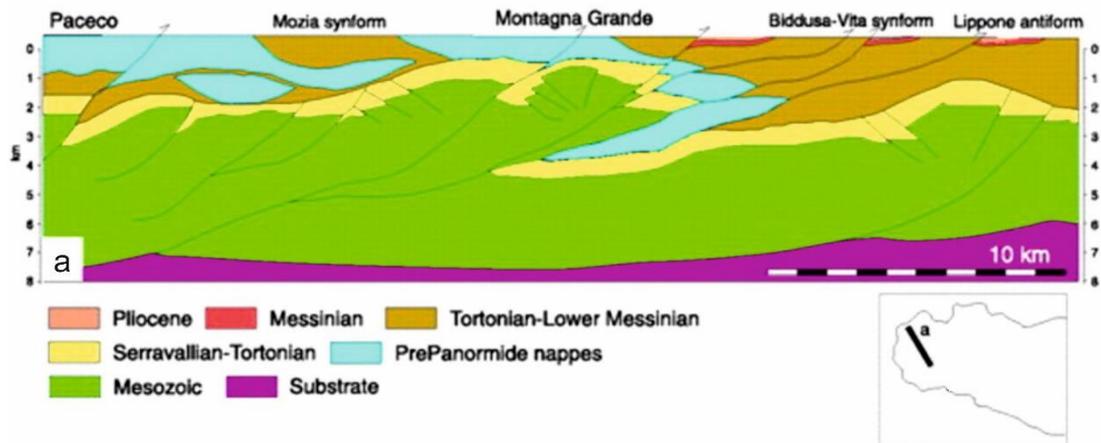
Fig. 6.2 – Geological cross section showing the structural geometries at depth. Location is also reported in Figure 6.1. (After CATALANO et al., 2002).

The submerged portion of the chain in the north-westernmost part of the Sicily Channel offshore the Egadi Islands corresponds to the Paceco and Montagna Grande culminations (Fig. 6.2; see also chapter III, Fig. 3.46). This sector consists of a pile of tectonic units, detached and accreted as thrust ramps and flats (ARGNANI et al., 1986; ANTONELLI et al., 1988; CATALANO et al., 1995b; 1998; CIVILE et al., 2014), which derive from the deformation of the Meso-Cenozoic carbonate platform domains. These successions exhibit stratigraphic and facies affinities with the innermost units of western Sicily (Pre-Panormide, Panormide and Trapanese) and with those of northern Tunisia (ANTONELLI et al., 1988). Differently, the marine zone between Mazara and Sciacca was considered mostly autochthonous based on well stratigraphic data (ANTONELLI et al., 1988).

In agreement with previous Authors, our analysis has documented that the offshore Egadi area was affected by a Middle-Upper Miocene compressive event related to emplacement of the Egadi Thrust System, ETS (Fig. 6.1). The leading edge of the ETS (ETF, Egadi Thrust Front, according to CATALANO et al., 1995b; or MTF, Maghrebian Thrust Front, according to ANTONELLI et al., 1988) is represented by a major thrust ramp separating the Pre-Panormide domain from the Trapanese-Saccense domain.

Younger contraction was transferred in the offshore of Mazara along the SE-vergent Adventure Thrust System (ATS, Fig. 6.1), on the eastern side of the Adventure Bank. This sector is in turn limited to the east by a major thrust front (ATF - Adventure Thrust Front; ARGNANI et al., 1987; or NFBF - Nilde Fold Belt Front, ANTONELLI et al., 1988). The ATS broadly coincides with the offshore extension of the Lippone antiform (Fig. 6.1; see also chapter III, Fig. 3.46).

Our detailed seismo-stratigraphic analysis revealed a prominent seismic reflector, dated to ~ 8 Ma by correlation between the seismic facies and on-land stratigraphic studies (BASILONE, 2012) which marks the passage from the conglomeratic to the sandy-pelitic member of the Terravecchia fm., that was instrumental to pinpoint the shift of activity from the ETS to the ATS.

Thus, contractional deformation acted during and after deposition within the Adventure foredeep basin. The ETS and ATS limited the north-western and south-eastern flank, respectively, of the NE-SW directed Miocene foredeep basin. The depozone of the basin coincides with the Adventure bank, where the foredeep sediments reach a maximum thickness of 2500-3000 m as evidenced by the isopach map (see chapter III, Fig. 3.45). Through the well calibration and seismic facies analysis, we were able to distinguish three seismo-stratigraphic facies pertaining to S4 seismic sequence, which fill the Miocene foredeep basin. The lower and middle facies are correlative of the Serravallian-Lower Tortonian Castellana fm. pelites and Terravecchia fm. conglomerates. The high amplitude-high frequency reflector described above separates the lower and middle seismic units from the upper unit, which is correlative of the sandy-pelitic sediments pertaining to the younger (Upper Tortonian-Messinian) member of the Terravecchia fm. (BASILONE, 2012).

The paleo-topographic reconstructions of the Miocene and the Plio-Pleistocene seismic units (see chapter III, Figs. 3.44, 3.45) allowed to appreciate the spatial features of the south-eastern and south-western tectonic

transport direction of the SFTB, respectively. Two segments of the chain in the north-western and south-eastern sectors of the Channel are separated by a transcurrent belt. As outlined above, the western segment migrated from the ETS in the NW to the ATS in the SE. This segment is separated from the eastern segment, which is represented by the GN, by means of the transcurrent belt, which includes the Selinunte (SELFB) and Sciacca (SFB) fault belts (Fig. 6.1). The Gela Nappe (GN), which is mapped in the south-eastern sector of the investigated area in the Eraclea Minoa offshore, shows a SW vergence and represents the outermost and youngest thrust sheet of the SFTB Sicilian chain. Also for the GN, integrated analysis of MCS and SCS profiles, allows to state that the deformation becomes younger toward the SW.

The availability of ENI seismic profiles was particularly instrumental for analysis on the GN, making possible to determine the exact location and seismic characteristic of the nappe and of the related foredeep basin. The Plio-Pleistocene isopach map shows the E-W trending Gela foredeep basin between Sciacca and Eraclea Minoa deformed by the Gela Nappe. The allochthonous body forms a wedge-shaped package of reflectors made up by multiple imbricates of Miocene to Pleistocene clastic, evaporitic and carbonate deposits, resting on the Pleistocene sediments of the foredeep. Based on the observation that the basal thrust dips, although gently, toward the land (so toward the chain; see chapter III, Fig. 3.33), we rule out a gravitational origin and agree with the content of a tectonic nature of the GN, as proposed by LENTINI (1982), ARGNANI (1987) and CAVALLARO et al. (2017). However, its emplacement produced a diffuse gravitational instability of the sediments resting on it (see Fig. 3.33, chapter III).

6.1.2 *Structural style and the role of inherited structures*

The extensive literature on the contractional structures exposed in Western Sicily (see CATALANO et al., 2011; MONTANARI et al., 2017 for a review) regards the structural evolution as characterized by two main tectonic

stages. An earlier (Early-Late Miocene p.p.) tectonic history was characterized by thin-skinned emplacement of thrust sheets made of Sicilide and Imerese basinal rocks above pre-Panormide and Panormide carbonate platform rocks. The platform rocks were in turn imbricated and thrust onto the Trapanese platform rocks, leading to the formation of the Paceco-Marsala antiform. This deformation characterizes also the more internal (northern) sector of the Channel between the Egadi Islands and Mazara offshore.

Oppositely, according to current models, the Late Miocene–Early Pleistocene deformation was characterized by SE-vergent thrusts with ramp and flat geometry, resulting from the deep-seated deformation of the Trapanese and Saccense carbonate platform domains. This deformation led to the growth of the Montagna Grande and Lippone antiforms. The Late Miocene-Pliocene deep-seated structures do not involve the basement in the deformation, and cannot be strictly considered as thick-skinned thrusts sensu COWARD (1983). Offshore, in the Sicily Channel, such model is typically applied to the ATS in the more external sector between Mazara and Capo Granitola.

Unlikely most of previous authors (CATALANO, 1987; CATALANO et al., 1995 a, b; ANTONELLI et al., 1988; ROURE et al., 2012; CIVILE et al., 2014), our tectonic model for the more internal (northern) sector of the Channel between the Egadi Islands and Mazara offshore is based on a deep-seated tectonic style. The ETS is characterized by an array of twelve SE-verging thrusts, which deformed Middle-Upper Miocene deposits (see Fig. 3.15, chapter 3). These thrusts are steep (~ 65° dip) and deep-seated, since they cut, with a broadly planar geometry, at least down to the investigation depth (~ 7 km) allowed by MCS profiles (see Fig. 3.18, chapter III). Similarly to the ETS, the ATS is expressed at the front by a NW-dipping reverse fault traceable up to ~ 8 km with a dip angle of 69°. Thus, the ETS and ATS, previously regarded as characterized by contrasting structural styles and geometries, are in fact very similar.

As regards the offshore area between Capo Granitola and Sciacca, ANTONELLI et al. (1988) based on well and seismic data proposed an extensional tectonic phase of a probably transtensional origin, involving the basement, which dismembered the area during the Early Tortonian and were later reactivated in transpression during the Plio-Pleistocene. In agreement with those and with other workers who studied the foreland-foredeep evolution onshore and offshore Sicily (COGAN et al., 1989; BILLI et al., 2006; CAVALLARO et al., 2017), we described the study area as affected by a compressive or transpressional reactivation of inherited high-angle extensional faults, which started during the Miocene and acted with major intensity during the Plio-Pleistocene. These faults, which are traceable up to ~ 8 km down-dip, formed during the Middle Miocene when they created half grabens completely filled by Middle-Upper Miocene sediments (see chapter III, Fig. 3.27). The normal faults origin could be related to the bending of the foreland plate ahead of the migrating orogen, as suggested for the foreland domain in SE Sicily (COGAN et al., 1989; BILLI et al., 2006) and its offshore (CAVALLARO et al., 2017) and for the Apulian platform in the southern Apennines (SHINER et al., 2004).

The reconstruction of geometry and position of the major structures presented in this work are supported by a modern analysis of the Bouguer gravity anomalies performed in the PhD work of LO RE (2017). Figure 6.3 below shows an overlay of the residual Bouguer anomalies (mGal) gathered by a layered density distribution model through the Sharp-Edged strategy inversion. The main maxima of gravity anomalies closely reproduce the depths of the Mesozoic-Cenozoic carbonate basement (see chapter III, Fig. 3.46). The values exhibit a good fit with the geological structures obtained by seismic profiles analysis demonstrating that the residual Bouguer anomalies largely depend on the geological setting relative to the first kilometres. It is worth to note the almost perfect correspondence between the depths of Miocene sediments (see chapter III, Fig. 3.46) deformed by normal faults that

reversed their movement, as described above, and the zones with higher or lower values of residual Bouguer anomalies, that is the zones of minor or major depths of the basement. In particular, the partial inversion of SELFB inferred by seismic images is evidenced also in the map of Figure 6.3b by lower values of anomalies with respect to the adjacent areas.

For what concerns the on-land sector, the high values of gravity anomalies in Mazara-Castelvetrano area agree with the presence of basement uplifts, as imaged by seismic profile analyses (e.g., Fig. 6.2), describing two main anomalies. The first anomaly on the west with a ENE-WSW trend and a second anomaly with a NE-SW trend. These two maxima can be related to Lippone anticline and CCA lineament, respectively (Fig. 6.1). As their intensity markedly decreases toward the coast, an offshore extension of the structures is excluded.
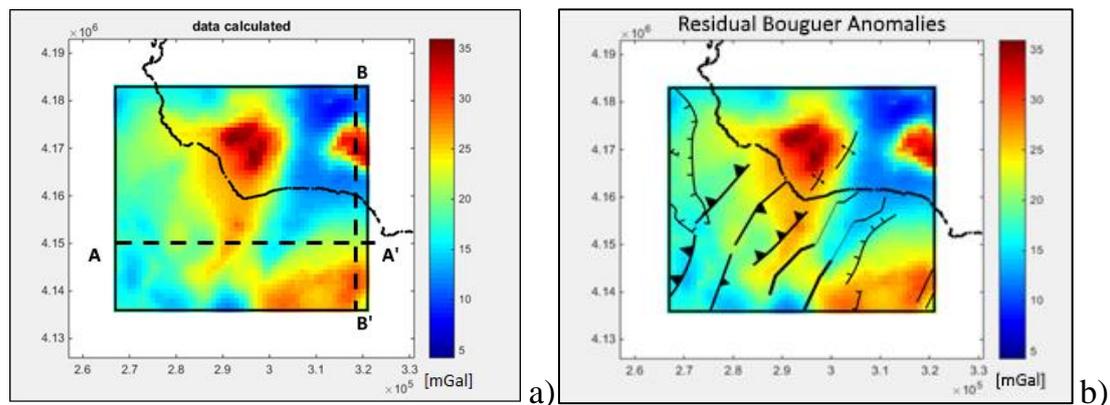
Fig. 6.3 – a) Data computed by the density distribution model obtained from the third stage of the Sharp-Edged Inversion strategy (LO RE, 2017). Axis in meters. Black dashed line A-A' is the trace of the cross-section of the density distribution model shown in Figure 6.4. b) Overlay of the residual Bouguer gravity anomaly map and the main structural features presented in this thesis (see chapter III, Fig. 3.15).

In figure 6.4 a tentative interpretation of the W-E trending density model cross-section (A-A' in Fig. 6.3a) is made taking into account the calibration of Oscar W well, where three density classes are defined based on the inversion of the velocity values attributed to geological formations within each class. Of

relevance, the geometry of the main tectonic structures allowed by the density model is consistent with a deep-seated model of deformation in the Sicily Channel between Mazara and Sciacca.
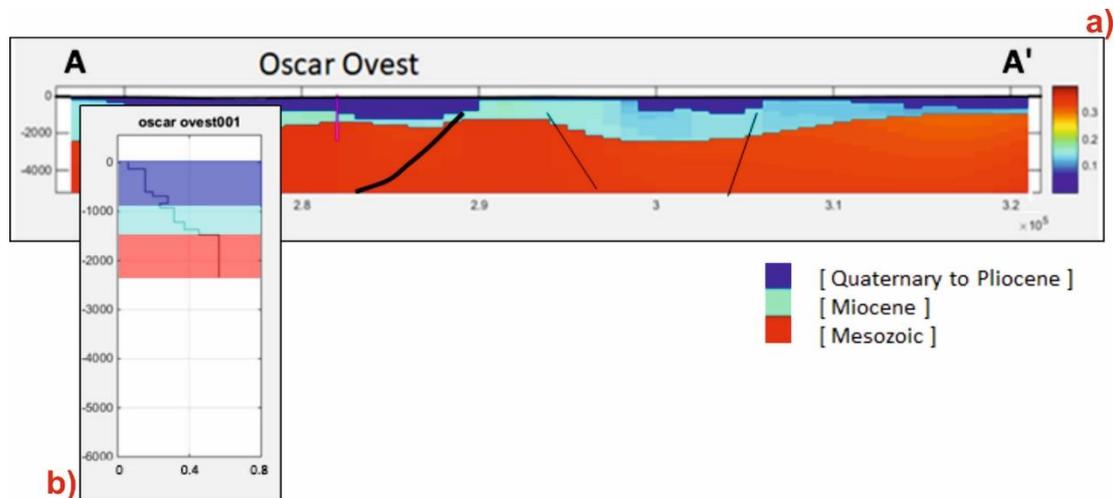
Fig. 6.4 – a) Density distribution cross section along the trace A-A' in Figure 6.3a. Color bar units are g/cm³, axis in metres. Magenta line is the well projection. Black lines are faults and thrust drawn according to the structural map in Figure 3.13b. b) Log of converted densities of Oscar Ovest well, with highlighted the three density classes used in the clustering. The three different homogeneous bodies are related to: Quaternary to Late Pliocene formations (blue), Miocene formations (cyan) and Mesozoic basement (red).

According to CATALANO et al. (1998) and MONTANARI et al. (2017), the formation in SW Sicily of the central antiform (Montagna Grande) during the second tectonic stage (Late Miocene-Early Pliocene) involved reactivation of a boundary between different paleogeographic domains. In fact, in their reconstruction, the transition between the Trapanese and Saccense domains runs along the Montagna Grande antiform and Marsala (see also CATALANO, 1987). The distinction is based on the facies characteristics of Oligocene-Miocene deposits, which are attributed to an open shelf environment in the Trapanese area, and to a reefal environment in the Saccense domain.

According to seismo-stratigraphic analysis of ANTONELLI et al. (1988), such transition occurs further to the east, offshore Mazara, and even further to east offshore Capo Granitola according to ARGNANI et al. (1986).

The results of our analysis based on well-logs and seismic data support the model of ANTONELLI et al. (1988), and allow to provide more detailed information regarding the location of the paleogeographic transition. Precisely, we map this transition along the Adventure Thrust System that separates Nuccia and Vallo wells to the north-west from Oscar W well to the south-east. These two groups of wells differ for the Triassic-Jurassic sedimentary facies evolution (for more details see chapter III, Fig. 3.6). In light of this, the ATS can be regarded as deriving from the inversion of an inherited Mesozoic crustal boundary between the Trapanese and Saccense domains (see chapter III, Fig. 3.24). Well-log analysis further documents that during the Miocene, this boundary was already active, and marked the transition, in the Terravecchia foredeep, from a proximal shelf facies to the northwest to a distal ramp facies to the southeast (see chapter III, Fig. 3.5). It is likely that the inheritance of a high-angle extensional fault is the primary cause for deep-seated activity on a steep (~ 65°) during the later reverse reactivation.

Our analysis also brings new highlights on the fault reactivation in the Egadi offshore, as previously suggested based on limited-resolution data (CIVILE et al., 2014 and references therein). Back-thrusts and high-angle faults cutting the seafloor bear evidence of a Plio-Quaternary activity of the ETS (see Figs. 3.20, 3.22, chapter III). The back-thrusts can be explained as related to a forced compressive strain of the chain in the recent phase of the collisional process. Whilst, the high-angle faults bound three banks (Talbot, Ante Talbot and the bank NAT, Figs. 3.20, 3.21, chapter III). CIVILE et al. (2015) consider the Talbot and the Ante Talbot banks as the surface expression of a Miocene structural high related to a thrust-anticline and to a transpressional (positive) flower structure, respectively. In addition to the findings of CIVILE et al. (2015), and based on the better resolution offered by the ENI seismic profiles, we argue that both sets of structures developed during Middle-Late Miocene contraction, and reactivated in transpression afterwards. The transpressional reactivation of these structures acted coeval to

the Plio-Pleistocene normal faults related to the opening of the rift system in the central Sicily Channel, as modelled by CORTI et al. (2006).

6.1.3 Extension and positive reactivation in the Sicily Channel Rift

In this work, we have studied the northern part of the rift where, starting from the Early Pliocene, the rift branch of Pantelleria formed south of the contractional structures. Through the analysis of industrial profiles, we define an asymmetric basin, which narrows from ~ 20 km in the south to ~ 7 km in the northwest of Pantelleria Island. The basin is characterized by NW trending extensional structures with a domino configuration, where half-grabens are separated by sub-vertical normal faults arrays with offsets of a few hundred meters. Fault activity is dated by syn-tectonic Lower Pliocene sediments, which are covered by a relatively undeformed Late Pliocene–Quaternary succession (see Figs. 3.35, 3.36, 3.37, chapter III). Volcanic extrusives and intrusives mask the tectonic structures in the central part of the through. The age of activity in this part of the Sicily Channel rift is in agreement with the extensive literature on the rift (e.g., FINETTI, 1984; ARGNANI, 1990; TORELLI et al., 1991; FINETTI and DEL BEN, 2005; CIVILE et al., 2010).

We also recognized some reverse faults in seismic images in the rift basins (see chapter III, Fig. 3.38), which can be connected to a local reactivation of normal faults, as already proposed by ARGNANI (1990). Based on age constraints, reactivation is coeval to the last compressive events of the chain in the offshore of Sciacca and Agrigento along the SFB and GN.

6.2 High-resolution Pleistocene tectono-stratigraphic evolution of the Capo Granitola and Sciacca offshore

6.2.1 Unveiling the structural-stratigraphic framework

The newly acquired high-resolution single-channel seismic reflection (SCS) profiles allowed a detailed reconstruction of the Quaternary structural

framework of the offshore area between Capo Granitola and Eraclea Minoa, which represents the central section of the part of the Channel investigated in this work.

Except for a single seismic line of the studied dataset presented in BARRECA et al. (2014), these profiles are unpublished to date and represent a starting point for a detailed description of the tectono-stratigraphic framework of the area. The analysis brings new implications regarding the recent activity of the main recognized structures.

Two seismo-stratigraphic unconformities (ES1 and ES2) and five seismic units (A, B, C, D, MD) were detected on the base of their internal configuration and correlated to the corresponding stratigraphic units by taking into account calibration with offshore and onshore deep exploration wells and correlation with on-land outcrops (see chapter IV, Table 4.1).

The lowermost unit A is assigned to the latest Pleistocene-Holocene; unit B to the Middle-Late Pleistocene; unit C to the Lower– Middle Pleistocene silty clays (Marsala Synthem and older sediments exposed on-land); unit D to the Pliocene substratum (Belice marly-arenaceous and Trubi formations). As regard unit MD, it is locally recognised only above unit C, and is buried by unit B or by unit A or at the seafloor.

The correlation with on-land outcrops concerns the Marsala-Marinella area, where the older outcropping Quaternary deposits are Emilian p.p.-Sicilian in age and are assigned to the Marsala Synthem. These deposits are attributed to a long-lived highstand prograding system formed prior to the onset of regional uplift of south-western Sicily, or at least when regional uplift occurred at limited rate so that the depositional system could prograde without significant break in sedimentation. Offshore, they are correlative to unit C.

By considering its stratigraphic position, unconformity ES1 is assigned to the LGM. Conversely, ES2 is considered as a polyphase surface whose composite origin is related to the deposition and subsequent deformation of Pleistocene sediments during the cycles of sea-level fluctuation and tectonic

events probably connected to the so-called Roman Regression, which embraces the Marine Isotopic Stages 18, 19 and 20 (D'ANGELO & VERNUCCIO, 1996). This interval is particularly important for deciphering the morphotectonic evolution of the study area because during this time the transition from high-frequency, low amplitude to low-frequency, high-amplitude eustatic fluctuations established on the earth (LISIECKI & RAYMO, 2005).
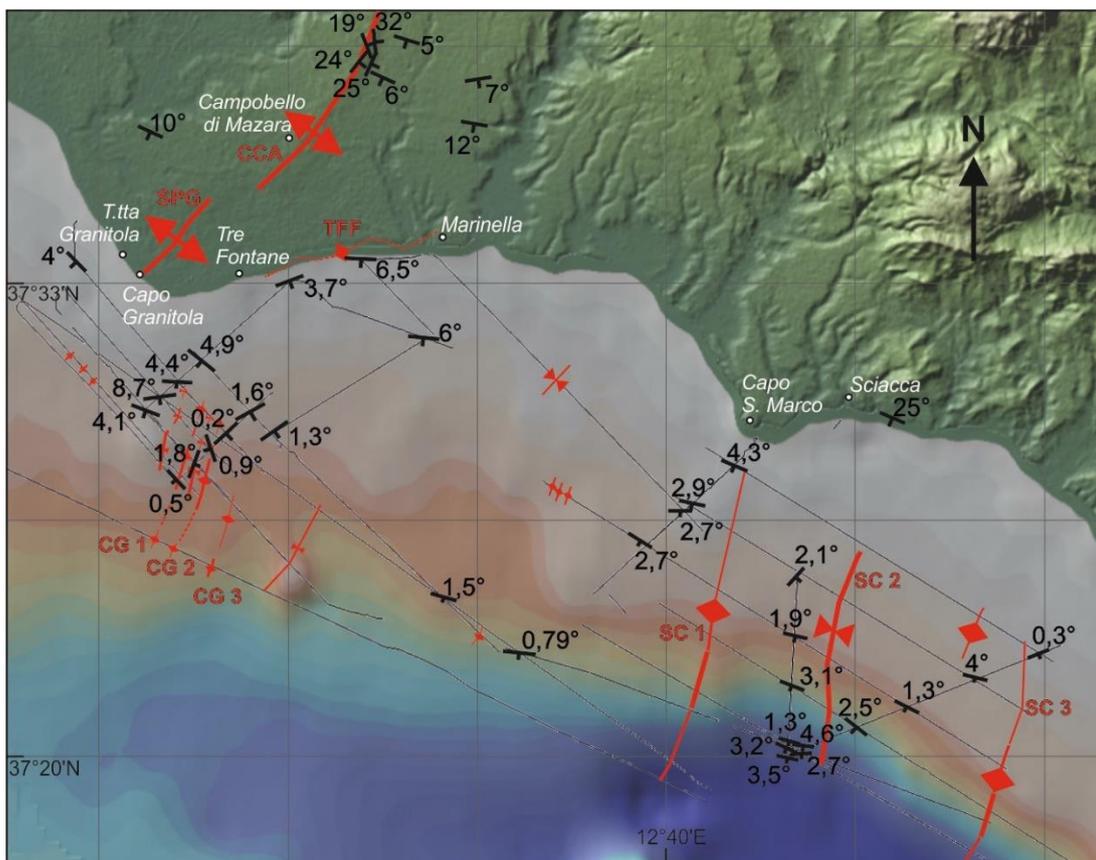
Fig. 6.5 – Bathymetric map of western Sicily offshore with location of main structural features and dip directions and dip angles computed for a horizon within unit C, gathered by SCS profiles analysis; and with dip direction of Quaternary deposits in western Sicily, inferred by a geological campaign (see text for more details).

The area of interest was divided in two sectors based on the different expression of deformation. Area 1, between Torretta Granitola and Capo San Marco, is characterized by a prominent fault escarpment with a maximum height of 33 m, and by three main folds, CG1, CG2 and CG3 (Fig. 6.5). These

folds deform an ~ 3 km wide and ~ 8 km long area, and are well developed within unit C, along with syn-sedimentary slumping, during uplift of underlying unit D. The folds developed at different rates during the Middle-Late Pleistocene as evidenced by growing strata. The associated faults and fractures are often the preferential path of fluid escapes that at places originated mounds grouped in unit MD (see chapter IV, Fig. 4.38).

Area 2, between Capo San Marco and Eraclea Minoa, is affected by a NNE-SSW trending, ~ 3 km wide fault zone that features a broad anticline fold (SC1) separated by a syncline from a second anticline (SC3) to the east (Fig. 6.5). These folds are locally associated to blanking and semi-transparent fault zones and fractures. The high angle faults deform unit C and B and were active during the Pleistocene.

6.2.2. Comparison between coastal and offshore Quaternary structures

The graphic reconstruction of the true attitude of several reflectors within unit C confirms the control on unit C deposition exerted by thrust uplift of unit D (Fig. 6.5). The reflectors within this unit presents marked variation in the dip direction when approaching the structures that deform there during deposition. This pattern can be compared to the attitude of Marsala calcarenites on-land (Fig. 6.5) which, as in the comparative submarine portion, exhibits strong changes in correspondence of the CCA lineaments.

The on-land map was built from data gathered during a multidisciplinary geological field work in the frame of an INGV project devoted to the seismotectonic study of SW Sicily.

The detailed analysis of geometrical parameters of the folds presented in chapter IV, allows a quantitative comparison between the offshore structures and those previously recognized on-land.

To this aim, we consider two graphs (Figs. 6.6a, b) showing the maximum height of scarps CCA and SPG, respectively, measured along the

profiles of Fig. 1.6 (chapter I) in the area between Castelvetrano and Capo Granitola and plotted along a longitudinal profile (GUZZETTA, 2014). The height of CCA displays a gradual increase from NNE toward SSW with a maximum of 58 m in the area of Castelvetrano between profiles 11 and 12 (Fig. 6.6 b). Then, the height rapidly decreases up to 10 m in the Straglio area (Fig. 6.1) depicting a bell-shape geometry. The longitudinal profile of SPG (Fig. 6.6 a) is composed by two minor bell-shaped profiles when compared to CCA, with a maximum height of ~ 10 m and with overlying slopes in between them.

The bell-shaped topographic profiles suggest the presence of underlying structures grown in a "characteristic" way (sensu SCHWARZ & COPPERSMITH, 1984). According to GUZZETTA (2014), the scarps represents the forelimb of thrust-related folds developed above blind thrust ramps at depth of ~ 2 km (Fig. 6.2). These ramps cut the upper 8-10 km crust at a high-angle.

A similar interpretation of "characteristics" grown of structures can be applied to the offshore escarpment and folds described in chapter IV (Figs. 4.40 to 4.46).

By correlating the geometry (amplitude, length) of the on-land escarpments with the scarp and folds related to the offshore structures, we note that these are comparable and thus reflect a similar genetic process. The cumulative structures can be categorized in two classes of length: ~ 5 km (for SPG and CG escarpment) and ~ 10 km (for CCA, CG1 and CG2), respectively. The segments SPG and CG exhibit similar length band comparable value of height (10 and 33 m, respectively). Conversely, CCA (maximum height of 58 m) can be compared with CG1 and CG2 folds, that show a maximum amplitude of 125 m and 47 m, respectively.

In light of this, it can be argued that, starting from the CCA in the north, the deformation belt tends to lose intensity toward the coast in the SSW direction along the SPG segment, which represents a relay zone, and resumes offshore further to east, with a left step, along the CG1 and CG2. These latter

folds can be thus considered the en-echelon structures that continue offshore the deformation accrued on-land on the CCA (Fig. 6.1).
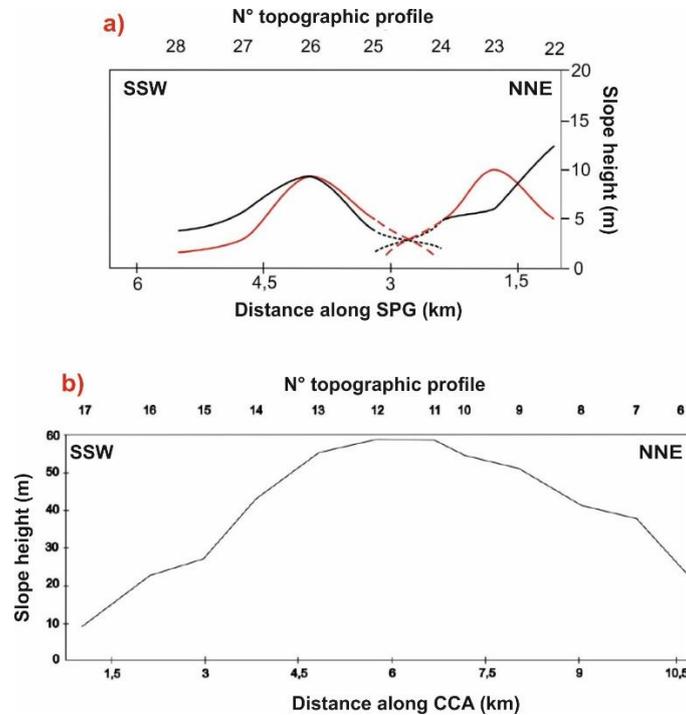
Fig. 6.6 – a) Longitudinal profile of SPG lineament. b) Longitudinal profile of CCA lineament that shows two folds (black and red). From GUZZETTA, 2014.

6.3 Integration of MCS and SCS reflection profiles

6.3.1 Structural pattern

In this section, we compare the structural and kinematic pattern of the central part of the investigated Channel (offshore zone between Mazara del Vallo and Eraclea Minoa), for which both high penetration (MCS) and high resolution (SCS) reflection profiles are available.

At a regional scale, the examined area was characterized by an intense Miocene extensional deformation expressed by NNW and SSE dipping normal faults. During the Pliocene-Pleistocene, the faults reversed their movements within a compressive/transcurrent regime that originated two tectonic lineaments, labeled SELFB and SFB (Fig. 6.1). These fault systems

experienced a positive inversion and development of flower structures (see chapter III, Figs. 3.25, 3.27, 3.28, 3.29).

Joint analysis of MCS and SCS profiles allowed to highlight spatial and geometric correspondence between structures separately studied in the two datasets. These datasets provide information at different resolution and depth, upper crustal (max 9 km) for MCS and near-bottom (200-400 m) for SCS profiles.

The location of the Selinunte anticline and Sciacca fold retrieved from analysis of MCS profiles (Fig. 6.1), is spatially coincident with those recognized along SCS profiles, i.e. CG 1, CG 2, CG3 and SC1 (Fig. 6.5).

Based on spatial correspondence of the upper crustal and near-bottom structures offshore Capo Granitola and Sciacca, we infer that they are different scale expression of two fault systems (SELFB and SFB, respectively). The two systems were inverted since the Pliocene (as documented by MCS profiles), with inversion still active (as documented by folding of recent reflectors and by pervasive fluid escapes SCS profiles).

If we consider the geometrical parameters of the structures at different scales of observation, a distinction can be made for Selinunte anticline and its recent folding and for Sciacca fold with its recent structures.

SELF 1 and SELF 2, retrieved from analysis of MCS profiles, exhibit a typical bell-shaped curve for ratio of displacement vs. fault trace length, highlighting a maximum displacement at ~ 20 km away from the coast with a value of 221 m for SELF 1 and 88 m for SELF 2 (Fig. 6.8). The same trend is obtained for the recent folds (CG1 and CG2) retrieved in the SCS profiles (and corresponding spatially to the SELF1 and SELF2, respectively) that show a maximum amplitude of 100 m and 47 m respectively (Fig. 6.7).
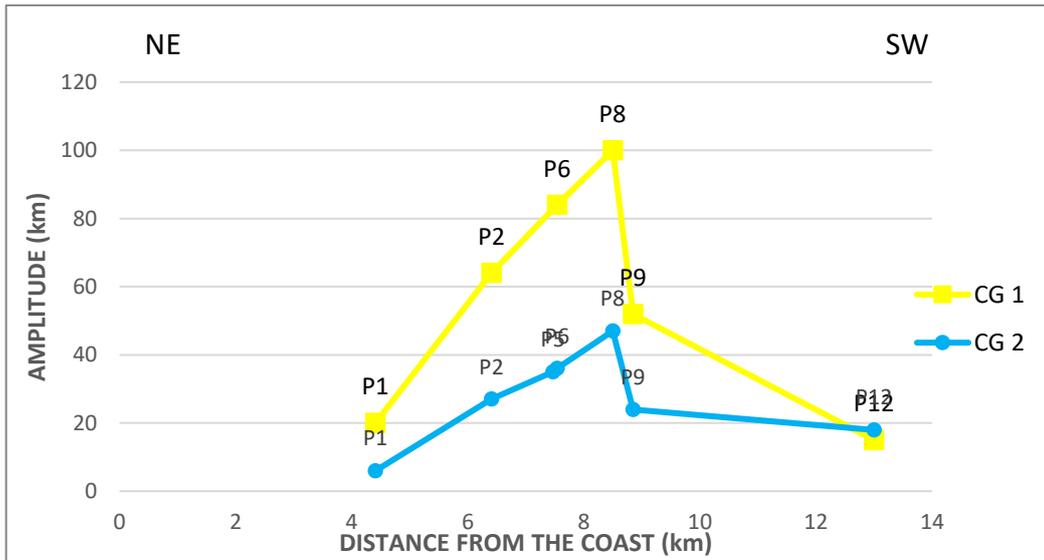
Fig. 6.7 – Graph of amplitude vs. distance from the coast relative to CG1 (yellow line) and CG2 (blue line) gathered by SCS reflection profiles analyses.
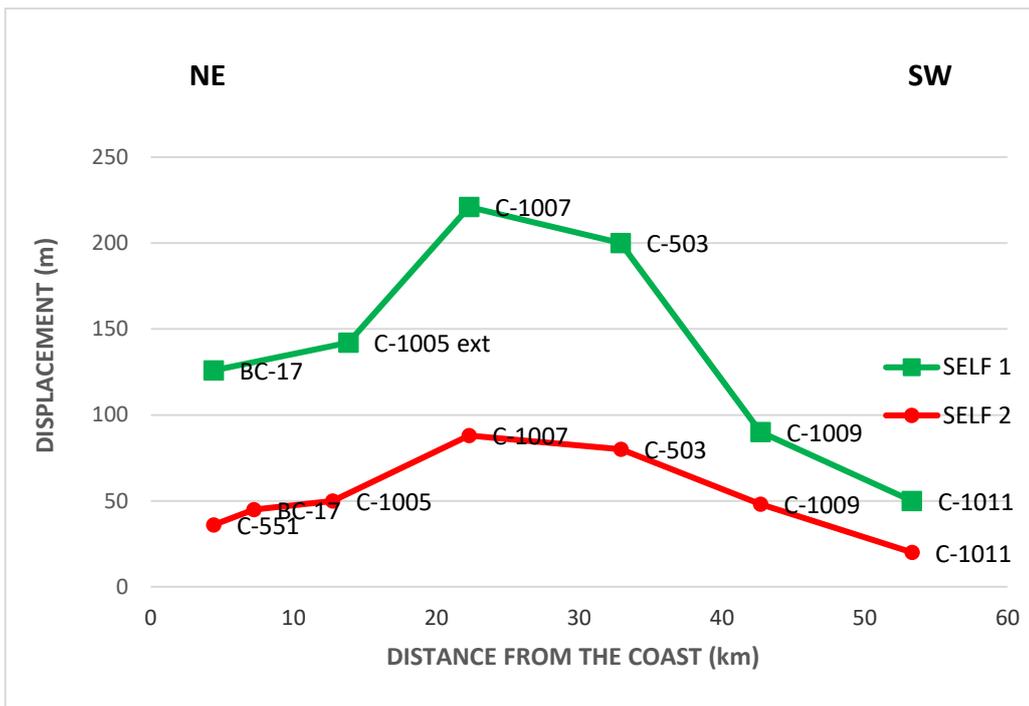
Fig. 6.8 – Graph of displacement vs. distance from the coast with respect to horizon M relative to SELF 1 (green line) and SELF 2 (red line,) gathered by MCS reflection profiles analyses.

For what concerns the Sciacca fold, the fold trends achieved by MCS and SCS profiles analyses show similarity in the curve pattern (Fig. 6.9). The shape of the curves appears to persist through time reproducing the same

232

deformation with different magnitude over shorter and longer timescales. Taking into account the different features of Selinunte anticline and Sciacca fold highlighted in seismic images, as described in chapter III and IV and above summarized, and the different trend patterns on the base of geometrical analysis, we forward the hypothesis that while Selinunte anticline developed in a compression regime of fault reactivation, Sciacca fold is related to a transcurrent regime with a component of contraction (transpression).
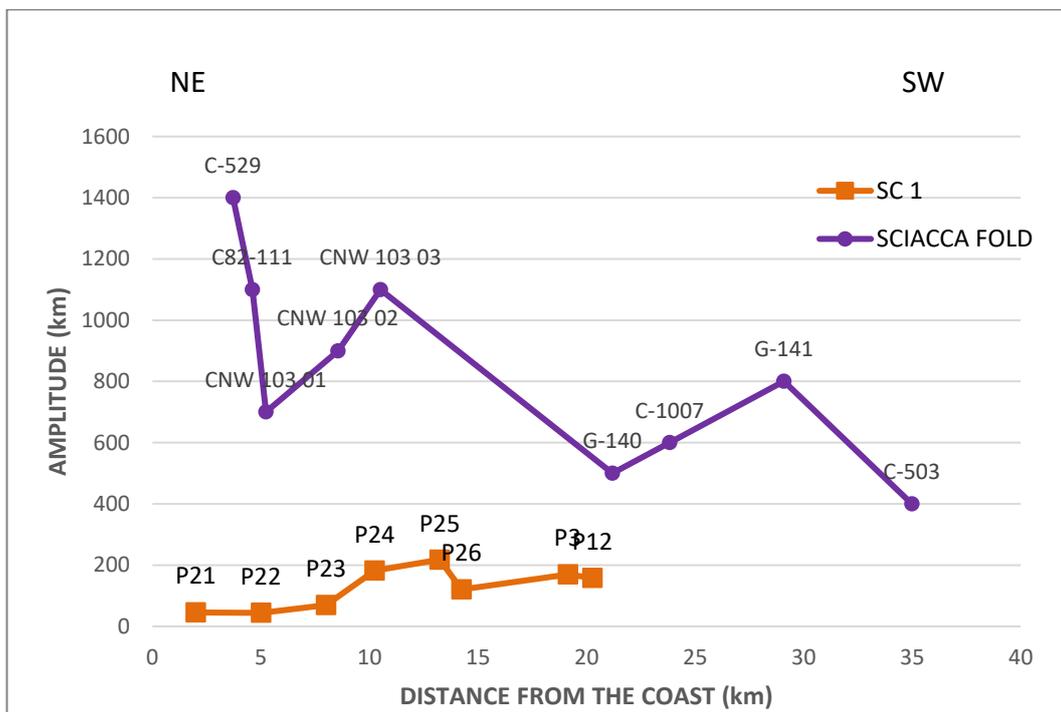
Fig. 6.9 – Graph of fold amplitude vs. distance from the coast relative to Sciacca fold (MCS), violet curve, and SC 1 (SCS), orange curve.

Furthermore, considering the GN (Fig. 6.1) we noted that the recent folds which deform the Eraclea offshore (grouped into a single fold, SC3; Fig. 6.5) are spatially coincident with the nappe. Despite the MCS profiles (see chapter III, Fig. 3.33) do not show a recent activity for the nappe, this evidence can be gathered by the SCS profiles. Hence, the emplacement of the Gela Nappe is considered still active, as recently suggested by CAVALLARO et al. (2017)

based on longer and lesser-resolution Sparker profiles; motion of the nappe trigger mass-transport events (see chapter IV, Fig. 4.29).

6.3.2 Fold-grow rate

Fault slip rate is one of the most important issues in active tectonic by providing information on the seismic potential in a region. Many studies that discuss variable fault activity refer to temporal earthquake clustering with intermittent periods of relative quiescence (COWIE et al., 2012 and reference therein). The difference between short- and long-term slip rates can be explained as due to the fact that deformation proceeds with a non-linear mode, instead for progressive steps. In this case, the short-term slip rate could coincide with a prominent temporal grouping of larger slip events overestimating the true value. Slip rates can be computed directly (on the fault) as done by paleo-seismological studies, or indirectly by using tectonic structures created by slip.

For the area under study, we made a quantitative estimate of uplift (fold-growth) rates for the considered time interval on the fault-related folds (Tables 6.1 and 6.2). Based on the conceptual model of deformation reconstructed in this work, with the folds being expression of motion of underlying blind thrusts, the estimate of fold-growth rate can be taken as a proxy for the vertical slip-rate on the underlying blind faults.

As regards Area 1 (between Mazara and Capo Granitola), we made two distinct estimations of uplift referred to the last 1.5 Ma, by using well data and geometrical parameters of the structures, respectively. Firstly, we considered the difference in thickness of the Pleistocene sediments characterized by the occurrence of *Hyalinea Baltica* between Marinella (600 m) and Oscar wells (265 m). The two wells are located in the footwall and hanging-wall of Selinunte anticline, respectively (see chapter IV, Fig. 4.16), and thus the thickness difference between the two locations reflects the relative uplift

across the thrust-related fold. By dividing this difference (335 m) by 1.5 Ma, that is the onset of the Emilian sub-stage (i.e. the time of first appearance of Hyalinea; RUGGIERI, 1975), we obtain a rate of 0.22 mm/yr for the uplift (fold-growth) rate.

In the second approach, we calculated the vertical fold-growth rate for CG1 and CG2 considering the sum of their maximum values of fold amplitude, equal to 172 m, and an average time activity of ~ 1.5 Ma. The derived uplift rate is of 0.11 mm/yr. The two values of fold-growth rate are comparable.

TABLE 6.1

AREA 1						
DATA USED	**MARKERS**	**UPLIFT (m)**	**AGE (Ma)**	**UPLIFT RATE (mm/yr)**	**UPLIFT RATE (mm/yr) CORRECTED**	
WELL DATA	Hyalinea baltica	335	1.5	0.22	~ 0.11	SHORT-TERM
FOLD AMPLITUDE (CG1)	horizon within unit C	125	1.5	0.08	~ 0.04	SHORT-TERM
FOLD AMPLITUDE (CG1)	horizon within unit C	47	1.5	0.03	~ 0.015	SHORT-TERM
FOLD AMPLITUDE (CG1+CG2)	horizon within unit C	172	1.5	0.11	~ 0.06	SHORT-TERM
FAULT DISPLACEMENT (SELF1)	horizon M	221	5.332	0.04	~ 0.02	LONG-TERM
FAULT DISPLACEMENT (SELF2)	horizon M	88	5.332	0.02	~ 0.01	LONG-TERM
FAULT DISPLACEMENT (SELF1+SELF2)	horizon M	309	5.332	0.06	~ 0.03	LONG-TERM

In order to evaluate the long-term vertical fold-growth rate which is representative of the average slip behaviour on underlying faults, we used the

235

parameters relative to SELF 1 and SELF 2 considering the onset age of the Selinunte anticline during the Early Pliocene (5.3 Ma).

The estimates of fold-growth rates are 0.04 mm/yr and 0.02 mm/yr for SELF 1 and SELF 2, respectively, yielding a cumulative value of 0.06 mm/yr.

When a ~ 50% decrease is applied to the estimated fold-growth rates to account for the lack of decompaction correction for seismic units (MAESANO et al., 2013), average vertical rates estimates decrease to ~ 0.1 mm/yr and to ~ 0.03 mm/yr for the short-term (1.5 Ma) and long-term (5.3 Ma) interval, respectively.

For what concerns Area 2, between Capo Granitola and Sciacca, we estimated the vertical fold-growth rate for the Sciacca Fold since the Miocene. The results evidence an uplift rate of 0.26 mm/yr. A similar value is obtained for the Pleistocene rates (0.15 mm/yr) measured for SC1, using a maximum fold amplitude of 218 m.

TABLE 6.2

AREA 2						
DATA USED	MARKERS	UPLIFT (m)	AGE (Ma)	UPLIFT RATE (mm/yr)	UPLIFT RATE (mm/yr) CORRECTED	
FOLD AMPLITUDE (SC1)	horizon within unit C	218	1.5	0.15	~ 0.08	SHORT-TERM
FOLD AMPLITUDE (SF)	horizon M	1400	5.332	0.26	~ 0.13	LONG-TERM

The similarity in growth rates values over different time interval for Sciacca Fold (i.e., long term ~ 0.13 mm/yr and Pleistocene ~ 0.1 mm/yr) supports the view that the regional shortening rates for this fold belt may not have changed. Note that this estimate reflects less directly the slip rates on the underlying fault, which, as suggested by the different fold parameters relative to the Selinunte folds, we believe is a high-angle strike-slip fault.

In addition, observing the along-strike displacement profiles for the two time-windows (Miocene for SELF1, SELF2, Sciacca Fold; Pleistocene for CG1, CG2, SC1), it can be noted that the shape of the profiles appears to persist through time. So, the shape of profiles is independent of the time-window of observation.

6.4 Geodynamic and seismo-tectonic implications

The NW Sicily Channel represents the link between the outcropping orogenic belts in Tunisia and Sicily derived from the long-lasting convergence between Nubia/Eurasia since the Late Cretaceous. At the scale of the Mediterranean region, the African margin underwent an early stage of subduction, which is accompanied by an increasing of slab rollback under the combined action of decreasing velocity of the African plate and increasing slab pull force (JOLIVET & FACCENNA, 2000; FACCENNA et al., 2004; BILLI et al., 2011). Rupture of the slab and decoupling of the margin from the sinking oceanic slab favoured, in Late Tortonian, the onset of continental collision and the building of the Maghrebides thrust belt along the Tunisian-Sicily northern coast (ARGNANI, 2009). During a second slab break-off episode (5–4 Ma), an intense back-arc extension occurred in the South Tyrrhenian Sea and, according to ARGNANI (2009), thrusting ended in the Adventure thrust belt. The Sicily Channel rift, which opened contemporaneously with the Tyrrhenian basin by slab pull-related forces, could be the upper crustal process accompanying this second slab break-off (FACCENNA et al., 2004). The rift system in the Sicily Channel, developed in the African foreland area and cutting the inactive thrust system, is characterized by Quaternary magmatic activity (ARGNANI, 2009).

CORTI et al. (2006) considered the Sicily Channel as an archetypic area where two geodynamic processes expressed by the Maghrebides-Apennines thrust accretion and by the Sicily Channel rifting acted together since the Pliocene.

Our seismo-stratigraphic and structural analysis of MCS and SCS reflection profiles in the Sicily Channel bears further and high-resolution details to the coexisting of the two geodynamic processes. The resulting complex deformational pattern is represented by superimposed structural features with normal and reverse sense of motion. In particular, the Adventure Bank is affected by a prevalent compression regime and a minor extension mostly localized west of Nameless bank (Fig. 6.1). When we consider the NE-SW trend of the extension in the central Channel and the NW-SE direction of the axis of shortening, we tentatively attribute to the combination of these two processes the cause of ~ N-S orientation of Talbot, Ante Talbot and NAT banks. The seismic analysis revealed that they developed within the Miocene compressive regime related to the emplacement of the SFTB, and later reactivated in transpression and deformed by minor normal faults.

The NW-SE trending extensional faults in Egadi-Marsala offshore which separate Nereo bank from the sector approaching the coast were probably an extensional corridor during the Pliocene together with the near parallel main Channel rift.

Toward the south-east, away from the frontal chain, extension tends to prevail and high angle normal faults bound volcanic banks (e.g., Nameless, Graham).

NE-SW trending normal faults are present in the area between Capo Granitola and Sciacca showing a different trend respect to the extensional structures related to the rift, which as stated before show a NW-SE direction. The origin of the former set of faults may be associated to the bending of foreland during the orogenesis.

Our updated geodetic analysis presented in chapter V supports this general tectonic frame. The estimated geodetic strain-rate confirms and refines previous findings (PALANO et al., 2012) that the eastern part of the Pelagian block between sites PZIN, LAMP and MALT is presently experiencing both NW-SE contraction and NE-SW extension. In addition, our new solution

based on a longer time series provides an improved estimation of the strain occurring between the Pelagian islands and mainland Sicily (see chapter V, Fig. 5.7).

Although the transition between different strain domains appears smooth as a result of the gridded analysis, it is remarkable how the limits of these domains broadly retrace the boundaries of tectonic domains resulting from our regional analysis. Specifically, Lampedusa and the region north-northeast of it until the Sicily shore at Agrigento is reached, and probably swinging to NW toward Campobello, has similar greatest contractional and extensional vector magnitudes, which reflect a strike-slip deformation regime.

Moving northeast of Lampedusa toward Malta and the southeast Sicily shore, the magnitude of the extensional vector gradually prevails, starting from the area where we mapped Plio-Quaternary extensional basins. Between Lampedusa, Pantelleria and the north-western part of the Sicily shore of the channel, a NW-SE trending contractional axis dominates, reflecting an increasing transpression degree. Hence, the deformation gradually changes from compressive in the northwest to transpressive south-eastward but is also influenced by extensional processes.

Overall, the greatest contractional axes across the whole Sicily Channel are aligned to the geodetically estimated Nubia-Eurasia geodetic relative motion (see PALANO et al., 2015), indicating that the plate-driving forces related to the convergence process control the observed crustal deformation pattern, locally modulated by active faults. The orientation and magnitude of the strain field axes suitably fits the strain expected on individual geologic structures during the Late Miocene-Quaternary.

For what concerns the Lampedusa shelf, the geodetic contraction axis is broadly coaxial with the geological shortening axis evidenced by

structural analysis (see chapter V, Fig. 5.5) and with the reconstructed plate convergence direction for the last ~ 20 Ma (see chapter V, Fig. 5.4a). The geodetic estimate, coupled to the occurrence around the Lampedusa Plateau of strike-slip earthquakes that have E-W trending nodal planes whose orientation and kinematics (see chapter I, Fig. 1.7) are consistent with the geological faults presented here, support the contention that strike-slip and transpression have been a permanent feature of the plateau since the Miocene.

As regards the inferences on the active deformation pattern, seismic profile analysis reveals that deformation is active in the Egadi offshore, expressed by back-thrusts and transpressional/transtensional structures, and in the Mazara-Sciacca offshore by folding and faulting of Pleistocene sediments associated to the transcurrent belt.

One of the goal of this thesis was to determine the offshore prosecution of the active thrust system in south-western Sicily. This area is spatially adjacent to the macro-seismic zone of the destructive 1968 Belice earthquake sequence where the active compression at the front of the Sicilian chain is accommodate by south-eastward verging deep-seated thrusts with poor surface expression. Recently, BARRECA et al. (2014) have found that in the southwestern prosecution of the Belice area, an active tectonic lineament is present between Castelvetrano and Campobello di Mazara and till the coast, which GUZZETTA (2014) interpreted as the forelimb of a fault-related fold.

We suggest that the active contraction is mostly transferred in the submerged SELFB which started during the Early Pliocene and is still active as inferred by MCS and SCS reflection profiles. Specifically, as testified by merged MCS and SCS profiles, the Selinunte anticline is the most candidate en-echelon prosecution of the active deformation belt.

In addition, we not only pinpoint the active frontal belt offshore, but also find that current shortening is also accommodated elsewhere in the Channel and notably in the Egadi offshore. The back-thrusts shown in figure 3.22 (chapter III) are so far the only known geological evidence of the long active

deformation belt that, offshore northern Sicily, accommodate the bulk of Africa and Sardinia convergence (see chapter I, Fig. 1.1; BILLI et al., 2011). Thus, the belt offshore northern Sicily and the deformation at the front in southwestern Sicily are concurrent in the Channel and indicate that contractional deformation is diffuse, as typically occurs in collisional zones. Similarly, active strike-slip related to the folding offshore Sciacca supports the notion that the foreland block is strongly fractured, with inherited shear zones focusing the locus of current strain in the general convergence context.

Furthermore, the active GN that proceed toward the SW could trigger new mass-transport events, with important implications for geological hazard in a densely populated coast such as the Sicilian coasts.

CHAPTER VII

7. CONCLUSIONS

In summary, this thesis proposes an updated interpretation of the tectonic evolution of the NW Sicily Channel and the Lampedusa Plateau by integrating available ministerial data (MCS reflection profiles and boreholes from ViDEPI database), industrial (MCS reflection profiles from ENI database) and newly acquired (SCS) high resolution data, and is corroborated by independent geological and geodetic data. The emphasis of this work was on contributing to understanding the geodynamic processes that govern an important area as it bounds densely populated Sicily shore.

The results evidence a complex scenario of deformation related to the convergence of Nubia-Eurasia plates and modulated by a mixture of shortening, strike-slip and extension.

In the NW Sicily Channel, the structures imaged by MCS and SCS seismic profiles exhibit different geometries and kinematics. We distinguished six main fault systems from the oldest to youngest: 1) ETS, which deforms Lower-Middle Miocene deposits through high angle reverse faults bounded by a thrust front with listric geometry (ETF); some of these high-angle faults were recently reactivated; 2) ATS, which is considered the Middle-Upper Miocene front; 3) SELFB and 4) SFB, that are expressed by Miocene (and possibly older) normal faults which were inverted in reverse-oblique slip and formed positive flower structures of Plio-Pleistocene age; these are still active as imaged by SCS lines; 5) GN, represented by a NE-dipping basal thrust which delineates the youngest thrust sheet of the Apennine-Maghrebide chain; 6) the Pantelleria graben characterized by extensional faults active mostly during the Early Pliocene, also extending toward NE on the Adventure Plateau and toward Terrible Bank.

The low resolution of MCS profiles, which provide information at depth of 7-8 km, is not conclusive on the tectonic style (basement-involved or not) of the recognized structures. However, it is most reasonable associate the faults geometry to a deep-seated deformational pattern, as also suggested by residual Bouguer anomalies.

Detailed analyses of Capo Granitola and Sciacca offshore on the base of high-penetration multi-channel and high-resolution single-channel reflection profiles, integrated with correlation with the recent sedimentary succession outcropping in western Sicily coasts, support the inference that the offshore continuation of the forelimb of the thrust-related fold in Castelvetrano area is represented by the Selinunte anticline (related to the SELFB), which forms a left step-over fault segment compared to the on-land structure.

In the perspective of a collisional contest, our study pinpoints the locus of current deformation which is accommodated in different sectors of the Channel. We indicate three principal zones of active deformation expressed by back-thrusts in the Egadi offshore, and by recent folding and faulting in the area of Capo Granitola and Sciacca.

Seismic profile analysis and field work in the Lampedusa Plateau suggests that this region forms a broad anticlinorium modulated by narrower highs and lows. The major high that stands above the regional arch culminates with Lampione and Lampedusa islands. These folds are bounded by reverse and transpressional faults of relatively minor offset in seismic profiles.

Growth of the anticlinorium ensues from the long-lived convergence between Nubia and Europe, and intraplate shortening was already documented in lower Paleogene strata (GRASSO et al., 1999). Compared to this previous work, we focused mostly on the Late Paleogene and Neogene-Quaternary evolution. We argue, based on seismic profiles and reconstruction of the trajectory of Lampedusa relative to Europe, that N-S intraplate shortening also continued during Eocene to Miocene, albeit at a lower rate. From Miocene

onwards, a change to NNW-SSE in plate convergence direction caused reactivation of the previous structural fabrics in transpression.

In the eastern part of Lampedusa, the CCF, which according to GRASSO & PEDLEY (1985) was active during Tortonian-Early Messinian sedimentation, was reactivated more recently causing formation of brittle fabrics indicative of transpression.

During early Pliocene, NE-SW stretching probably related to formation of the Linosa half-graben affected the region to the northeast of the Lampedusa Plateau, forming underfilled basins above tilted blocks.

Geodetic velocities analysed in an already published work (MECCARIELLO et al., 2017) indicate that NW-SE contraction continues today between Lampedusa and Pantelleria, and NE-SW stretching is taking place between Lampedusa and Malta. Geodetic strain seems to indicate that the Transcurrent Belt area and the Lampedusa Plateau continue to be affected by transpression as it was since the Pliocene and Miocene, respectively.

Although observations on Lampedusa indicate a lack of recent most activity, transpression could be accommodated somewhere else in the plateau. Detailed work on high-resolution seismic profiles is deemed to test this hypothesis and detect the more recent deformation suggested by geodesy under the plateau.

REFERENCES

ABATE, B., DI MAGGIO, C., INCANDELA, A., & RENDA, P. (1993) – *Carta geologica dei Monti di Capo San Vito, scala 1: 25.000*. Dipartimento di Geologia e Geodesia dell'Univ. di Palermo (in Italian).

AMOROSI, A., COLALONGO, M. L. (2005) – *The linkage between alluvial and coeval nearshore marine successions: evidence from the Late Quaternary record of the Po River Plain, Italy.* Fluvial Sedimentology VII, 255-275.

ANTONELLI, M., FRANCIOSI, R., PEZZI, G., QUERCI, A., RONCO, G. P., & VEZZANI, F. (1988) – *Paleogeographic evolution and structural setting of the northern side of the Sicily Channel.* Mem. Soc. Geol. It, **41**(1), 141-157.

ANZIDEI, M., BALDI, P., CASULA, G., GALVANI, A., MANTOVANI, E., PESCI, A., RIGUZZI, F., & SERPELLONI, E. (2001) – *Insights into present-day crustal motion in the central Mediterranean area from GPS surveys*. Geophysical Journal International, **146**(1), 98-110.

ARGNANI, A., CORNINI, S., TORELLI, L., & ZITELLINI, N. (1986) – *Neogene-Quaternary foredeep system in the Strait of Sicily.* Memorie Società Geologica Italiana, **36**, 123-30.

ARGNANI, A. (1987) – *The Gela Nappe: Evidence of accretionary melange in the Maghrebian foredeep of Sicily,* Mem. Soc. Geol. It., **38**, 419-428.

ARGNANI, A., CORNINI, S., TORELLI, L., & ZITELLINI, N. (1987) – *Diachronous foredeep-system in the Neogene-Quaternary of the Strait of Sicily.* Mem. Soc. Geol. It, **38**, 407-417.

ARGNANI, A. (1990) – *The Strait of Sicily rift zone: foreland deformation related to the evolution of a back-arc basin.* Journal of Geodynamics, **12**, 311-331.

ARGNANI, A. (1993a) – *Neogene tectonics of the Strait of Sicily*. In: Max MD, Colantoni P (eds.) Geological development of the Sicilian-Tunisian Platform. UNESCO Report in marine science, **58**, 55–60.

ARGNANI, A. (1993b) – *Neogene basins in the Strait of Sicily (Central Mediterranean): tectonic settings and geodynamic implications*. In: Boschi E et al (eds) Recent evolution and seismicity of the Mediterranean region. Kluwer Academic Publication, Dordrecht, 173–187.

ARGNANI, A., & SAVELLI, C. (1999) – *Cenozoic volcanism and tectonics in the southernTyrrhenian sea: space-time distribution and geodynamic significance.* Journal of Geodynamics, 27(4), 409-432.

ARGNANI, A., & TORELLI, L. (2001) – *The Pelagian Shelf and its graben system (Italy/Tunisia).* In: P.A. Ziegler, W. Cavazza, A.H.F. Robertson & S. Crasquin-Soleau (eds),

Pei-Tethys Memoir 6: Peri-Tethyan Rift/Wrench Basins and Passive Margins. Mèm. Mus. Natn. Hist. nat., **186**, 529-544. Paris ISBN: 2-85653-528-3.

ARGNANI, A., & BONAZZI C. (2005) – *Malta Escarpment fault zone offshore eastern Sicily: Pliocene-Quaternary tectonic evolution based on new multichannel seismic data.* Tectonics, **24** (4).

AVELLONE, G., BARCHI, M. R., CATALANO, R., MORTICELLI, M. G., & SULLI, A. (2010) – Interference between shallow and deep-seated structures in the Sicilian fold and thrust belt, Italy. Journal of the Geological Society, **167**(1), 109-126.

BARRECA, G., BRUNO, V., COCORULLO, C., CULTRERA, F., FERRANTI, L., GUGLIELMINO, F., GUZZETTA, L., MATTIA, M., MONACO, C., & PEPE, F. (2014) – *Geodetic and geological evidence of active tectonics in south-western Sicily (Italy).* Journal of Geodynamics, **82**, 138-149.

BASILONE, L. (2012) – *Litostratigrafia della Sicilia.* Palermo: Dipartimento di Scienze della Terra e del Mare - Università degli Studi di Palermo.

BECCALUVA, L., COLANTONI, P., DI GIROLAMO, P., SAVELLI, C. (1981) – *Upper submarine volcanism in the Strait of Sicily (Banco Senza Nome).* Bull Volcanol **44,** 573–581.

BELLO, M., FRANCHINO, A., & MERLINI, S. (2000) – *Structural model of eastern Sicily.* Mem. Soc. Geol. It, **55**, 61-70.

BEN-AVRAHAM, Z., NUR, A., CELLO, G. (1987) – *Active transcurrent fault system along the north African passive margin.* Tectonophysics, **141,** 249–260.

BEN AVRAHAM, Z., BOCCALETTI, M., CELLO, G., GRASSO, M., LENTINI, F., TORELLI, L., & TORTORICI, L. (1990) – *Principali domini strutturali originatisi dalla collisione neogenico-quaternaria nel Mediterraneo Centrale.* Mem. Soc. Geol. Ital., **45**, 453-462.

BEN-AVRAHAM, Z., & GRASSO, M. (1991) - *Crustal structure variations and transcurrent faulting at the eastern and western margins of the eastern Mediterranean.* Tectonophysics, **196.3**, 269-277.

BILLI, A., PORRECA, M., FACCENNA, C., & MATTEI, M. (2006) – *Magnetic and structural constraints for the noncylindrical evolution of a continental forebulge (Hyblea, Italy).* Tectonics, **25**(3).

BILLI, A., PRESTI, D., FACCENNA, C., NERI, G., & ORECCHIO, B. (2007) – *Seismotectonics of the Nubia plate compressive margin in the south Tyrrhenian region, Italy: Clues for subduction inception.* Journal of Geophysical Research: Solid Earth, **112**(B8).

BILLI, A., FACCENNA, C., BELLIER, O., MINELLI, L., NERI, G., PIROMALLO, C., PRESTI, D., SCROCCA, D., AND SERPELLONI, E. (2011) – *Recent tectonic reorganization of the Nubia-Eurasia convergent boundary heading for the closure of the western Mediterranean.* Bull. Soc. Geol. Fr., **182**(4), 279–303.

BOCCALETTI, M., CELLO, G., & TORTORICI, L. (1987) – *Transtensional tectonics in the Sicily Channel.* Journal of Structural Geology, **9**(7), 869-876.

BOTTARI, C., STIROS, S.C., TERAMO, A. (2009) – *Archaeological evidence for destructiveearthquakes in Sicily between 400 B.C. and A.D. 600.* Geoarchaeology, **24**(2),147–175, http://dx.doi.org/10.1002/gea.20260.

BULLIMORE, S., HENRIKSEN, S., LIESTØL, F. M., HELLAND-HANSEN, W. (2005) – *Clinoform stacking patterns, shelf edge trajectories and facies associations in Tertiary coastal deltas, offshore Norway: Implications for the prediction of lithology in prograding systems.* Norwegian Journal of Geology/Norsk geologisk Forening, **85**.

BUROLLET, P. F., MUGNIOT, J.M., & SWEENWY, P. (1978) – *The Geology of the Pelagian Block: The margins and basins off southern Tunisia and Tripolitania.* In: The Ocean Basins and Margins, The Eastern Mediterranean (ed. By A.E.M. Nairn, W.H. Kanes and F.G. Stehly), **4**B, 337-359. Plenum Press, New York.

CALANCHI, N., COLANTONI, P., ROSSI, P.L., SAITTA, M., SERRI, G. (1989) – *The Strait of Sicily continental rift systems: physiography and petrochemistry of the submarine volcanic centres.* Mar. Geol., **87**, 55–83.

CATALANO, R. (1987) – *Northeastern Sicily straits. Stratigraphy and structures from seismic reflection profiles.* Rend. Soc. Geol. It, **9**(2), 103-112.

CATALANO R., AGATE M., AVELLONE G., BASILONE L., GASPARO MORTICELLI M., GUGLIOTTA C., SULLI A., VALENTI V. & GIBILARO C., PIERINI S. (2011) – *Walking along a crustal profile across the Sicily Fold and Thrust Belt.* AAPG International Conference & Exhibition, 23-26 October 2011, Milan, Italy, Post-Conference Field Trip 4/27-29 October 2011, Palermo, Italy. ISBN: 978-88-97559-02-3

CATALANO, R., & D'ARGENIO, B. (1978) – *An essay of palinspastic restoration across western Sicily.* Geologica Romana, **17**, 145-159.

CATALANO, R., & D'ARGENIO, B. (1982) – *Schema geologico della Sicilia. Guida alla geologia della Sicilia occidentale*, **24**, 9-41.

CATALANO, R., D'ARGENIO, B., MONTANARI, L., MORLOTTI, E., & TORELLI, L. (1985) – *Marine geology of the NW Sicily offshore (Sardinia Channel) and its relationships with mainland structures.* Bollettino della Societa Geologica Italiana, **104**(2), 207-215.

CATALANO, R., D'ARGENIO, B., & TORELLI, L. (1989) – *From Sardinia Channel to Sicily Strait. A geologic section based on seismic and field data.* The Lithosphere in Italy, 109-127.

CATALANO, S., DE GUIDI, G., LANZAFAME, G., MONACO, C., & TORTORICI, L. (2009) – *Late Quaternary deformation on the island on Pantelleria: New constraints for the recent tectonic evolution of the Sicily Channel Rift (southern Italy).* Journal of Geodynamics, **48**(2), 75-82.

CATALANO, R., DI STEFANO, P., SULLI, A., VITALE, F.P. (1996) – *Paleogeography and structure of the Central Mediterranean: Sicily and its offshore area.* Tectonophysics, **260**, 291–323.

CATALANO, R., DI STEFANO, P., VITALE, F.P. (1995a) – *Structural trends and palaeogeography of the central and western Sicily belt: new insights.* Terra Nova, **7**, 189–199.

CATALANO, R., FRANCHINO, A., MERLINI, S., SULLI, A. (1998) – *Assetto Strutturale Profondo della Sicilia Occidentale.* Atti del 79° Congresso Nazionale. Società Geologica Italiana 1998. **A**, 257–260.

CATALANO, R., FRANCHINO, A., MERLINI, S., SULLI, A. (2000). *Central western Sicily structural setting interpreted from seismic reflection profiles.* Mem. Soc. Geol. Ital., **55**, 5–16.

CATALANO R., INFUSO S. & SULLI A. (1994) – *The submerged Alpidic chain from southern Sardinia shelf to the Pelagian rifting: tectonic history.* Boll. Geofis. Teor., **36**, 139-158.

CATALANO R., INFUSO S. & SULLI A. (1995b) – *Tectonic history of the submerged Maghrebian Chain from the Southern Tyrrhenian Sea to the Pelagian Foreland.* Terra Nova, **7**, 179-188.

CATALANO, R., MERLINI, S., SULLI, A. (2002). *The structure of western Sicily, central Mediterranean.* Pet. Geosci., **8**, 7–18.

CATALANO, R., VALENTI, V., ALBANESE, C., ACCAINO, F., SULLI, A., TINIVELLA, U., GASPARO MORTICELLI, M., ZANOLLA, C., & GIUSTINIANI, M. (2013) – *Sicily's fold–thrust belt and slab roll-back: the SI. RI. PRO. seismic crustal transect.* Journal of the Geological Society, **170**(3), 451-464.

CATTANEO, A., TRINCARDI, F. (1999) – *The Late-Quaternary transgressive record in the Adriatic epicontinental sea: basin widening and facies partitioning.* Society for Sedimentary Geology Special Publication, **64**, 127-146.

CATUNEANU, O. (2006) – *Principles of sequence stratigraphy.* Elsevier.

CAVALLARO, D., MONACO, C., POLONIA, A., SULLI, A., & DI STEFANO, A. (2017) – E*vidence of positive tectonic inversion in the north-central sector of the Sicily Channel (Central Mediterranean).* Natural Hazards, **86**(2), 233-251.

CELLO, G. (1987) – *Structure and deformation processes in the Strait of Sicily ''rift zone''.* Tectonophysics, **141**, 237–247.

CHIARABBA, C., DE GORI, P., & SPERANZA, F. (2008) – *The southern Tyrrhenian subduction zone: deep geometry, magmatism and Plio-Pleistocene evolution.* Earth and Planetary Science Letters, **268**(3), 408-423.

CIVILE, D., LODOLO, E., ACCETTELLA, D., GELETTI, R., BEN-AVRAHAM, Z., DEPONTE, M., & ROMEO, R. (2010) – *The Pantelleria graben (Sicily Channel, Central Mediterranean): an example of intraplate 'passive' rift.* Tectonophysics, **490**(3), 173-183.

CIVILE, D., LODOLO, E., ALP, H., BEN-AVRAHAM, Z., COVA, A., BARADELLO, L., ACCETTELLA, D., BURCA, M., & CENTONZE, J. (2014) – *Seismic stratigraphy and structural setting of the Adventure Plateau (Sicily Channel).* Marine Geophysical Research, **35**(1), 37-53.

COGAN, J., RIGO, L., GRASSO, M., LERCHE, I. (1989) – *Flexural tectonics of SE Sicily.* J. Geodyn., **11**, 189–241.

COLANTONI, P. (1975) – *Note di geologia marina sul Canale di Sicilia.* Giornale di geologia, **40**, 181-207.

COLANTONI, P., DEL MONTE, M., GALLIGNANI, P., ZARUDZKI, EFK (1975) – *Il Banco Graham: un vulcano recente del Canale di Sicilia.* Giorn. Geol., **40**, 141–162.

COLTELLI, M., CAVALLARO, D., D'ANNA, G., D'ALESSANDRO, A., GRASSA, F., MANGANO, G., PATANÈ, D., GRESTA, S. (2016) – *Exploring the submarine Graham bank in the Sicily Channel.* Annals of Geophysics, **59** (2), DOI: 10.4401/ag-6929.

CORTI, G., BONINI, M., CLOETINGH, S., INNOCENTI, F., MANETTI, P., AND SOKOUTIS, D. (2003) – *Analogue modelling of continental extension: A review focused on the relations between the patterns of deformation and the presence of magma.* Earth-Science Reviews, **63**, 169–247, doi: 10.1016/S0012-8252(03)00035-7.

CORTI, G., CUFFARO, M., DOGLIONI, C., INNOCENTI, F., & MANETTI, P. (2006) – *Coexisting geodynamic processes in the Sicily Channel.* Geological Society of America Special Papers, **409**, 83-96.

COWARD, M. P. (1983). *Thrust tectonics, thin skinned or thick skinned, and the continuation of thrusts to deep in the crust.* Journal of Structural Geology, **5**, 113–123.

COWIE, P. A., & SCHOLZ, C. H. (1992) – *Displacement-length scaling relationship for faults: data synthesis and discussion.* Journal of Structural Geology, **14**(10), 1149-1156.

D'ANGELO, U., & VERNUCCIO, S. (1992) – *Carta geologica del foglio 617 "Marsala" (scala 1:50.000)* – Dipartimeto di Geologia e Geodesia dell'Università degli studi di Palermo.

D'ANGELO, U., AND VERNUCCIO, S. (1994) – "*Note illustrative della carta geological Marsala (F degrees 617 scala 1: 50.000)".* Bollettino della Societa Geologica Italiana, **113**(1), 55-67.

D'ANGELO, U., AND VERNUCCIO, S. (1996) – "*I terrazzi marini quaternari della estremità occidentale della Sicilia."* Mem. Soc. Geol. It*,* **51,** 585-594.

DEMETS, C., GORDON, R. G., & ARGUS, D. F. (2010) – *Geologically current plate motions*. Geophys. J. Int., **181**, 1-80, doi:10.1111/j.1365-246X.2009.04491.x.

DEMETS, C., IAFFALDANO, G., & MERKOURIEV, S. (2015) – *High-resolution Neogene and Quaternary estimates of Nubia-Eurasia-North America Plate motion*. Geophys. J. Int., **203**, 416-427, doi:10.1093/gji/ggv277.

DEVOTI, R., ESPOSITO, A., PIETRANTONIO, G., PISANI, A. R., & RIGUZZI, F. (2011) – *Evidence of large scale deformation patterns from GPS data in the Italian subduction boundary*. Earth and Planetary Science Letters, **311**(3), 230-241.

DEWEY, J. F., HELMAN, M. L., KNOTT, S. D., TURCO, E. & HUTTON, D.H.W. (1989) – *Kinematics of the western Mediterranean*. Geological Society, London, Special Publications, **45**(1), 265-283.

DI MAGGIO, C., AGATE, M., CONTINO, A., BASILONE, L. & CATALANO, R. (2009) – *Unità a limiti inconformi utilizzate per la cartografia dei depositi quaternari nei fogli CARG della Sicilia nord-occidentale.* Italian Journal of Quaternary Sciences, **22**(2), 345-364.

DISS Working Group, 2010. http://diss.rm.ingv.it/diss/, © INGV 2010.

FACCENNA, C., DAVY, P., BRUN, J.P., FUNICIELLO, R., GIARDINI, D., MATTEI, M., & NALPAS, T. (1996) – *The dynamics of back-arc extensions: An experimental approach to the opening of the Tyrrhenian Sea.* Geophys. J. Int., **126,** 781-785.

FACCENNA, C., PIROMALLO, C., CRESPO-BLANC, A., JOLIVET, L., & ROSSETTI, F. (2004) – *Lateral slab deformation and the origin of the western Mediterranean arcs*. Tectonics, **23**(1).

FACCENNA, C., CIVETTA, L., D'ANTONIO, M., FUNICIELLO, F., MARGHERITI, L., & PIROMALLO, C. (2005) – *Constraints on mantle circulation around the deforming Calabrian slab.* Geophysical Research Letters, **32**(6).

FACCENNA, C., FUNICIELLO, F., CIVETTA, L., D'ANTONIO, M., MORONI, M., & PIROMALLO, C. (2007) – *Slab disruption, mantle circulation, and the opening of the Tyrrhenian basins.* Geological Society of America Special Papers, **418**, 153-169.

FACCENNA, C., BECKER, T. W., AUER, L., BILLI, A., BOSCHI, L., BRUN, J. P., CAPITANIO, F. A., FUNICIELLO, F., HORVÀTH, F., AND JOLIVET L. (2014) – *Mantle dynamics in the Mediterranean*, Rev. Geophys., **52**, 283–332, doi:10.1002/2013RG000444.

FERRANTI, L., OLDOW, J.S., D'ARGENIO, B., CATALANO, R., LEWIS, D., MARSELLA, E., AVELLONE, G., MASCHIO, L., PAPPONE, G., PEPE, F., & SULLI, A. (2008) – *Active deformation in southern Italy, Sicily and southern Sardinia from GPS velocities of the Peri-Tyrrhenian Geodetic Array* (PTGA). Boll. Soc. Geol. Ital, **127**(2), 299-316.

FERRANTI, L., BURRATO, P., PEPE, F., SANTORO, E., MAZZELLA, M. E., MORELLI, D., PASSARO S. & VANNUCCI, G. (2014) – *An active oblique-contractional belt at the transition between the Southern Apennines and Calabrian Arc: The Amendolara Ridge, Ionian Sea, Italy*. Tectonics, **33**(11), 2169-2194.

FERRANTI, L., BURRATO, P., FORLANO, S., DI DONATO, V., & AMORE, O.F. (2016) – *Mid-late Quaternary uplift of the coastal sector between Mazara and Selinunte (SW Sicily): hints on active tectonic structures*. Abstract 88 Congresso SGI 2016, Napoli. Rend. Online Soc. Geol. It., **40**, suppl. 1, 322.

FINETTI, I. (1984) – *Geophysical study of the Sicily Channel rift zone*. Boll. Geofis. Teor. Appl., **26**, 3–28.

FINETTI, I., & DEL BEN, A. (1986) – *Geophysical study of the Tyrrhenian opening*. Boll. Geof. Teor. Appl., **28**, 110.

FINETTI, I., & MORELLI, C. (1973) – *Geophysical exploration of the Mediterranean Sea*. Osservatorio geofisico sperimentale.

FINETTI, I.R., LENTINI, F., CARBONE, S., DEL BEN, A., DI STEFANO, A., FORLIN, E., GUARNIERI, P., PIPAN, M., PRIZZON, A. (2005) – *Geological outline of Sicily and Litospheric Tectono-Dynamics of its Tyrrenian Margin from new CROP Seismic Data*. In: FINETTI I.R. (Ed.), CROP PROJECT: Deep Seismic Exploration of the Central Mediterranean and Central Italy, 2005 Elsevier B.V.

FINETTI, I.R., & DEL BEN, A. (2005) – *Crustal tectono-stratigraphic setting of the Pelagian foreland from new CROP seismic data*. CROP PROJECT. Deep Seismic Exploration of the Central Mediterranean and Italy, 581-595.

GHISETTI, F. C., GORMAN, A. R., GRASSO, M., & VEZZANI, L. (2009) – *Imprint of foreland structure on the deformation of a thrust sheet: The Plio-Pleistocene Gela Nappe (southern Sicily, Italy)*. Tectonics, **28**(4).

GRASSO, M., & PEDLEY, H. M. (1985) – *The Pelagian Islands: a new geological interpretation from sedimentological and tectonic studies and its bearing on the evolution of the central Mediterranean Sea (Pelagian Block)*. Geologica Rom., **24**, 13-34.

GRASSO, M., & PEDLEY, H. M. (1988) – *Geological Map of the Island of Lampedusa (Pelagian Island – Central Mediterranean Sea) 1:10.000 Scale*. SE.L.CA, Florence.

GRASSO, M., MAZZOLDI, G. & TORELLI, L. (1993) – *Structural and stratigraphic framework of the Tunisian shelf surrounding the islands of Lampione and Lampedusa (Pelagian Sea)*. In: Max, M. D. and Colantoni P. (Eds). Geological Development of the Sicilian-Tunisian Platform, Proceedings of International Scientific Meeting held at the University of Urbino, Italy, 4-6 November, 1992. UNESCO reports in Marine Science, **58**, 65-70.

GRASSO, M., TORELLI, L., & MAZZOLDI, G. (1999) – *Cretaceous-Palaeogene sedimentation patterns and structural evolution of the Tunisian shelf, offshore the Pelagian Islands (Central Mediterranean).* Tectonophysics, **315**, 235-250.

GRASSO, M. (2001) – *The Apenninic-Maghrebian orogen in southern Italy, Sicily and adjacent areas.* In: Vai GB, Martini IP (eds)Anatomy of an orogen: the Apennines and adjacent Mediterranean basins: Norwell. Kluwer Academic Publishers, Massachusetts, 255–286.

GUIDOBONI, E., MUGGIA, A., MARCONI, C., BOSCHI, E. (2002) – *A case study in archaeo-seismology. The collapses of the Selinunte Temples (Southwestern Sicily): two earthquakes identified.* Bull. Seismol. Soc. Am., **92**, 2961–2982.

GUZZETTA, L. G. (2014) – *Integrazione di dati geodetici e geologici per lo studio dei processi di deformazione attiva in Sicilia Sud-Occidentale.* PhD Thesis. University of Naples Federico II.

HELLAND-HANSEN, W., AND HAMPSON, G.J. (2009) – *Trajectory analysis: concepts and applications.* Basin Research, **21**(5), 454-483.

HERNÁNDEZ-MOLINA, F.J., STOW, D.A.V., ALVAREZ-ZARIKIAN, C.A., ACTON, G., BAHR, A., BALESTRA, B., DUCASSOU, E., FLOOD, R., FLORES, J.-A., FUROTA, S., GRUNERT, P., HODELL, D., JIMENEZ-ESPEJO, F., KIM, J.K., KRISSEK, L., KURODA, J., LI, B., LLAVE, E., LOFI, J., LOURENS, L., MILLER, M., NANAYAMA, F., NISHIDA, N., RICHTER, C., ROQUE, C., PEREIRA, H., SANCHEZ GOÑI, M.F., SIERRO, F.J., SINGH, A.D., SLOSS, C., TAKASHIMIZU, Y., TZANOVA, A., VOELKER, A., WILLIAMS, T., AND XUAN, C. (2014) – *Onset of Mediterranean outflow into the North Atlantic.* Science, **344**(6189), 1244–1250.

HOLLAND, C. W., ETIOPE, G., MILKOV, A. V., MICHELOZZI, E., & FAVALI, P. (2003) – *Mud volcanoes discovered offshore Sicily.* Marine Geology, *199*(1), 1-6.

HORNBACH, M. J., RUPPEL, C., & VAN DOVER, C. L. (2007) – *Three-dimensional structure of fluid conduits sustaining an active deep marine cold seep.* Geophysical Research Letters, **34**(5).

HSÜ, K. J., MONTADERT, L., BERNOULLI, D., CITA, M. B., ERICKSON, A., GARRISON, R. E., & WRIGHT, R. (1977) – *History of the Mediterranean salinity crisis.* Nature, **267**(5610), 399-403.

HUNT, D., AND TUCKER, M. E. (1992) – *Stranded parasequences and the forced regressive wedge systems tract: deposition during base level fall.* Sedimentary Geology, **81**, 1–9.

ILLIES, J.H. (1981) – *Graben formation—the Maltese Islands—a case history.* Tectonophysics, **73**, 151–168.

INCANDELA, A. (1995) – *Lineamenti stratigrafico-strutturali dell'estremità nord-occidentale della Sicilia e delle Isole di Favignana e Levanzo (Arcipelago delle Egadi).* Unpublished PhD Thesis. University of Palermo.

JOLIVET, L., & FACCENNA, C. (2000) – *Mediterranean extension and the Africa-Eurasia collision.* Tectonics, **19**(6), 1095-1106.

JONGSMA, D, VAN HINTE, J.E., WOODSIDE, J.M. (1985) – *Geologic structure and neotectonics of the North African continental margin south of Sicily*. Mar. Pet. Geol., **2**, 156–179.

JUDD, A. G., AND HOVLAND, M. (2007) – Seabed Fluid Flow: The Impact on Geology, Biology and the Marine Environment. Cambridge: Cambridge University Press. doi:10.1017/CBO9780511535918.

KIM, Y. S., & SANDERSON, D. J. (2005) – *The relationship between displacement and length of faults: a review*. Earth-science reviews, **68**(3), 317-334.

LAVECCHIA, G., FERRARINI, F., DE NARDIS, R., VISINI, F., & BARBANO, M. S. (2007) – *Active thrusting as a possible seismogenic source in Sicily (Southern Italy): Some insights from integrated structural–kinematic and seismological data.* Tectonophysics, **445**(3), 145-167.

LENTINI, F. (1982) – *The geology of the Mt. Etna basement*. Mem. Soc. Geol. Ital., **23,** 7–25.

LENTINI, F., CARBONE, S., & GUARNIERI, P. (2006) – *Collisional and postcollisional tectonics of the Apenninic-Maghrebian orogen (southern Italy).* Geological Society of America Special Papers, **409**, 57-81.

LICKORISH, W. H., GRASSO, M., BUTLER, R. W., ARGNANI, A., & MANISCALCO, R. (1999). *Structural styles and regional tectonic setting of the "Gela Nappe" and frontal part of the Maghrebian thrust belt in Sicily.* Tectonics, **18**(4), 655-668.

LISIECKI, L. E., & RAYMO, M. E. (2005). *A Pliocene-Pleistocene stack of 57 globally distributed benthic δ18O records.* Paleoceanography, **20**(1).

LO RE, D. (2017). *Constraining potential field interpretation by geological data: examples from geophysical mapping, inverse and forward modelling*. PhD Thesis. University of Naples Federico II.

LODOLO, E., CIVILE, D., ZANOLLA, C., GELETTI, R. (2012) – *Magnetic signature of the Sicily Channel volcanism.* Mar. Geophys .Res., **33**, 33–44.

MAESANO, F.E., TOSCANI, G., BURRATO, P., MIRABELLA, F., D'AMBROGI, C., BASILI, R. (2013) – *Deriving thrust fault slip rates from geological modelling: examples from the Marche coastal and offshore contraction belt, Northern Apennines, Italy.* Marine and Petroleum Geology, **42**, 122-134.

MALINVERNO, A., CAFIERO, M., RYAN, W. B. F., & CITA, M. B. (1981) – *Distribution of messinian sediments and erosional surfaces beneath the tyrrhenian sea-geodynamic implications*. Oceanologica Acta, **4**(4), 489-495.

MALINVERNO, A., & RYAN, W.B.F. (1986) – *Extension in the tyrrhenian sea and shortening in the apennines as result of arc migration driven by sinking of the lithosphere*. Tectonics, **5**(2), 227-245.

MECCARIELLO, M. (2014) – *Ricostruzione dell'assetto strutturale della parte nord-occidentale del Canale di Sicilia in base all'analisi di profili sismici a riflessione*. Tesi magistrale. Università degli studi di Napoli Federico II, 124 pp.

MECCARIELLO M., FERRANTI L. & PEPE F. (2014) – *The NW sector of the Sicily Channel: geometry and evolution of inverted structural lineaments*. Abstract. Rend. Online Soc. Geol. It., **31**(1).

MECCARIELLO, M., FERRANTI, L., BARRECA, G., & PALANO, M. (2017) – *New insights on the tectonics of the Lampedusa Plateau from the integration of offshore, on-land and space geodetic data.* Italian Journal of Geosciences, **136**(2), 206-219.

MELLERE, D.O., PLINK-BJORKLUND, P., STEEL, R. (2002) – *Anatomy of shelf deltas at the edge of a prograding Eocene shelf margin, Spitsbergen*. Sedimentology, **49**, 1181-1206.

MILKOV, A.V. (2000) – *Worldwide distribution of submarine mud volcanoes and associated gas hydrates.* Marine Geology, **167**, 29–42.

MITCHUM, R. M. JR., AND VAIL, P. R. (1977). *Seismic stratigraphy and global changes of sea-level, part 7: stratigraphic interpretation of seismic reflection patterns in depositional sequences.* In Seismic Stratigraphy–Applications to Hydrocarbon Exploration (C. E. Payton, Ed.) American Association of Petroleum Geologists Memoir **26**, 135–144.

MITCHUM, R. M. JR., VAIL, P. R., AND THOMPSON, S. (1977) – *Seismic stratigraphy and global changes of sea-level, part 2: the depositional sequence as a basic unit for stratigraphic analysis.* In: Seismic Stratigraphy–Applications to Hydrocarbon Exploration (C. E. Payton, Ed.), American Association of Petroleum Geologists Memoir, **26**, 53–62.

MONACO, C., MAZZOLI, S., & TORTORICI, L. (1996) – *Active thrust tectonics in western Sicily (southern Italy): the 1968 Belice earthquake sequence.* Terra Nova, **8**(4), 372-381.

MONACO, C., TORTORICI, L., CATALANO, S. (2000) – *Tectonic escape in the Sicanian mountains (western Sicily).* Memorie della Società Geologica Italiana, **55**, 17–25.

MONACO, C., BALDASSINI, N., BARRECA, G., CAVALLARO, D., DI STEFANO, A., FERRANTI, L., MECCARIELLO, M. (2015) – *Geological framework of the Sicily Channel.* In: Establishment of an integrated Italy–Malta cross–border system of civil protection. Geological aspects. ISBN 978-88-548-8255-3. DOI 10.4399/97888548825533.

MONTANARI, D., MINISSALE, A., DOVERI, M., GOLA, G., TRUMPY, E., SANTILANO, A., & MANZELLA, A. (2017) – *Geothermal resources within carbonate reservoirs in western Sicily (Italy): A review.* Earth-Science Reviews, **169**, 180-201.

MORELLI, A., PONDRELLI, S. (1998) – Il terremoto del Belice del 1968. In: Poster presented at Conference "Trenta anni di terremoti in Italia: dal Belice a Colfiorito", Erice, Sicily 14–18 July.

NEAL, J., & ABREU, V. (2009) – *Sequence stratigraphy hierarchy and the accommodation succession method.* Geology, **37**(9), 779-782.

NERI, G., ORECCHIO, B., TOTARO, C., FALCONE, G., & PRESTI, D. (2009). *Subduction beneath southern Italy close the ending: Results from seismic tomography.* Seismological Research Letters, **80**(1), 63-70.

OGNIBEN, L. (1969). *Schema introduttivo alla geologia del confine calabro-lucano.* Mem. Soc. Geol. It., **8**, 453-763.

PALANO, M., FERRANTI, L., MONACO, C., MATTIA, M., ALOISI, M., BRUNO, V., CANNAVÒ, F., & SILIGATO, G. (2012) – *GPS velocity and strain fields in Sicily and southern Calabria, Italy: Updated geodetic constraints on tectonic block interaction in the central Mediterranean.* Journal of Geophysical Research, **117**, b07401, doi:10.1029/2012jb009254, 2012.

PALANO, M. (2015) – *On the present-day crustal stress, strain-rate fields and mantle anisotropy pattern of Italy.* Geophys. J. Int., **200**, 969-985, doi:10.1093/gji/ggu45.

PALANO, M., GONZÁLEZ, P.J., & FERNÁNDEZ, J. (2015) – *The diffuse plate boundary of Nubia and Iberia in the Western Mediterranean: Crustal deformation evidence for viscous coupling and fragmented lithosphere.* Earth and Planetary Science letters, **430**, 439-447, doi:10.1016/j.epsl.2015.08.040.

PATACCA, E., SCANDONE, P., GIUNTA, G., AND LIGUORI, V. (1979) – *Mesozoic paleotectonic evolution of the Ragusa zone (Southeastern Sicily).* Geologica Romana, 1979, **18**, 331-369.

PEPE, F., SULLI, A., BERTOTTI, G., & CELLA, F. (2010) – *Architecture and Neogene to Recent evolution of the western Calabrian continental margin: An upper plate perspective to the Ionian subduction system, central Mediterranean.* Tectonics, **29**(3).

PEPE, F., BERTOTTI, G., FERRANTI, L., SACCHI, M., COLLURA, A. M., PASSARO, S., & SULLI, A. (2014) – Pattern and rate of post-20 ka vertical tectonic motion around the Capo Vaticano Promontory (W Calabria, Italy) based on offshore geomorphological indicators. Quaternary International, **332**, 85-98.

POSAMENTIER, H. W., JERVEY, M. T., AND VAIL, P. R. (1988) – *Eustatic controls on clastic deposition I – conceptual framework.* In Sea Level Changes–An Integrated Approach

(C. K. Wilgus, B. S. Hastings, C. G. St. C. Kendall, H. W. Posamentier, C. A. Ross and J. C. Van Wagoner, Eds.). SEPM Special Publication **42**, 110–124.

RABINEAU, M., BERNÉ, S., ASLANIAN, D., OLIVET, J. L., JOSEPH, P., GUILLOCHEAU, F., GRANJEON, D. (2005) – *Sedimentary sequences in the Gulf of Lion: a record of 100,000 years climatic cycles.* Marine and Petroleum Geology, **22**(6), 775-804.

RANUCCI, M., & MONTI, F. (1963) – *Note sui rilievi sismici.* Volume I. Sismica a riflessione. Generalità-Elaborazione dei sismogrammi e procedimenti di calcolo.

REBESCO, M., HERNÁNDEZ-MOLINA, F. J., VAN ROOIJ, D., WAHLIN, A., (2014) – *Contourites and associated sediments controlled by deep-water circulation processes: state-of-the-art and future considerations.* Marine Geology, **352**, 111-154.

REUTHER, C.D., & EISBACHER, G.H. (1985) – *Pantelleria rift-crustal extension in a convergent intraplate setting.* Geol. Rundsch., **74**, 585–597.

REUTHER, C. D., BEN-AVRAHAM, Z., & GRASSO, M. (1993*). Origin and role of major strike-slip transfers during plate collision in the central Mediterranean.* Terra Nova, **5**(3), 249-257.

RIGO, M., & BARBIERI, F. (1959) – Stratigrafia pratica applicata in Sicilia. Boll. Serv. Geol. Italia, **80**, 351-442, Roma.

RYAN, W.B.F., & CITA, M.B. (1978) – *The nature and distribution of Messinian erosional surfaces-indicators of several kilometer deep Mediterranean in the Miocene.* Mar. Geol., **27**, 193-230, doi:10.1016/0025-3227(78)90032-4.

RODA-BOLUDA, D. C., & WHITTAKER, A. C. (2016) – *Normal fault evolution and coupled landscape response: examples from the Southern Apennines, Italy*. Basin Research. doi: 10.1111/bre.12215.

ROSENBAUM, G., LISTER, G.S., & DUBOZ, C. (2002) – *Relative motions of Africa, Iberia, and Europe during the Alpine orogeny*. Tectonophysics, **359,** 117-129.

ROSENBAUM, G., & LISTER, G. S. (2004) – *Neogene and Quaternary rollback evolution of the Tyrrhenian Sea, the Apennines, and the Sicilian Maghrebides*. Tectonics, **23**(1).

ROTOLO, S.G., CASTORINA, F., CELLULA, D., POMPILIO, M. (2006) – *Petrology and geochemistry of submarine volcanism in the Sicily Channel*. J. Geol., **114**, 355–365.

ROURE, F., CASERO, P., & ADDOUM, B. (2012). *Alpine inversion of the North African margin and delamination of its continental lithosphere.* Tectonics, **31**(3).

RUGGIERI, G., & TORRE, G. (1973) – *Geologia delle zone investite dal terremoto del Belice.* Estratto dalla Riv. Min. Sic, **139**(141), 27-48.

RUGGIERI, G., UNTI, A., UNTI, M., MORONI, M. A. (1977) – *La calcarenite di Marsala (pleistocene inferiore) ei terreni contermini*. Estratto dal Bollettino Società Geologica Italiana, **94**, 1623-1655, 2 ff.

SARIA, E., CALAIS, E., ALTAMIMI, Z., WILLIS, P., & FARAH, H. (2013) – *A new velocity field for Africa from combined GPS and DORIS space geodetic solutions: Contribution to the definition of the African reference frame (AFREF)*. J. Geophys. Res. Solid Earth, **118**, 1677-1697, doi:10.1002/jgrb.50137.

SEBEI, K., INOUBLI, M. H., BOUSSIGA, H., TLIG, S., ALOUANI, R. & BOUJAMAOUI, M. (2007) – *Seismic stratigraphy, tectonics and depositional history in the Halk el Menzel region, NE Tunisia*. Journal of African Earth Sciences, **47**(1), 9-29.

SELLI, R. (1960) – *Il Messiniano Mayer-Eymar 1867. Proposta di un Neostratotipo*. Giornale di Geologia, Ser. 2, **28**, 1-33, Bologna.

SCHMIDT DI FRIEDBERG, P. (1962) – *Introduction a la géologie pétrolière de la Sicile*. Revue Inst. Franc. du Pétr., **17** (5), 35-668.

SCHWARTZ, D.P., & COPPERSMITH, K.J. (1984) – *Fault behaviour and characteristic earthquake: Examples from the Wasatch and San Andreas Fault Zones*. J. Geophys. Res., **89**, 5681–5698

SHINER, P., BECCACINI, A., & MAZZOLI, S. (2004) – *Thin-skinned versus thick-skinned structural models for Apulian carbonate reservoirs: constraints from the Val d'Agri Fields, S Apennines, Italy*. Marine and Petroleum Geology, **21**(7), 805-827.

SIMONETTI, A., KNAPP, J. H., KNAPP, C. C., MACELLONI, L., & LUTKEN, C. B. (2011) – *Defining the hydrocarbon leakage zone and the possible accumulation model for marine gas hydrates in a salt tectonic driven cold seep: examples from Woolsey Mound, MC118, northern Gulf of Mexico*. In Proceedings of the 7th International Conference on Gas Hydrates (ICGH 2011), Edinburgh, Scotland, United Kingdom.

SOUMAYA, A., BEN AYED, N., DELVAUX, D., & GHANMI, M. (2015) – *Spatial variation of present-day stress field and tectonic regime in Tunisia and surroundings from formal inversion of focal mechanisms: Geodynamic implications for central Mediterranean*. Tectonics, **34**, 1154-1180. doi: 10.1002/2015TC003895.

SUESS, E. (2010) – Marine cold seeps. In *Handbook of hydrocarbon and lipid microbiology,* 185-203. Springer Berlin Heidelberg.

TALUKDER, A.R. (2012). – *Review of submarine cold seep plumbing systems: leakage to seepage and venting*. Terra Nova, **24**(4), 255-272.

TAVARNELLI, E., BUTLER, R.W. H., DECANDIA, F. A., CALAMITA, F., GRASSO, M., ALVAREZ, W., & RENDA, P. (2004) – *Implications of fault reactivation and structural inheritance in the Cenozoic tectonic evolution of Italy*. The Geology of Italy, Special, **1**, 209-222.

TORELLI, L., ZITELLINI, N., ARGNANI, A., BRANCOLINI, G., DE CILLIA, C., PEIS, D., & TRICART, P. (1991) – *Sezione geologica crostale dall'avampaese Pelagiano al Bacino di retroarco Tirrenico (Mediterraneo centrale).* Mem. Soc. Geol. Ital, **47**, 385-399.

TORELLI, L., TRICART, P., ZITELLINI, N., ARGNANI, A., BOUHLEL, I., BRANCOLINI, G., DE CILLIA, C., DE SANTIS, L., & PEIS, D. (1992) – *Une Section sismique profonde de la chaine Maghrebides-Apennins, du bassin Tyrrhenien a la plateforme Pelagienne (Mediterranée centrale).* Comptes rendus de l'Académie des sciences. Série 2, Mécanique, Physique, Chimie, Sciences de l'univers, Sciences de la Terre, **315**(5), 617-622.

TORELLI, L., ZITELLINI, N., ARGNANI, A., BRANCOLINI, G., DE CILLIA, C., PEIS, D., TRICART, P. (1993) – Sezione geologica crostale dall'avampaese Pelagiano al bacino di retroarco Tirrenico (Mediterraneo Centrale). Mem. Soc. Geol. It., **47**, 385–399.

TORELLI, L., GRASSO, M., MAZZOLDI, G., PEIS, D. & GORI, D. (1995) – *Cretaceous to Neogene structural evolution of the Lampedusa Shelf (Pelagian Sea, Central Mediterranean).* Terra Nova, **7**, 200-212.

VAIL, P.R. (1987) – *Seismic stratigraphy interpretation procedure.* In Atlas of Seismic Stratigraphy (A. W. Bally, Ed.), 1–10. American Association of Petroleum Geologists Studies in Geology, **27**.

VAIL, P.R., MITCHUM, J.R., R. M. & THOMPSON, S. (1977) – *Seismic Stratigraphy and Global Changes of Sea Level: Part 4. Global Cycles of Relative Changes of Sea Level.: Section 2. Application of Seismic Reflection Configuration to Stratigraphic Interpretation.*

VAN WAGONER, J. C., POSAMENTIER, H. W., MITCHUM, R. M. JR., VAIL, P. R., SARG, J. F., LOUTIT, T. S., AND HARDENBOL, J. (1988) – *An overview of sequence stratigraphy and key definitions.* In Sea Level Changes–An Integrated Approach C. K. Wilgus, B. S. Hastings, C. G. St. C. Kendall, H. W. Posamentier, C. A. Ross and J. C. Van Wagoner, Eds.), 39–45. SEPM Special Publication 42.

VIDEPI project. http://unmig.sviluppoeconomico.gov.it/videpi/videpi.asp

VITALE, F.P. (1990) – *Studi sulla valle del medio Belice, Sicilia centro occidentale: l'avanfossa plio-pleistocenica nel quadro dell'evoluzione paleotettonica dell'area.* Tesi di dottorato.

VITALE, F. (1996) – *I bacini Plio-Pleistocenici della Sicilia: un laboratorio naturale per lo studio delle interazioni tra tettonica e glacio-eustatismo.* Riunione Gruppo Sedimentologia CNR, Catania, 10-14.

WAELBROECK, C., LABEYRIE, L., MICHEL, E., DUPLESSY, J. C., MCMANUS, J. F., LAMBECK, K., BALBON, E., & LABRACHERIE, M. (2002) – *Sea-level and deep water temperature changes derived from benthic foraminifera isotopic records.* Quaternary Science Reviews, **21**(1), 295-305.

WESSEL, P., & BERCOVICI, D. (1998) – *Interpolation with splines in tension: a Green's function approach.* Mathematical Geology, **30**(1), 77-93.

WILLIAMS, G. D., POWELL, C. M., & COOPER, M. A., (1989) – *Geometry and kinematics of inversion tectonics.* Geological Society, London, Special Publications, **44**(1), 3-15.

WINNOCK, E. (1981) – *Structure du bloc pélagien.* Sedimentary basins of Mediterranean margins, 445-464.

ACKNOWLEDGEMENTS

I am grateful to all the people that supported me during this research starting from my supervisors: Luigi Ferranti, who improved my knowledge in structural geology and tectonics and encouraged me constantly; and Fabrizio Pepe, who introduced me to high-resolution data processing.

I am grateful to Mimmo Palano and Giovanni Barreca who made a valid contribution to the publication of the research regarding the Lampedusa Plateau.

I wish to thank all the crew of R/V Minerva Uno with whom I worked and had a good time during the 10 days oceanographic cruise. I will never forget this experience.

I am grateful to Andrea Billi and Attilio Sulli who critically reviewed the thesis and encouraged me to publish the results of this research.

I wish to thank all my University friends and colleagues for sharing with me their knowledge and pleasant times.

Last but not least, I am very grateful to all my family and close friends that have always believed in me.